Distribution Agreement

In presenting this thesis or dissertation as a partial fulfillment of the requirements for an advanced degree from Emory University, I hereby grant to Emory University and its agents the non-exclusive license to archive, make accessible, and display my thesis or dissertation in whole or in part in all forms of media, now or hereafter known, including display on the world wide web. I understand that I may select some access restrictions as part of the online submission of this thesis or dissertation. I retain all ownership rights to the copyright of the thesis or dissertation. I also retain the right to use in future works (such as articles or books) all or part of this thesis or dissertation.

Signature:

_____ _____

Rachel E. Turn Date

The ELMOD Family of ARF GAPs: Proposed Roles in Inter-pathway Communication

By

Rachel Elizabeth Turn
Doctor of Philosophy

Graduate Division of Biological and Biomedical Science
Biochemistry, Cell and Developmental Biology

_____

Richard A. Kahn, Ph.D.
Advisor

_____

Lawrence H. Boise, Ph.D.
Committee Member

_____

John R. Hepler, Ph.D.
Committee Member

_____

Anna M. Kenney, Ph.D.
Committee Member

_____

Dorothy A. Lerit, Ph.D.
Committee Member

Accepted:

_____

Lisa A. Tedesco, Ph.D.
Dean of the James T. Laney School of Graduate Studies

_____

Date

The ELMOD Family of ARF GAPs: Proposed Roles in Inter-pathway Communication

By

Rachel Elizabeth Turn
B.A, Harriet L. Wilkes Honors College, FAU, 2015

Advisor: Richard A. Kahn, Ph.D.

An abstract of
A dissertation submitted to the Faculty of the
James T. Laney School of Graduate Studies of Emory University
in partial fulfillment of the requirements for the degree of
Doctor of Philosophy
in Biochemistry, Cell and Developmental Biology
2020

Abstract

The ELMOD Family of ARF GAPs: Proposed Roles in Inter-pathway Communication

By Rachel E. Turn

The ARF family of small GTPases are regulators of diverse cellular pathways. Because of the numerous functions that a single GTPase can mediate (e.g vesicular traffic, cytoskeletal dynamics, ciliary function), we propose that the ARFs are drivers of inter-pathway communication, or "higher order signaling." The mechanisms by which ARF GTPases would regulate higher order signaling, though, remain unclear. The focus of my dissertation work has been on the ELMODs, a 3-member family of ARF GAPs that regulate the on/off state of ARF GTPases. I have discovered new, diverse functions for the ELMODs in cells, lending to our model that the regulators of the GTPases themselves may also drive inter-pathway communication to mediate essential cell functions.

The majority of my dissertation work has been with one of the family members, ELMOD2. Previous lab members and I worked to probe for functions of ELMOD2 in mitochondrial fusion. I generated ELMOD2 KO cells using CRISPR-Cas9 to probe for mechanism. This model system served as a springboard for my own project, as I discovered that the loss of ELMOD2 led to the disruption of a number of cellular processes. As detailed in my first-author manuscript, I discovered numerous phenotypes consistent with defects in microtubules and cell cycle. I discovered that ELMOD2 works in two additional pathways: with ARL2 to regulate microtubule anchoring at centrosomes, and with ARF6 to regulate cytokinesis from the Flemming body. Another large portion of my dissertation work has been exploring functions for ELMDO2 in yet another pathway, acting in concert with ciliary rootlets and ARL2 to inhibit spurious ciliogenesis. Altogether, these findings shed light on the mechanisms by which ARFs and their GAPs regulate cell signaling and pave the way for understanding how such discrete cell functions as microtubule anchoring, ciliogenesis, and cytokinesis coordinate to ensure cell survival. My findings will pave the way for future study of other ELMOD family members as well as ARF GTPases, with the ultimate goal of understanding how the vast network of signaling pathways communicate with one another.

The ELMOD Family of ARF GAPs: Proposed Roles in Inter-pathway Communication

By

Rachel Elizabeth Turn
B.A., Harriet L. Wilkes Honors College, FAU, 2015

Advisor: Richard A. Kahn, Ph.D.

A dissertation submitted to the Faculty of the
James T. Laney School of Graduate Studies of Emory University
in partial fulfillment of the requirements for the degree of
Doctor of Philosophy
in Biochemistry, Cell and Developmental Biology
2020

Acknowledgements

There are many people I have to thank for making this work possible. First and foremost, I would like to thank my mentor, Rick Kahn. Thank you for all of your years of sage wisdom, for pushing me to be the best version of myself and to grow as a scientist, for reading all the awful drafts of my manuscripts and grants, for giving me the freedom to trailblaze and to make my own name in the field, and for inspiring me to pursue my dreams of becoming a principal investigator. None of this would have been possible without you. Thank you to my wonderful committee: Dorothy, Anna, John, and Larry. You've been an amazing team, helping me test my models and to figure out the best approaches to get at the heart of my questions. You've all been so supportive, answering my many questions, and I'm so grateful to have had the chance to work with you. Thanks also to all my collaborators who have provided me much needed resources and with great advice to get my project off the ground. Win and Tamara, you've been amazing at helping me find a new home in the field of cilia and centrosomes. I can't wait to work with you in the future, even if I'm a coast away! To my beautiful, ever growing, ever changing lab family: thanks for everything. Laura, Josh, Anna, Cara, Skylar, Darius, Kate, Nicky, Yihan, Randy, Dennis, Elle- you've all been amazing. Thanks for simultaneously making science an exciting new adventure, while also making the lab feel like a home. These have been some of the best years of my life, and I will always think of you as my family. Laura and Cara, the foundresses of the Nerd Girl Squad, I'll be seeing you in California soon.

Outside of the lab, I first would like to thank all of BCDB. I'm grateful to have been a part of such a wonderful, supportive program. Thanks to Mike, Graeme, Susan, and all the Exec Board past and present for helping keep our graduate program running. Thank you to all the amazing teachers I had in Foundations and Grant Writing class- you provided me with all the tools I needed

to succeed in my graduate career. I'm grateful to my wonderful cohort for helping me through some of the craziest years of grad school, and for all of the brothers and sisters I've made in the years below and above me in BCDB. So grateful for all of you. Special thanks to all the friends I've made through GIVE. You are some of the most loving and generous people I know, and I'm so excited to hear what great things GIVE has in store for the future. Warm thanks to all my former science mentors: Nick Quintyne, April Schimmel, Paul Kirchman, Haiqing Zhao, Patsy McDonald, Crystal Gigante, and Emmanuel Sturchler. Each of you guided me on my journey to becoming a better scientist, and I will always be grateful. Sam, Tyler, Courtney, Zane, George, Binta, Laura, Cara, Hale, Rachel- thanks for being some of the best friends I could ever ask for. Outside of Emory, thanks to my Habitat for Humanity family, my STM family, and my undergrad friends who've stayed around through thick and thin. Thank you to my family- my parents, Christina, Jeffrey, Grandmom, aunts and uncles—I wouldn't be who I am today if it wasn't for you. And last but not least, I'm grateful for Chris and Chloe- I'm looking forward to making a new life with you.

Table of Contents

Abbreviations

ARL2 = ADP ribosylation like factor 2

ARL3 = ADP ribosylation like factor 3

ARF6 = ADP ribosylation factor 6

CP110 = Centriolar coiled coil protein 110

Cep164 = Centrosomal protein 164

CEP290 = Centrosomal protein 290

D2 = ELMOD2

ELMOD = Engulfment & motility domain containing protein

FBS = Fetal bovine serum

FIP3 = Rab11 Family Interacting Protein 3

GAP = GTPase activating protein

GEF = Guanine nucleotide exchange factor

GFP = Green fluorescent protein

gSTED = Gated stimulated emission depletion microscope

IF = Immunofluorescence

IFT = Intraflagellar transport

IMS = Inner membrane space

KO = Knockout

MEF = Mouse embryonic fibroblast

NPHP4 = Nephrocystin-4

PTM = Post-translational modification

Rab11 = Ras-related protein 11

SIM = Structured illumination microscopy

TBCD = Tubulin folding cofactor D

TZ = Transition zone

WB = Western blot

WT = Wild-type

γTuRC = γ-tubulin ring complex

Chapter 1: Introduction

ARF Family GTPases and their Regulators

ADP Ribosylation Factor (ARF) was first discovered in 1984 by Richard Kahn during his tenure in Al Gilman's lab (Kahn and Gilman, 1984). The first family member, later termed ARF1, was originally purified from multiple mammalian sources and named because of its role as cofactor in the ADP-ribosylation of Gs (the heterotrimeric G-protein activator of adenylyl cyclase) by cholera toxin (Kahn and Gilman, 1984). Future work led to the cloning and identification of a number of proteins that had high homology to ARF1, so this in vitro assay was originally used to classify the expanding group of GTPases as either ARFs (which possess the activity) or ARF-like or ARLs (which do not). With genome sequencing came the recognition that, together, ARFs and ARLs form a family (later identified as a superfamily) with 29 members in humans: 5 ARFs, 21 ARLs, 2 SARs, and Trim23 (Sztul et al., 2019). For the sake of simplicity, I will refer to the ARF family as a whole as ARFs, and when I refer to specific subfamily members (*e.g* ARF vs ARL), I will make note of it. Homologies range from 96% identity between ARF1-3 to at least 40% identity between all ARFs and ARLs, with SARs and Trim23 lower. These proteins are ancient, with sixteen family members having been traced back to the last eukaryotic common ancestor (Sztul et al., 2019). Metagenomic studies from the Asgard archaea (or archaea that are believed to be the progenitors of eukaryotic cells) reveal clear evidence of a close relative of ARFs that would later form the origins of the ARF GTPase superfamily (Spang et al., 2015; Zaremba-Niedzwiedzka et al., 2017). Because these players are so old and highly conserved, one would predict that ARFs play critical, conserved cellular functions.

ARFs and other GTPases function by cycling between guanine nucleotide binding states, allowing them to be turned "on" upon exchange of bound GDP with GTP and "off" with GTP hydrolysis and release of inorganic phosphate, to return the GTPase to its basal GDP-bound state. Nucleotide binding allows for conformational changes that alter GTPase function, whether it is changing conformation of the canonical switches 1 or 2 to alter affinity for binding partners and release of its N-terminally myristolated α-helix to allow membrane recruitment. This activation-dependent translocation on and off membranes is a hallmark

of the ARFs, also found in some but not all ARLs. It is also a contributor, though not sole determinant, to the findings that most ARF family GTPases localize to and act at multiple sites in cells. The cycling between nucleotide binding states provides temporal control for the GTPase functionalities but fails to explain (at least completely) how spatial regulation is maintained or regulated. What allows for the differential recruitment of ARFs to different sites, presumably to meet the changing needs of the cell? We believe that it can be partially explained by access to regulators of the GTPases: Guanine Nucleotide Exchange Factors (GEFs) and GTPase Activating Proteins (GAPs). GEFs act upstream to promote the GTPase "on" state by speeding the rate of GDP release, clearing the way for GTP loading. GAPs, on the other hand, promote the "off" state by increasing the rate of GTP hydrolysis. Even more fascinating about ARF GAPs, though, is that in practically every instance studied to date, ARF GAPs also function as effectors. This means that, rather than simply regulating the rate of inactivation, the binding of an activated ARF to an ARF GAP also results in propagation of a signal "downstream" that results in a biological consequence, thus is an obligate step in the signaling pathway(s) to which they are associated (East and Kahn, 2011; Zhang et al., 1998). Because of their ability to both indirectly and directly modulate signaling pathways, ARF GAPs have become an important field of study for teasing apart the diverse signaling pathways that ARF GTPases regulate.

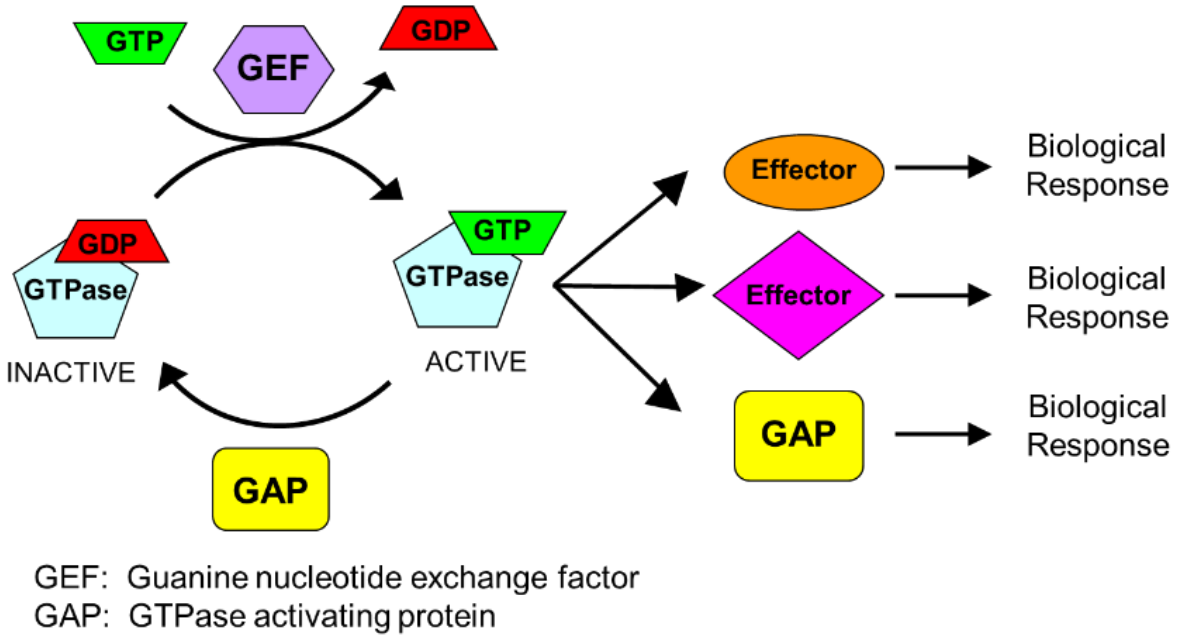

Figure 1: ARF GTPases are molecular switches that provide spatial and temporal control of signaling. *Like other small regulatory GTPases, ARFs behave as molecular switches that cycle between "on" and "off" states. As shown in the diagram above, a GTPase is activated when it is GTP bound and inactivated when it is GDP bound. To regulate this cycling, GEFs (light purple) increase the rate of GDP release to promote GTPase activation, while GAPs increase the rate of GTP hydrolysis and, thus, GTPase inactivation. This cycling between inactivation and activation alters the ARF's ability to bind effectors which help propagate downstream signals. Interesting to note, and important for this dissertation, is that GAPs can also play dual roles as effectors to yield biological responses.*

ARF GTPases and their regulators drive diverse signaling pathways

Although first purified based on an activity that has proven uninformative for its roles in cellular biology, ARFs have been heavily studied because of their ability to regulate diverse cellular pathways. Some of the earliest roles found for ARFs in cells were for ARF1-6 in vesicular traffic, as they regulate the recruitment of coat proteins and complexes to nascent, budding vesicles that recruit vesicular cargoes at multiple intracellular compartments (*e.g.*, endosomes, Golgi, *trans*-Golgi network, and plasma membrane (Boman et al., 2000; D'Souza-Schorey and Chavrier, 2006; Kahn, 2009; Kahn et al., 2005; Volpicelli-Daley et al., 2005; Yu and Lee, 2017)). Further study revealed other functions for the ARFs as direct allosteric activators of lipid modifying enzymes (*e.g.*, phospholipase D or PI4P-5kinase; (Brown et al., 1993; Hernandez-Deviez et al., 2004)) and the remodeling of cortical actin to dictate cell motility, adhesion, and cell division (Caviston et al., 2014; Song et al., 1998). With the study of ARL GTPases, the number of known cellular functions and compartments to which these GTPases localize increased dramatically. While ARL1 shares the most in common with ARF1-6 via its functions in endosomal traffic, many of the other ARLs are quite disparate in cellular activities. ARL2 alone has been linked to mitochondrial fusion (Newman et al., 2017), tubulin folding (Francis et al., 2017a; Francis et al., 2017b), anchorage of microtubules at centrosomes (Cunningham and Kahn, 2008; Zhou et al., 2006), rods and rings (Schiavon et al., 2018), transport of isoprenylated cargoes (Ismail et al., 2011; Renault et al., 2001), and ciliary function in retinal cells (Davidson et al., 2013; Wright et al., 2018). ARL3 is ARL2's closest paralog, sharing 53% identity and strong structural conservation (Hanzal-Bayer et al., 2002; Hillig et al., 2000). Although they both localize to centrosomes and both function in the transport of prenylated cargoes, ARL2 and ARL3 are unique in cell activities. ARL3, rather than working in mitochondrial fusion and tubulin folding, has functions in cytokinesis (Zhou et al., 2006), transport of myristolated cargoes (Ismail et al., 2012), Golgi function (Zhou et al., 2006), and GEF activity for ARL13B in cilia (Gotthardt et al., 2015; Ivanova et al., 2017). This is just one example of the range of overlapping and distinct roles shared by ARF GTPases, drawing to mind fundamental questions. How can a single protein have so many diverse

functions? What would be the reason that a cell would have a single protein mediate multiple pathways, rather than have many proteins perform their own discrete functions? What are the sources and determinants of specificity within the ARF family? And technically, how best to deconvolute such extensive overlaps and interconnections?

To address these questions, I hypothesize that ARFs have maintained limited expansion in the genome with most active at multiple sites specifically to allow integration of those distinct signals at distinct sites. Thus, in addition to regulating specific pathways they also serve as mediators of "inter-pathway communication," or the ability of multiple different signaling pathways to integrate with one another to mediate life's processes. Though much of signaling research has focused on teasing apart linear pathways that drive specific, single cellular functions, cell biology is much more complicated than that. Rather, a single cellular function often requires multiple cellular compartments to coordinate with one another. Cell division alone requires DNA to replicate, centrosomes to amplify, microtubules and actin to organize correctly at the right time and place, mitochondria to fragment, cilia to resorb, and so many more cellular compartments to coordinate. How these divergent pathways all communicate with one another, though, remains a mystery. Our lab previously discussed the potential of ARFs as mediators of inter-pathway communication (or "higher order signaling") (Francis et al., 2016), suggesting that having a protein at the crossroads of multiple cellular pathways that can be selectively driven to promote one function versus another may be key to inter-pathway communication. The selective driving of ARFs to promote one pathway versus another would explain how signaling events can adapt to the changing needs of the cell, but the question remains: what mechanisms are employed to ensure that an ARF performs the right functions at the right place and time? To give just one example, recruitment of an ARF family GTPase to one site results in its deficiency at other sites, particularly if the protein is expressed to only low levels. I propose that the regulators of ARFs, GAPs and GEFs, modulate ARF functions in their respective pathways, as they also have been shown to localize to multiple different cellular compartments and to

function in multiple pathways. In the next section, I will turn my focus to ARF GAPs and how they, too, may facilitate inter-pathway communication.

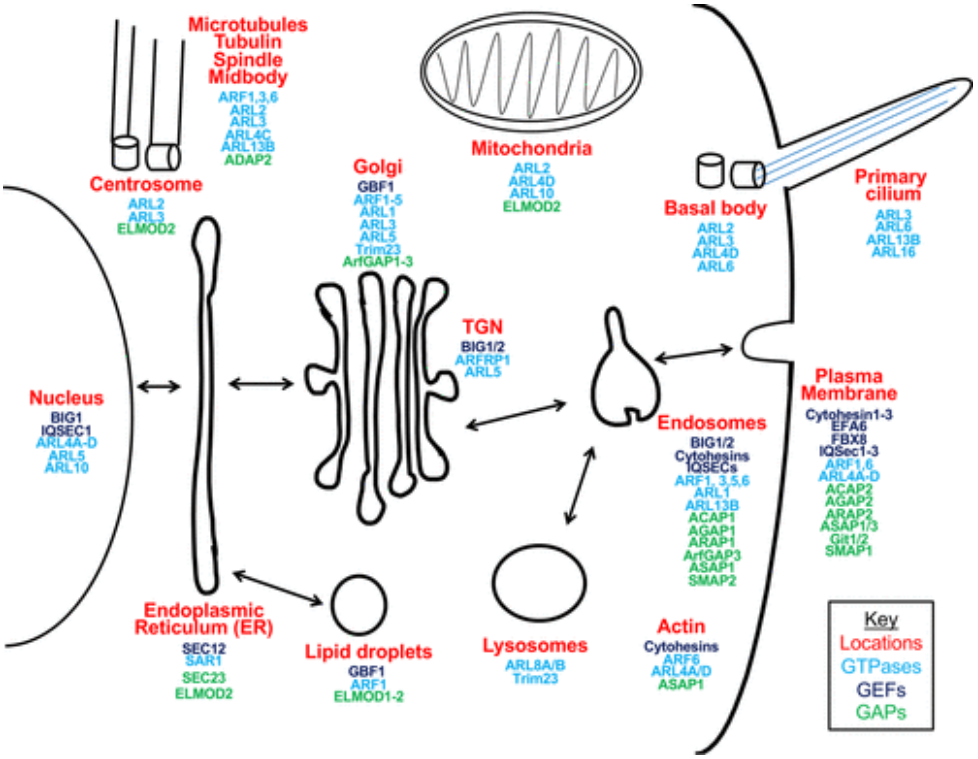

Figure 2: ARF GTPases and their regulators coordinate diverse cellular compartments. *This diagram highlights how ARFs and their regulators (GEFs and GAPs) can be found at virtually every cellular compartment mediating critical cellular functions. Cell compartments are labeled in red, ARFs in blue, GEFs in purple, and GAPs in green. How GTPases and their regulators are temporally and spatially regulated in their cellular functions and how this contributes to inter-pathway communication remains unclear. Figure obtained from (Sztul et al., 2019). Reprinted with permission.*

ARF GAPs

To date, a total of 28 ARF GAPs have been discovered in humans (Gillingham and Munro, 2007; Sztul et al., 2019). Though there are multiple subfamilies of ARF GAPs (typically consisting of 2-3 members each, except in the case of RP2), all share a common catalytic domain, the ARF GAP domain, that garners them GAP activity (Randazzo and Hirsch, 2004; Spang et al., 2010). Specifically, this domain contains an arginine residue within a highly conserved motif sequence ($CX_2CX_{16}CX_2CX_4R$) that the GAP can insert inside the nucleotide binding pocket of the ARF to help stabilize the transition state during GTP hydrolysis (Ahmadian et al., 1997; Kahn et al., 2008; Scheffzek et al., 1998a; Scheffzek et al., 1998b). The vast majority of ARF GAPs have only been tested for GAP activity towards a small subset of the ARF family, most often just ARF1 and ARF6. These ARF GAPs act in multiple different pathways, including in regulation of actin cytoskeleton (Randazzo et al., 2007), cell adhesion and motility (Casalou et al., 2016; Ha et al., 2008a; Ha et al., 2008b; Luo et al., 2019; Vitali et al., 2019), regulation of kinase activity in signaling cascades, and recruitment of coat proteins to membranes (Donaldson and Jackson, 2011; Gillingham and Munro, 2007; Randazzo and Hirsch, 2004; Spang et al., 2010).

Like the ARFs, ARF GAPs are also believed to be highly conserved in evolutionary history. At least 6 ARF GAPs and 2 ELMODs have been traced back to the Last Eukaryotic Common Ancestor (LECA) (East et al., 2012; Schlacht et al., 2013). However, most of the known specificities for 24 of the ARF GAPs are based on testing specificity of GAP activity against only a few ARFs and no ARLs. Therefore, much of what is known about ARF GAP functions is limited to actin remodeling, vesicular traffic, and focal adhesion pathways. Whether any of the 24 known ARF GAPs that share the ARF GAP domain mediate functions at cilia, microtubules, centrosomes, and mitochondria is largely unknown. Alternatively, whether there are additional GAPs yet to be discovered (and clearly if such additional GAPs exist, their specificities) is also unknown. Thus, the mechanisms by which ARFs and ARLs mediate functions at these sites, and the extent of any potential functional overlap, are incompletely understood. The only ARF GAP family members with proven in vitro GAP activity for ARFs, despite lacking an ARF GAP

domain, are the ELMODs (or Engulfment and Motility Domain proteins). Furthermore, the ELMODs are the only ARF GAPs with demonstrated in vitro activity against both ARFs and ARLs (Ivanova et al., 2014). It is this family of ARF GAPs, which I posit to be regulators of inter-pathway communication, that is the central focus of this dissertation research.

GAP	Which ARF?	Localization	Function
ACAP1/CentB1	ARF6	Rab11+ recycling endosomes	Integrin and TfnR recycling
ACAP2/CentB2	ARF6	plasma membrane, phagocytic cup, ARF6 endosomes	Neurite outgrowth, FcγR-mediated phagocytosis
ACAP3/CentB5	ARF6		Neurite outgrowth, neuronal migration
ADAP1/CentA1	ARF6	membrane ruffles, mitochondria, dendrites, synapses	Salmonella invasion, beta2-AR internalization, dendritic differentiation
ADAP2/CentA2	ARF6		
AGAP1		AP-3 endosomes	endosome-lysosome transport
AGAP2/PIKE		focal adhesions, Rab4/AP-1 endosomes	Cell migration, neurite outgrowth, invasion, TfnR recycling
AGAP3		endosomes	
AGFG1/HRB, RIP		Clathrin/AP-2/EPS15 vesicles	HIV-1 replication, TfnR endocytosis
AGFG2			
ARAP1		early endosomes, podosomes, circular dorsal ruffles	EGFR endocytosis, macropinocytosis, secretory lysosomes
ARAP2		focal adhesions, APPL early endosomes	focal adhesion turnover, stress fiber formation, integrin endocytosis
ARAP3		podosome-like adhesions	Cell migration, invasion, RhoGAP stimulation
ARFGAP1		Golgi	ER protein retrieval
ARFGAP2		Golgi	
ARFGAP3		trans-Golgi-network, early endosomes	early endosome - late endosome transport of M6PR and EGFR
ASAP1	ARF1	plasma membrane, focal adhesions, podosomes/invadopodia, circular dorsal ruffles	Cell migration, invasion, stress fiber formation, integrin and EGFR recycling
ASAP2	ARF1	cell periphery, phagocytic cup	Cell migration, FcγR-mediated phagocytosis
ASAP3	ARF1	plasma membrane, circular dorsal ruffles	cell migration, integrin recycling, invasion
ELMOD1	ARL2, ARL3, ARF1, ARF3, ARF6	Golgi, nuclear speckles, lipid droplets	
ELMOD2	ARL2, ARL3, ARF1, ARF3, ARF6	mitochondria, rods and rings, lipid droplets, endoplasmic reticulum	mitochondrial fusion, lipid metabolism?
ELMOD3	ARL2, ARL3, ARF1, ARF3, ARF6	plasma membrane, lagging edge, actin	
GIT1		focal adhesions, SNX27 endosomes, recycling endosomes, early endosomes	Cell migration, invasion, EGFR traffic/degradation
GIT2		plasma membrane, focal adhesions	Cell migration, invasion, beta2-Adrenergic R down-regulation
SMAP1		plasma membrane	TfnR endocytosis
SMAP2		early endosomes, trans Golgi network	early endosome - trans golgi network transport
RP2		plasma membrane, microtubules, nucleus	ciliary traffic

Figure 3: Summary of known ARF GAP specificities, localizations, and functions. *This table lists the known ARF GAPs and summarizes their previously described cellular locations, functions, and ARFs for which they are known to have in vitro GAP activity. As evidenced by the table, there are large holes in our knowledge of these ARF GAPS. In particular, little is known about their GAP activities. In fact, the majority of the GAPs, only a handle of ARFs were tested for GAP activity. Information from this table was obtained from (Sztul et. al, 2019).*

ELMOD Family of ARF GAPs

The ELMO-domain containing (ELMOD) family is in many ways distinct from the other families of ARF GAPs. First and foremost, they lack the conserved ARF GAP domain which all other known ARF GAPs share except for RP2. The other ARF GAPs typically contain multiple different domains, while the only domain that the 3 ELMODs (ELMOD1-3) share is a single ELMO (Engulfment and Cell Motility) domain (Figure 3). This domain is also found in ELMO proteins that lack ARF GAP activity in in vitro assays (East et al., 2012), suggesting that having an ELMO domain itself does not give the protein GAP function. Instead, the ELMO domain in ELMODs is distinct because, like the ARF GAPs, it contains a conserved motif within which lies the catalytic arginine residue that is essential for GAP activity (East et al., 2012). The three ELMODs share a consensus sequence flanking the critical arginine residue ($WX_3G(F/W)QX_3PXTD(F/L)RGXGX_3LX_2L$) that is not shared with other ARF GAPs (East et al., 2012).

The ELMOD family was discovered to have GAP activity when ELMOD2 was purified from bovine testes based on its GAP activity for ARL2 (Bowzard et al., 2007). At the time of this discovery, cellular functions for ELMOD2 were completely unknown. Later studies revealed that ELMOD1 and ELMOD3 also had GAP activities (Ivanova et al., 2014). Interestingly, though, the ELMODs showed in vitro GAP activity for both ARFs and ARLs. Thus, these are the first and only known ARF GAPs to have such broad specificity, but perhaps largely because virtually none of the ARF GAPs have ever been screened for activity against ARLs (Bowzard et al., 2007; Ivanova et al., 2014). The fact that the ELMOD family has uniquely promiscuous GAP activity for multiple different ARFs makes these proteins strong candidates as mediators of inter-pathway communication.

Despite in vitro data revealing that ELMODs have promiscuous GAP activity, relatively little was known concerning the cellular functions for the ELMODs at the onset of this project. The ELMODs have been implicated in multiple different diseases, including, in the case of ELMOD1 and ELMOD3, deafness in mice and humans (Jaworek et al., 2013; Johnson et al., 2012; Lahbib et al., 2019; Li et al., 2019; Li et al., 2018) and mental retardation in humans (Bacchelli et al., 2019; Loi et al., 2020; Miryounesi et al.,

2019; Pandey et al., 2014). On the other hand, ELMOD2 appears to have its own slate of associated pathologies, including idiopathic pulmonary fibrosis (Hodgson et al., 2006; Lawson et al., 2011), defective antiviral response (Pulkkinen et al., 2010), and pulmonary hypertension (Duga et al., 2014). Previous work from our lab identified functions for ELMOD1 at Golgi (East et al., 2012), and more recent studies implicate ELMOD1 in stabilization of apical actin in stereocilia along with ARF6 (Krey et al., 2018). ELMOD3's cellular functions remain uncharacterized. ELMOD2, which is the focus of this dissertation research and described further below, has reported cellular functions in mitochondria and lipid droplets. At the onset of this project, limited information was available concerning the functions of ELMOD1-3, much less whether these proteins were promiscuous GAPs (*i.e.*, working on multiple ARFs/ARLs) in a cellular context. The study of these proteins is further stymied because of the limited accessibility to reagents, such as specific antibodies that work for Western/immunofluorescence, inefficient knockdown via siRNA (and also a lack of good antibodies to detect the efficacy of said knockdown), and poor protein expression. Therefore, to gain a fundamental understanding of how these proteins function in cells as a family and independently, a better set of reagents and approaches was needed to tackle higher order questions.

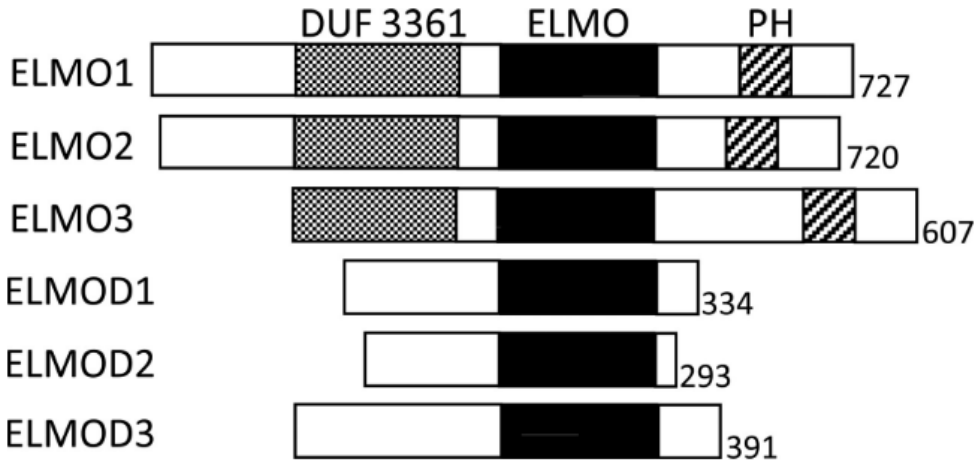

Figure 4: Summary of the mammalian ELMOD family of 6 ELMO-domain containing family members. *Figured borrowed with permission from East, et al (East et al., 2012). Even though all six proteins share a common ELMO domain (shown in black), there is not much homology shared between the ELMOs and ELMODs. The ELMOs have domain of unknown function 3361 (DUF 3361) (grey) and pleckstrin homology (PH) (striped) domains and show no evidence of in vitro GAP activity. ELMODs, on the other hand, only share a single domain and their ELMO domain includes the conserved GAP sequence motif and catalytic arginine..*

ELMOD2

Over the past few years, our lab has been exploring cellular functions of mammalian (human and mouse) ELMOD2. This 293 amino acid, ~35 kDa protein was previously reported to localize to the following cellular compartments: mitochondria (Newman et al., 2014), lipid droplets (Suzuki et al., 2015), rods and rings (Schiavon et al., 2018), and endoplasmic reticulum (ER) (Suzuki et al., 2015). A 2015 study suggested that ELMOD2 acts at lipid droplets to regulate cellular lipid metabolism through Arf1-COPI (Suzuki et al., 2015). Otherwise, not much else was known concerning ELMOD2 function.

In collaboration with senior lab members Laura Newman, PhD and Cara Schiavon, PhD, we began to tease apart the cellular functions for ELMOD2 in mitochondria. We built off the findings of Laura Newman and previous lab members and discovered that ELMOD2 works as an effector of ARL2 to mediate mitochondrial fusion (Schiavon et al., 2019). Specifically, we discovered that ELMOD2 and ARL2 are working through the mitofusins to facilitate fusion of the outer mitochondrial membrane (OMM), acting from the intramitochondrial space (Newman et al., 2017; Newman et al., 2014; Schiavon et al., 2019). ELMOD2 and ARL2 were shown to localize periodically along the length of mitochondria in concert with mitochondrial fusion and motility-associated proteins via g-STED microscopy (Schiavon et al., 2019). Together, these data led us to propose a model in which ELMOD2 and ARL2 are acting in a complex with components of mitochondrial motility and fusion (Schiavon et al., 2019). These data, combined with Cara Schiavon's discovery of ARL2 and ELMOD2 at rods and rings (Schiavon et al., 2018), began to open up the prospects that ELMOD2 may play additional, even multiple roles in cell biology.

My original goal was to contribute to the ELMOD2 at mitochondria model by generating ELMOD2 KO cells via CRISPR-Cas9. We chose to use immortalized mouse embryonic fibroblasts (MEFs) as the model system for a number of reasons: 1) the other knockout lines used to study the function of ELMOD2 in mitochondria (*e.g.* $OPA1^{-/-}$ and $MFN1/2^{-/-}$) were also MEFs and from the same background, allowing for ready comparison, 2) MEFs are excellent for imaging, which would prove useful for future phenotyping, and 3) MEFs have pretty uniform phenotypes (*e.g.* one nucleus, 1-2 centrosomes, relatively normal

mitochondria, only one primary cilium, etc.) allowing for ready identification of defects, and 4) MEFs are often available from Knock Out Mouse Project (KOMP) that contain deletions of a large number of genes that might also help us in our analyses. We sought to create a system in which we could cleanly tease apart the functions of ELMOD2 and the mechanisms by which they mediate these functions. I generated at least two different clonal populations of cells from at least two different CRISPR guides to ensure that any phenotypes discovered were not a product of off-target effects or clonal variation. I simultaneously generated ELMOD1-3 KO lines to assess the degree of functional redundancy among the family members. Together, these findings allow us to identify which pathways are altered or lost in response to deletion of any ELMOD, which pathways may be shared between more than one ELMOD, and also which of the phenotypes identified can be linked to distinct ARF family members.

Together, my early studies served as a powerful tool for defining the role of ELMOD2 in mitochondria. Upon closer investigation, though, I discovered a number of novel phenotypes in all three ELMOD knockout populations that pointed to previously unknown functions for ELMODs in cells. These studies revealed that ELMOD1 and ELMOD3 share similarities in function, as each show defects in traffic of ARL13B to primary cilia and in cell attachment. Current and future lab members will carry this story forward as it is currently incomplete. The focus of my dissertation work, though, was on ELMOD2. It revealed novel cellular functions for ELMOD2 in cell division (Chapter 2), microtubule anchoring (Chapter 2), and ciliogenesis (Chapter 3) that led to the production of two primary manuscripts. Together, the overall focus of this work was to shed light on the diversity of cellular functions that the ELMOD family mediates in cells, laying the groundwork for future study into how regulatory proteins like ELMODs may serve a pivotal role in driving inter-pathway communication. In chapter 4, I will discuss the impact of these findings and future directions for the field.

References

Ahmadian, M.R., P. Stege, K. Scheffzek, and A. Wittinghofer. 1997. Confirmation of the arginine-finger hypothesis for the GAP-stimulated GTP-hydrolysis reaction of Ras. *Nat Struct Biol*. 4:686-689.

Bacchelli, E., E. Loi, C. Cameli, L. Moi, A.F. Vega-Benedetti, S. Blois, A. Fadda, E. Bonora, S. Mattu, R. Fadda, R. Chessa, E. Maestrini, G. Doneddu, and P. Zavattari. 2019. Analysis of a Sardinian Multiplex Family with Autism Spectrum Disorder Points to Post-Synaptic Density Gene Variants and Identifies CAPG as a Functionally Relevant Candidate Gene. *J Clin Med*. 8.

Boman, A.L., C. Zhang, X. Zhu, and R.A. Kahn. 2000. A family of ADP-ribosylation factor effectors that can alter membrane transport through the trans-Golgi. *Mol Biol Cell*. 11:1241-1255.

Bowzard, J.B., D. Cheng, J. Peng, and R.A. Kahn. 2007. ELMOD2 is an Arl2 GTPase-activating protein that also acts on Arfs. *J Biol Chem*. 282:17568-17580.

Brown, H.A., S. Gutowski, C.R. Moomaw, C. Slaughter, and P.C. Sternweis. 1993. ADP-ribosylation factor, a small GTP-dependent regulatory protein, stimulates phospholipase D activity [see comments]. *Cell*. 75:1137-1144.

Casalou, C., A. Faustino, and D.C. Barral. 2016. Arf proteins in cancer cell migration. *Small GTPases*. 7:270-282.

Caviston, J.P., L.A. Cohen, and J.G. Donaldson. 2014. Arf1 and Arf6 promote ventral actin structures formed by acute activation of protein kinase C and Src. *Cytoskeleton (Hoboken)*. 71:380-394.

Cunningham, L.A., and R.A. Kahn. 2008. Cofactor D functions as a centrosomal protein and is required for the recruitment of the gamma-tubulin ring complex at centrosomes and organization of the mitotic spindle. *J Biol Chem*. 283:7155-7165.

D'Souza-Schorey, C., and P. Chavrier. 2006. ARF proteins: roles in membrane traffic and beyond. *Nat Rev Mol Cell Biol*. 7:347-358.

Davidson, A.E., N. Schwarz, L. Zelinger, G. Stern-Schneider, A. Shoemark, B. Spitzbarth, M. Gross, U. Laxer, J. Sosna, P.I. Sergouniotis, N.H. Waseem, R. Wilson, R.A. Kahn, V. Plagnol, U. Wolfrum, E. Banin, A.J. Hardcastle, M.E. Cheetham, D. Sharon, and A.R. Webster. 2013. Mutations in ARL2BP, encoding ADP-ribosylation-factor-like 2 binding protein, cause autosomal-recessive retinitis pigmentosa. *Am J Hum Genet*. 93:321-329.

Donaldson, J.G., and C.L. Jackson. 2011. ARF family G proteins and their regulators: roles in membrane transport, development and disease. *Nat Rev Mol Cell Biol*. 12:362-375.

Duga, B., M. Czako, K. Komlosi, K. Hadzsiev, K. Torok, K. Sumegi, P. Kisfali, G. Kosztolanyi, and B. Melegh. 2014. Deletion of 4q28.3-31.23 in the background of multiple malformations with pulmonary hypertension. *Mol Cytogenet*. 7:36.

East, M.P., J.B. Bowzard, J.B. Dacks, and R.A. Kahn. 2012. ELMO domains, evolutionary and functional characterization of a novel GTPase-activating protein (GAP) domain for Arf protein family GTPases. *J Biol Chem*. 287:39538-39553.

East, M.P., and R.A. Kahn. 2011. Models for the functions of Arf GAPs. *Semin Cell Dev Biol*. 22:3-9.

Francis, J.W., D. Goswami, S.J. Novick, B.D. Pascal, E.R. Weikum, E.A. Ortlund, P.R. Griffin, and R.A. Kahn. 2017a. Nucleotide Binding to ARL2 in the TBCDARL2beta-Tubulin Complex Drives Conformational Changes in beta-Tubulin. *J Mol Biol*. 429:3696-3716.

Francis, J.W., L.E. Newman, L.A. Cunningham, and R.A. Kahn. 2017b. A Trimer Consisting of the Tubulin-specific Chaperone D (TBCD), Regulatory GTPase ARL2, and beta-Tubulin Is Required for Maintaining the Microtubule Network. *J Biol Chem*. 292:4336-4349.

Francis, J.W., R.E. Turn, L.E. Newman, C. Schiavon, and R.A. Kahn. 2016. Higher order signaling: ARL2 as regulator of both mitochondrial fusion and microtubule dynamics allows integration of 2 essential cell functions. *Small GTPases*. 7:188-196.

Gillingham, A.K., and S. Munro. 2007. The small G proteins of the Arf family and their regulators. *Annu Rev Cell Dev Biol*. 23:579-611.

Gotthardt, K., M. Lokaj, C. Koerner, N. Falk, A. Giessl, and A. Wittinghofer. 2015. A G-protein activation cascade from Arl13B to Arl3 and implications for ciliary targeting of lipidated proteins. *Elife*. 4.

Ha, V.L., S. Bharti, H. Inoue, W.C. Vass, F. Campa, Z. Nie, A. de Gramont, Y. Ward, and P.A. Randazzo. 2008a. ASAP3 is a focal adhesion-associated Arf GAP that functions in cell migration and invasion. *J Biol Chem*. 283:14915-14926.

Ha, V.L., R. Luo, Z. Nie, and P.A. Randazzo. 2008b. Contribution of AZAP-Type Arf GAPs to cancer cell migration and invasion. *Adv Cancer Res*. 101:1-28.

Hanzal-Bayer, M., L. Renault, P. Roversi, A. Wittinghofer, and R.C. Hillig. 2002. The complex of Arl2-GTP and PDE delta: from structure to function. *EMBO J*. 21:2095-2106.

Hernandez-Deviez, D.J., M.G. Roth, J.E. Casanova, and J.M. Wilson. 2004. ARNO and ARF6 regulate axonal elongation and branching through downstream activation of phosphatidylinositol 4-phosphate 5-kinase alpha. *Mol Biol Cell*. 15:111-120.

Hillig, R.C., M. Hanzal-Bayer, M. Linari, J. Becker, A. Wittinghofer, and L. Renault. 2000. Structural and biochemical properties show ARL3-GDP as a distinct GTP binding protein. *Structure*. 8:1239-1245.

Hodgson, U., V. Pulkkinen, M. Dixon, M. Peyrard-Janvid, M. Rehn, P. Lahermo, V. Ollikainen, K. Salmenkivi, V. Kinnula, J. Kere, P. Tukiainen, and T. Laitinen. 2006. ELMOD2 is a candidate gene for familial idiopathic pulmonary fibrosis. *Am J Hum Genet*. 79:149-154.

Ismail, S.A., Y.X. Chen, M. Miertzschke, I.R. Vetter, C. Koerner, and A. Wittinghofer. 2012. Structural basis for Arl3-specific release of myristoylated ciliary cargo from UNC119. *EMBO J*. 31:4085-4094.

Ismail, S.A., Y.X. Chen, A. Rusinova, A. Chandra, M. Bierbaum, L. Gremer, G. Triola, H. Waldmann, P.I. Bastiaens, and A. Wittinghofer. 2011. Arl2-GTP and Arl3-GTP regulate a GDI-like transport system for farnesylated cargo. *Nat Chem Biol*. 7:942-949.

Ivanova, A.A., T. Caspary, N.T. Seyfried, D.M. Duong, A.B. West, Z. Liu, and R.A. Kahn. 2017. Biochemical characterization of purified mammalian ARL13B protein indicates that it is an atypical GTPase and ARL3 guanine nucleotide exchange factor (GEF). *J Biol Chem*. 292:11091-11108.

Ivanova, A.A., M.P. East, S.L. Yi, and R.A. Kahn. 2014. Characterization of recombinant ELMOD (cell engulfment and motility domain) proteins as GTPase-activating proteins (GAPs) for ARF family GTPases. *J Biol Chem*. 289:11111-11121.

Jaworek, T.J., E.M. Richard, A.A. Ivanova, A.P. Giese, D.I. Choo, S.N. Khan, S. Riazuddin, R.A. Kahn, and S. Riazuddin. 2013. An alteration in ELMOD3, an Arl2 GTPase-activating protein, is associated with hearing impairment in humans. *PLoS Genet*. 9:e1003774.

Johnson, K.R., C.M. Longo-Guess, and L.H. Gagnon. 2012. Mutations of the mouse ELMO domain containing 1 gene (Elmod1) link small GTPase signaling to actin cytoskeleton dynamics in hair cell stereocilia. *PLoS One*. 7:e36074.

Kahn, R.A. 2009. Toward a model for Arf GTPases as regulators of traffic at the Golgi. *FEBS Lett*. 583:3872-3879.

Kahn, R.A., E. Bruford, H. Inoue, J.M. Logsdon, Jr., Z. Nie, R.T. Premont, P.A. Randazzo, M. Satake, A.B. Theibert, M.L. Zapp, and D. Cassel. 2008. Consensus nomenclature for the human ArfGAP domain-containing proteins. *J Cell Biol*. 182:1039-1044.

Kahn, R.A., and A.G. Gilman. 1984. Purification of a protein cofactor required for ADP-ribosylation of the stimulatory regulatory component of adenylate cyclase by cholera toxin. *J Biol Chem*. 259:6228-6234.

Kahn, R.A., L. Volpicelli-Daley, B. Bowzard, P. Shrivastava-Ranjan, Y. Li, C. Zhou, and L. Cunningham. 2005. Arf family GTPases: roles in membrane traffic and microtubule dynamics. *Biochem Soc Trans*. 33:1269-1272.

Krey, J.F., R.A. Dumont, P.A. Wilmarth, L.L. David, K.R. Johnson, and P.G. Barr-Gillespie. 2018. ELMOD1 Stimulates ARF6-GTP Hydrolysis to Stabilize Apical Structures in Developing Vestibular Hair Cells. *J Neurosci*. 38:843-857.

Lahbib, S., C.S. Leblond, M. Hamza, B. Regnault, L. Lemee, A. Mathieu, H. Jaouadi, R. Mkaouar, I.B. Youssef-Turki, A. Belhadj, I. Kraoua, T. Bourgeron, and S. Abdelhak. 2019. Homozygous 2p11.2 deletion supports the implication of ELMOD3 in hearing loss and reveals the potential association of CAPG with ASD/ID etiology. *J Appl Genet*. 60:49-56.

Lawson, W.E., J.E. Loyd, and A.L. Degryse. 2011. Genetics in pulmonary fibrosis--familial cases provide clues to the pathogenesis of idiopathic pulmonary fibrosis. *Am J Med Sci*. 341:439-443.

Li, W., Y. Feng, A. Chen, T. Li, S. Huang, J. Liu, X. Liu, Y. Liu, J. Gao, D. Yan, J. Sun, L. Mei, X. Liu, and J. Ling. 2019. Elmod3 knockout leads to progressive hearing loss and abnormalities in cochlear hair cell stereocilia. *Hum Mol Genet*. 28:4103-4112.

Li, W., J. Sun, J. Ling, J. Li, C. He, Y. Liu, H. Chen, M. Men, Z. Niu, Y. Deng, M. Li, T. Li, J. Wen, S. Sang, H. Li, Z. Wan, E.M. Richard, P. Chapagain, D. Yan, X.Z. Liu, L. Mei, and Y. Feng. 2018. ELMOD3, a novel causative gene, associated with human autosomal dominant nonsyndromic and progressive hearing loss. *Hum Genet*. 137:329-342.

Loi, E., L. Moi, S. Blois, E. Bacchelli, A.F. Vega Benedetti, C. Cameli, R. Fadda, E. Maestrini, M. Carta, G. Doneddu, and P. Zavattari. 2020. ELMOD3-SH2D6 gene fusion as a possible co-star actor in autism spectrum disorder scenario. *J Cell Mol Med*. 24:2064-2069.

Luo, R., C.E. Reed, J.A. Sload, L. Wordeman, P.A. Randazzo, and P.W. Chen. 2019. Arf GAPs and molecular motors. *Small GTPases*. 10:196-209.

Miryounesi, M., S. Bahari, S. Salehpour, N. Alipour, and S. Ghafouri-Fard. 2019. ELMO Domain Containing 1 (ELMOD1) Gene Mutation Is Associated with Mental Retardation and Autism Spectrum Disorder. *J Mol Neurosci*. 69:312-315.

Newman, L.E., C.R. Schiavon, R.E. Turn, and R.A. Kahn. 2017. The ARL2 GTPase regulates mitochondrial fusion from the intermembrane space. *Cell Logist*. 7:e1340104.

Newman, L.E., C.J. Zhou, S. Mudigonda, A.L. Mattheyses, E. Paradies, C.M. Marobbio, and R.A. Kahn. 2014. The ARL2 GTPase is required for mitochondrial morphology, motility, and maintenance of ATP levels. *PLoS One*. 9:e99270.

Pandey, A.K., L. Lu, X. Wang, R. Homayouni, and R.W. Williams. 2014. Functionally enigmatic genes: a case study of the brain ignorome. *PLoS One*. 9:e88889.

Pulkkinen, V., S. Bruce, J. Rintahaka, U. Hodgson, T. Laitinen, H. Alenius, V.L. Kinnula, M. Myllarniemi, S. Matikainen, and J. Kere. 2010. ELMOD2, a candidate gene for idiopathic pulmonary fibrosis, regulates antiviral responses. *Faseb J*. 24:1167-1177.

Randazzo, P.A., and D.S. Hirsch. 2004. Arf GAPs: multifunctional proteins that regulate membrane traffic and actin remodelling. *Cell Signal*. 16:401-413.

Randazzo, P.A., H. Inoue, and S. Bharti. 2007. Arf GAPs as regulators of the actin cytoskeleton. *Biol Cell*. 99:583-600.

Renault, L., M. Hanzal-Bayer, and R.C. Hillig. 2001. Coexpression, copurification, crystallization and preliminary X-ray analysis of a complex of ARL2-GTP and PDE delta. *Acta Crystallogr D Biol Crystallogr*. 57:1167-1170.

Scheffzek, K., M.R. Ahmadian, L. Wiesmuller, W. Kabsch, P. Stege, F. Schmitz, and A. Wittinghofer. 1998a. Structural analysis of the GAP-related domain from neurofibromin and its implications. *EMBO J*. 17:4313-4327.

Scheffzek, K., M.R. Ahmadian, and A. Wittinghofer. 1998b. GTPase-activating proteins: helping hands to complement an active site. *Trends Biochem Sci*. 23:257-262.

Schiavon, C.R., M.E. Griffin, M. Pirozzi, R. Parashuraman, W. Zhou, H.A. Jinnah, D. Reines, and R.A. Kahn. 2018. Compositional complexity of rods and rings. *Mol Biol Cell*. 29:2303-2316.

Schiavon, C.R., R.E. Turn, L.E. Newman, and R.A. Kahn. 2019. ELMOD2 regulates mitochondrial fusion in a mitofusin-dependent manner, downstream of ARL2. *Mol Biol Cell*. 30:1198-1213.

Schlacht, A., K. Mowbrey, M. Elias, R.A. Kahn, and J.B. Dacks. 2013. Ancient complexity, opisthokont plasticity, and discovery of the 11th subfamily of Arf GAP proteins. *Traffic*. 14:636-649.

Song, J., Z. Khachikian, H. Radhakrishna, and J.G. Donaldson. 1998. Localization of endogenous ARF6 to sites of cortical actin rearrangement and involvement of ARF6 in cell spreading. *J Cell Sci*. 111 (Pt 15):2257-2267.

Spang, A., J.H. Saw, S.L. Jorgensen, K. Zaremba-Niedzwiedzka, J. Martijn, A.E. Lind, R. van Eijk, C. Schleper, L. Guy, and T.J.G. Ettema. 2015. Complex archaea that bridge the gap between prokaryotes and eukaryotes. *Nature*. 521:173-179.

Spang, A., Y. Shiba, and P.A. Randazzo. 2010. Arf GAPs: gatekeepers of vesicle generation. *FEBS Lett*. 584:2646-2651.

Suzuki, M., T. Murakami, J. Cheng, H. Kano, M. Fukata, and T. Fujimoto. 2015. ELMOD2 is anchored to lipid droplets by palmitoylation and regulates adipocyte triglyceride lipase recruitment. *Mol Biol Cell*. 26:2333-2342.

Sztul, E., P.W. Chen, J.E. Casanova, J. Cherfils, J.B. Dacks, D.G. Lambright, F.S. Lee, P.A. Randazzo, L.C. Santy, A. Schurmann, I. Wilhelmi, M.E. Yohe, and R.A. Kahn. 2019. ARF GTPases and their GEFs and GAPs: concepts and challenges. *Mol Biol Cell*. 30:1249-1271.

Vitali, T., S. Girald-Berlingeri, P.A. Randazzo, and P.W. Chen. 2019. Arf GAPs: A family of proteins with disparate functions that converge on a common structure, the integrin adhesion complex. *Small GTPases*. 10:280-288.

Volpicelli-Daley, L.A., Y. Li, C.J. Zhang, and R.A. Kahn. 2005. Isoform-selective effects of the depletion of ADP-ribosylation factors 1-5 on membrane traffic. *Mol Biol Cell*. 16:4495-4508.

Wright, Z.C., Y. Loskutov, D. Murphy, P. Stoilov, E. Pugacheva, A.F.X. Goldberg, and V. Ramamurthy. 2018. ADP-Ribosylation Factor-Like 2 (ARL2) regulates cilia stability and development of outer segments in rod photoreceptor neurons. *Sci Rep*. 8:16967.

Yu, C.J., and F.J. Lee. 2017. Multiple activities of Arl1 GTPase in the trans-Golgi network. *J Cell Sci*. 130:1691-1699.

Zaremba-Niedzwiedzka, K., E.F. Caceres, J.H. Saw, D. Backstrom, L. Juzokaite, E. Vancaester, K.W. Seitz, K. Anantharaman, P. Starnawski, K.U. Kjeldsen, M.B. Stott, T. Nunoura, J.F. Banfield, A. Schramm, B.J. Baker, A. Spang, and T.J. Ettema. 2017. Asgard archaea illuminate the origin of eukaryotic cellular complexity. *Nature*. 541:353-358.

Zhang, C.J., M.M. Cavenagh, and R.A. Kahn. 1998. A family of Arf effectors defined as suppressors of the loss of Arf function in the yeast Saccharomyces cerevisiae. *J Biol Chem*. 273:19792-19796.

Zhou, C., L. Cunningham, A.I. Marcus, Y. Li, and R.A. Kahn. 2006. Arl2 and Arl3 regulate different microtubule-dependent processes. *Mol Biol Cell*. 17:2476-2487.

Chapter 2: The ARF GAP ELMOD2 acts with different GTPases to regulate centrosomal microtubule nucleation and cytokinesis

This chapter was published as:

Turn, R.E., East M.P., Prekeris R., and Kahn R.A. 2020. The ARF GAP ELMOD2 acts with different GTPases to regulate centrosomal microtubule nucleation and cytokinesis. MBoC. 31:2070-2091.

Abstract

ELMOD2 is a ~32 kDa protein first purified by its GAP activity towards ARL2 and later shown to have uniquely broad specificity toward ARF family GTPases in *in vitro* assays. To begin the task of defining its functions in cells, we deleted ELMOD2 in immortalized mouse embryonic fibroblasts (MEFs) and discovered a number of cellular defects, which are reversed upon expression of ELMOD2-myc. We show that these defects, resulting from the loss of ELMOD2, are linked to two different pathways and two different GTPases: with ARL2 and TBCD to support microtubule nucleation from centrosomes and with ARF6 in cytokinesis. These data highlight key aspects of signaling by ARF family GAPs which contribute to previously under-appreciated sources of complexity, including GAPs acting from multiple sites in cells, working with multiple GTPases, and contributing to the spatial and temporal control of regulatory GTPases by serving as both GAPs and effectors.

Introduction

To carry out essential cellular processes, a cell requires diverse cellular compartments to communicate and synchronize with one another. Cell division alone requires DNA replication and condensation, nuclear envelope breakdown, mitochondrial fragmentation, actin and microtubule cytoskeletal rearrangement, centrosome duplication and migration, ciliary resorption, and many other events performed and timed correctly to facilitate the generation of two new cells. It stands to reason that there must be signaling network(s) to allow for these discrete processes to communicate. Regulatory GTPases are strong candidates as keys to such communication and integration of cellular processes because of their ability to act from multiple locations and with different partners and regulators in the same cells. The ARF superfamily of regulatory GTPases

(in mammals represented by 6 ARFs, 22 ARLs (ARF-like proteins), and 2 SARs (Sztul et al., 2019) is one such example not only because many of the members localize to diverse cellular compartments and work with multiple different effectors, but also because they are ancient (most members found in eukaryotes were predicted to have been present in the last eukaryotic common ancestor), very highly conserved, and ubiquitous in eukaryotes (Klinger et al., 2016; Li et al., 2004; Sztul et al., 2019).

While the ARFs are best known for their roles in the regulation of membrane traffic (D'Souza-Schorey and Chavrier, 2006; Jackson and Bouvet, 2014; Kahn et al., 2005), ARF family GTPases are also critical regulators of a diverse array of essential cellular functions (Burd et al., 2004; D'Souza-Schorey and Chavrier, 2006; Donaldson and Jackson, 2011; Gillingham and Munro, 2007; Nie et al., 2003; Seixas et al., 2013). In several instances, single members of this family regulate multiple processes at distinct sites, making dissection and elucidation of each molecular pathway challenging (Francis et al., 2016; Sztul et al., 2019). In other cases, multiple family members share overlapping or redundant functionalities, making clear demonstrations of the role(s) of any one a challenge (*e.g.*, ARF1-3 all share >96% identity, overlapping localization and common binding partners). A further complication to clear understanding of any one signaling pathway is that the proteins tasked with turning off these GTPases, the ARF GTPase activating proteins or ARF GAPs, are also almost always effectors contributing to the propagation of the signal from the GTPase to a biological response (East and Kahn, 2011; Inoue and Randazzo, 2007; Vitali et al., 2017; Zhang et al., 2003; Zhang et al., 1998). While a challenge to researchers, the ability of one cell regulator to act on multiple essential cellular processes and at distinct sites has also been posited to provide an important means of communication between those functions and

between the distinct cellular locations from which they act (East and Kahn, 2011; Sztul et al., 2019).

Multiplicity of functions at distinct locations is perhaps most clearly demonstrated for ARL2. It is found predominantly in a cytosolic, heterotrimeric complex with TBCD and β-tubulin (Bhamidipati et al., 2000; Francis et al., 2017a; Shultz et al., 2008) but also localizes to centrosomes (Zhou et al., 2006), mitochondria (Newman et al., 2017a; Newman et al., 2014), and rods and rings (Schiavon et al., 2018). Genetic screens in multiple model organisms identified ARL2 and TBCD orthologs as key players affecting microtubules and cell division (Antoshechkin and Han, 2002; McElver et al., 2000; Price et al., 2010; Radcliffe et al., 2000). Stearns, *et al* (Stearns et al., 1990) identified mutants in *S. cerevisiae* of ARL2 (*CIN4*) and TBCD (*CIN1*) based on super-sensitivity to benomyl, while a related screen linked mutations in these same genes to increased chromosome loss and defects in nuclear migration and nuclear fusion (Hoyt et al., 1990). Nick Cowan's group discovered five cofactors required for tubulin heterodimer formation (termed tubulin-specific chaperones A-E; TBCA-E (Tian et al., 1996)) and first posited a specific role for ARL2 working with TBCD in a tubulin folding pathway (Tian et al., 2010). An obligate role for ARL2 in the folding of the αβ-tubulin heterodimer was later expanded upon with structural studies (Francis et al., 2017a; Francis et al., 2017b). Other studies suggest a role for ARL2 and TBCD in microtubule polymerization, acting from centrosomes (Cunningham and Kahn, 2008; Zhou et al., 2006). ARL2 was later shown to mediate mitochondrial fusion from the inner membrane space (Newman et al., 2017a; Newman et al., 2014; Schiavon et al., 2019; Sharer et al., 2002). Still other studies have revealed roles for ARL2 in transport of farnesylated cargoes to the transition zone of primary cilia (Ismail et al., 2011; Watzlich et al., 2013), in STAT3 signaling in the nucleus (Muromoto et al., 2008), and as a component of rods and rings (Schiavon et al., 2018). That one

protein regulates so many pathways and from so many different locations highlights the complexity involved in generating models of its actions at any one site. Yet, it offers the promise of important insights into cell regulation with better models of the mechanisms that drive inter-pathway communication.

Another example of diversity in function by one ARF family member is ARF6. This GTPase is found at the plasma membrane, cytoplasm, cleavage furrows, and Flemming bodies (Cavenagh et al., 1996; D'Souza-Schorey et al., 1995; Hosaka et al., 1996). ARF6 facilitates membrane and actin remodeling, and activated ARF6 is recruited to the cleavage furrow where it supports ingression in early cytokinesis (D'Souza-Schorey et al., 1998; Frank et al., 1998; Radhakrishna and Donaldson, 1997; Song et al., 1998). Depletion of ARF6 leads to failures in cytokinesis (Makyio et al., 2012; Schweitzer and D'Souza-Schorey, 2002; Schweitzer and D'Souza-Schorey, 2005; Ueda et al., 2013). Other studies have revealed the importance of its binding to MKLP1 at the Flemming body in the completion of cytokinesis (Hanai et al., 2016; Makyio et al., 2012; Takahashi et al., 2011; Ueda et al., 2013), where it is predicted to either mediate the traffic of key factors to and from the midbody to facilitate the proper docking of endosomes or to promote the recruitment of FIP3 (Takahashi et al., 2011).

Like the ARF superfamily, the family of ARF GAPs are also highly conserved and ancient (Schlacht et al., 2013), with 24 genes/proteins in mammals that all share the ARF GAP domain (Donaldson and Jackson, 2011; East and Kahn, 2011; Randazzo et al., 2007; Spang et al., 2010; Sztul et al., 2019; Vitali et al., 2017). However, these ARF GAPs have consistently been shown to act only on the six ARFs and not on the ARLs. In contrast, ELMOD2 was purified based on its GAP activity toward ARL2 and later was shown to act *in vitro* on both a number of ARLs and ARFs (Bowzard et al., 2007; Ivanova et al., 2014). There are three ELMOD family members

(ELMOD1-3) in mammals which share a common ELMO domain with the three ELMO proteins (ELMO1-3), though only the ELMODs have GAP activities for ARFs and ARLs (Bowzard et al., 2007; East et al., 2012). Thus, ELMODs have uniquely broad substrate specificity that includes several GTPases tested in the ARF family; these include ARL1, ARL2, ARL3, ARF1, and ARF6 but not ARL13B (Bowzard et al., 2007; Ivanova et al., 2014). The ELMOD family is also ancient, predicted to have been present in the last eukaryotic common ancestor (East et al., 2012), and linked to various pathologies; these include idiopathic pulmonary fibrosis (ELMOD2 (Hodgson et al., 2006)), deafness (ELMOD1 and ELMOD3 (Johnson et al., 2012; Li et al., 2019; Li et al., 2018)), intellectual disability (ELMOD1 and ELMOD3 (Loi et al., 2019; Miryounesi et al., 2019)), and antiviral response (ELMOD2 (Pulkkinen et al., 2010)). The broad specificity of ELMODs for GTPases in the ARF family in *in vitro* GAP assays increases the likelihood that it works with multiple (currently unknown) GTPases in cells. This promiscuity makes teasing apart the biological functions of ELMODs more complicated to dissect, but also makes ELMODs more likely to serve key roles in multiple pathways.

The cellular functions and specificity of ELMODs as GAPs in cells have not yet been characterized. These proteins are only expressed to low levels, making their detection and quantification challenging. Of the three, ELMOD2 displayed the highest *in vitro* GAP activities (Ivanova et al., 2014) and has been localized to mitochondria, ER, and lipid droplets. Yet, functions at these locations have only been shown for ELMOD2 and ARL2 acting from the intermembrane space to regulate mitochondrial fusion (Schiavon et al., 2019). Here, we used CRISPR/Cas9 to generate frameshifting/null mutations of ELMOD2 in immortalized mouse embryo fibroblasts (MEFs). These lines not only proved useful earlier for gaining mechanistic insight into ELMOD2's role(s) in mitochondrial fusion (Schiavon et al., 2019), but they also revealed a host of unexpected

phenotypes that were not apparent from previous knockdown or overexpression studies. Our data highlight both the importance of this protein to two essential cellular processes and the complexities involved in dissecting signaling by ARF GTPases and their interactors.

Materials and Methods

Reagents, antibodies, plasmids: The antibodies raised against the following proteins were purchased: α-tubulin (Sigma; T9026), β-tubulin (Sigma; T4026), α-tubulin (Millipore-Sigma; rat monoclonal; MAB1864), γ-tubulin (Sigma; T6557), γ-tubulin (Abcam; ab11317), centrin (Sigma; 04-1624), RAB11 (Transduction Laboratories; R56320), myc (Invitrogen; R950-25), HA (Covance; MMS-101P), acetylated tubulin (Sigma; T6793-2ML). The following rabbit polyclonal antibodies were generated against their respective human proteins and have been described previously: ARL1 (Van Valkenburgh et al., 2001), ARL2 (Sharer and Kahn, 1999; Sharer et al., 2002), ARL3 (Cavenagh et al., 1994), BART (Sharer et al., 2002), TBCD (Francis et al., 2017b), and ELMOD2 (Newman et al., 2014). RHOA (Abcam; ab54835) and ARF 1D9 monoclonal (Affinity Bioreagents; MA3-060; (Cavenagh et al., 1996)) antibodies were obtained commercially. We are grateful for the generous gifts of other antibodies: ARF6 polyclonal antibody from Jim Casanova (Univ. of Virginia), rabbit polyclonal antibodies directed against FIP1 and FIP5 from Rytis Prekeris (Univ. of Colorado), polyclonal sheep-anti-FIP3 from Jim Goldenring (Vanderbilt Univ), and mouse monoclonal antibodies against MKLP1 from Ryoko Kuriyama (Univ of Minnesota) (Kuriyama et al., 1994).

The CRISPR-Cas9 system used for transfection into MEFs was obtained commercially from Addgene (pSpCas9(BB)-2A-Puro (PX459) V2.0 (#62988)). Plasmids directing expression of human ARL2, ARL2[Q70L], ELMOD2-myc, ELMOD2-HA, or ELMOD2[R167K]-myc/his in

pcDNA3.1 were described previously (Bowzard et al., 2007; East et al., 2012; Zhou et al., 2006). The following plasmids were gifted to us by Rytis Prekeris: FIP1-GFP and FIP5-GFP. Jim Goldenring gifted us with FIP3-GFP (Hickson et al., 2003). Jim Casanova provided us with plasmids used for transient expression of ARF6-HA, ARF6[Q71L]-HA, or ARF6[T157A]-HA. All fast cycling point mutants were generated in pcDNA3.1 vectors using site-directed mutagenesis. The following reagents were purchased: nocodazole (VWR; 102515-934), thymidine (Sigma; T1895-10G), RO-3306 CDK1 inhibitor (Sigma; SML0569-25MG), oleic acid (Sigma; O1383-5G).

Cell Culture: Cells used in this study were grown in DMEM supplemented with 10% FBS (Atlanta Biologicals; S11150) and 2mM glutamine at 37°C, 5% CO_2. WT MEFs were obtained from ATCC (CRL-2991). Antibiotics are not used in routine cell culture, and cells are regularly checked for mycoplasma contamination. All phenotypes described were monitored in MEF lines maintained below passage 10, to avoid the potential selection against cell cycle defects observed in ELMOD2 nulls. Cells with different genotypes were all maintained with careful attention to ensure the same feeding, passaging, and plating density, though densities at plating may differ between assays. For all experiments described below, we consider replicates of individual lines repeated on different days as technical replicates, and the averages of technical replicates performed for each line are considered biological replicates.

Generation of CRISPR null lines: WT (parental; ATCC CRL-2991) immortalized MEFs served as the parental population for the ELMOD2 KO lines generated via CRISPR-Cas9. Benchling software (https://www.benchling.com/academic/) was used to design four 20 nt guides.

To facilitate expression from the U6 promoter, a "G" was substituted for the first nucleotide for each guide RNA. Overlapping primers with BbsI overhangs at the 5'-end were purchased from IDT based on the following templates: 5'-CACC$(N)_{20}$-3' and 5'-AAAC$(NR)_{20}$-3' where $(N)_{20}$ and $(NR)_{20}$ refer to the 20 nt protospacer sequence and its reverse complement, respectively. The two complimentary oligos were annealed and cloned into pSpCas9(BB)-2A-Puro (PX459) V2.0 vector (Addgene) at the BbsI sites. These guides were targeted close to the N-terminus of the protein to optimize the likelihood of null alleles that yield little of the ELMOD2 protein. Our goal was to generate at least two different clones from at least two different guides, each with frameshifting mutations on both alleles.

Low passage MEFs were grown to 90% confluence in 6-well dishes, transfected with a 1:3 ratio of DNA (guide RNA plasmids) to Lipofectamine 2000 for 4 hr in OptiMEM medium, and then re-plated onto 10 cm plates for growth overnight. Puromycin (3 µg/ml, Sigma #P8833) was added the next day and maintained for four days to enrich for transfected cells. Individual clones were isolated via limited dilution in 96 well plates, followed by expansion, cryopreservation, and sequencing of genomic DNA around the target site.

To ensure that any phenotypes we identified were solely the consequence of a loss of ELMOD2, we used the following controls: 1) generated at least two different clones from at least two different guides, and 2) performed rescue experiments by expressing ELMOD2-myc using lentivirus transduction into null cells, as well as WT cells which served as further controls. All phenotypes described here were present in all 10 null lines, though varied in magnitude when scored. Four of the 10 null lines were chosen at random for more detailed studies and quantification.

Transfection of MEFs: For all other transfections of WT or ELMOD2 null MEFs, PEI transfection was used instead of Lipofectamine as it proved to be less toxic and yielded higher transfection efficiencies. Cells were transfected with a 1:3 ratio of DNA to PEI for 24 hr in medium containing 2% serum before being re-plated onto coverslips. In most cases, 4 µg of DNA, 12 µg PEI, and 100 µL of serum-free medium per reaction were combined in an Eppendorf tube, vortexed, and allowed to incubate for 20 min. The DNA/PEI mixture was added dropwise to each respective well, and samples were returned to 37°C to incubate overnight. The next day, cells were re-plated as needed for different experiments.

Lentiviral Transduction: A lentivirus directing expression of mouse ELMOD2-myc was generated by Emory's Viral Vector Core, using the pFUGW vector into which the mouse ELMOD2-myc open reading frame was engineered at EcoRI and BamHI sites. About 10,000 cells were plated into wells of a 24-well plate and were treated with lentivirus 2 hr later. Medium was replaced after 48 hrs. Efficacy of lentiviral transduction was checked using immunocytochemistry, staining for myc expression. Transduction efficiency was estimated between 70-90% depending on the line. For all following rescue experiments, all cells were counted under the assumption that the majority of the cells scored express ELMOD2-myc. This may account for the heterogeneity in phenotypic rescue and may also result in underestimates of the magnitude of the rescue achieved.

Lipid droplet staining: Cells were plated onto Matrigel coated coverslips and the next day were treated with or without oleic acid (30µM at 37˚C for 24 hr; vortexed in solution with DMEM +10% FBS + 1%BSA prior to addition to cells) to increase lipid droplet accumulation. Cells were fixed with 4% PFA for 15 min at 37˚C and permeabilized with 0.1% Triton X-100 for 15 min. To

visualize lipid droplets, cells were stained for 30 min with a 1:100 dilution of BODIPY 493/502 (Invitrogen, D3922) (0.5mg/mL stock) in PBS. Brightfield (20x magnification) and widefield fluorescence microscopy (100x magnification) were used to assess lipid droplet numbers and sizes by visual inspection.

Scoring mitotic cells and high cell density: Cells were grown to high confluence (>90%) on glass coverslips and fixed with 4% paraformaldehyde in PBS (137 mM NaCl, 2.7 mM KCl, 10 mM Na_2HPO_4, 1.8 mM KH_2PO_4, pH 7.4). Cells were permeabilized with 0.1% Triton X-100, blocked with 1% BSA in PBS, and stained with Hoechst (10 mg/mL stock in water; diluted 1:5000 in PBS and stained for 4 min), tubulin, and γ-tubulin to track mitotic indices. Five hundred cells were scored per replicate. Cells were binned based on the following features: DNA condensation at prophase, aligning of DNA at the metaphase plate and mitotic spindle staining during metaphase, separation of condensed DNA without cleavage furrow formation during anaphase, cleavage furrow formation during telophase, and midbody staining and DNA de-condensation during late cytokinesis.

Growth in Soft Agar: Anchorage independent growth, or the ability to grow in soft agar, was assessed as previously described (Borowicz et al., 2014). Briefly, 20,000 cells were plated in individual wells of a 6-well dish in soft (1 mL, 0.7%) agar over a base of 1 mL 1.0% agar in DMEM with 10% FBS. Cells were monitored over 30 days, with addition of fresh medium dropwise every few days to prevent dehydration. Cells were stained with 0.5 mL 0.005% crystal violet in methanol for 2 hr at room temperature before rinsing three times with water. Colonies

that are positive for crystal violet and at least three cells in diameter (≥~10 cells) were scored using brightfield microscopy.

Nocodazole Sensitivity: Cells were treated with a range of concentrations of nocodazole (0-100ng/µL) for 2 hr. Cells were then fixed with ice-cold methanol for 5 min at -20°C. They were then blocked and stained for α-tubulin to identify microtubule networks and γ-tubulin to identify centrosomes. Cells were visualized via widefield microscopy and binned by visual inspection based on whether they had intact versus defective microtubule networks. Microtubule networks were defined as "defective" if they had either an obvious decrease or complete loss of microtubule network compared to that seen in WT cells (see Supplemental Figures for example).

Cold Sensitivity: Cold sensitivity was determined by removing cells from the incubator and exposing them to either room temperature or putting them on ice (as indicated in the text) for a defined period of time ranging between 0-30 min. Immediately after, the cells were fixed with pre-warmed (37°C) 4% PFA and permeabilized with 0.1% Triton X-100. Samples were stained for α-tubulin to denote microtubule networks and γ-tubulin to identify centrosomes. Like the nocodazole sensitivity assay described above, microtubule network density was assessed by visual inspection (see Figure S4 for example).

For cold sensitivity recovery experiments, cells were removed from the incubator and incubated on ice for 30 min. Afterward, cells were returned to the incubator at 37˚C and allowed to recover for a range of time points extending from 0 min to 1 hr recovery. Cells were either fixed with 4% PFA and permeabilized with 0.1% Triton X-100 to look at microtubules and γ-tubulin or with ice-cold methanol for 5 min to visualize centrin at centrioles. The latter condition was also

used to visualize ARL2 and TBCD at centrosomes. Cells were visualized with either widefield microscopy for basic scoring or confocal microscopy to generate z-projections to score microtubules at asters.

Scoring microtubules at centrosomes after cold recovery. Cells were treated as described above for cold sensitivity recovery, incubating the cells for the specified time points at 37˚C to allow partial regrowth of microtubules. Cells were fixed with 4% PFA for 15 min at 37˚C, permeabilized with 0.1% Triton X-100 for 10 min, and stained for γ-tubulin to look at recovery at centrosomes and for α-tubulin to look at microtubule formation at asters. Cells were imaged using confocal microscopy (as described below) taking z-projections with 0.37 μm steps. These z-projections were processed using FIJI software to look at individual slices of cells and to visualize microtubules emanating from centrosomes. Microtubules were scored if (1) one of the ends of the microtubule could be seen extending from a γ-tubulin positive centrosome, and (2) if the tubule was at least 0.5 μm long, as determined using FIJI. The number of microtubules emanating from that centrosome were scored in each slice, and the slice with the highest number of microtubules was used to score that aster. After analyzing cells from multiple replicates, a total of at least 38 asters were scored per line.

Aster Formation Assay: The extent of aster formation as a function of time after removal of nocodazole was used as a way to measure the rate of growth of new microtubules at centrosomes, as previously described (Cunningham and Kahn, 2008; Sankaran et al., 2005; Tulu et al., 2006; Zhou et al., 2006). Microtubules were found to be eliminated, with minimal cellular toxicity, by treating with 50 ng/μL nocodazole for 2 hr at 37°C. The drug was then removed, cells

were washed once, and fresh pre-warmed medium added. Cells were fixed at 0, 0.5, 1, 2, 5, 7, and 10 min after release from nocodazole using 4% PFA and 0.1% Triton X-100 permeabilization. Cells were stained for α-tubulin and γ-tubulin, as described above. The size of asters as well as the morphology of the growing microtubule network were then assessed. To quantify aster size, the diameter of individual asters was measured using FIJI imaging software's measuring tool. For each aster, the largest diameter was determined and then tabulated. At least 50 asters were quantified per line per replicate, and the average aster diameter was determined per line (see Figure S5 for example).

Scoring of cell phenotypes: To score numbers of nuclei, cells were plated onto glass coverslips at 50-60% confluence to facilitate scoring of individual cells. The next day, cells were fixed with 37°C 4% PFA in PBS for 15 min at room temperature. Cells were permeabilized for 10 minutes with 0.1% Triton X-100 in PBS and blocked for 1 hr with PBS with 1% BSA. Primary antibodies were incubated at least 1 hr to overnight. The next day, cells were washed 4x with PBS and incubated with secondary antibody in PBS with 1% BSA. Cells were washed twice with PBS, stained with 1:5000 Hoechst 33342 for 4 min, and washed twice again with PBS before being mounted onto slides with 1:9 solution of PPD (p-phenylenediamine dihydrochloride; ACROS Organics; 624-18-0) in MOWIOL 4-88 Reagent (CALBIOCHEM; 475904). Cells were scored in triplicate for each of the 21 lines studied, 100 cells per replicate.

Scoring of centrosomes was performed using immunofluorescence, after methanol fixation, using two centrosomal markers (centrin and γ-tubulin). At least 100 cells were scored per condition per line, and this experiment was repeated at least three times.

Live Cell Imaging: Cells were plated on 8-well Ibidi glass-bottom slides (Ibidi #80827) at medium density and 24 hr later medium was replaced with imaging medium (phenol red-free DMEM with 25 mM HEPES, 10% FBS (Invitrogen #21063)). Cell cycle was tracked with phase contrast illumination at 40x magnification (0.60 NA) using a BioTek Lionheart FX widefield microscope. Several fields of cells were collected over a 24 hr time course at 37°C, 5% CO_2 every 10 min. Z-projections were generated to detect all cells, including those detaching from the plate during cell division. To track stages of cell division, different aspects of cell morphology were noted including cell rounding (indicative of prophase/metaphase), cell elongation and cleavage furrow formation (anaphase proceeding into telophase), cleavage furrow narrowing into midbodies (cytokinesis), and cells splitting apart during abscission.

Scoring of cell cycling and synchronization: Cells were grown on Matrigel coated coverslips to ~50% density and treated with the CDK1 Inhibitor (RO-3306; 7.5 µg/mL) in DMEM with 10% FBS. After 18 hr, cells were rinsed once and grown in fresh medium, taking time points after release from drug every 10 min for 2 hr. Cells were fixed in 4% PFA in PBS for 15 min at room temperature, rinsed 3 times in PBS, then permeabilized with 0.1% Triton X-100 in PBS for 10 min, followed by blocking with 1% BSA in PBS for one hr. The cells were stained with antibodies directed against α-tubulin (to mark mitotic spindles and midbodies) and γ-tubulin (to mark centrosome migration throughout the cell cycle and midbodies), and Hoechst 3052 (diluted 1:5000 in PBS from 5mM stock). Cells were scored as mitotic if DNA was condensed and aligned along the midplate and a mitotic spindle was evident, or if nuclear envelopes had formed and the midbody was evident from the α-tubulin staining. We use the term “mitotic indices” to indicate

cells bearing traits of anywhere from prophase to late cytokinesis, *e.g.* DNA condensation, mitotic spindle formation, cleavage furrowing/ingression, midbody formation.

Analyzing DNA content: Cell synchronization was performed using a double thymidine block followed by nocodazole using the following protocol: cells at ~50% confluence were treated for 16 hr in 2 mM thymidine, then allowed to recover for 8 hr in drug-free medium after 3x washes with PBS, another 16 hr thymidine block, followed by a 5 hr recovery in drug-free medium after 3x washes in PBS, and then 9 hr in medium containing nocodazole (20 ng/mL). Immediately after nocodazole synchronization, cells were prepared for analysis by flow cytometry by collecting cells, washing with ice-cold PBS, and fixing with ice-cold 70% ethanol in PBS. Note that all cells were collected and fixed at this stage to ensure a full representation of the cell population. Immediately prior to cytometry, cells were washed twice with phosphate citrate buffer (0.1M citric acid in PBS, pH 7.8), treated with RNase (100 µg/mL; Sigma; R5125), and stained with propidium iodide (50 µg/mL; Sigma, P4170) to measure DNA content. The voltage was set based on WT cells for each run, centering the G1 peak at 50K. These same settings were applied to all subsequent samples run that day, to ensure that we accurately track 2N, 4N, and >4N peaks. Data were plotted using FloJo software.

Microscopy: For all immunocytochemistry experiments, Matrigel (BD Bioscience) coated 18 mm glass coverslips (#1.5, Fisher Scientific; 12-545-81) were used. Imaging was performed on confocal (Olympus FV1000 microscope and Olympus Fluoview v1.7 software; 100x magnification (1.45 NA, Oil); 405, 488, and 543 laser lines used, 0.37µm step size for z-stacks) and widefield microscopes (Olympus IX81 microscope and Slidebook software; 100x

magnification (UPIanFI, 1.30 NA Oil), as indicated in the provided figures. Images were processed (and analyzed, in the case of aster formation assays) using FIJI imaging software. For all data appearing in any one figure, the same acquisition, brightness, contrast, cropping, and other processing settings were used across the experimental test group to ensure the accuracy of comparisons.

Reproducibility/Statistics: All experiments performed in this paper were scored at least in duplicate and performed at least in triplicate. Unless otherwise stated, at least 100 cells were scored per sample. Error bars presented in the graphs indicate standard error of the mean (SEM), and box-and-whisker plots indicate the range of the data along with the median and upper/lower quartiles. One-Way or Two-Way ANOVA tests were used to determine if there were significant differences between test groups. The number of stars indicate the level of statistical significance: * = $p < 0.05$; ** = $p < 0.01$; *** = $p < 0.0001$. For all experiments shown, we treated individual replicates (separate samples from experiments performed on separate days) of each individual line as technical replicates. We consider the individual lines as biological replicates. Therefore, if we report that a sample has an N=4, this indicates that four different lines were scored in duplicate, and the averages of those duplicates are presented in the graphs.

Results

With the goal of identifying cellular functions for ELMOD2, we generated cell lines specifically deleted for ELMOD2. We used CRISPR/Cas9 genome editing to introduce frame-shifting mutations of both alleles in MEFs, as described earlier (Schiavon et al., 2019). By targeting close to the 5' end of the open reading frame and upstream of the sole, catalytic ELMO domain

(Figure S1A), we expect that any protein fragments made from the mutated ELMOD2 gene will be inactive, as well as potentially rapidly degraded. We will refer to such lines herein as null or knockout (KO) lines, even though a short N-terminal peptide might exist in cells. To strengthen any conclusions drawn from characterization of these lines and specifically to protect against off-target effects that can occur from CRISPR, we generated multiple cell lines from two different guide RNAs. A total of 10 independently cloned KO lines were obtained (Figure S1B). Screening of cell lines was performed by genomic DNA sequencing after PCR amplification of the region targeted. We also generated a lentivirus that directs expression of mouse ELMOD2 with a C-terminal myc epitope (ELMOD2-myc) and used it to transduce our MEF lines to further strengthen the link between any observed phenotypes and the loss of cellular ELMOD2. Clones found to have no changes in the targeted exon are referred to as "CRISPR WT" and are retained as controls, as they have been through the same transfection, selection, and cloning processes as the nulls. We narrowed down the number of test samples to include four KO lines (KO #4, 6, 8, and 10; see Figure S1), the same four KO lines after transduction with virus to drive expression of ELMOD2-myc, two WT lines (one parental population, one CRISPR WT), and the same two WT lines expressing ELMOD2-myc. Hereafter, we will refer to these cells as our "12 standard lines." Finally, we note that every phenotype described below was evident in all 10 KO lines when tested and differed only in the magnitude of the changes. These are typically shown as the range, with more detailed analyses performed on the 12 standard lines.

We screened ELMOD2 null lines using markers of various cellular compartments to assess both potential global changes in organelle morphology as well as to specifically look for changes in compartments to which ELMOD2 had been localized (*i.e.*, mitochondria and lipid droplets). As predicted and demonstrated earlier, we observed mitochondrial defects (fragmentation) consistent

with ELMOD2 acting with ARL2 in mitochondrial fusion (Schiavon et al., 2019). In contrast, staining of WT and ELMOD2 null cells with BODIPY, either untreated or after a 24 hr exposure to 30 mM oleic acid, showed no changes in the number or size of lipid droplets that might be ascribed to the deletion of ELMOD2 (Figure S2). These early, broad screens did reveal a number of other cellular changes to result from deletion of ELMOD2 that we describe and analyze further below.

ELMOD2 null MEFs display multiple defects linked to microtubules

During routine handling and culture of ELMOD2 null cells, we observed some obvious differences from WT cells, *e.g.*, in cell morphology. Cell rounding was evident in each of our 10 ELMOD2 null lines and appeared to correlate with time spent out of the 37°C incubator, at room temperature, but was not seen in our WT or rescued lines. Cell rounding can result from defects in any of several different processes. Given the established links between ELMOD2 and ARL2, though, as well as the roles of ARL2 and its partner TBCD in tubulin heterodimer assembly, microtubule stability, γ-tubulin ring complex (γ-TuRC) recruitment, and links to chromosome instability, we hypothesized that cold sensitivity of ELMOD2 null MEFs was tied to the changes in microtubules (Bowzard et al., 2007; Francis et al., 2017a; Hoyt et al., 1990; Ivanova et al., 2014; Newman et al., 2017b; Zhou et al., 2006).

A time course study revealed that changes in cell morphology became evident within one minute at room temperature, progressing and persisting for at least two hr. Approximately 50% of cells became rounded within the first 15 min, and those that did not remained flat for at least two hr. We chose 15 min for more detailed analyses as a time at which changes were prominent in null cells but not in WT. Cells were removed from the incubator and either fixed immediately or after

15 min at room temperature (~22°C). Tubulin staining was not obviously different in WT and null cells fixed immediately upon removal from the incubator; microtubules fill the majority of the cell body and are ordered in appearance (Figure 1A). Quantification revealed that the percentage of cells with depleted microtubule networks was slightly increased in KO (17.1%) compared to controls (3.3%; $p<0.05$; Figure 1B). In contrast, within 15 min at room temperature, ELMOD2 KOs displayed a pronounced loss of microtubule staining compared to WT MEFs (77.8% in KO lines versus 8.8% in WT lines; Figure 1A, B). This is evident from the loss of overall microtubule staining and less frequent evidence of their organization around a centrosome in the nulls (see Figure S4 for details on binning of MT density). In marked contrast, there was little or no evidence of changes in the microtubule network of WT cells between the 0 and 15 min time points (Figure 1A, B). Quantification of loss of microtubule networks (Figure 1B) included scoring of both rounded and flat cells, as rounded cells were also depleted of microtubules. While both WT and null cells display loss of microtubules and cell rounding at 4°C, these changes are initiated more rapidly and are more evident in the null lines (not shown). Thus, ELMOD2 nulls clearly display an increased cold sensitivity for microtubules. Expression of ELMOD2-myc in nulls resulted in the near complete rescue of cold sensitivity, in that cell rounding and microtubule network densities each reverted to near WT levels (Figure 1A, B (KO+D2)). Expression of ELMOD2-myc in WT cells had no apparent effect on either parameter (Figure 1A).

Changes in microtubule sensitivity can also be assessed through their response to drugs that act on microtubules, such as nocodazole, as previously used in genetic screens in model organisms (Hoyt et al., 1990; Stearns et al., 1990). Nocodazole sensitivity was assessed in our 12 standard lines, grown to ~70% confluence, after treating with increasing concentrations of nocodazole (0 to 100 ng/mL) for 2 hr, followed by fixation and staining for α-tubulin, as described

under Materials and Methods. Cell rounding occurred in response to nocodazole, and such cells lacked evidence of, or had a greatly reduced, microtubule network. WT cells begin demonstrating clear evidence of microtubule loss at 5-10 ng/mL nocodazole and are most sensitive to changes in the drug at these concentrations, under these conditions (Figure 1C). In contrast, comparable loss of microtubules was evident in ELMOD2 KO cells with as little as 2 ng/mL nocodazole (Figure 1C). At 5ng/mL, ELMOD2 KO cells have >3-fold more cells displaying loss of microtubules (average of WT = 18.5%, range 13.5-23.5%; average of KO = 63.1%, range 59.5-66.75%). The expression of ELMOD2-myc in rescued lines reversed the nocodazole super-sensitivity of ELMOD2 null MEFs (average = 17.1%, range 15.75-18.5%) but had no effect on WT cells. At 20 ng/mL, all 12 lines presented with 100% of cells with microtubule loss (Figure 1C). Thus, the absence of ELMOD2 in MEFs causes the microtubule network to become more sensitive to both cold and nocodazole.

ELMOD2 localizes to centrosomes and its deletion causes delay in the recruitment of γ-TuRC and in microtubule nucleation from centrosomes

Microtubule network organization, regulation, and function(s) rely upon a variety of different factors. Increased sensitivity to cold and nocodazole could be the product of increased microtubule catastrophe, delays in microtubule nucleation, changes in pools of polymerizable tubulin, altered microtubule anchorage, or other means. To begin narrowing in on the role of ELMOD2, we used the aster formation assay (Cunningham and Kahn, 2008) to assess the rate of microtubule polymerization from centrosomes. We treated cells with 50 ng/mL nocodazole (optimized to increase the number of cells with complete microtubule loss while minimizing toxicity) for 2 hr, before replacing the drug with fresh medium and monitoring the formation of

asters by staining fixed cells for tubulin. The cells were fixed at time points up to 20 min after release from nocodazole; the 30 sec and 10 min time points are shown in Figure 1E. Cells were stained for α- and γ-tubulin to track aster formation. Both WT and null cells show at least some asters at the earliest time point (30 seconds after nocodazole washout). However, the rate at which asters grow or new asters appear was clearly slower in the null lines (Figure 1D, E; $p<0.001$). Scoring of this assay is described further in Figure S5. We also noted the presence of >2 asters in some ELMOD2 null cells, resulting from microtubule nucleation from supernumerary centrosomes (see below). By 10 min, WT cells have recovered microtubule arrays and cell morphology comparable to untreated cells. ELMOD2 nulls also have restored microtubule networks, though their networks are less ordered, emanate less obviously from centrosome-nucleated asters, and frequently do not extend to the cell periphery (Figure 1E, 10 min recovery).

The presence of microtubules but lack of an obvious microtubule organizing center in many ELMOD2 null cells recovering from nocodazole prompted us to ask whether nucleation of new microtubule growth was specifically defective at centrosomes, and perhaps retained at other sites (*e.g.*, Golgi or plasma membrane (Bugnard et al., 2005; Chabin-Brion et al., 2001; Efimov et al., 2007; Petry and Vale, 2015; Rios, 2014; Tassin et al., 1985a; Tassin et al., 1985b; Wu and Akhmanova, 2017; Zhu and Kaverina, 2013)). Therefore, cells were incubated on ice for 30 min to deplete the microtubule network and then returned to 37˚C for different times before fixation with 4% PFA, permeabilization with 0.1% TritonX-100, and staining for α-tubulin and γ-tubulin. At 0 min recovery from cold exposure, both WT and ELMOD2 null cells presented with a greatly depleted microtubule network, showing little or no evidence of a centrosomal microtubule organizing center. Peripheral microtubules were still present in both WT and null cells and at similar levels, though the microtubules were clearly less organized than in untreated cells. At each

time point of recovery from cold, peripheral microtubules in both WT and null cells appeared to recover at indistinguishable rates. Cells fixed immediately after cold exposure show little to no γ-tubulin positive centrosomes. In both WT and KO cells, the majority of the cells show background, punctate γ-tubulin staining, but no obvious bright foci consistent with centrosomes (Figure 2A). This indicates that the cold treatment used here causes at least partial changes in γ-tubulin, and thus γ-TuRC, at centrosomes, or more specifically at the pericentriolar material (PCM). After 5 min of recovery from cold, the vast majority (87.5%; range 83-92%; Figure 2B) of WT cells show the return of γ-tubulin positive centrosomes. In contrast, our KO lines show delayed recovery, with an average of only 21.3% (range 13-29%; Figure 2B) of cells showing γ-tubulin at centrosomes with 5 min recovery. Rescue with ELMOD2-myc in null cells reversed this effect to near WT levels (82.6%; range 76-88%). By 10 min, γ-tubulin positive centrosomes have recovered in practically all cells.

This loss or delay in γ-tubulin at centrosomes after cold was also accompanied by a decrease in the number of microtubules emanating from them even after its return. We quantified the number of microtubules at γ-tubulin positive centrosomes, as described under Materials and Methods and illustrated in Figure S6, at the 5 min time point. While WT cells had an average of 12.4 microtubules (range 11.6-13.2) at γ-tubulin positive centrosomes, the four KO lines had an average of 5.1 (range 5.0-5.3) microtubules. These four rescue lines showed numbers approaching those seen in wild type cells (average 9.5 microtubules, range 9.4-9.6; Figure 2C). Note that in this assay we scored only cells with γ-tubulin positive centrosomes and because we earlier found that KO lines show loss or delay in return of γ-tubulin to centrosomes, these data underestimate the severity of the differences in microtubules at asters during recovery from cold.

Taken together, these data point to a role for ELMOD2 in the recruitment of γ-tubulin, and by extension γ-TuRC, to centrosomes. However, ELMOD2 has not previously been localized to centrosomes. We had earlier generated rabbit polyclonal antibodies directed against ELMOD2 and used them to demonstrate localization in mitochondria (Newman et al., 2017b). Others have reported its presence at lipid droplets using proteomics or immunoblotting of purified preparations as well as exogenous expression of tagged protein (Bouchoux et al., 2011; East et al., 2012; Suzuki et al., 2015). Previous immunofluorescence experiments with our ELMOD2 antibody used fixation with paraformaldehyde and permeabilization with saponin or Triton X-100, which are conditions often used to visualize antigens in or on membranous compartments. However, protein dense structures like centrosomes and midbodies typically do not immunostain well under those conditions. Rather, it is common to fix and permeabilize in cold methanol, as described under Materials and Methods. WT MEFs were stained with our rabbit polyclonal antibody to ELMOD2 along with markers of microtubules (α-tubulin) and centrosomes (γ-tubulin) (Figure 5A). These studies revealed specific staining of ELMOD2 at both centrosomes and Flemming bodies, though not at cleavage furrows or the intercellular bridge (ICB) of midbodies (similar to ARL2, which also localizes to both centrosomes and Flemming bodies (Figure S3)). ELMOD2 staining was strongly decreased or completely absent from centrosomes and midbodies when the primary antibody was first incubated with purified GST-ELMOD2 (*i.e.*, antigen competition). In addition, staining of ELMOD2 at centrosomes and Flemming bodies was not observed in KO lines. These two important controls for immunostaining confirm the specific localization of endogenous ELMOD2 to centrosomes and midbodies in MEFs and provide novel potential sites at which it may act to alter microtubule dynamics or cytokinesis (see below) when deleted.

Previous data from our lab revealed a role for ARL2 and its binding partner TBCD in γ-TuRC anchoring (Cunningham and Kahn, 2008) and for ARL2 binding ELMOD2 (Bowzard et al., 2007; Ivanova et al., 2014). Thus, we also asked whether deletion of ELMOD2 affected the localization/recruitment of ARL2 or TBCD to centrosomes under cold stress. Using the same conditions for recovery from cold described above, cells were co-stained for centrin (to mark centrioles) and for either ARL2 or TBCD, as described under Materials and Methods. At each time point, centriolar staining of centrin is evident in all our cell lines, suggesting that cold exposure does not disrupt its localization to centrioles. In contrast, we observed loss of ARL2 and TBCD in response to cold stress in all cells, though this effect was more pronounced in the KO lines than in WT or rescued lines. Upon 0 min recovery from cold, 20.8% of WT cells were positive for TBCD staining at centrosomes (range 16-24%), and 27% were positive for ARL2 at centrosomes (range 21-35%). In contrast, 1.8% of KO cells displayed TBCD staining at centrosomes (range 0-4%), and 4% had ARL2 (range 0-8%). The decreased TBCD and ARL2 recruitment is reversed upon rescue with ELMOD2-myc, 21.3% (range 14-30%) and 25% (range 18-30%), respectively. After 5 min of recovery, 86.3% of centrosomes in WT cells were positive for TBCD (range 85-88%) and 77.5% for ARL2 (range 74-81%), while only 31.1% of null cells had TBCD (range 24-40%) and 41.3% (range 38-47%) had ARL2. This decrease in ARL2 and TBCD recruitment in ELMOD2 null cells, compared to WT, was reversed upon expression of ELMOD2-myc as we found 82.4% of null cells positive for TBCD (range 77-89%) and 81.3% (range 73-88%) for ARL2. By 10 min of recovery from cold, both ARL2 and TBCD staining recovered at centrosomes in both WT and KO cells. Thus, the loss of ELMOD2 in MEFs causes instability in the binding of γ-TuRC, ARL2, and TBCD at centrosomes in response to cold stress and delays in their ability to be recruited back to centrosomes during recovery from cold. We noted a small but statistically significant ($p<0.01$)

increase in the percentages of WT cells retaining centrosomal TBCD after cold (0 min recovery) when expressing ELMOD2-myc, as well as an elevated percentage of centrosomes retaining ARL2, though the latter is not statistically significant. This is consistent with a model in which ELMOD2 is a key component in regulating the recruitment of these two other proteins, though clearly requires more detailed study. Deletions of these other proteins or live cell imaging and determining the kinetics of each of these under different stressors may provide important insights into the ordering of recruitment but was deemed beyond the scope of the current study. However, because ELMOD2 was identified as an ARL2 GAP, we pushed our analyses in this direction further, in efforts to assess (1) whether ELMOD2 is acting as a GAP in these responses, (2) whether increasing ARL2 activity can reverse effects seen in the absence of ELMOD2, and (3) if so, if this effect is specific to ARL2.

Reversal of cold sensitivity by ELMOD2 requires its GAP activity or activated ARL2

Because ARF GAPs can function in cells as both terminators of GTPase signaling and as effectors of those same GTPases, we tested whether expression of the previously described (East et al., 2012) GAP dead mutant, ELMOD2[R167K], rescues the cold sensitive phenotype that we described above. We note that the mitochondrial fragmentation that occurs in MFN1 null MEFs is reversed upon expression of either WT or GAP dead ELMOD2, which supports the model that ELMOD2 acts as an effector of ARL2 inside mitochondria (Schiavon et al., 2019). As seen in Fig. 2H, expression of ELMOD2-myc reverses the effects of ELMOD2 deletion on cold sensitivity of microtubules. Two WT and four KO lines were transiently transfected with a pCDNA3.1-based vector either “empty” (serving as negative control) or directing expression of ELMOD2[R167K]-myc. The following day, cells were fixed and stained for α-tubulin and myc both immediately after

removal from the incubator and after a 15 min incubation at room temperature. No differences were found between scoring of cold sensitivity-induced changes in tubulin staining in untransfected cells (not shown), those transfected with empty vector, or those expressing ELMOD2[R167K]-myc (Figure 2H). Thus, GAP activity appears to be required for the actions of ELMOD2 that impact microtubule densities and cold sensitivity of cell morphology.

If the GAP activity of ELMOD2 is required for reversal of cold sensitivity, we reasoned that increasing the activity of the GTPase that it is working with in this pathway may also reverse the effects resulting from ELMOD2 deletion. Though ELMOD2 was purified as an ARL2 GAP, it was later shown to be promiscuous and to act on multiple ARF family GTPases (including both ARLs and ARFs) using *in vitro* GAP assays (Bowzard et al., 2007; Ivanova et al., 2014). Within the ARF family, only ARL2 and its closest paralog, ARL3, have been linked to microtubules (Zhou et al., 2006). We asked if cold sensitivity of microtubules could be rescued by increasing the activity of either GTPase through expression of activating mutants. The dominant, activating mutant ARL2[Q70L] has previously been shown to cause strong and irreversible effects on microtubules and other structures in CHO cells (Newman et al., 2014; Zhou et al., 2006). We saw similar strong effects of ARL2[Q70L] in MEFs, with essentially complete loss of microtubules in all expressing cells (not shown). We were concerned that such strong effects would prove difficult to sort out from those resulting from loss of ELMOD2. This mutant is analogous to RAS[Q61L] (Adari et al., 1988; Chipperfield et al., 1985) or ARF1[Q71L] (Zhang et al., 1994), as each is activating as a result of the loss of GTP hydrolysis and thus cannot inactivate the GTPases. An alternative means of generating activating GTPases is to increase the rate limiting step in their *activation* (release of bound GDP) via mutation of a conserved threonine. This residue lies in the nucleotide binding pocket making direct contact with the guanine ring (Aspenstrom, 2018; Santy,

2002) and is situated in the highly conserved “T(C/S)AT” or G-5 motif. The site is T157 in ARF6 and is homologous to V160 in ARL2 and L131 in ARL3. Such mutants were first described in RAS and RHO GTPases (Aspenstrom, 2018; Fidyk et al., 2006; Lin et al., 1997; Lin et al., 1999; Reinstein et al., 1991). Santy later demonstrated the utility of analogous mutants of ARF6 (Santy, 2002), and this was later extended to other family members (D'Souza et al., 2020; Moravec et al., 2012). These mutants increase the turnover of the activation/deactivation cycle and are thus also referred to as “fast cycling” activating mutants and, importantly here, remain sensitive to GAPs. Therefore, they can be more informative than the Q to L mutants which are locked into only the activated conformation, preventing cycling.

Expression of fast cycling ARL2 (ARL2[V160A]) in WT MEF lines caused little or no changes to the microtubule network and thus offered a means of attempting rescue with this activating mutant (Figure 2H; average 19.5%, range 18-21%). The cold sensitive microtubule loss in ELMOD2 null lines (Figure 2H; average 89.8%, range 84.5-95%) was strongly reversed upon expression of ARL2[V160A] in each of the 4 KO lines assayed (Figure 2H; average 31.9%, range 29.5-36.5%, $p<0.0001$) to almost the same extent as seen with ELMOD2-HA. Even wild type ARL2 has a small ability to reverse the loss of microtubules ($p<0.01$). In contrast, expression of activating mutants of other ARF family GTPases (ARL3 (ARL3[L131A]), ARF6 (ARF6[T157A]), and the dominant activated ARF6 (ARF6[Q71L])) had no effect on the microtubule defects in ELMOD2 KO lines (Figure 2H). Thus, ARL2 is uniquely capable of rescuing the microtubule defects seen in ELMOD2 null MEFs. This result is consistent with ELMOD2 and ARL2 acting in a single common, or perhaps two parallel, pathways that influence microtubule stability.

*KO lines are multinucleated, polyploid, and have supernumerary centrosome*s

While performing the experiments described above, it was evident that other things were aberrant in our KO lines that seemed to point to dysfunction in some aspect of cell division. These included apparent increases in the number of centrosomes, evident when staining for γ-TuRC or centrin, and multinucleation, evident from Hoechst staining. So, we next set out to quantify these effects and test whether they are consequences of the changes in microtubules, described above, or separate pathways that may also have a requirement for ELMOD2.

We saw no consistent differences in rates of cell proliferation correlating with genotype while cloning the KO lines or during routine maintenance of them. However, simply staining for DNA (with Hoechst) revealed a large increase in the incidence of multinucleation in ELMOD2 KO lines. All 10 KO lines were analyzed (technical triplicates of 100 cells counted per line) for nuclear number, and we found that an average of 17.1% (range of 10 lines 10.0-20.3%) of ELMOD2 KO cells have 2 or more nuclei, compared to 1.6% of WT cells (range 1.3-2.0%; Figure 3A). This experiment was scored in triplicate but was repeated many times with consistent results, as we routinely stain for Hoechst in immunocytochemistry experiments. Although we use the term multinucleation, the clear majority of multinucleated cells are binucleated.

Multinucleation was largely reversed upon expression of ELMOD2-myc (Figure 3A; $p<0.0001$). While the average percentage of multinucleated cells in our standard KO lines was 20.6% (range 20.0-21.3%), this was reduced to 5.0% (range 3.3%-6.7%) after expression of ELMOD2-myc. Because lentivirus infection efficiency was between 70 and 90% (positive for myc staining), scoring was performed for all cells. As a result, the presence of at least 10% of cells in the culture that do not express ELMOD2-myc is expected to at least partially account for the

incomplete rescue. Thus, it is evident that multinucleation is a common phenotype observed in cells lacking ELMOD2 that is reversed upon its re-introduction.

To assess DNA content, we used flow cytometry with propidium iodide staining of DNA. The 12 standard lines were each analyzed in technical triplicate. The six other null lines were each analyzed at least once, with none displaying results that deviated clearly from the data summarized here. Even without cell synchronization, null lines often presented with an increased G2/M (4N) peak compared to WT cells, and often also displayed 8N peaks (Figure 3B). These results are consistent with a subpopulation of null cells either being multinucleated or polyploid. To better assess the nature of the lesion, cells were synchronized using a double thymidine block followed by nocodazole to maximize the number of cells in G2/M (4N), as described under Materials and Methods. After synchronization, an 8N population of cells emerged in all null lines and was quite prominent in several of them (Figure 3B). Because the apparent percentage of cells with 8N is clearly in excess over the percentage of multinucleated cells (~20%, Figure 3C), we conclude that polyploidy is not occurring exclusively in mononucleated cells. While multinucleation was reversed upon expression of ELMOD2-myc in KO lines, this was not the case for polyploidy. Reversal of polyploidy may require more time than does multinucleation, as cells do not have a known mechanism for removing excess DNA. All the data reported herein use low passage numbers (<10) to minimize the impact of phenotypic drift over time.

Multinucleation is often the result of failure in cytokinesis and frequently is associated with increased incidence of supernumerary centrosomes. To examine centrosome numbers, cells were plated at ~70% confluence, fixed the next day, and stained for two markers of centrosomes: γ-tubulin and centrin. The two WT lines displayed an average of 98.9% of cells having 1 or 2 centrosomes, or 1.1% having >2 centrosomes (Figure 3C). In marked contrast, in the 10 KO lines,

an average of 25.0% of cells had >2 centrosomes (Figure 3C; range = 14.3-29.3%; $p<0.0001$). The majority of these cells have 3-4 centrosomes, though some cells had as many as 20 centrosomes. All multinucleated cells displayed supernumerary centrosomes, but not all cells with supernumerary centrosomes were multinucleated. Number and arrangement of centrosomes appeared to vary widely from cell to cell (*e.g.*, there was no obvious trend in centrosomes being clustered, and there was no obvious preference for even numbers of centrosomes). This phenotype was largely reversed upon expression of ELMOD2-myc in all four KO lines tested, as the average in these four lines dropped from 27.1% to 5.3% post-transduction. Because both these phenotypes are reversed upon expression of ELMOD2-myc, multinucleation and centrosome amplification result from the loss of ELMOD2 and not from potential off-target effects of CRISPR/Cas9.

ELMOD2 null cells display higher rates of cytokinesis failures

Multinucleation, polyploidy, and centrosome amplification can each result from defects in cell division. We sought to determine if a specific stage in cell division is compromised in cells lacking ELMOD2. Our 12 standard lines were imaged by brightfield microscopy over 24 hr at 37°C, capturing z-projections every 10 min (Figure 4A). We observed no failures in cell division in WT cells. In contrast, ELMOD2 null cells frequently displayed defects in the later stages of cell division that included late failure in cytokinesis: the cells generated a midbody, but they were incapable of completing abscission (Figure 4A, top row). We also noted common instances in which cells complete cytokinesis with apparently normal nuclear division, but the cells take a markedly prolonged time to complete cytokinesis (Figure 4 A, bottom row). To gain a better perspective, as well as increase the numbers of cells analyzed at specific points in the cell cycle, we continued these studies using fixed synchronized cell populations.

Cells were treated with the CDK1 inhibitor RO-3306 (7.5 μg/mL) for 18 hr to block cells at the beginning of mitosis. The drug was removed, and cells were fixed at time points up to 5 hr before staining for α-tubulin, γ-tubulin, and Hoechst to track mitotic indices and cell division (see Materials and Methods, and Figure S7). WT cells displayed a wave of cell divisions with clearly increased mitotic indices within 10 min of drug removal, peaking at 20 min at an average of 42.5% mitotic cells, followed by lower mitotic indices (9-16% on average) throughout the remainder of the 5 hr imaging window (Figure 4B). ELMOD2 nulls had a similar onset of increased mitotic index and achieved a maximum average of 51.3% 30 min after release from inhibitor. In contrast to WT cells that had a short-lived peak in mitotic indices, this level plateaued and was sustained at ≥40% of cells throughout most of the 5 hr time course in KO lines. Mitotic indices of ELMOD2 nulls never returned to the levels seen in WT MEFs, even 5 hr after release from CDK1 inhibitor (32.5%). Thus, the lack of ELMOD2 results in long delays in completion of cytokinesis. This result is consistent with the live cell imaging data, as the most common defects observed were either stalling or failure at late cytokinesis.

Consistent with delays in completion of cytokinesis, both synchronized and unsynchronized ELMOD2 null lines display a higher percentage of cells with midbodies (as visualized by α-tubulin staining). At no time point after washout of the drug did WT MEFs have more than 6.5% of cells with a midbody throughout the 5 hr imaging window. In contrast, the average of the four KO lines have a maximum of ~20% of cells with midbodies, and this is maintained throughout the 5 hr imaging window (Figure 4C). The increased fraction of cells displaying midbodies was also accompanied by an increase in the number of very long midbodies and midbody remnants (residual midbodies that persist after abscission). Remarkably, there were also instances in which one cell was attached to two others via distinct midbodies. These were

each uncommon (estimated at 1% but not rigorously quantified), though never observed in WT lines. Expression of ELMOD2-myc in WT lines had little to no effect on the percentage of cells with midbodies at any time point but was sufficient to return the percentage of cells with midbodies in ELMOD2 null lines nearly to WT levels (Figure 4C). Together, these data support a role for ELMOD2 in late cytokinesis, though defects at other stages have not been excluded.

ELMOD2 null MEFs have reduced recruitment of ARF6 to midbodies

The later stages of cytokinesis, including abscission, require the selective recruitment of multiple regulatory proteins to key sites (including centrosomes, cleavage furrows, recycling endosomes, and midbodies) via mechanisms that are often incompletely understood (Agromayor and Martin-Serrano, 2013; Nahse et al., 2017; Nakayama, 2016; Peterman and Prekeris, 2019). Such proteins may traffic to the mitotic spindle or cleavage furrow during metaphase and anaphase, and later to specific parts of the midbody to facilitate abscission. Some inconsistency in terminology exists in the literature. So, to be clear, we refer to the entire structure that bridges two dividing cells as the midbody, which consists of two inter-cellular bridges (ICBs) on either side of a central Flemming body. We sought to better define potential sites and mechanisms of ELMOD2 action to tease apart its role(s) in cytokinesis. We monitored the recruitment and retention of a number of other components at these sites at different stages in the cell cycle, with the aim of determining if ELMOD2 can be linked to any known cytokinesis pathways. We focused on both markers of the key compartments/processes as well as on proteins previously linked to ARF family GTPases. Sixteen endogenous proteins were localized in WT and ELMOD2 null MEFs (plated at the same density) using cold methanol fixation and specific antibodies directed against ARL1, ARL2, ARL3, ARFs (monoclonal 1D9), ARF6, RHOA, RAB11, RAB11-FIP3 (hereafter termed

FIP3), MKLP1, α- and γ-tubulin, acetylated tubulin, centrin, BART/ARL2BP, TBCD, and ELMOD2, as described under Materials and Methods. A summary of localizations observed for these proteins in MEFs is shown in Figure 5B.

Almost all previously described markers of the Flemming body (*e.g.*, MKLP1, RHOA, and FIP3 (Figure S1A)) and ICB (α-tubulin, γ-tubulin, acetylated tubulin, and RAB11 (Figure S3B)) localize indistinguishably in WT and ELMOD2 null cells. We have previously shown ARL3, TBCD, and BART to localize to the Flemming body, and these, too, were unaltered in ELMOD2 null MEFs compared to WTs. ARL2 has not previously been localized to the Flemming body, but it also is unaltered in staining in both WT and null MEFs (Figure S3C). ARL2, ARL3, and TBCD staining at centrosomes appears unchanged in null versus WT cells, though as noted above cold stress does promote the release of ARL2 and TBCD to a greater extent in KO than WT cells.

In marked contrast, ARF6 is no longer found at the Flemming body of ELMOD2 nulls (Figure 5C, D). This loss of ARF6 staining is reversed upon expression of ELMOD2-myc. We examined four KO lines, and ARF6 was absent from Flemming bodies in each case, while staining of ARF6 was restored in every case upon expression of ELMOD2-myc (Figure 6D; $p<0.0001$). Thus, the loss of ELMOD2 in cells and from Flemming bodies is accompanied by the specific loss of ARF6 from Flemming bodies.

ELMOD2 nulls show reduced RAB11 and increased ARF6 recruitment to FIP3-GFP positive endosomes

To begin to test the model that ELMOD2 is acting with ARF6 to mediate cytokinesis, we next checked to see if other factors in this pathway were disrupted by loss of ELMOD2. Prior to their recruitment to midbodies, ARF6, RAB11, and FIP3 are each recruited to recycling

endosomes adjacent to centrosomes (Prigent et al., 2003; Schiel et al., 2012). From there, ARF6 traffics to the cleavage furrow to facilitate furrow ingression, and later to the Flemming body during cytokinesis. RAB11 and FIP3 are recruited to the ICB. Just before abscission, it is thought that FIP3 moves from the ICB to the Flemming body, where ARF6 has already been recruited (Schiel et al., 2012). Their location at the Flemming body is critical for the final stages of abscission. To visualize these processes, we used FIP3-GFP expression to identify the relevant recycling endosomes and to follow changes in localization of these key proteins at these sites, as previously described (Schiel et al., 2012).

Expression of FIP3-GFP in WT cells results in bright staining (Figure 6A, top panel) of a cluster that has been shown previously to be recycling endosomes adjacent to or surrounding the centrosome (Schiel et al., 2012). In a small subset (<10%) of WT cells, we also observed evidence of a diffuse GFP signal as well as a mixture of clustered and diffuse staining, quantified in Figure 6B. Cells expressing FIP3-GFP were also stained with antibodies to FIP3 and yielded the same results, arguing against GFP being cleaved from FIP3 and confusing interpretations. The FIP3-GFP recycling endosomal clusters also stained strongly for RAB11, though cytosolic staining of RAB11 was also always evident (Figure 6C). We repeated this experiment several times with different WT lines and always obtained the same results. We also investigated ARF6 localization to recycling endosomes. WT cells expressing FIP3-GFP display ARF6 staining that is diffuse/cytosolic, with little to no evidence of enrichment at FIP3-positive clusters over background (Figure 6D).

In contrast, FIP3-GFP staining was much more diffuse in all four ELMOD2 null lines analyzed (Figure 6A, B). A subpopulation (<30%) of these cells retain a strong GFP signal at clusters with little diffuse staining, while another ~30% show retention of a clear cluster but with

obvious, diffuse staining. The remainder (~40%) only have diffuse GFP signal (all quantified in Figure 6B). In ELMOD2 null lines, there is a uniform and pronounced loss of RAB11 staining at recycling endosomes, regardless of whether FIP3-GFP is clustered (Figure 6C). This effect is quite strong, though occasionally a weak RAB11 signal can still be seen to co-stain FIP3-GFP clusters. The partial or complete loss of FIP3-GFP clustering and of RAB11 co-staining at recycling endosomes was reversed upon expression of ELMOD2-myc in all four rescued lines.

All members of the FIP family (RAB11-FIP1 through 5) bind to and are recruited to endosomes in concert with RAB11, though only FIP3 and FIP4 bind to ARF6 (Fielding et al., 2005; Hickson et al., 2003; Horgan and McCaffrey, 2009; Wilson et al., 2005). As a test of the specificity of FIP family members being sensitive to the loss of ELMOD2, we immunostained FIP3-GFP transfected cells for FIP1 or FIP5. FIP3-GFP positive clusters in WT cells stain positive for both FIP1 and FIP5 (Figure 6E, F), and this staining was not altered upon deletion of ELMOD2. Furthermore, even in ELMOD2 null cells with diffuse FIP3-GFP staining, FIP1 and FIP5 are still recruited to clusters. This suggests that FIP1 and FIP5 localization to endosomes is unaffected by the loss of ELMOD2, and thus the effect is specific to the ARF6 binder FIP3.

In contrast to WT cells, in which ARF6 staining at FIP3-GFP clusters was either faint or not evident, our ELMOD2 nulls displayed uniformly strong ARF6 staining at recycling endosome clusters (Figure 6D). This increased ARF6 staining was reversed upon expression of ELMOD2-myc in KO lines. Thus, loss of ELMOD2 results in compromised FIP3-GFP clustering, no changes in FIP1 or FIP5 clustering, (near) complete loss of RAB11, and strong increases in ARF6 at that site. These data lead us to propose a model in which RAB11 and ARF6 compete for the binding of FIP3 at recycling endosomes (see Discussion).

ELMOD2 GAP activity is required for rescue of multinucleation and centrosome amplification

Having identified a novel role for ELMOD2 in cell division, we next sought to understand the mechanism(s) by which ELMOD2 mediates cytokinesis. To determine if ELMOD2 is acting as a GAP in cytokinesis, we transfected the standard 2 WT and 4 KO lines with a plasmid directing expression of ELMOD2[R167K]-myc to determine if it could reverse supernumerary centrosomes and multinucleation, as shown previously for ELMOD2-myc (see above). Cells were transfected, fixed 48 hr later, and stained for myc, γ-tubulin, and Hoechst, as described under Materials and Methods. WT MEFs expressing the GAP-dead ELMOD2 appeared normal in morphology (*e.g.*, mononucleated, 1-2 centrosomes) with only an average of 1.5% of cells being multinucleated and 1.2% of cells having supernumerary centrosomes (Figure 6G, H). KO lines that express ELMOD2[R167K] display comparable levels of multinucleation (22.7%) and supernumerary centrosomes (27.4%) as empty vector controls (19.3% and 27.6%, respectively) or untransfected ELMOD2 nulls (17.1% and 25.0%, respectively). Because we showed above that ELMOD2-myc reverses multinucleation and centrosome amplification but the GAP dead point mutant shows virtually no such rescue, we conclude that, in contrast to ELMOD2's role with ARL2 in mitochondrial fusion (Schiavon et al., 2019) but like its role in microtubules, GAP activity *is* required for its function(s) in these processes.

Expression of activated ARF6-HA rescues cytokinesis defects seen in ELMOD2 null MEFs

Given the prior evidence demonstrating effects of ARF6 mutants on endosomes and cell division (*e.g.*, (D'Souza-Schorey et al., 1998; Donaldson and Radhakrishna, 2001), we hypothesized that ELMOD2 may act as a GAP to inactivate ARF6 at recycling endosomes to mediate cytokinesis. This could explain the accumulation of ARF6 at FIP3-GFP positive

endosome clusters, if inactivation of ARF6 is required for its release from that site. To begin to address such a model, we expressed ARF6-HA, dominant activating point mutant (ARF6[Q67L]-HA), or empty vector control, into the standard 12 cell lines. Cells were fixed 48 hr later, stained, and scored for multinucleation and centrosome amplification, as described in Materials and Methods. Neither transfection controls (empty vector) nor expression of ARF6-HA resulted in changes in the extent of multinucleation (2.0% and 3.3%, respectively) or centrosome amplification (2.3% and 3.3%, respectively) in WT cells (Figure 6G, H, respectively). In contrast, expression of ARF6[Q67L]-HA in WT cells led to large increases in both multinucleation (average = 23.0%; Figure 6G; $p<0.0001$) and supernumerary centrosomes (30.8%; Figure 6H $p<0.0001$), consistent with the consequences of excessive ARF6 activity to the cell cycle, as previously reported (Schweitzer and D'Souza-Schorey, 2002). The effects of increased ARF6 activity in WT cells are comparable to the consequences of deletion of ELMOD2 (17.1% multinucleation, range of 10-21.3%, and 25.0% centrosome amplification, range of 14.3-33.3%, respectively (Figure 6 G,H)).

Multinucleation and centrosome amplification in ELMOD2 nulls were unaffected by transfection (empty vector) or expression of ARF6-HA (19.3% and 18.0% multinucleation; and 27.6% and 31.4%, supernumerary centrosomes, respectively) (Figure 6G,H). In marked contrast, expression of ARF6[Q67L]-HA resulted in substantial reversal of both multinucleation and supernumerary centrosome defects in ELMOD2 nulls (8.4% multinucleation; 8.0% supernumerary centrosomes (Figure 6G,H).

Though ARF6[Q67L]-HA can rescue the defects seen in ELMOD2 nulls, the fact that it causes multinucleation and supernumerary centrosome defects in WT cells complicates interpretations. Similar effects of ARF6[Q67L] on midbodies and cytokinesis have been reported

in HeLa and Jurkat cells (Schweitzer and D'Souza-Schorey, 2002). To further examine the role of ARF6 in cells deleted for ELMOD2, we used the same rationale described above in use of fast cycling ARL2 to rescue changes in microtubules. The corresponding activating mutation in ARF6 is ARF6[T157A]-HA, and we compared it to ARF6[Q71L] in both WT and KO lines. Interestingly, only ARF6[Q71L]-HA caused increases in multinucleation in WT cells; ARF6[V160A]-HA did not (multinucleation: average 1.75%, range 1.5-2.0%; supernumerary centrosome: average 2.25%, range 1.5-3%) (Figure 6G). This is consistent with the ARF6[Q71L] mutant "locking" its pathway in an activated state and preventing cycling. In doing so, this mutant may actually be inhibiting the pathway, perhaps analogous to that seen upon depletion of ARF6 (Schweitzer and D'Souza-Schorey, 2005). While ARF6[T157A]-HA does not cause multinucleation in WT cells, it is as effective as ARF6[Q71L]-HA in reversing the effects of ELMOD2 deletion (Figure 6H; $p<0.0001$), again demonstrating the utility of such fast cycling mutants in ARF family members by avoiding irreversible or toxic effects of the GTPase defective mutants (Santy, 2002).

Because of the roles we found for ELMOD2 in microtubules, we did not want to exclude the possibility that at least part of the cell cycle defects could be a product of an ARL2-related pathway. Therefore, we also compared the effects of expressing the activating ARL2[V160A] or ARL3[L131A] mutants on multinucleation and supernumerary centrosomes. Neither appeared to have effects on these phenotypes in WT cells. Neither ARL2[V160A] nor ARF6-HA caused a significant change in the percentage of multinucleated cells in KO lines, but expression of ARL3[L131A] led to a small increase (from 22.0 to 27.5%; Figure 6G) in multinucleation in null lines that was statistically significant ($p<0.05$). Thus, two different activating ARF6 mutants were

highly specific, at least among this small subset of ARF family members, in reversing the increased nuclear number seen in ELMOD2 nulls.

Similar results were obtained upon scoring centrosome numbers (Figure 6G) in that both activating ARF6 mutants strongly reversed the supernumerary centrosome phenotype in KO lines ($p<0.0001$). Like multinucleation, the ARF6[Q71L] caused increased centrosome numbers in WT cells, despite reversing the phenotype in nulls, while ARF6[T157A] had no effect on WT cells, yielding a cleaner and more readily interpretable result. Although small effects of activated ARL2 or ARL3 were seen in WT cells, these did not rise to the level of statistical significance ($p<0.05$) and were well below that seen in ARF6[Q71L]-HA expressing cells. We saw no effects on centrosome numbers upon expression of ARF6-HA or ARL3[L131A]. Interestingly, expression of ARL2[V160A] yielded a partial reversal that was statistically significant ($p<0.01$). Thus, only the two activating ARF6 mutants were found to strongly (essentially completely) reverse the increases in both the percentages of cells with multinucleation and supernumerary centrosomes; each appeared to be comparable in effectiveness.

These results demonstrate close functional links between ARF6 and ELMOD2 activities in MEFs with respect to their effects on nuclear and centrosome numbers. This stands in marked contrast to the specific functional ties between microtubule defects and ARL2 in ELMOD2 null lines, suggesting that ELMOD2 directs two different essential cellular functions through distinct GTPases.

ELMOD2 KO lines have lost contact inhibition and anchorage independent growth

During the course of the investigations described above, we also noted two other phenotypes linked to ELMOD2 deletion. We include a brief description of them here, not to focus

on additional mechanisms but simply to highlight the likelihood that ELMOD2 plays additional roles in the cell We are still far from understanding all of its actions and how these functions may be integrated.

If cells were allowed to reach high cell densities, at or approaching confluence, we noted that ELMOD2 null lines displayed a higher percentage of cells undergoing cell division compared to wild type lines (Figure 7A, B). This higher mitotic index in confluent cultures is interpreted as evidence of the loss of contact inhibition. Our standard 12 lines were scored in technical triplicate (counting 500 cells/line) and revealed that an average of 11.5% of KO lines were mitotic (ranging from 8.8% to 15.2%) while only 2.6% (range of 1.9-3.3%) of WT cells were dividing under these conditions (Figure 7A, B). Expression of ELMOD2-myc resulted in reversal of this phenotype in KOs, as the average of the four lines dropped from 11.5% to 3.7%, while the WT lines showed no difference after transduction (2.6% vs 2.9%). Thus, deletion of ELMOD2 in MEFs causes reduced contact inhibition, and this phenotype is rescued by expression of ELMOD2-myc.

Loss of contact inhibition is a common feature of cell transformation, so we next assessed another such property: the ability to grow in soft agar or anchorage independent growth. We plated $2x10^4$ cells in soft agar and monitored growth at 37°C over the course of 30 days, as described under Materials and Methods. The 12 standard lines were quantified in technical triplicate, with two biological replicates (Figure 7C, D). While WT and ELMOD2-myc expressing WT cells had an average of 24 and 78 colonies, respectively, ELMOD2 nulls had >10-fold more colonies than WT (average of 4 lines = 379 colonies, range of 245-503 colonies) (Figure 7D). In addition, the few colonies seen in WT cultures were small (typically containing only a few cells), round, and symmetric. In contrast, the colonies from KO cultures were larger and often asymmetric in morphology. Thus, the loss of ELMOD2 in immortalized MEFs is accompanied by acquisition of

at least two phenotypes associated with cell transformation: loss of contact inhibition and gain of anchorage independent growth. Neither of these phenotypes is predicted be secondary to the effects described above on microtubules or cell division. Rather, these data are included simply to highlight the fact that additional cellular roles for ELMOD2 are evident. With each one, both the complexity and importance of this protein grows, as do the challenges in developing strong models for each action.

Discussion

The generation of null MEF lines has revealed novel roles for the ARF GAP ELMOD2 in cytokinesis and microtubule stability and nucleation that are in addition to its previously documented roles in mitochondrial fusion (Newman et al., 2017a; Schiavon et al., 2019), in lipase recruitment to lipid droplets (Bouchoux et al., 2011; Suzuki et al., 2015), and in meiosis in oocytes (Zhou et al., 2017). Our initial observations of cold sensitivity of cell morphology with loss of microtubules and multinucleation in ELMOD2 null cells were pursued through the use of multiple cell-based assays targeting different potential causes of these defects; our goal was to identify the sites and mechanisms of action. These assays have revealed a host of changes in cell functions resulting from the deletion of ELMOD2 that we believe can be traced back to fundamental defects in the recruitment of γ-TuRC to centrosomes, with consequent microtubule instability, and to the release of ARF6 from recycling endosomes resulting in downstream defects/failures in late cytokinesis or abscission (Figure 8). We also provide evidence that the defects observed in ELMOD2 nulls are linked to pathways involving (at least) two different ARF family GTPases: γ-TuRC recruitment with ARL2, and cytokinesis with ARF6. While pathways involving distinct GTPases have been demonstrated here, we cannot definitively rule out the possibility that defects

in one impact the others. For example, altered microtubule stability or dynamics cannot be excluded from contributing to the delay in cell cycle. Similarly, we believe other essential cell processes are likely to be affected by the loss of ELMOD2, as evidenced by the loss of contact inhibition and gain of ability to grow in soft agar. These two features of cell transformation were not further explored mechanistically, but we believe that they speak to the fundamental and far-reaching cellular roles of ELMOD2 and, by extension, the GTPases with which it acts.

We interpret cold sensitivity and nocodazole super-sensitivity of the microtubule network in the ELMOD2 nulls as most consistent with a decrease in the overall stability of the microtubule network. The regulation of microtubules and their dynamics is incredibly complex but, based on our data, we predict that ELMOD2 acts with ARL2 at centrosomes at least in part to promote the recruitment of the γ-TuRC. We cannot exclude other possibilities for how ELMOD2 may be working with ARL2, as ARL2 is also a critical player in regulating the assembly of αβ-tubulin heterodimers through the tubulin folding pathway (Beghin et al., 2007; Bhamidipati et al., 2000; Francis et al., 2017a; Francis et al., 2017b; Francis et al., 2016; Nithianantham et al., 2015; Radcliffe et al., 2000; Tian et al., 2010). However, our data reveal delays in γ-tubulin, ARL2, and TBCD recruitment during recovery from cold, leading us to propose a model (Figure 8) in which ELMOD2 regulated ARL2 activity and perhaps less directly TBCD and γ-TuRC. Furthermore, the decreased aster size and number of microtubules emanating from asters suggest that even when γ-tubulin does recruit, there is still a delay in microtubule growth (Figs. 1 and 2). Further studies into the ordering of recruitment of these components to centrosomes and mechanisms by which they work together to regulate microtubule nucleation at centrosomes is warranted and predicted to reveal further insights into the actions of each of these proteins.

With our earlier focus on the role of ELMOD2 inside mitochondria, we used fixation and permeabilization methods optimal for that organelle and missed the fact that ELMOD2 also localizes to centrosomes, or more specifically the pericentriolar material (PCM). After switching to the most common fixative for looking at centrosomal proteins (cold methanol), we were able to demonstrate the specific localization of ELMOD2 at that site, where we had previously shown ARL2 and TBCD to be present (Cunningham and Kahn, 2008; Zhou et al., 2006). The greater cold induced release of all of these, along with γ-TuRC, and delays in their return in ELMOD2 null cells (compared to WT) provide correlative evidence of them acting together. Work from our and other labs have demonstrated direct interactions between ARL2 and ELMOD2 and between ARL2, TBCD, and β-tubulin, though not previously at centrosomes. The finding that rescue of the ELMOD2 loss requires its GAP activity supports the conclusion that it is acting through ARL2 in this pathway. The fact that fast cycling ARL2 (which is still sensitive to GAP action) rescues the cold sensitivity is consistent with ELMOD2 regulating the cycling, and thus the half-life, of activated ARL2 at centrosomes. Clearly more work is needed to provide molecular mechanisms by which ARL2 and ELMOD2 are acting at the PCM to influence γ-TuRC recruitment and microtubule growth/stability, but these initial findings reveal novel roles for each that also will need to be dissected from their other essential cellular roles.

Placing a population of ELMOD2 at centrosomes could also potentially explain the effects of its deletion on the recruitment of FIP3, RAB11, and ARF6 to recycling endosomes. Although we did not detect ELMOD2 staining in the endosome clusters that are defined by FIP3-GFP, their close proximity to centrosomes may suggest a functional link. Deletion of ELMOD2 caused defects that can be attributed to either a delay or a failure in cell division late in the process, perhaps immediately preceding abscission. The delay is most evident from the extended stalling observed

in time required to complete cytokinesis after removal of CDK1 inhibitor (Figure 4B) and the large increase in the percentage of cells having midbodies (Figure 4C). Multinucleation, supernumerary centrosomes, and polyploidy (Figure 3) typically result from failure in cytokinesis. In efforts to identify a specific lesion present in cells lacking ELMOD2, we used immunofluorescence to monitor the localization of multiple markers of cytokinesis that are recruited to specific sites (recycling endosomes, midbodies, ICB, or Flemming body) at precise times during cytokinesis. Most of these were unchanged between WT and ELMOD2 null cells. In contrast, staining of ARF6 is lost at the Flemming body in ELMOD2 KO cells. MKLP1 binds to activated ARFs and recruits ARF6 to the Flemming body (Boman et al., 1999; Makyio et al., 2012; Van Valkenburgh et al., 2001). ARF6 is required for completion of cytokinesis (Schweitzer and D'Souza-Schorey, 2002; Schweitzer and D'Souza-Schorey, 2005; Schweitzer et al., 2011). MKLP1 is still present in null cells while ARF6 is not. We propose (Fig. 8) that the lack of ELMOD2 causes a defect in the translocation of ARF6 to that site, with consequent increased failures in abscission. This might result from a defect in the spatial and/or temporal activation of ARF6 that is required for its functionality at that site, *e.g.*, a role for ELMOD2 in recruiting an ARF6 GEF in a GTPase network (Mizuno-Yamasaki et al., 2012). This is also consistent with the finding that the fast cycling, activated ARF6 reverses this defect upon expression in null cells (Figure 6G,H). The mechanism by which ELMOD2 plays a role in ARF6 recruitment to the midbody (and how ELMOD2 itself recruits to the midbody) requires further exploration. Despite the lack of specific ELMOD2 staining at recycling endosomes, we cannot exclude the possibility that it also can be recruited to recycling endosomes. As suggested above, the close physical proximity of these recycling endosomes to the PCM might allow for transient protein interactions that do not survive fixation.

While RAB11 staining was reduced, we saw the opposite changes in ARF6 staining at FIP3 positive recycling endosomes in response to deletion of ELMOD2; ARF6 was strongly increased (Figure 6). The order and specific interactions involved in recruitment of FIP3, RAB11, and ARF6 to recycling endosomes is unresolved, though FIP3 can bind to RAB11 and ARF6 and potentially even at the same time, based on *in vitro* binding assays (Fielding et al., 2005; Schonteich et al., 2007; Shiba et al., 2006; Takahashi et al., 2011). Our data support a role for ELMOD2 in this process. Fielding, *et al* (Fielding et al., 2005) also showed staining of ARF6 at the ICB but not at the Flemming body. In contrast, we found ARF6 at the Flemming body but not evident at the ICB. Much (though not all) of the evidence that ARF6 localizes to the ICB in this earlier study was obtained using ARF6[Q71L] and thus may result in trapping of the mutant that is incapable of cycling between active and inactive conformations. Expression of FIP3-GFP in WT cells allows visualization of the pericentrosomal pool of recycling endosomes, and that stains strongly for RAB11 but not for ARF6 (Figure 6). ELMOD2 deletion hampers the recruitment of FIP3 to these endosome clusters, causes a severe loss of RAB11 staining there, and is accompanied by large increases in ARF6. However, when FIP3 staining is diffuse and FIP3-GFP positive endosomes are no longer evident, ARF6 also does not localize to endosomal clusters. Thus, we interpret these findings as consistent with a model in which ARF6 is recruited to recycling endosomes by FIP3 and competes for this binding with RAB11. The presence of ELMOD2 in WT cells at or nearby this site may result in rapid inactivation of ARF6 and favor the binding of RAB11 to FIP3.

Because the binding of RAB11 or ARF6 to FIP3 is dependent on activation (GTP-binding), there are two likely ways that ELMOD2 might increase RAB11 and decrease ARF6 at recycling endosomes: it could recruit a RAB11 GEF or act as an ARF6 GAP. Given the established activity of ELMOD2 as an ARF/ARL GAP, we clearly favor the latter of these and conclude that the

deletion of ELMOD2 causes ARF6 to accumulate on recycling endosome by decreasing the cell's ability to inactivate the GTPase there. That increase in ARF6 competes effectively with RAB11 for the binding to FIP3. It is not clear whether ELMOD2 might have some additional effect resulting in the loss in FIP3 recruitment to recycling endosomes. It could be the case that FIP3 is more stably bound at this site when complexed with RAB11 than to ARF6. The strong and specific effects of activated ARF6 to reverse the multinucleation and supernumerary centrosome phenotypes (Figure 6) in ELMOD2 are consistent with those phenotypes being linked.

Because of the central role of microtubules in the mitotic spindle and cell division, we expected to find close ties between the cytokinesis failure and the changes in microtubules observed, but instead we interpret our findings as evidence of two different roles for ELMOD2 in cells and acting with two different GTPases. While ARF6 is capable of influencing actin at the cell surface (D'Souza-Schorey and Chavrier, 2006), there are no published links between ARF6 and microtubules/tubulins. ARL2, though, has well documented roles in assembly of the αβ-tubulin heterodimer and in altering microtubule networks when over-activate; *e.g.*, upon expression of the dominant activated mutant ARL2[Q70L] (Zhou et al., 2006). Indeed, decreased stability of microtubules and increased sensitivity to microtubule destabilizing drugs were among the first phenotypes found for mutants of ARL2 in multiple genetic model systems (Antoshechkin and Han, 2002; Hoyt et al., 1990; Stearns et al., 1990; Steinborn et al., 2002). The fact that we first purified ELMOD2 as a GAP for ARL2 also prompted us to focus on this GTPase as likely to be playing a central role in the microtubule defects seen in ELMOD2 null cells. The specificity of rescue by activated ARL2 but not ARL3 or ARF6 further supports it acting with ARL2 here. We currently model the actions of ELMOD2 in cells, specifically in microtubule stability and cytokinesis, as acting in distinct pathways that use distinct ARF family GTPases. Consistent with this, we

observed no clear evidence of a defect in mitotic spindles or midbody bridge morphology in the nulls, based on α-tubulin or γ-tubulin staining, suggesting that any cytokinesis defects we observe are not an overt consequence of ELMOD2-related microtubule instability. Our results are similar though different from Zhou, et al (Zhou et al., 2017) in which they found aneuploidy in mouse oocytes knocked down for ELMOD2 but with "severe abnormalities in spindle organization" that we did not observe in null cells. Furthermore, fast cycling ARL2 only partially rescued cell cycle-related defects, and active ARF6 did not rescue the microtubule defects. Thus, despite our original conjecture that the microtubule and cell cycle related phenotypes may result from a single lesion arising from the absence of ELMOD2, our data clearly argue for at least two distinct lesions each of which can be mitigated through increased activation of distinct GTPases.

This study also describes for the first time the use of multiple "fast cycling" mutants for ARF family GTPases, first described by Lorraine Santy for ARF6 (Santy, 2002) and later employed by others for multiple family members (D'Souza et al., 2020; Moravec et al., 2012). This and structural studies have confirmed the conserved function of homologous residues in the GTP binding pocket in making direct contacts with the guanine base. Mutations that decrease this interaction result in weakened affinity for GDP and thus increase the rate limiting step in GTPase activation: release of GDP. These mutants provide an important adjunct to the common use of glutamine mutants (*e.g.*, Q70L in ARL2) that are also activating in cells. The stronger Q to L mutants may be so strong as to generate phenotypes that obscure or make analyses of other actions unfeasible. This is particularly problematic when studying a regulator of the GTPase that acts at multiple sites and with multiple GTPases. We believe this is the case with ARL2[Q70L], further demonstrating the value of fast cycling mutants.

Similarly novel, and perhaps confusing, is the use of activated GTPase mutants to rescue the deletion of a GAP. Clearly, in this use the "rescuing GTPase" cannot be acting as the substrate for the deleted GAP (ELMOD2). In such a case where a GEF activates the GTPase and the GAP silences that activity, one should not see "rescue" by further increasing the activity of the GTPase in question. Instead, we are speculating that rescue is achieved in one of two, not mutually exclusive, ways. Our preferred hypothesis is that the pathways in question are acting as GTPase networks such as those described by Mizuno-Yamasaki, et al (Mizuno-Yamasaki et al., 2012). In this scenario, an activated GTPase recruits its own GAP and effectors, and one of those effectors also possesses GEF activity for another GTPase acting downstream of the first. Thus, if activated ARF6 or ARL2 rescues a defect observed upon deletion of ELMOD2, we are not concluding in either case that ELMOD2 normally acts as a GAP on the GTPase in that pathway and location. Rather, we propose that those GTPases share a common pathway with ELMOD2 but instead act downstream. Yet, we cannot exclude the possibility that the same GTPase *also* acts upstream of ELMOD2. For example, a number of the ARF family GTPases that ELMOD2 acts on *in vitro* (including ARF1, ARF3, and ARF6) have been shown previously to regulate aspects of cytokinesis and to localize to key sites in this process (*e.g.* centrosomes, cleavage furrows, and midbodies (D'Souza-Schorey and Chavrier, 2006; Hanai et al., 2016)). Further research should be devoted to finding which GTPase(s) ELMOD2 acts with directly to mediate these functions and identifying the mechanism by which it regulates both cytokinesis and γ-TuRC recruitment. The other possibility is that the cell system under study involves parallel pathways, only one of which involves ELMOD2 and the other is under regulation by the rescuing, activated GTPase. Of course, these are not mutually exclusive, pointing to the potential for complexities and the amount of work

left to do in deconvoluting mechanisms of regulation of these essential cell processes (Sztul et al., 2019).

Two other issues that we considered as having the potential to influence the interpretation of our data are the existence of two other ELMOD family members and three other ELMO proteins (East et al., 2012). Parallel studies using CRISPR/Cas9 generated deletions of ELMOD1 and ELMOD3 in MEFs have revealed none of the same phenotypes described here for ELMOD2, though they, too, are implicated in multiple processes (manuscript in preparation). Though quantification of these three proteins is difficult because of their low abundance, we used qRT-PCR in that study and found no evidence of up-regulation of other ELMOD family members in response to deletion of any one. Thus, we do not believe the results described here are explained by changes in activities of ELMOD1 or ELMOD3, though of course cannot exclude some level of functional redundancy or actions of either protein in microtubule dynamics or cell division. In addition, ELMO proteins share the ELMO domain with the ELMODs and are found in cells bound to DOCK proteins (*e.g.*, DOCK180) that possess RAC/RHO GEF activity (Brugnera et al., 2002; Gumienny et al., 2001; Lu et al., 2004). Furthermore, ARF6 and its GEF ARNO (aka Cytohesin 2) activate RAC via ELMO1/DOCK180 (Santy et al., 2005), influencing actin dynamics and cell motility. To date, there have been no studies showing functional redundancies between ELMOD and ELMO proteins. It is worth noting the existence of each, though, particularly as they share some common pathway components (*e.g.*, ARF6).

In summary, this work provides evidence for essential roles for ELMOD2 in both cytokinesis and microtubule dynamics. To our knowledge, this is the first evidence of one ARF GAP acting in cells to influence pathways involving both ARF(s) and ARL(s). The previously described (Ivanova et al., 2014) biochemical promiscuity of ELMODs as GAPs makes them prone to even

greater complexity in serving as signaling hubs to bring together disparate, but highly regulated, processes. Future studies into the mechanisms by which ELMOD2 modulates cytokinesis and microtubule stability should provide further insights into those processes as well as if and how apparently diverse pathways may communicate with one another. When these results are considered together with those demonstrating roles for ELMOD2 in mitochondrial fusion (Newman et al., 2017a; Schiavon et al., 2019), in fat metabolism at lipid droplets (Suzuki et al., 2015), and in anchorage independent growth (Figure 7), there is clearly need for further study of these pathways and their potential for inter-connections. Together, these results significantly extend the functions and locations at which ELMOD2 acts in cells, working with multiple GTPases to mediate these processes.

Acknowledgements This work was supported by NIH Grants R35GM122568 to RAK and 1F31CA236493-02 to RET. We thank colleagues for their generous sharing of key reagents: Jim Casanova (University of Virginia; ARF6 antibody and ARF6 mutant plasmids), Jim Goldenring (Vanderbilt University; FIP3 plasmid and antibody), and Ryoko Kuriyama (University of Minnesota, MKLP1 antibodies). This research was supported in part by the Emory University Integrated Cellular Imaging (ICI) Microscopy Core and Emory Viral Vector Core of the Emory Neuroscience NINDS Core Facilities Grant 5P30NS055077. We would like to thank the Emory Biochemistry Department and Laney Graduate School for all the support and shared resources provided.

Author Contributions RET designed, performed, and analyzed experiments, and prepared figures. MPE provided critical training for CRISPR-Cas9 technologies. RP provided critical

insight into experimental design and model-building. RET and RAK developed this study and prepared the manuscript. All authors reviewed the findings and edited and approved the final version.

References

Adari, H., D.R. Lowy, B.M. Willumsen, C.J. Der, and F. McCormick. 1988. Guanosine triphosphatase activating protein (GAP) interacts with the p21 ras effector binding domain. *Science*. 240:518-521.

Agromayor, M., and J. Martin-Serrano. 2013. Knowing when to cut and run: mechanisms that control cytokinetic abscission. *Trends Cell Biol*. 23:433-441.

Antoshechkin, I., and M. Han. 2002. The C. elegans evl-20 gene is a homolog of the small GTPase ARL2 and regulates cytoskeleton dynamics during cytokinesis and morphogenesis. *Dev Cell*. 2:579-591.

Aspenstrom, P. 2018. Fast-cycling Rho GTPases. *Small GTPases*:1-8.

Beghin, A., S. Honore, C. Messana, E.L. Matera, J. Aim, S. Burlinchon, D. Braguer, and C. Dumontet. 2007. ADP ribosylation factor like 2 (Arl2) protein influences microtubule dynamics in breast cancer cells. *Exp Cell Res*. 313:473-485.

Bhamidipati, A., S.A. Lewis, and N.J. Cowan. 2000. ADP ribosylation factor-like protein 2 (Arl2) regulates the interaction of tubulin-folding cofactor D with native tubulin. *J Cell Biol*. 149:1087-1096.

Boman, A.L., J. Kuai, X. Zhu, J. Chen, R. Kuriyama, and R.A. Kahn. 1999. Arf proteins bind to mitotic kinesin-like protein 1 (MKLP1) in a GTP-dependent fashion. *Cell Motil Cytoskel*. 44:119-132.

Borowicz, S., M. Van Scoyk, S. Avasarala, M.K. Karuppusamy Rathinam, J. Tauler, R.K. Bikkavilli, and R.A. Winn. 2014. The soft agar colony formation assay. *J Vis Exp*:e51998.

Bouchoux, J., F. Beilstein, T. Pauquai, I.C. Guerrera, D. Chateau, N. Ly, M. Alqub, C. Klein, J. Chambaz, M. Rousset, J.M. Lacorte, E. Morel, and S. Demignot. 2011. The proteome of cytosolic lipid droplets isolated from differentiated Caco-2/TC7 enterocytes reveals cell-specific characteristics. *Biol Cell*. 103:499-517.

Bowzard, J.B., D. Cheng, J. Peng, and R.A. Kahn. 2007. ELMOD2 is an Arl2 GTPase-activating protein that also acts on Arfs. *J Biol Chem*. 282:17568-17580.

Brugnera, E., L. Haney, C. Grimsley, M. Lu, S.F. Walk, A.C. Tosello-Trampont, I.G. Macara, H. Madhani, G.R. Fink, and K.S. Ravichandran. 2002. Unconventional Rac-GEF activity is mediated through the Dock180-ELMO complex. *Nat Cell Biol*. 4:574-582.

Bugnard, E., K.J. Zaal, and E. Ralston. 2005. Reorganization of microtubule nucleation during muscle differentiation. *Cell Motil Cytoskeleton*. 60:1-13.

Burd, C.G., T.I. Strochlic, and S.R. Gangi Setty. 2004. Arf-like GTPases: not so Arf-like after all. *Trends Cell Biol*. 14:687-694.

Cavenagh, M.M., M. Breiner, A. Schurmann, A.G. Rosenwald, T. Terui, C. Zhang, P.A. Randazzo, M. Adams, H.G. Joost, and R.A. Kahn. 1994. ADP-ribosylation factor (ARF)-like 3, a new member of the ARF family of GTP-binding proteins cloned from human and rat tissues. *J Biol Chem*. 269:18937-18942.

Cavenagh, M.M., J.A. Whitney, K. Carroll, C. Zhang, A.L. Boman, A.G. Rosenwald, I. Mellman, and R.A. Kahn. 1996. Intracellular distribution of Arf proteins in mammalian

cells. Arf6 is uniquely localized to the plasma membrane. *J Biol Chem*. 271:21767-21774.

Chabin-Brion, K., J. Marceiller, F. Perez, C. Settegrana, A. Drechou, G. Durand, and C. Pous. 2001. The Golgi complex is a microtubule-organizing organelle. *Mol Biol Cell*. 12:2047-2060.

Chipperfield, R.G., S.S. Jones, K.M. Lo, and R.A. Weinberg. 1985. Activation of Ha-ras p21 by substitution, deletion, and insertion mutations. *Mol Cell Biol*. 5:1809-1813.

Cunningham, L.A., and R.A. Kahn. 2008. Cofactor D functions as a centrosomal protein and is required for the recruitment of the gamma-tubulin ring complex at centrosomes and organization of the mitotic spindle. *J Biol Chem*. 283:7155-7165.

D'Souza-Schorey, C., and P. Chavrier. 2006. ARF proteins: roles in membrane traffic and beyond. *Nat Rev Mol Cell Biol*. 7:347-358.

D'Souza-Schorey, C., G. Li, M.I. Colombo, and P.D. Stahl. 1995. A regulatory role for ARF6 in receptor-mediated endocytosis. *Science*. 267:1175-1178.

D'Souza-Schorey, C., E. van Donselaar, V.W. Hsu, C. Yang, P.D. Stahl, and P.J. Peters. 1998. ARF6 targets recycling vesicles to the plasma membrane: insights from an ultrastructural investigation. *J Cell Biol*. 140:603-616.

D'Souza, R.S., J.Y. Lim, A. Turgut, K. Servage, J. Zhang, K. Orth, N. Sosale, M. Lazzara, J. Allegood, and J.E. Casanova. 2020. Calcium-stimulated disassembly of focal adhesions mediated by an ORP3/IQSec1 complex. *Elife*. 9.

Donaldson, J.G., and C.L. Jackson. 2011. ARF family G proteins and their regulators: roles in membrane transport, development and disease. *Nat Rev Mol Cell Biol*. 12:362-375.

Donaldson, J.G., and H. Radhakrishna. 2001. Expression and properties of ADP-ribosylation factor (ARF6) in endocytic pathways. *Methods Enzymol*. 329:247-256.

East, M.P., J.B. Bowzard, J.B. Dacks, and R.A. Kahn. 2012. ELMO Domains, Evolutionary and Functional Characterization of a Novel GTPase-activating Protein (GAP) Domain for Arf Protein Family GTPases. *J Biol Chem*. 287:39538-39553.

East, M.P., and R.A. Kahn. 2011. Models for the functions of Arf GAPs. *Semin Cell Dev Biol*. 22:3-9.

Efimov, A., A. Kharitonov, N. Efimova, J. Loncarek, P.M. Miller, N. Andreyeva, P. Gleeson, N. Galjart, A.R. Maia, I.X. McLeod, J.R. Yates, 3rd, H. Maiato, A. Khodjakov, A. Akhmanova, and I. Kaverina. 2007. Asymmetric CLASP-dependent nucleation of noncentrosomal microtubules at the trans-Golgi network. *Dev Cell*. 12:917-930.

Fidyk, N., J.B. Wang, and R.A. Cerione. 2006. Influencing cellular transformation by modulating the rates of GTP hydrolysis by Cdc42. *Biochemistry*. 45:7750-7762.

Fielding, A.B., E. Schonteich, J. Matheson, G. Wilson, X. Yu, G.R. Hickson, S. Srivastava, S.A. Baldwin, R. Prekeris, and G.W. Gould. 2005. Rab11-FIP3 and FIP4 interact with Arf6 and the Exocyst to control membrane traffic in cytokinesis. *EMBO J*. 24:3389-3399.

Francis, J.W., D. Goswami, S.J. Novick, B.D. Pascal, E.R. Weikum, E.A. Ortlund, P.R. Griffin, and R.A. Kahn. 2017a. Nucleotide Binding to ARL2 in the TBCDARL2beta-Tubulin Complex Drives Conformational Changes in beta-Tubulin. *J Mol Biol*. 429:3696-3716.

Francis, J.W., L.E. Newman, L.A. Cunningham, and R.A. Kahn. 2017b. A Trimer Consisting of the Tubulin-specific Chaperone D (TBCD), Regulatory GTPase ARL2, and beta-Tubulin Is Required for Maintaining the Microtubule Network. *J Biol Chem*. 292:4336-4349.

Francis, J.W., R.E. Turn, L.E. Newman, C. Schiavon, and R.A. Kahn. 2016. Higher order signaling: ARL2 as regulator of both mitochondrial fusion and microtubule dynamics allows integration of 2 essential cell functions. *Small GTPases*. 7:188-196.

Frank, S.R., J.C. Hatfield, and J.E. Casanova. 1998. Remodeling of the actin cytoskeleton is coordinately regulated by protein kinase C and the ADP-ribosylation factor nucleotide exchange factor ARNO. *Mol Biol Cell*. 9:3133-3146.

Gillingham, A.K., and S. Munro. 2007. The small G proteins of the Arf family and their regulators. *Annu Rev Cell Dev Biol*. 23:579-611.

Gumienny, T.L., E. Brugnera, A.C. Tosello-Trampont, J.M. Kinchen, L.B. Haney, K. Nishiwaki, S.F. Walk, M.E. Nemergut, I.G. Macara, R. Francis, T. Schedl, Y. Qin, L. Van Aelst, M.O. Hengartner, and K.S. Ravichandran. 2001. CED-12/ELMO, a novel member of the CrkII/Dock180/Rac pathway, is required for phagocytosis and cell migration. *Cell*. 107:27-41.

Hanai, A., M. Ohgi, C. Yagi, T. Ueda, H.W. Shin, and K. Nakayama. 2016. Class I Arfs (Arf1 and Arf3) and Arf6 are localized to the Flemming body and play important roles in cytokinesis. *Journal of biochemistry*. 159:201-208.

Hickson, G.R.X., J. Matheson, B. Riggs, V.H. Maier, A.B. Fielding, R. Prekeris, W. Sullivan, F.A. Barr, and G.W. Gould. 2003. Arfophilins Are Dual Arf/Rab 11 Binding Proteins That Regulate Recycling Endosome Distribution and Are Related to Drosophila Nuclear Fallout. *Mol. Biol. Cell*. 14:2908-2920.

Hodgson, U., V. Pulkkinen, M. Dixon, M. Peyrard-Janvid, M. Rehn, P. Lahermo, V. Ollikainen, K. Salmenkivi, V. Kinnula, J. Kere, P. Tukiainen, and T. Laitinen. 2006. ELMOD2 is a candidate gene for familial idiopathic pulmonary fibrosis. *Am J Hum Genet*. 79:149-154.

Horgan, C.P., and M.W. McCaffrey. 2009. The dynamic Rab11-FIPs. *Biochem Soc Trans*. 37:1032-1036.

Hosaka, M., K. Toda, H. Takatsu, S. Torii, K. Murakami, and K. Nakayama. 1996. Structure and intracellular localization of mouse ADP-ribosylation factors type 1 to type 6 (ARF1-ARF6). *J Biochem (Tokyo)*. 120:813-819.

Hoyt, M.A., T. Stearns, and D. Botstein. 1990. Chromosome instability mutants of Saccharomyces cerevisiae that are defective in microtubule-mediated processes. *Mol Cell Biol*. 10:223-234.

Inoue, H., and P.A. Randazzo. 2007. Arf GAPs and their interacting proteins. *Traffic*. 8:1465-1475.

Ismail, S.A., Y.X. Chen, A. Rusinova, A. Chandra, M. Bierbaum, L. Gremer, G. Triola, H. Waldmann, P.I. Bastiaens, and A. Wittinghofer. 2011. Arl2-GTP and Arl3-GTP regulate a GDI-like transport system for farnesylated cargo. *Nature chemical biology*. 7:942-949.

Ivanova, A.A., M.P. East, S.L. Yi, and R.A. Kahn. 2014. Characterization of recombinant ELMOD (cell engulfment and motility domain) proteins as GTPase-activating proteins (GAPs) for ARF family GTPases. *J Biol Chem*. 289:11111-11121.

Jackson, C.L., and S. Bouvet. 2014. Arfs at a glance. *J Cell Sci*. 127:4103-4109.

Johnson, K.R., C.M. Longo-Guess, and L.H. Gagnon. 2012. Mutations of the mouse ELMO domain containing 1 gene (Elmod1) link small GTPase signaling to actin cytoskeleton dynamics in hair cell stereocilia. *PloS one*. 7:e36074.

Kahn, R.A., L. Volpicelli-Daley, B. Bowzard, P. Shrivastava-Ranjan, Y. Li, C. Zhou, and L. Cunningham. 2005. Arf family GTPases: roles in membrane traffic and microtubule dynamics. *Biochem Soc Trans*. 33:1269-1272.

Klinger, C.M., A. Spang, J.B. Dacks, and T.J. Ettema. 2016. Tracing the Archaeal Origins of Eukaryotic Membrane-Trafficking System Building Blocks. *Molecular biology and evolution*. 33:1528-1541.

Kuriyama, R., S. Dragas-Granoic, T. Maekawa, A. Vassilev, A. Khodjakov, and H. Kobayashi. 1994. Heterogeneity and microtubule interaction of the CHO1 antigen, a mitosis-specific kinesin-like protein. Analysis of subdomains expressed in insect sf9 cells. *J Cell Sci*. 107 (Pt 12):3485-3499.

Li, W., Y. Feng, A. Chen, T. Li, S. Huang, J. Liu, X. Liu, Y. Liu, J. Gao, D. Yan, J. Sun, L. Mei, X. Liu, and J. Ling. 2019. Elmod3 knockout leads to progressive hearing loss and abnormalities in cochlear hair cell stereocilia. *Hum Mol Genet*. 28:4103-4112.

Li, W., J. Sun, J. Ling, J. Li, C. He, Y. Liu, H. Chen, M. Men, Z. Niu, Y. Deng, M. Li, T. Li, J. Wen, S. Sang, H. Li, Z. Wan, E.M. Richard, P. Chapagain, D. Yan, X.Z. Liu, L. Mei, and Y. Feng. 2018. ELMOD3, a novel causative gene, associated with human autosomal dominant nonsyndromic and progressive hearing loss. *Human genetics*. 137:329-342.

Li, Y., W.G. Kelly, J.M. Logsdon, Jr., A.M. Schurko, B.D. Harfe, K.L. Hill-Harfe, and R.A. Kahn. 2004. Functional genomic analysis of the ADP-ribosylation factor family of GTPases: phylogeny among diverse eukaryotes and function in C. elegans. *FASEB J*. 18:1834-1850.

Lin, R., S. Bagrodia, R. Cerione, and D. Manor. 1997. A novel Cdc42Hs mutant induces cellular transformation. *Curr Biol*. 7:794-797.

Lin, R., R.A. Cerione, and D. Manor. 1999. Specific contributions of the small GTPases Rho, Rac, and Cdc42 to Dbl transformation. *J Biol Chem*. 274:23633-23641.

Loi, E., L. Moi, S. Blois, E. Bacchelli, A.F. Vega Benedetti, C. Cameli, R. Fadda, E. Maestrini, M. Carta, G. Doneddu, and P. Zavattari. 2019. ELMOD3-SH2D6 gene fusion as a possible co-star actor in autism spectrum disorder scenario. *Journal of cellular and molecular medicine*.

Lu, M., J.M. Kinchen, K.L. Rossman, C. Grimsley, C. deBakker, E. Brugnera, A.C. Tosello-Trampont, L.B. Haney, D. Klingele, J. Sondek, M.O. Hengartner, and K.S. Ravichandran. 2004. PH domain of ELMO functions in trans to regulate Rac activation via Dock180. *Nat Struct Mol Biol*. 11:756-762.

Makyio, H., M. Ohgi, T. Takei, S. Takahashi, H. Takatsu, Y. Katoh, A. Hanai, T. Ueda, Y. Kanaho, Y. Xie, H.W. Shin, H. Kamikubo, M. Kataoka, M. Kawasaki, R. Kato, S. Wakatsuki, and K. Nakayama. 2012. Structural basis for Arf6-MKLP1 complex formation on the Flemming body responsible for cytokinesis. *EMBO J*. 31:2590-2603.

McElver, J., D. Patton, M. Rumbaugh, C. Liu, L.J. Yang, and D. Meinke. 2000. The TITAN5 gene of Arabidopsis encodes a protein related to the ADP ribosylation factor family of GTP binding proteins. *The Plant cell*. 12:1379-1392.

Miryounesi, M., S. Bahari, S. Salehpour, N. Alipour, and S. Ghafouri-Fard. 2019. ELMO Domain Containing 1 (ELMOD1) Gene Mutation Is Associated with Mental Retardation and Autism Spectrum Disorder. *Journal of molecular neuroscience : MN*. 69:312-315.

Mizuno-Yamasaki, E., F. Rivera-Molina, and P. Novick. 2012. GTPase networks in membrane traffic. *Annu Rev Biochem*. 81:637-659.

Moravec, R., K.K. Conger, R. D'Souza, A.B. Allison, and J.E. Casanova. 2012. BRAG2/GEP100/IQSec1 interacts with clathrin and regulates alpha5beta1 integrin

endocytosis through activation of ADP ribosylation factor 5 (Arf5). *J Biol Chem*. 287:31138-31147.

Muromoto, R., Y. Sekine, S. Imoto, O. Ikeda, T. Okayama, N. Sato, and T. Matsuda. 2008. BART is essential for nuclear retention of STAT3. *International immunology*. 20:395-403.

Nahse, V., L. Christ, H. Stenmark, and C. Campsteijn. 2017. The Abscission Checkpoint: Making It to the Final Cut. *Trends Cell Biol*. 27:1-11.

Nakayama, K. 2016. Regulation of cytokinesis by membrane trafficking involving small GTPases and the ESCRT machinery. *Critical reviews in biochemistry and molecular biology*. 51:1-6.

Newman, L.E., C.R. Schiavon, R.E. Turn, and R.A. Kahn. 2017a. The ARL2 GTPase regulates mitochondrial fusion from the intermembrane space. *Cellular logistics*. 7:e1340104.

Newman, L.E., C.R. Schiavon, C. Zhou, and R.A. Kahn. 2017b. The abundance of the ARL2 GTPase and its GAP, ELMOD2, at mitochondria are modulated by the fusogenic activity of mitofusins and stressors. *PloS one*. 12:e0175164.

Newman, L.E., C.J. Zhou, S. Mudigonda, A.L. Mattheyses, E. Paradies, C.M. Marobbio, and R.A. Kahn. 2014. The ARL2 GTPase is required for mitochondrial morphology, motility, and maintenance of ATP levels. *PloS one*. 9:e99270.

Nie, Z., D.S. Hirsch, and P.A. Randazzo. 2003. Arf and its many interactors. *Curr Opin Cell Biol*. 15:396-404.

Nithianantham, S., S. Le, E. Seto, W. Jia, J. Leary, K.D. Corbett, J.K. Moore, and J. Al-Bassam. 2015. Tubulin cofactors and Arl2 are cage-like chaperones that regulate the soluble alphabeta-tubulin pool for microtubule dynamics. *eLife*. 4.

Peterman, E., and R. Prekeris. 2019. The postmitotic midbody: Regulating polarity, stemness, and proliferation. *J Cell Biol*. 218:3903-3911.

Petry, S., and R.D. Vale. 2015. Microtubule nucleation at the centrosome and beyond. *Nat Cell Biol*. 17:1089-1093.

Price, H.P., A. Peltan, M. Stark, and D.F. Smith. 2010. The small GTPase ARL2 is required for cytokinesis in Trypanosoma brucei. *Mol Biochem Parasitol*. 173:123-131.

Prigent, M., T. Dubois, G. Raposo, V. Derrien, D. Tenza, C. Rosse, J. Camonis, and P. Chavrier. 2003. ARF6 controls post-endocytic recycling through its downstream exocyst complex effector. *J Cell Biol*. 163:1111-1121.

Pulkkinen, V., S. Bruce, J. Rintahaka, U. Hodgson, T. Laitinen, H. Alenius, V.L. Kinnula, M. Myllarniemi, S. Matikainen, and J. Kere. 2010. ELMOD2, a candidate gene for idiopathic pulmonary fibrosis, regulates antiviral responses. *FASEB J*. 24:1167-1177.

Radcliffe, P.A., L. Vardy, and T. Toda. 2000. A conserved small GTP-binding protein Alp41 is essential for the cofactor-dependent biogenesis of microtubules in fission yeast. *FEBS Lett*. 468:84-88.

Radhakrishna, H., and J.G. Donaldson. 1997. ADP-ribosylation factor 6 regulates a novel plasma membrane recycling pathway. *J Cell Biol*. 139:49-61.

Randazzo, P.A., H. Inoue, and S. Bharti. 2007. Arf GAPs as regulators of the actin cytoskeleton. *Biol Cell*. 99:583-600.

Reinstein, J., I. Schlichting, M. Frech, R.S. Goody, and A. Wittinghofer. 1991. p21 with a phenylalanine 28----leucine mutation reacts normally with the GTPase activating protein GAP but nevertheless has transforming properties. *J Biol Chem*. 266:17700-17706.

Rios, R.M. 2014. The centrosome-Golgi apparatus nexus. *Philos Trans R Soc Lond B Biol Sci*. 369.

Sankaran, S., L.M. Starita, A.C. Groen, M.J. Ko, and J.D. Parvin. 2005. Centrosomal microtubule nucleation activity is inhibited by BRCA1-dependent ubiquitination. *Mol Cell Biol*. 25:8656-8668.

Santy, L.C. 2002. Characterization of a Fast Cycling ADP-ribosylation Factor 6 Mutant. *J Biol Chem*. 277:40185-40188.

Santy, L.C., K.S. Ravichandran, and J.E. Casanova. 2005. The DOCK180/Elmo complex couples ARNO-mediated Arf6 activation to the downstream activation of Rac1. *Curr Biol*. 15:1749-1754.

Schiavon, C.R., M.E. Griffin, M. Pirozzi, R. Parashuraman, W. Zhou, H.A. Jinnah, D. Reines, and R.A. Kahn. 2018. Compositional complexity of rods and rings. *Mol Biol Cell*. 29:2303-2316.

Schiavon, C.R., R.E. Turn, L.E. Newman, and R.A. Kahn. 2019. ELMOD2 regulates mitochondrial fusion in a mitofusin-dependent manner, downstream of ARL2. *Mol Biol Cell*. 30:1198-1213.

Schiel, J.A., G.C. Simon, C. Zaharris, J. Weisz, D. Castle, C.C. Wu, and R. Prekeris. 2012. FIP3-endosome-dependent formation of the secondary ingression mediates ESCRT-III recruitment during cytokinesis. *Nat Cell Biol*. 14:1068-1078.

Schlacht, A., K. Mowbrey, M. Elias, R.A. Kahn, and J.B. Dacks. 2013. Ancient Complexity, Opisthokont Plasticity, and Discovery of the 11th Subfamily of Arf GAP Proteins. *Traffic*. 14:636-649.

Schonteich, E., M. Pilli, G.C. Simon, H.T. Matern, J.R. Junutula, D. Sentz, R.K. Holmes, and R. Prekeris. 2007. Molecular characterization of Rab11-FIP3 binding to ARF GTPases. *Eur J Cell Biol*. 86:417-431.

Schweitzer, J.K., and C. D'Souza-Schorey. 2002. Localization and Activation of the ARF6 GTPase during Cleavage Furrow Ingression and Cytokinesis. *J Biol Chem*. 277:27210-27216.

Schweitzer, J.K., and C. D'Souza-Schorey. 2005. A requirement for ARF6 during the completion of cytokinesis. *Exp Cell Res*. 311:74-83.

Schweitzer, J.K., A.E. Sedgwick, and C. D'Souza-Schorey. 2011. ARF6-mediated endocytic recycling impacts cell movement, cell division and lipid homeostasis. *Semin Cell Dev Biol*. 22:39-47.

Seixas, E., M. Barros, M.C. Seabra, and D.C. Barral. 2013. Rab and Arf proteins in genetic diseases. *Traffic*. 14:871-885.

Sharer, J.D., and R.A. Kahn. 1999. The ARF-like 2 (ARL2)-binding protein, BART. Purification, cloning, and initial characterization. *J Biol Chem*. 274:27553-27561.

Sharer, J.D., J.F. Shern, H. Van Valkenburgh, D.C. Wallace, and R.A. Kahn. 2002. ARL2 and BART enter mitochondria and bind the adenine nucleotide transporter. *Mol Biol Cell*. 13:71-83.

Shiba, T., H. Koga, H.W. Shin, M. Kawasaki, R. Kato, K. Nakayama, and S. Wakatsuki. 2006. Structural basis for Rab11-dependent membrane recruitment of a family of Rab11-interacting protein 3 (FIP3)/Arfophilin-1. *Proc Natl Acad Sci U S A*. 103:15416-15421.

Shultz, T., M. Shmuel, T. Hyman, and Y. Altschuler. 2008. Beta-tubulin cofactor D and ARL2 take part in apical junctional complex disassembly and abrogate epithelial structure. *FASEB J*. 22:168-182.

Song, J., Z. Khachikian, H. Radhakrishna, and J.G. Donaldson. 1998. Localization of endogenous ARF6 to sites of cortical actin rearrangement and involvement of ARF6 in cell spreading. *J Cell Sci*. 111 (Pt 15):2257-2267.

Spang, A., Y. Shiba, and P.A. Randazzo. 2010. Arf GAPs: gatekeepers of vesicle generation. *FEBS Lett*. 584:2646-2651.

Stearns, T., M.A. Hoyt, and D. Botstein. 1990. Yeast mutants sensitive to antimicrotubule drugs define three genes that affect microtubule function. *Genetics*. 124:251-262.

Steinborn, K., C. Maulbetsch, B. Priester, S. Trautmann, T. Pacher, B. Geiges, F. Kuttner, L. Lepiniec, Y.D. Stierhof, H. Schwarz, G. Jurgens, and U. Mayer. 2002. The Arabidopsis PILZ group genes encode tubulin-folding cofactor orthologs required for cell division but not cell growth. *Genes Dev*. 16:959-971.

Suzuki, M., T. Murakami, J. Cheng, H. Kano, M. Fukata, and T. Fujimoto. 2015. ELMOD2 is anchored to lipid droplets by palmitoylation and regulates adipocyte triglyceride lipase recruitment. *Mol Biol Cell*. 26:2333-2342.

Sztul, E., P.W. Chen, J.E. Casanova, J. Cherfils, J.B. Dacks, D.G. Lambright, F.S. Lee, P.A. Randazzo, L.C. Santy, A. Schurmann, I. Wilhelmi, M.E. Yohe, and R.A. Kahn. 2019. ARF GTPases and their GEFs and GAPs: concepts and challenges. *Mol Biol Cell*. 30:1249-1271.

Takahashi, S., T. Takei, H. Koga, H. Takatsu, H.W. Shin, and K. Nakayama. 2011. Distinct roles of Rab11 and Arf6 in the regulation of Rab11-FIP3/arfophilin-1 localization in mitotic cells. *Genes to cells : devoted to molecular & cellular mechanisms*. 16:938-950.

Tassin, A.M., B. Maro, and M. Bornens. 1985a. Fate of microtubule-organizing centers during myogenesis in vitro. *J Cell Biol*. 100:35-46.

Tassin, A.M., M. Paintrand, E.G. Berger, and M. Bornens. 1985b. The Golgi apparatus remains associated with microtubule organizing centers during myogenesis. *J Cell Biol*. 101:630-638.

Tian, G., Y. Huang, H. Rommelaere, J. Vandekerckhove, C. Ampe, and N.J. Cowan. 1996. Pathway leading to correctly folded beta-tubulin. *Cell*. 86:287-296.

Tian, G., S. Thomas, and N.J. Cowan. 2010. Effect of TBCD and its regulatory interactor Arl2 on tubulin and microtubule integrity. *Cytoskeleton (Hoboken)*. 67:706-714.

Tulu, U.S., C. Fagerstrom, N.P. Ferenz, and P. Wadsworth. 2006. Molecular requirements for kinetochore-associated microtubule formation in mammalian cells. *Curr Biol*. 16:536-541.

Ueda, T., A. Hanai, T. Takei, K. Kubo, M. Ohgi, H. Sakagami, S. Takahashi, H.W. Shin, and K. Nakayama. 2013. EFA6 activates Arf6 and participates in its targeting to the Flemming body during cytokinesis. *FEBS Lett*. 587:1617-1623.

Van Valkenburgh, H., J.F. Shern, J.D. Sharer, X. Zhu, and R.A. Kahn. 2001. ADP-ribosylation factors (ARFs) and ARF-like 1 (ARL1) have both specific and shared effectors: characterizing ARL1-binding proteins. *J Biol Chem*. 276:22826-22837.

Vitali, T., S. Girald-Berlingeri, P.A. Randazzo, and P.W. Chen. 2017. Arf GAPs: A family of proteins with disparate functions that converge on a common structure, the integrin adhesion complex. *Small GTPases*:1-9.

Watzlich, D., I. Vetter, K. Gotthardt, M. Miertzschke, Y.X. Chen, A. Wittinghofer, and S. Ismail. 2013. The interplay between RPGR, PDEdelta and Arl2/3 regulate the ciliary targeting of farnesylated cargo. *EMBO Rep*. 14:465-472.

Wilson, G.M., A.B. Fielding, G.C. Simon, X. Yu, P.D. Andrews, R.S. Hames, A.M. Frey, A.A. Peden, G.W. Gould, and R. Prekeris. 2005. The FIP3-Rab11 protein complex regulates recycling endosome targeting to the cleavage furrow during late cytokinesis. *Mol Biol Cell*. 16:849-860.

Wu, J., and A. Akhmanova. 2017. Microtubule-Organizing Centers. *Annu Rev Cell Dev Biol*. 33:51-75.

Zhang, C.J., J.B. Bowzard, A. Anido, and R.A. Kahn. 2003. Four ARF GAPs in Saccharomyces cerevisiae have both overlapping and distinct functions. *Yeast*. 20:315-330.

Zhang, C.J., M.M. Cavenagh, and R.A. Kahn. 1998. A family of Arf effectors defined as suppressors of the loss of Arf function in the yeast Saccharomyces cerevisiae. *J Biol Chem*. 273:19792-19796.

Zhang, C.J., A.G. Rosenwald, M.C. Willingham, S. Skuntz, J. Clark, and R.A. Kahn. 1994. Expression of a dominant allele of human ARF1 inhibits membrane traffic in vivo. *J Cell Biol*. 124:289-300.

Zhou, C., L. Cunningham, A.I. Marcus, Y. Li, and R.A. Kahn. 2006. Arl2 and Arl3 regulate different microtubule-dependent processes. *Mol Biol Cell*. 17:2476-2487.

Zhou, C.X., L.Y. Shi, R.C. Li, Y.H. Liu, B.Q. Xu, J.W. Liu, B. Yuan, Z.X. Yang, X.Y. Ying, and D. Zhang. 2017. GTPase-activating protein Elmod2 is essential for meiotic progression in mouse oocytes. *Cell Cycle*. 16:852-860.

Zhu, X., and I. Kaverina. 2013. Golgi as an MTOC: making microtubules for its own good. *Histochem Cell Biol*. 140:361-367.

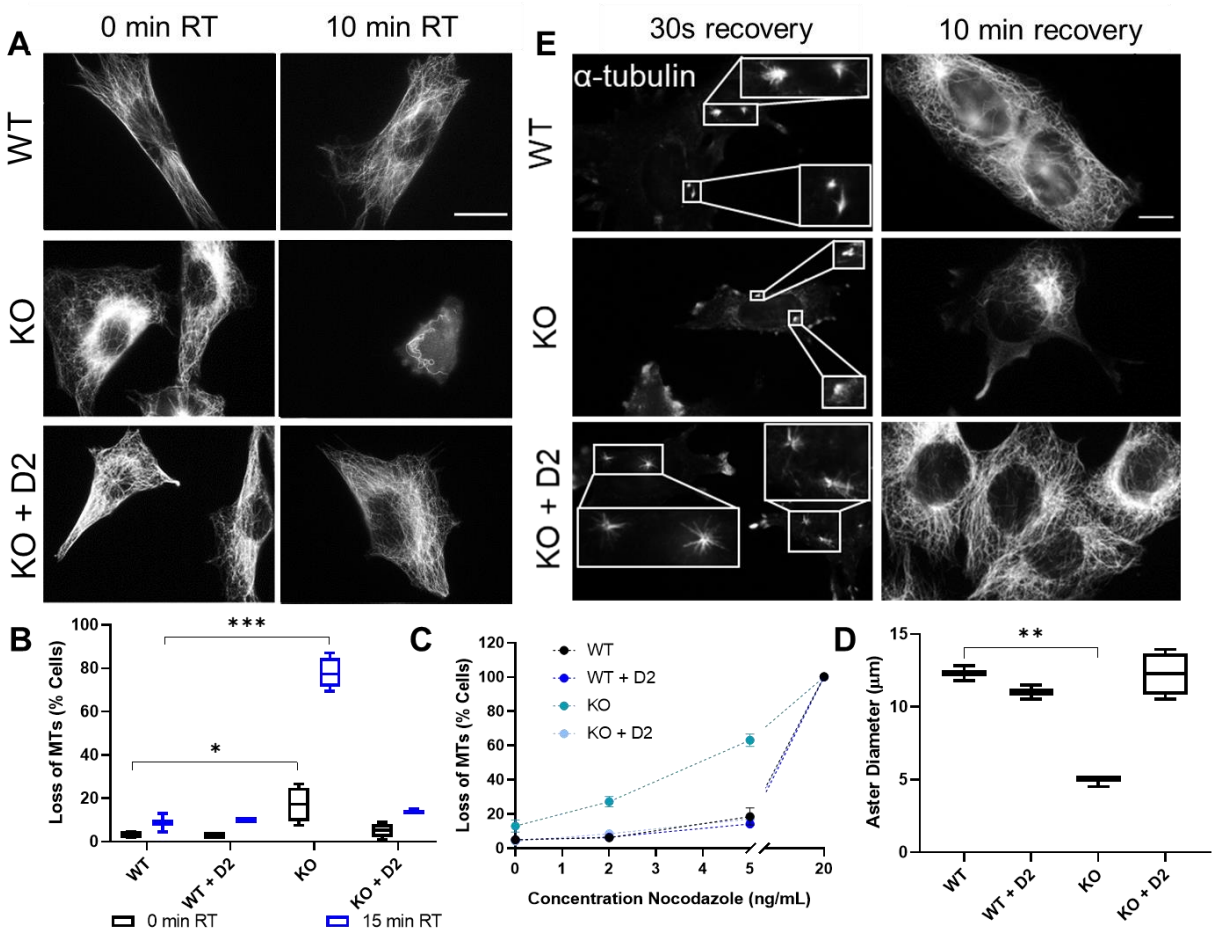

Figure 1: **Loss of ELMOD2 leads to decreased microtubule stability.** (**A**) Microtubules in ELMOD2 null MEFs display increased cold sensitivity compared to WT cells. Cells grown at the same densities were fixed either immediately after removal from the incubator (left panels) or after 15 min at room temperature (~23°C; right panels), before staining for α-tubulin. Representative images collected via widefield microscopy at 100x magnification are shown. Scale bar = 10 µm. (**B**) Our 12 standard lines imaged as described in A and scored for obvious loss in microtubule densities, as described under Materials and Methods. For each cell line, 100 cells were scored in duplicate and averaged. WT, N=2 lines; WT + D2 (WT cells expressing ELMOD2-myc) N=2; KO (ELMOD2 nulls), N=4; KO + D2 (ELMOD2 nulls expressing ELMOD2-myc), N=4. Statistical significance was assessed using Two-Way ANOVA; *=p<0.05; ***=p<0.0001. (**C**) ELMOD2 KO

lines show increased sensitivity to nocodazole. The effects of increasing concentrations of nocodazole (0-100 ng/mL) on microtubule networks are shown for the different cell lines. Cells were stained for α-tubulin and scored for microtubule networks. Error bars represent the standard error of the mean (SEM), after scoring 100 cells in duplicate. Two-Way ANOVA statistical analysis reveals that KO cells have significantly ($p<0.0001$) increased nocodazole sensitivity at 2 ng/mL and 5 ng/mL. WT, N=2 lines; WT + D2 (WT cells expressing ELMOD2-myc) N=2; KO (ELMOD2 nulls), N=4; KO + D2 (ELMOD2 nulls expressing ELMOD2-myc), N=4. (**D**) Aster formation is delayed in ELMOD2 null MEFs after nocodazole washout. Cells were incubated with nocodazole (50 ng/mL) for 2 hrs, drug was washed out, and cells were fixed 30 sec later and stained for α-tubulin and γ-tubulin (not shown). Cells were imaged at 100x magnification on a widefield microscope, and images were taken of random fields of cells. A minimum of 50 asters were imaged for each of the 11 lines tested (N= 2 WT, 2 WT + D2, 3 KO, 4 KO + D2) in duplicates. Aster diameters were measured via Fiji software. Note that differences in KO lines are larger than they appear in this graph, as we did not score α-tubulin-negative centrosome staining at this early time point after release from drug; these were clearly more numerous in KO lines. (**E**) Asters were imaged at either 30 sec or 10 min after washout of nocodazole, as described in panel D. Asters are boxed and shown at higher magnification for ready comparison. Statistical significance was assessed using One-Way ANOVA; **=$p<0.01$. Scale bar = 10 μm.

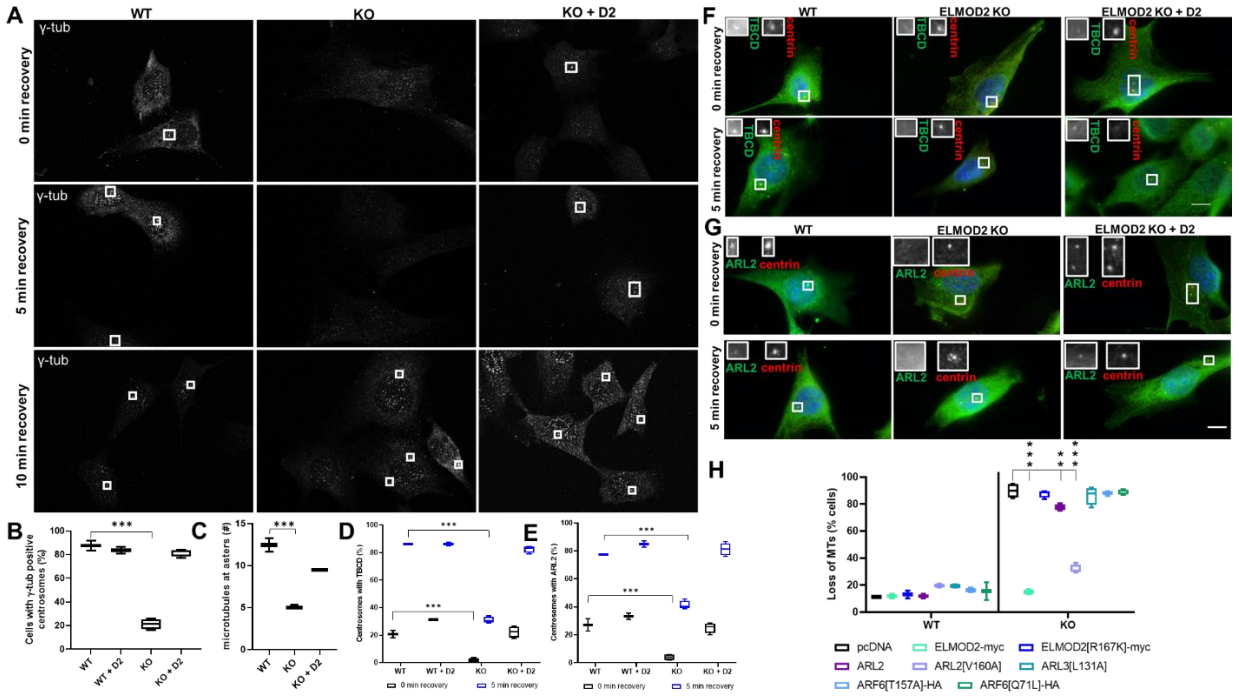

Figure 2: **ELMOD2 nulls are slow to recruit γ-TuRC, ARL2, and TBCD to centrosomes during recovery from cold.** Cells were incubated on ice for 30 min to deplete the microtubule network, then returned to 37˚C and fixed at different times during recovery before being stained for γ-tubulin to mark centrosomes. (**A**) Widefield images shown (100x magnification) are representative of the number of cells displaying γ-tubulin positive centrosomes. (**B**) Scoring of the percentage of cells with γ-tubulin positive centrosomes was performed, as described under Materials and Methods, after 5 min recovery. Statistical significance was assessed using One-Way ANOVA; ***=p<0.0001 (**C**) 2 WT, 3 KO, and 2 rescued lines were fixed after 5 min of recovery from cold and stained for α- and γ-tubulin. Z-stacks were collected. These images were analyzed using FIJI software, and the numbers of microtubules protruding from each centrosome were manually counted from each layer of the z-stack. The cut-off for what was considered a microtubule (using FIJI measuring tool) was 0.5μm. The z-section with the largest number of microtubules protruding from the centrosome was recorded, and the average of these values for

each cell line is shown, as described under Materials and Methods. Statistical significance was assessed using One-Way ANOVA; ***=p<0.0001 (**D-G**) Cells were fixed using ice-cold methanol and stained for centrin and ARL2 or TBCD, as described under Materials and Methods, at either 0 or 5 min of recovery at 37˚C from cold exposure. Widefield imaging was used to score for centrin (to mark centrosomes) and ARL2 or TBCD. (**D-E**) The standard 12 cell lines were scored in duplicate experiments with 100 cells per condition and averaged. Statistical significance was assessed using Two-Way ANOVA; ***=p<0.0001 (**F-G**) Representative widefield images at 100x magnification are shown. (**H**) Two WT and 4 ELMOD2 KO lines were transfected with either empty vector (pcDNA) or the same vector directing expression of ELMOD2-myc, ELMOD2[R167K]-myc, ARL2 ARL2[V160A], ARL3[L131A], ARF6[T157A]-HA, or ARF6[Q71L]-HA, as indicated. The next day, cells were maintained at room temperature for 15 min prior to fixation and staining for α-tubulin and either myc, ARL2, ARL3, or HA to identify transfected cells. Density of microtubule networks of transfected cells were scored in duplicate and averaged, as described under Materials and Methods. Statistical significance was assessed using One-Way ANOVA; *=p<0.05; **=p<0.01, ***=p<0.0001. Only expression of ELMOD2-myc, ARL2, or ARL2[V160A] significantly reversed microtubule cold sensitivity in KO cells.

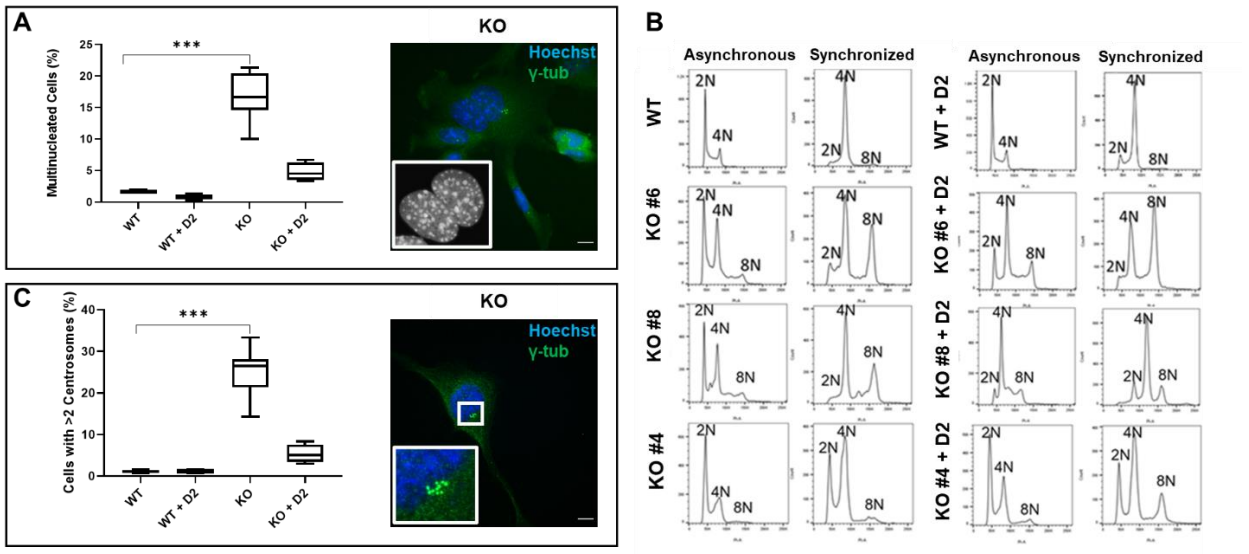

Figure 3: **Deletion of ELMOD2 causes multinucleation, supernumerary centrosomes, and polyploidy.** (**A**) Multinucleation was assessed by plating cells from 4 WT, 2 WT lines expressing ELMOD2-myc (WT+D2), 10 KO, and 4 KO lines expressing ELMOD2-myc (KO + D2), fixing the next day, staining for Hoechst to mark nuclei, and scoring the number of cells with 2 or more nuclei. Percent multinucleation was quantified in triplicate (100 cells per replicate) for all lines analyzed, with data being graphed as box-and-whisker plots. Statistical significance was assessed using One-Way ANOVA; *=p<0.05; **=p<0.01, ***=p<0.0001. A representative confocal (100x magnification, z-projection) image of ELMOD2 null (KO) cells is shown on the right. Inset shows higher magnification and in gray scale to highlight the two nuclei in the cell shown. Scale = 10 µm. (**B**) DNA content is increased in cells deleted for ELMOD2. Flow cytometry was used to quantify DNA content in at least 10,000 cells per condition, after staining with propidium iodine, as described under Materials and Methods. Both unsynchronized (left panels) and synchronized (double thymidine plus nocodazole block) (right panels) were analyzed. DNA content from WT (top panels) and three different KO lines are shown as graphs in the left set of panels. The panels on the right show the DNA content of the same four lines after transduction with ELMOD2-myc.

Graphs were generated using FloJo software, as described in Materials and Methods. (**C**) Cells plated at approximately 70% density were assessed for centrosome numbers after staining for γ-tubulin, centrin, and Hoechst. Averages of triplicate determinations for each of the lines tested are shown. Statistical significance was assessed using One-Way ANOVA; *=$p<0.05$; **=$p<0.01$, ***=$p<0.0001$. An image from a KO line, taken via confocal microscopy at 100x magnification, z-projected, is shown on the right. Scale = 10 μm.

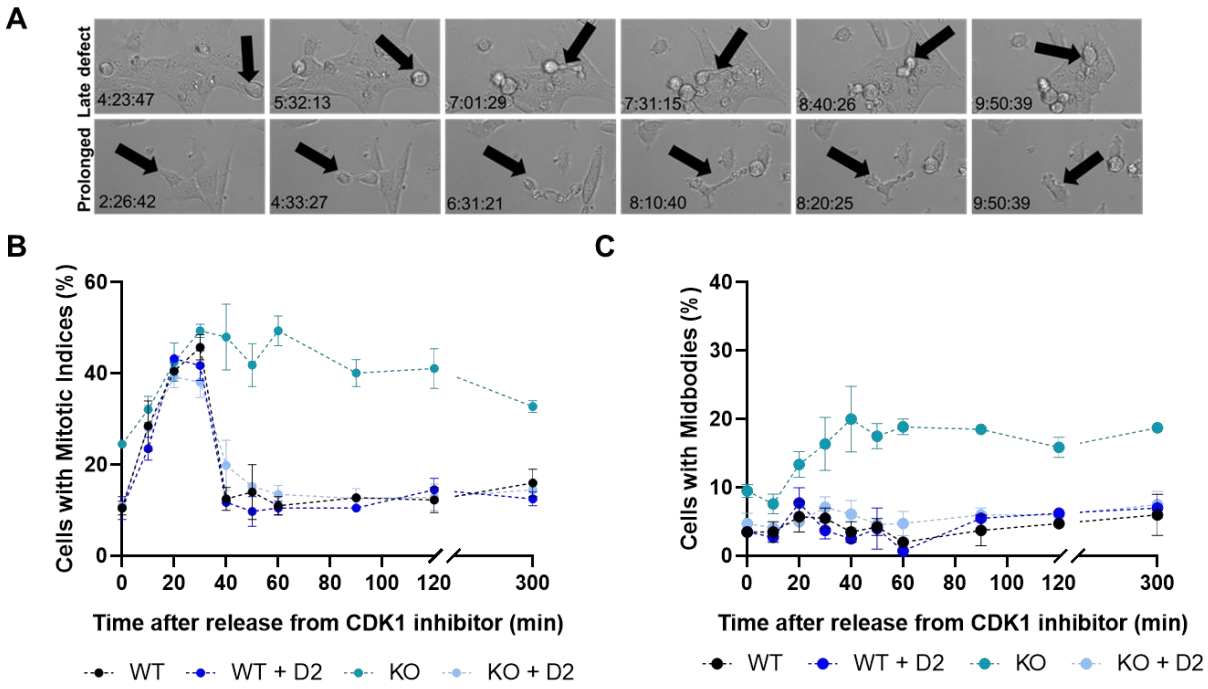

Figure 4: **ELMOD2 null cells display a prolonged cytokinesis and both early and late cytokinesis defects.** (**A**) Panels from time-lapse imaging collected from unsynchronized cells reveal cytokinesis defects in ELMOD2 nulls. Phase contrast images at 40x magnification were collected every 10 min using a Lionheart FX (BioTek) microscope. Images were selected to highlight defects observed, with time points indicated in the bottom left. (**B**) Cells were synchronized by treatment with CDK1 inhibitor (RO-3306; 7.5 µg/mL) for 18 hr; the drug was washed out, and cells were fixed at the time points indicated in the graphs. Cells were stained for α-tubulin, γ-tubulin, and Hoechst and visualized via widefield microscopy to track cells during stages of the cell cycle. Cells were binned into prophase, metaphase, anaphase, telophase, or late cytokinesis, as described in Materials and Methods (see Figure S7). These experiments were performed in triplicate, 100 cells per replicate, using the standard 12 lines. Ranging from 40-120 min after release from CDK1 inhibitor, KO cells show significantly ($p<0.0001$) increased mitotic indices compared to WT. This increase in mitotic indices persists even up to 300 min after release

($p<0.05$, measured by One-Way ANOVA). (**C**) The same samples described in panel B were scored for the presence of midbodies as markers of late cytokinesis, consistent with stalling late in cell division. Starting at 40 min after release from CDK1 inhibitor, KO lines have significantly ($p<0.01$) higher percentages of cells with midbodies than do WT (by One-Way ANOVA).

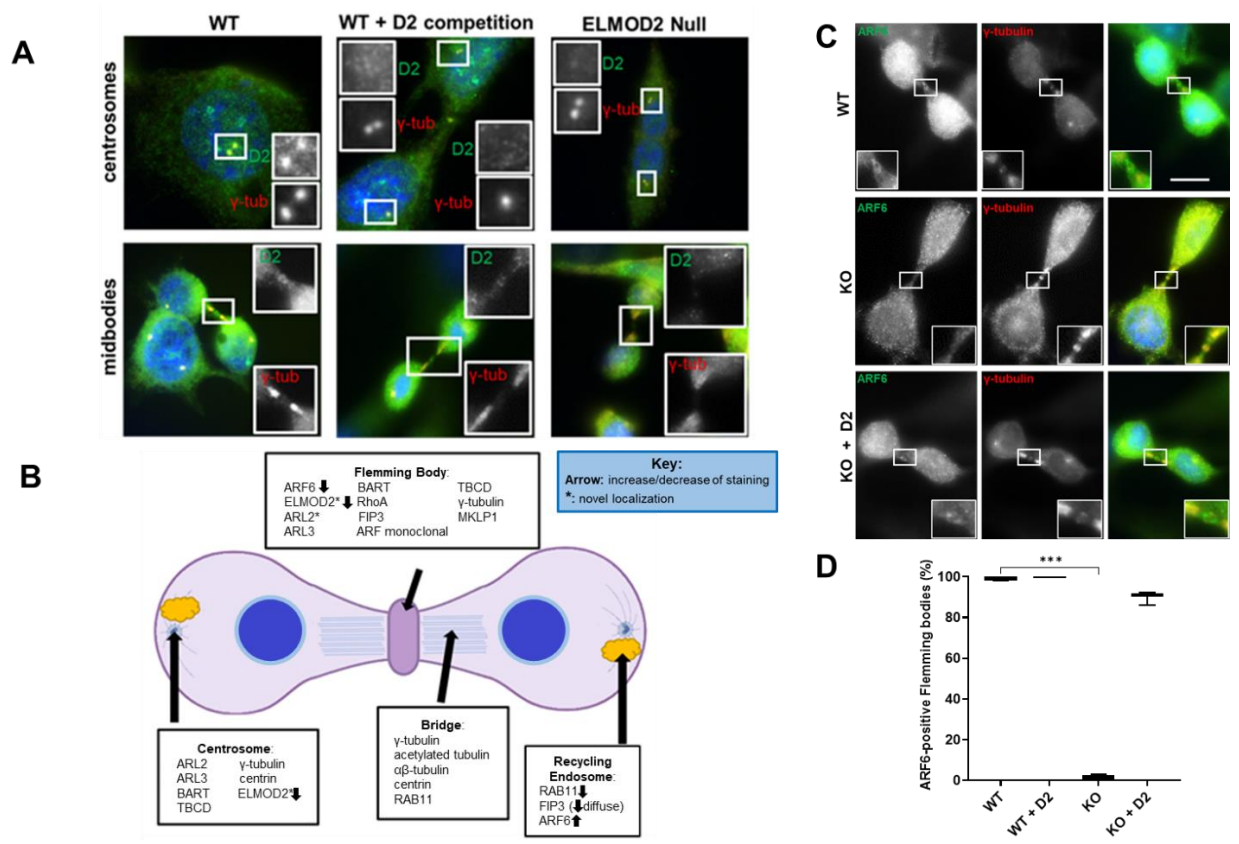

Figure 5: **ARF6, RAB11, and FIP3 are specifically altered in localization in ELMOD2 null cells.** (**A**) Localization of ELMOD2 at centrosomes (top panels) and midbodies (bottom panels) was identified via immunocytochemistry after methanol fixation (see Materials and Methods). Cells were stained for γ-tubulin (red), ELMOD2 (green), and Hoechst (blue). Antigen competition (WT + D2 competition) involved prior incubation of the ELMOD2 antibody with purified ELMOD2 protein, as described under Materials and Methods, and is shown in the center panels. Specificity of ELMOD2 staining at these sites was further supported as staining is lost in null cells, shown in panels on the right. (**B**) A summary of the 16 different markers of centrosomes, midbodies, Flemming bodies, and endosome clusters tested is shown. Black arrows indicate either increases or decreases in staining of these markers, and a black asterisk indicates a novel localization of the protein at the site indicated. (**C**) Widefield images (100x magnification) of

methanol-fixed cells stained for ARF6 and γ-tubulin reveal that ARF6 staining at midbodies is lost in null cells but is recovered upon rescue with ELMOD2-myc. Scale = 10μm. (**D**) The number of ARF6-positive Flemming bodies was quantified for 2 WT, 2 WT + D2, 4 KO, and 3 KO + D2 lines in duplicate (50 midbodies per replicate). The duplicates for each line were averaged, and results were tabulated in box-and-whisker plots in GraphPad Prism. Statistical significance was assessed using One-Way ANOVA; ***=$p<0.0001$.

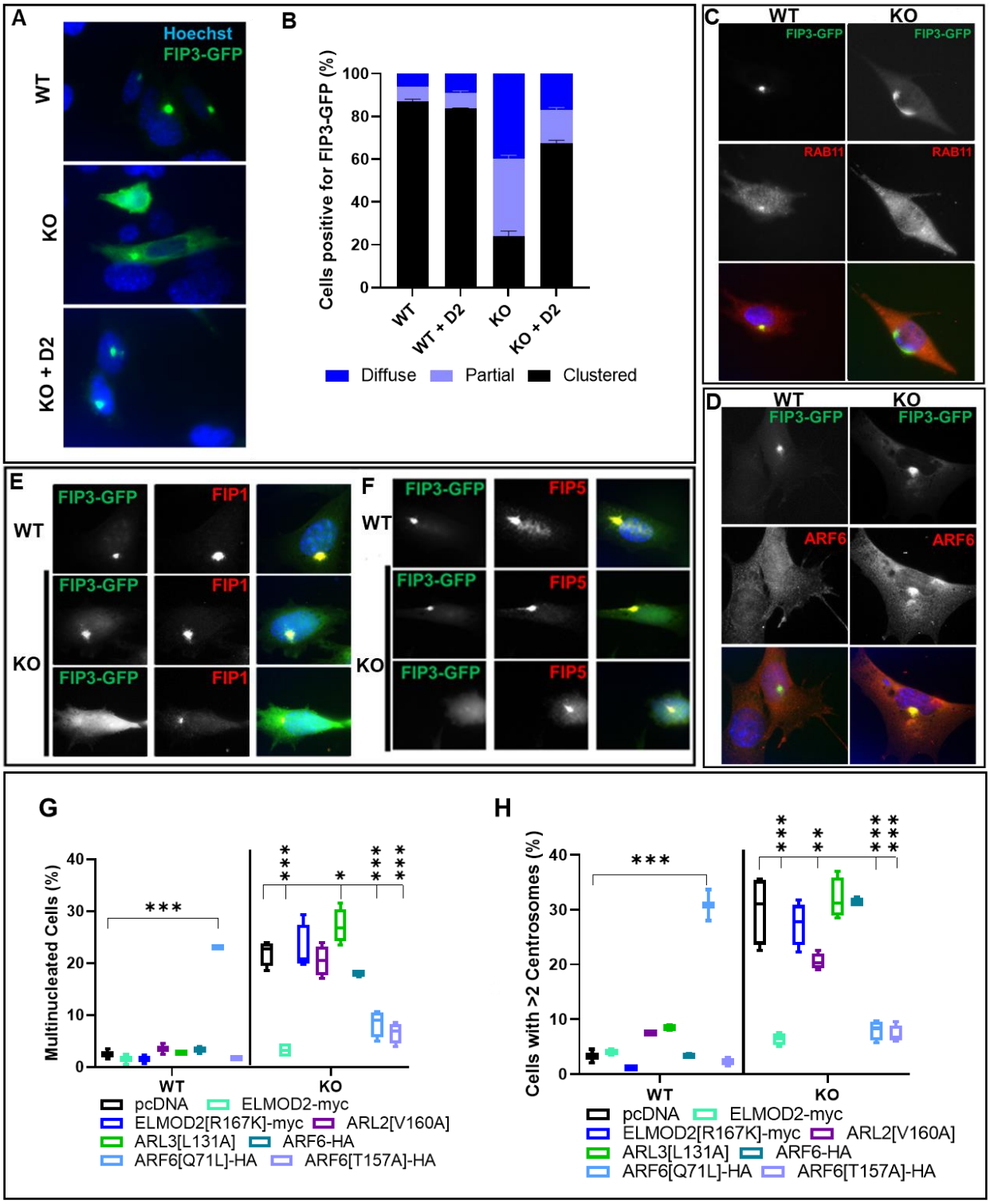

Figure 6: **ELMOD2 KO cells display decreased recruitment of FIP3-GFP, along with loss of RAB11 and increases in ARF6 at recycling endosome clusters.** (**A**) Standard lines were

transfected with FIP3-GFP (green) to visualize recycling endosome clusters. Cells were fixed with methanol and stained for Hoechst (blue), as described in Materials and Methods. Fluorescence images were collected via widefield microscopy at 100x magnification, scale = 10 μm. Note the loss of clustering (one more complete than the other) in the two cells expressing FIP3-GFP shown in the middle panel and the phenotypic reversal with expression of ELMOD2-myc (bottom panel). (**B**) The experiment described in (A) was scored in triplicate (100 cells each); results were binned into either complete clustered, partial clustered/partial diffuse, or completely diffuse staining of FIP3-GFP. Error bars represent the SEM of the cell lines scored for each genotype. Two-Way ANOVA analyses show that complete and partially diffuse FIP3-GFP staining are increased in null lines compared to WT ($p<0.0001$). (**C-F**) Representative images of 100x magnification widefield images were collected to determine co-localization of RAB11, ARF6, and FIP1/5 (each shown in red), with FIP3-GFP (green) positive clusters. Scale = 10μm. (**G-H**): GAP dead ELMOD2 cannot reverse the cytokinesis defects in ELMOD2 null cells but activated ARF6 specifically does. Cells from 2 WT and 4 KO lines were transfected with either empty vector or the same vector directing expression of ARL2[V160A], ARL3[L131A], ARF6-HA, ARF6[Q71L]-HA, ARF6[T157A]-HA, ELMOD2-myc, or ELMOD2[R167K]-myc. The next day, samples were fixed with methanol and stained for myc, γ-tubulin, and Hoechst. Multinucleation (**G**) and supernumerary centrosome (**H**) were scored in transfected cells, as described under Materials and Methods. These experiments were performed and analyzed in triplicate (100 cells per replicate), and the averages of each are shown, with lines representing the SEM. Statistical significance was assessed using One-Way ANOVA. Only the following were found to be statistically significant: ARL3[L131A] increased multinucleation, ARL2[V160A] decreased supernumerary centrosomes,

ARF6[Q71L]-HA increased both multinucleation and centrosome numbers in WT cells and decreased both in KO cells, and ARF6[T157A]-HA reversed both phenotypes.

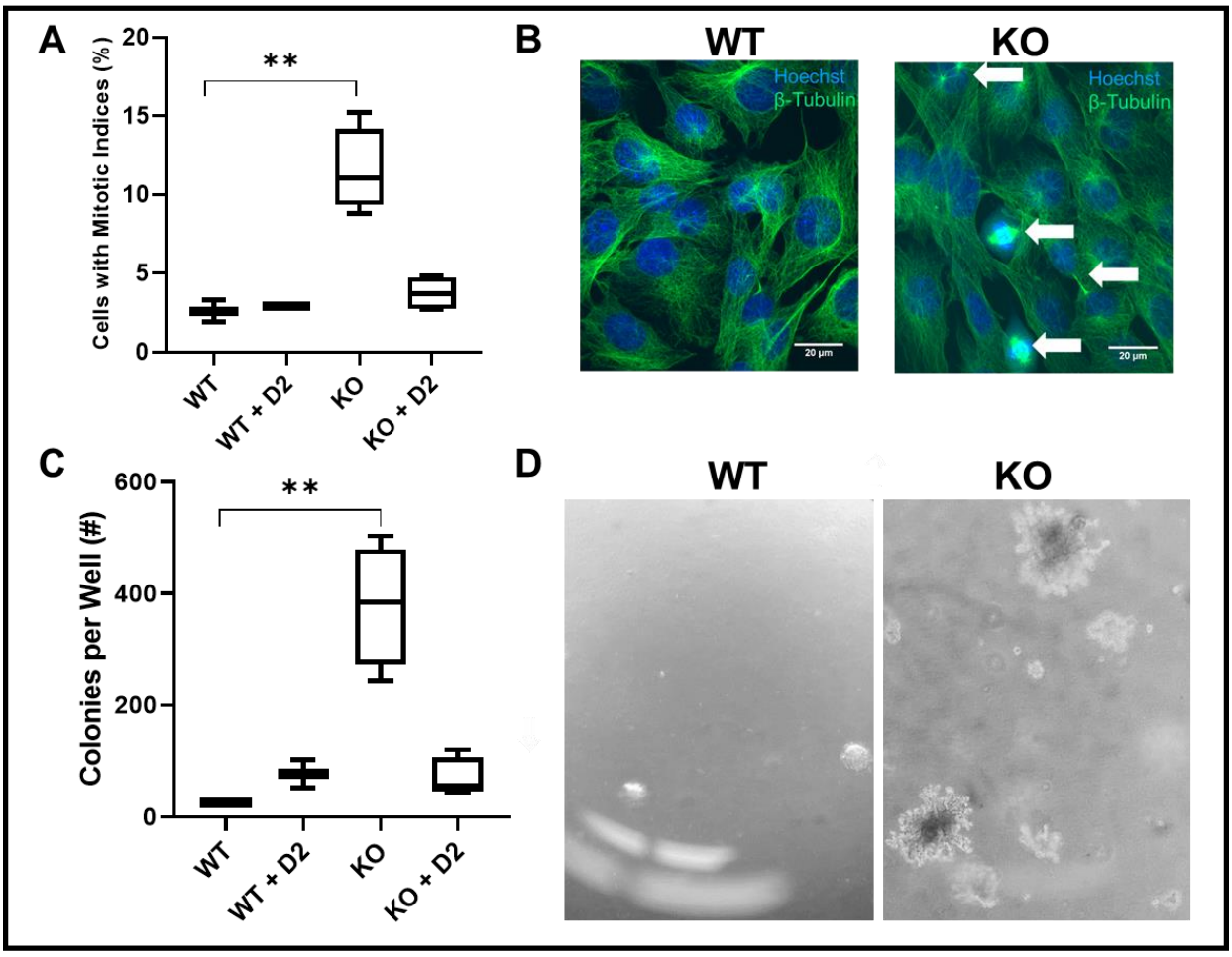

Figure 7: **ELMOD2 nulls have higher mitotic index at high densities and increased anchorage independent growth.** (**A**) Cells were grown to high density, at or near confluence, before fixing and staining for α-tubulin and Hoechst, as described in Materials and Methods. Mitotic cells were quantified in duplicate (100 cells per replicate), and averages were graphed as box-and-whisker plots via GraphPad Prism. Statistical significance was assessed using One-Way ANOVA; **=$p<0.01$. (**B**) Cells were prepared as described in A and imaged via confocal microscopy at 100x magnification, collecting z-stacks and generating a z-projection using FIJI software. White arrows indicate mitotic indices identified by DNA condensation and characteristic α-tubulin staining of mitotic spindles/midbodies. Scale = 20μm. (**C**) The standard 12 lines were plated (20,000 cells/well) in triplicate, and colonies scored after 30 days of growth in soft agar. This

experiment was performed twice. Colonies were quantified using a stereomicroscope after fixing and staining with crystal violet (see Materials and Methods). Statistical significance was assessed using One-Way ANOVA; **=$p<0.01$. (**D**) Colonies emerging after 30 days of culture, as described in (**C**), were imaged by brightfield at 4x magnification. Images shown are representative of morphologies of colonies observed in WT and null lines.

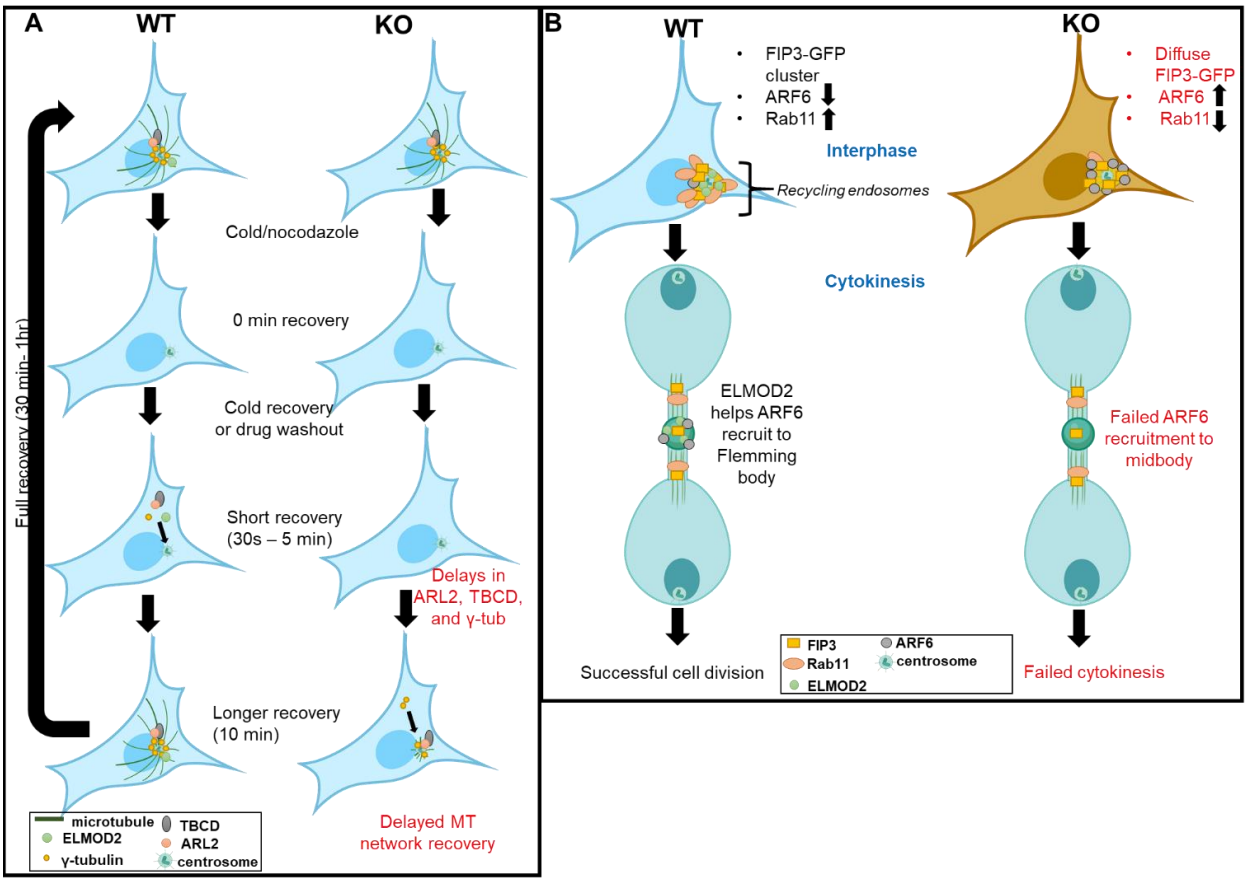

Figure 8: **Model of ELMOD2's role in microtubules and cytokinesis.** (**A**) We propose that the absence of ELMOD2 results in microtubule (cold and nocodazole) instability that is correlated with compromised retention and recruitment (during recovery) of γ-tubulin (and by extension γ-TuRC), ARL2, and TBCD at centrosomes. The higher retention of ARL2 and TBCD than γ-tubulin in all cells after cold treatment and effects of ELMOD2 overexpression (ELMOD2-myc) to increase ARL2 and TBCD retention in WT cells are suggestive of a role for ARL2 and TBCD in the recruitment of γ-tubulin to the PCM to allow centrosomal nucleation of microtubules. (**B**) We propose that ELMOD2 regulates cytokinesis through the ARF6/FIP3/Rab11 pathway(s). We propose that the absence of ELMOD2 results in altered binding of FIP3 (decreased), RAB11 (decreased), and ARF6 (increased) to endosomes, consistent with the previously proposed competition between ARF6 and RAB11 to bind FIP3. ARF6 fails to recruit to midbodies in the

absence of ELMOD2, despite the presence of its binding partner MKLP1, contributing to delayed or failed cytokinesis/abscission. Whether these two effects are directly linked is currently unknown, but we speculate that the action of ELMOD2 as an ARF6 GAP at recycling endosomes may promote its dissociation at that site and may facilitate its recruitment to midbodies.

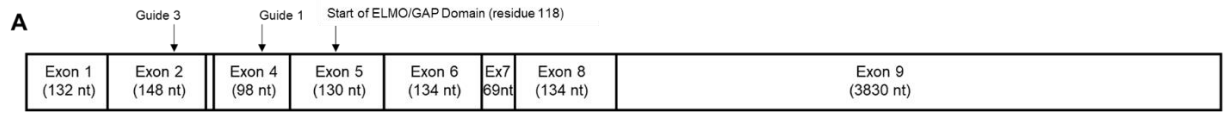

B

4 KO lines primarily used in experiments

Colonies	Guide	Alleles
ELMOD2 KO #4	1	1 and 2: 1 bp insertion; **AA sequence**: MFVSLWEFFYGHRFWMKWLLRQMTGKCELQRIFDTYGGAQRTYRIENSLTYSKNKVLQNATRVAQSELDRCIANINEGKEHLLREGHKVC
ELMOD2 KO #6	1	1: 1bp deletion; **AA sequence**: MFVSLWEFFYGHRFWMKWLLRQMTGKCELQRIFDTYGGAQRTYRIENSLTYSKNKVLQNATRVAQSELDRCIANI 2: 31bp deletion; **AA sequence**: MFVSLWEFFYGHRFWMKWLLRQMTGKCELQRIFDTYGGAQRTYRIENSLTYSKNKVLQNATRVAQSELDTSAPRRTQGMLTPSVTDVACSAEPCTVGLWCGR LVGETAQLCYPLSIEAQNADICTGCSRKAGPSHSIPEVK
ELMOD2 KO #8	3	1: 1 bp deletion; **AA Sequence**: MFVSLWEFFYGHFFRFWMKWLLRQMTGKCELQRIFDTEGHRGPTE 2: 10 bp deletion; **AA Sequence**: MFVSLWEFFYGHFFRFWMKWLLRQMTGKCELQRIMEGHRGPTE
ELMOD2 KO #10	3	1 and 2: 4 bp deletion; **AA Sequence**: MFVSLWEFFYGHFFRFWMKWLLRQMTGKCELQRIFAMEGHRGPTE
ELMOD2 KO #1	1	1: 1 bp insertion; **AA Sequence**: MFVSLWEFFYGHRFWMKWLLRQMTGKCELQRIFDTYGGAQRTYRIENSLTYSKNKVLQNATRVAQSELDRCIANINEGKEHLLREGHKVC 2: 2 bp deletion; **AA Sequence**: MFVSLWEFFYGHRFWMKWLLRQMTGKCELQRIFDTYGGAQRTYRIENSLTYSKNKVLQNATRVAQSELDRCIANK
ELMOD2 KO #2	1	1 and 2: 1 bp insertion; **AA Sequence**: MFVSLWEFFYGHRFWMKWLLRQMTGKCELQRIFDTYGGAQRTYRIENSLTYSKNKVLQNATRVAQSELDRCIANINEGKEHLLREGHKVC
ELMOD2 KO #3	1	1: 7 bp insertion; **AA Sequence**: MFVSLWEFFYGHRFWMKWLLRQMTGKCELQRIFDTYGGAQRTYRIENSLTYSKNKVLQNATRVAQSELDRCIANIRKRTSAPRRTQGMLTPSVTDVACSAEPC TVGLWCGRLVGETAQLCYPLSIEAQNADICTGCSRKAGPSHSIPEVK 2: 13 bp deletion; **AA Sequence**: MFVSLWEFFYGHRFWMKWLLRQMTGKCELQRIFDTYGGAQRTYRIENSLTYSKNKVLQNATRVAQSELDRCIANITSAPRRTQGMLTPSVTDVACSALWCGR LVGETAQLCYPLSIEAQNADICTGCSRKAGPSHSIPEVK
ELMOD2 KO #5	1	1: 1bp insertion; **AA Sequence**: MFVSLWEFFYGHRFWMKWLLRQMTGKCELQRIFDTYGGAQRTYRIENSLTYSKNKVLQNATRVAQSELDRCIANINEGKEHLLREGHKVC 2: 4bp deletion; **AA Sequence**: MFVSLWEFFYGHRFWMKWLLRQMTGKCELQRIFDTYGGAQRTYRIENSLTYSKNKVLQNATRVAQSELDRCIANIRKRTSAPRRTQGMLTPSVTDVACSAEP CTVGLWCGRLVGETAQLCYPLSIEAQNADICTGCSRKAGPSHSIPEVK
ELMOD2 KO #7	3	1: 5 bp deletion; **AA Sequence**: MFVSLWEFFYGHFFRFWMKWLLRQMTGKCELQRIFLWRGTEDLQNR 2: 14 bp deletion; **AA Sequence**: MFVSLWEFFYGHFFRFWMKWLLRQMTGKCELQLWRGTE
ELMOD2 KO #9	3	1 and 2: 1bp deletion; **AA Sequence**: MFVSLWEFFYGHFFRFWMKWLLRQMTGKCELQRIFDTEGHRGPTE

Figure S1: **Summary of ELMOD2 alleles in 10 KO MEF lines.** (**A**) The two guides used to generate the 10 KO lines targeted the region of the mouse ELMOD2 mRNA shown. The open reading frame is indicated below as well as where the ELMO domain (residues 126 to 273) begins in the protein. (**B**) Alleles of each of the 10 KO lines are shown: 4 from guide 3 and 6 from guide 1. Each of the ten clones have frameshifting mutations that lead to premature termination of protein translation. The four standard KO lines are indicated to the left. The underlined portion of the amino acid sequence indicates wild type sequence.

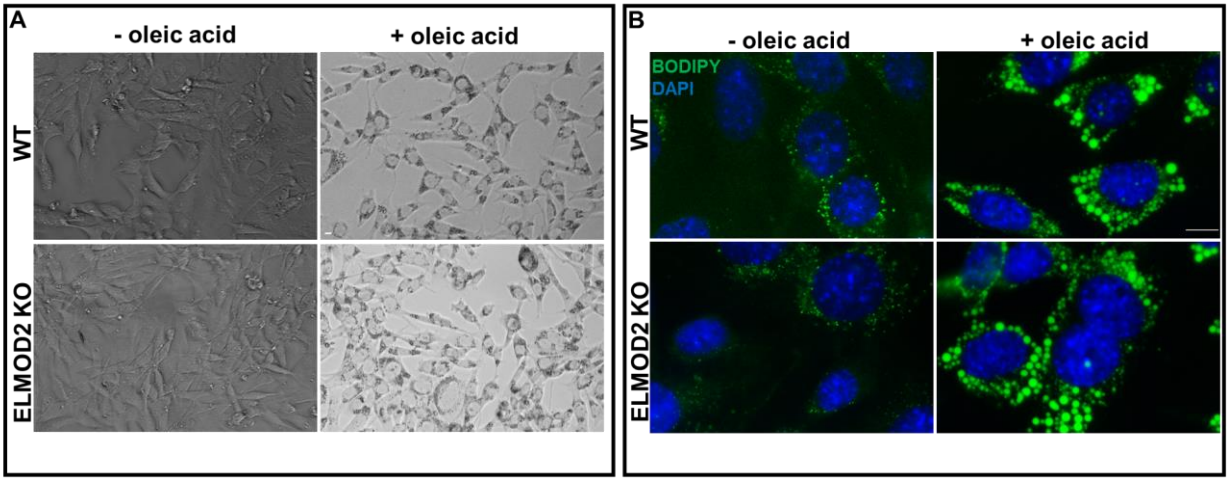

Figure S2: Lipid droplet sizes and abundance, with or without oleic acid treatment, are unchanged in ELMOD2 null cells. (**A**) Brightfield images (20x magnification (scale bar = 10µm)) of PFA-fixed, TritonX-100-permeabilized cells with or without oleic acid treatment (30µM for 24 hrs) reveal no obvious change in lipid droplets. (**B**) Widefield fluorescent microscopy (100x magnification) of the same cells stained for nuclei (Hoechst) and lipid droplets (BODIPY 493/502) reveal no obvious change.

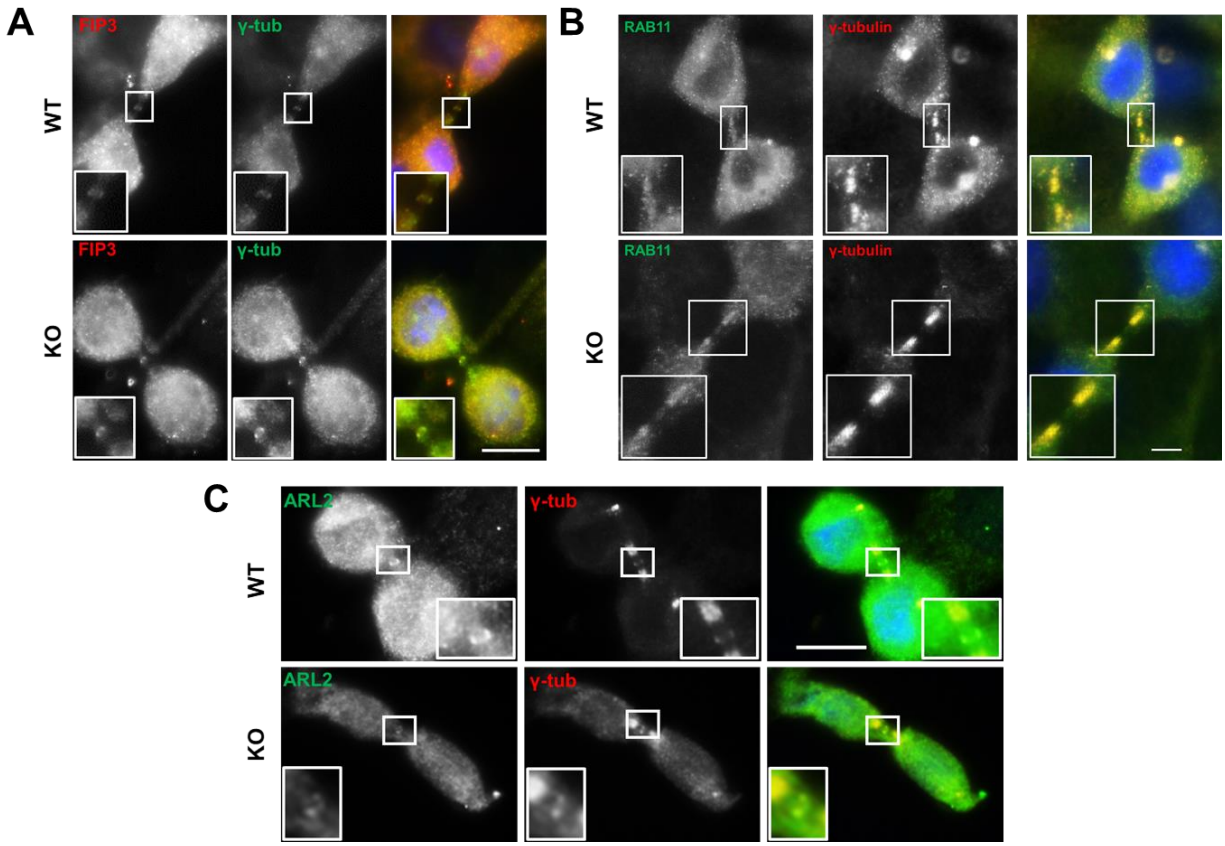

Figure S3: **Flemming body markers FIP3, RAB11, and ARL2 are unchanged in ELMOD2 null cells.** (**A-C**) Widefield images (100x magnification) of methanol-fixed cells co-stained for γ-tubulin and either FIP3, RAB11, or ARL2 reveal no clear differences between WT and ELMOD2 null cells. Scale = 10μm.

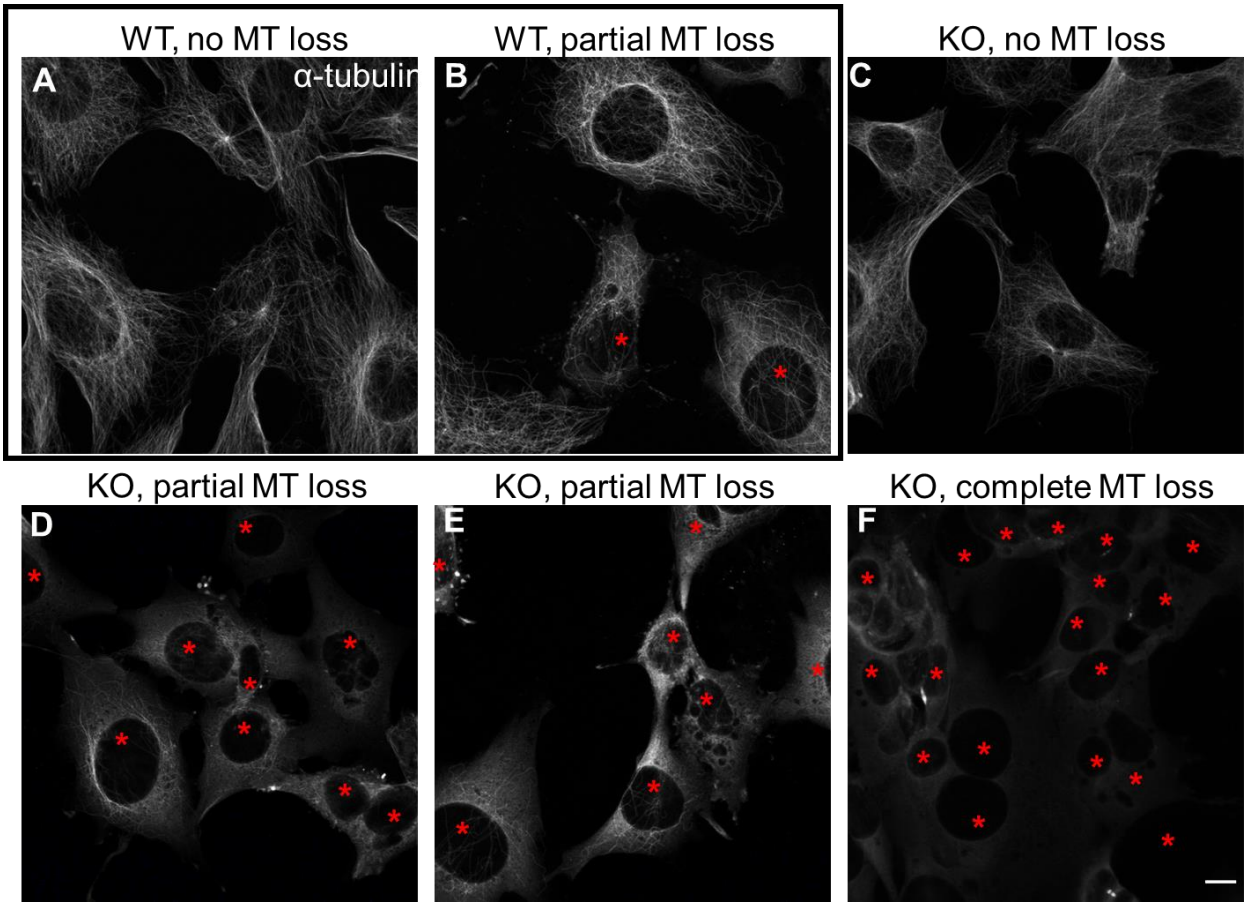

Figure S4: Binning cells into loss or no loss of MT network. WT or KO cells were maintained at 37°C (panels **A** and **C**) or removed from the incubator and maintained at room temperature (~23°C) for 10 min (panels **B**, **D-F**) before being fixed and stained for α-tubulin, as described under Methods. Z-projections of confocal images were generated from stacks with 0.37 µm step size, and representative images of fields of cells are shown. Fields are labeled as either no loss, partial loss, or complete loss of MTs to highlight the magnitude of the effect upon the network. Note that in some cases what appears to be strong tubulin staining (*e.g.*, panel **E**) is largely diffuse and not reticular, as seen for microtubules (*e.g.*, panels **A** or **C**). Cells marked with a red asterisk are those that would be binned as showing microtubule loss. Scale bar = 10 µm.

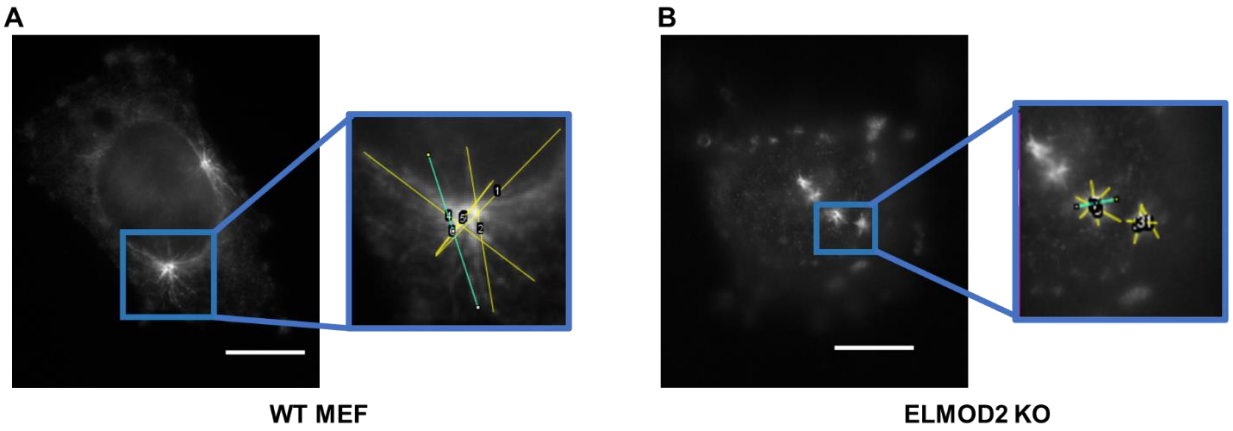

Figure S5: Measuring the diameter of asters. Cells were treated with nocodazole (50 ng/µL), as described under Materials and Methods, and 30 seconds after drug washout were fixed and stained for tubulin. Widefield images (100x magnification) were collected, and the largest diameter from each aster was determined using the FIJI measuring tool. Individual microtubules were delineated and saved as ROI's, and the lengths were recorded. The left side of each panel shows the image used in these examples, while the right side of each panel shows examples of the measurements along with the ROI's. Panel (**A**) shows examples of WT asters, while panel (**B**) shows examples of ELMOD2 KO asters. Scale bar = 10 µm. Note the clear differences, even to the naked eye.

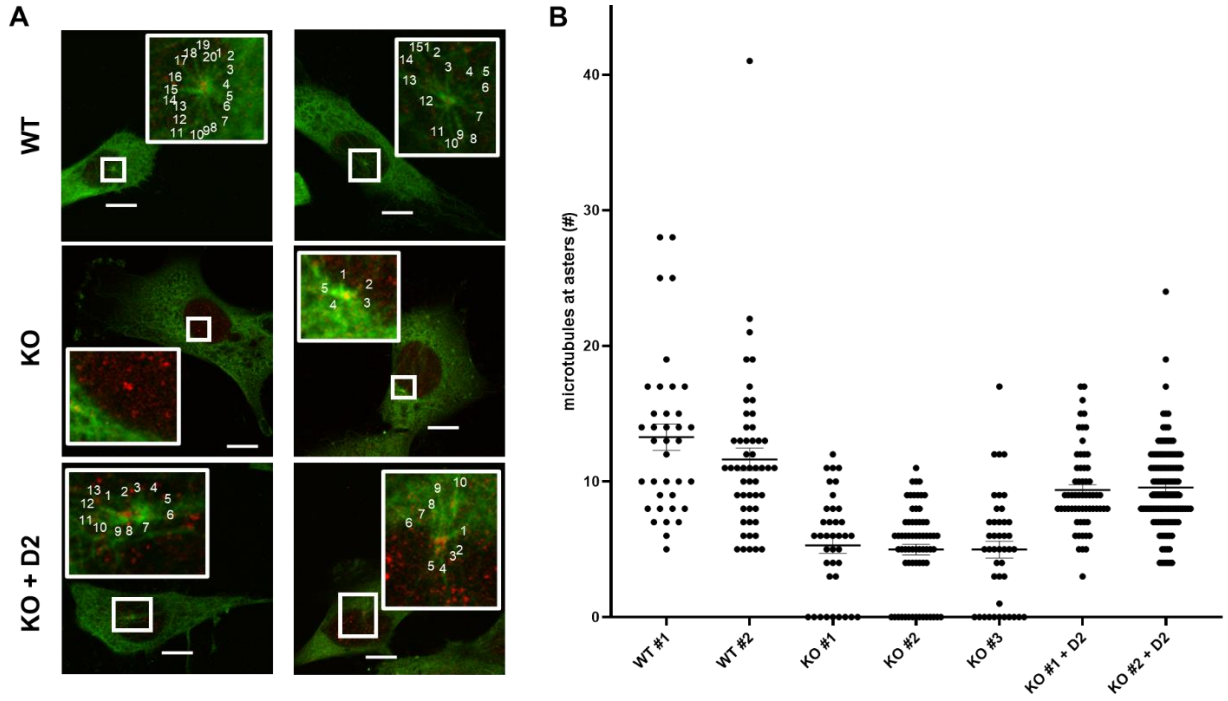

Figure S6: Scoring microtubules at asters during recovery from cold (4°C). (**A**) Cells were put on ice for 30 min and then returned to the 37°C incubator for 5 min before being fixed and stained for α-tubulin (green) and γ-tubulin (red). Images were collected for WT, KO, and KO + D2 lines 5 min after recovery from cold treatment (see Methods for details). Z-stack projections were generated by confocal microscopy at 100x magnification, and individual slices were scored for the number of microtubules projecting from centrosome at that plane. Only microtubules at least 0.5μm long were scored. (**B**) Numbers of microtubules emanating from γ-tubulin positive centrosomes are plotted for each cell analyzed, with at least 38 cells analyzed per cell type. Bars indicate the mean with SEM indicated. Data from two replicates of similar size have been merged.

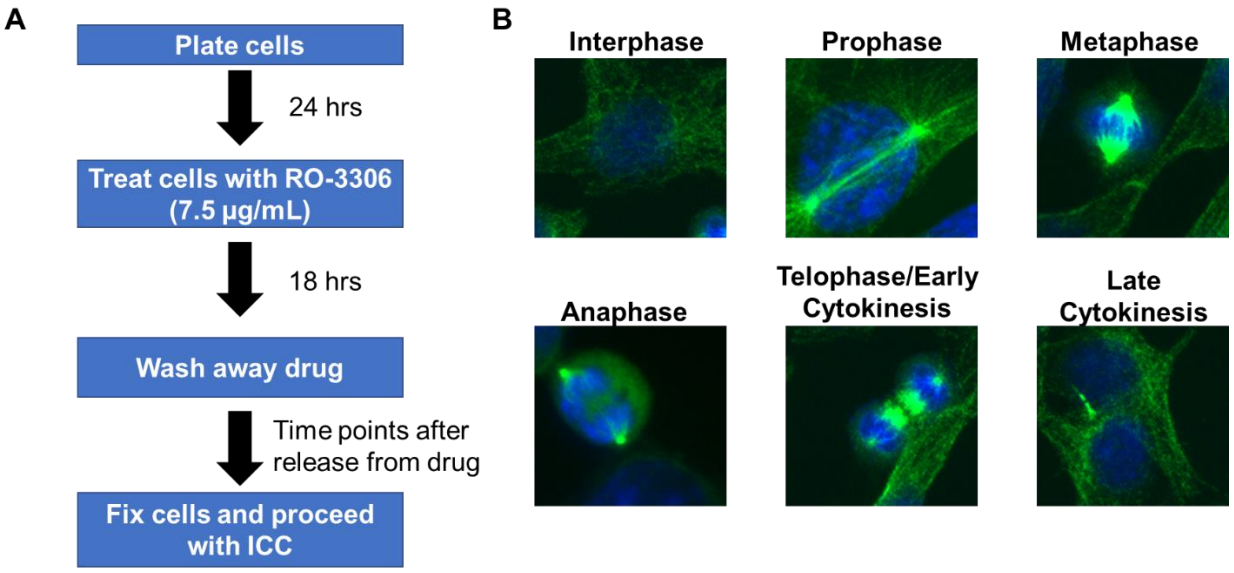

Figure S7: Workflow for scoring mitotic indices. (**A**) The workflow for scoring mitotic indices is shown (see Methods for additional details). Cell lines were plated onto glass coverslips at low density, treated with CDK1 inhibitor (RO-3306 at 7.5µg/mL) for 18hr to synchronize the cells at the G2/M transition, and then released from the drug by washing with PBS and replacing with drug-free medium. Cells were fixed with 4% PFA and permeabilized with 0.1% TritonX-100 as described in Materials and Methods. Time points were collected at 0, 10, 20, 30, 40, 50, 60, 90, 120, 300 min after release from drug. Cells were stained for α-tubulin and Hoechst to detect stages of cell cycle. (**B**) Representative images highlighting different stages in the cell cycle that were used in binning are shown. Interphase cells had relatively broadly distributed microtubule networks, and Hoechst staining revealed intact nuclei with no evidence of DNA condensation. Prophase cells are marked by polarization of microtubules at microtubule organizing centers, with evidence of early DNA condensation. At metaphase, the chromosomes have lined up at the metaphase plate and are flanked by the mitotic spindle. Anaphase is characterized by the increasing distance between sets of chromosomes and changes in the structure of the mitotic spindle, before indentation of the cleavage furrow. Telophase shows the formation of the cleavage furrow and the

formation of the microtubules that will later condense and form the midbody. Late cytokinesis is identified by the presence of decondensed nuclei with the two cells attached by a single midbody of varying length and width. These images were collected using widefield or confocal microscopy at 100x magnification and are shown as examples.

Chapter 3: Roles for ELMOD2 and Rootletin in Ciliogenesis

This chapter is under review at MBoC as:

Turn R.E., Linnert J., Gigante E.D., Wolfrum U., Caspary T, Kahn R.A. 2020. Roles for ELMOD2 and Rootletin in Ciliogenesis. MBoC. Under review.

Abstract

ELMOD2, a GTPase activating protein (GAP) with uniquely broad specificity for ARF family GTPases, has been shown previously to act with ARL2 in mitochondrial fusion and microtubule stability and with ARF6 during cytokinesis. Mouse embryonic fibroblasts deleted for ELMOD2 displayed increased ciliation, multiciliation, abnormal ciliary morphology, defective ciliary signaling, centrin accumulation in cilia, and loss of rootlets at centrosomes resulting in decreased centrosome cohesion. These effects were reversed upon increasing ARL2 activity and overexpressing rootletin. Deletion of rootletin yielded similar consequences, which could be rescued upon increasing activity of ARL2, but not ELMOD2 overexpression. Thus, ARL2, ELMOD2, and rootletin are proposed to all act in a common pathway that can suppress ciliation and maintain centrosome cohesion. Screening a number of markers of steps in the ciliation pathway support a model in which they act downstream of TTBK2 and upstream of CP110 to prevent spurious release of CP110 and to regulate ciliary vesicle docking. These data thus provide evidence supporting previously unknown roles for ELMOD2, ARL2, and rootletin in the regulation of ciliary licensing.

Introduction

Members of the ARF (ADP-ribosylation factor) family of regulatory GTPases, as well as their downstream effectors and GTPase activating proteins (GAPs) that mediate their effects, drive an incredibly diverse array of cellular functions (Casalou et al., 2020; Fisher et al., 2020; Francis et al., 2016; Sztul et al., 2019). Consisting of 6 ARFs, 22 ARLs (ARF-like proteins), and 2 SARs in mammals, the ARF family is ancient with multiple members traced back to the last eukaryotic common ancestor (Li et al., 2004). One critical feature of these proteins is that they localize to

multiple cellular compartments and can perform discrete functions at each site, making them both critical to healthy cell function and technically challenging to dissect each functionality. Because individual family members have been repeatedly found capable of regulating multiple processes at distinct cellular sites, they have been proposed as key players in interpathway communication or higher order signaling (Francis et al., 2016). Although the canonical model for regulatory GTPase actions is that a guanine nucleotide exchange factor (GEF) activates the GTPase (by promoting release of GDP and binding of GTP) and GAPs terminate the activated state (by promoting hydrolysis of the bound GTP), ARF GAPs have consistently been found to possess both GAP and effector activities, thereby providing temporal regulation as part of the signaling pathway (East and Kahn, 2011; Sztul et al., 2019; Zhang et al., 2003; Zhang et al., 1998). Because ARF GAPs consistently have been found to act as downstream mediators/effectors of the GTPases they bind, they too have been found to act in multiple pathways. This is particularly true for the ELMOD family of ARF GAPs at least in part due to their uniquely broad specificity towards both ARFs and ARLs (Ivanova et al., 2014). This is in contrast to the much larger family of 24 known ARF GAPs (including ACAPs, ASAPs, ARAPs) that bind and promote GTP hydrolysis only on ARFs, not ARLs (Cuthbert et al., 2008; Sztul et al., 2019; Vitali et al., 2019).

Like the ARF family, the ELMODs are also ancient, ubiquitous, and were present in the last eukaryotic common ancestor (East et al., 2012). The three mammalian family members share a single, common ELMO domain that gives the protein GAP activity. This domain contains a predicted “arginine finger” that is directly involved in helping the ARF family GTPases that they bind hydrolyze GTP (Ahmadian et al., 1997; East et al., 2012). Mutation of this single arginine is sufficient to eliminate in vitro GAP activity (Ivanova et al., 2014). Also like the ARF family GTPases, ELMODs are implicated in a number of pathologies, including deafness in mammals

(ELMOD1, ELMOD3; (Jaworek et al., 2013; Johnson et al., 2012; Lahbib et al., 2018; Li et al., 2019; Li et al., 2018)), intellectual disability (ELMOD1, ELMOD3; (Miryounesi et al., 2019)), idiopathic pulmonary fibrosis, and antiviral response (ELMOD2; (Hodgson et al., 2006; Pulkkinen et al., 2010)). The mechanisms by which disruption of these proteins causes disease are unclear. Because of the apparent importance of ELMODs to cell regulation and its predicted impact on our understanding of multiple disease states, we have undertaken a broad analysis of cellular roles for ELMODs using a number of technical approaches.

ELMOD2 is a ~37 kDa protein that was first purified as an ARL2 GAP (Bowzard et al., 2007) and found to localize at lipid droplets (Suzuki et al., 2015), ER (Suzuki et al., 2015), rods and rings (Schiavon et al., 2018), and mitochondria (Schiavon et al., 2019). Among its first known cellular functions was in mediating mitochondrial fusion as an ARL2 effector (Newman et al., 2017b; Schiavon et al., 2019). Recent studies from our lab, though, revealed that ELMOD2 also acts with ARL2 on aspects of microtubule biology and with ARF6 in cytokinesis/abscission (Turn et al., 2020). This recent study also provided evidence that ELMOD2 localizes to centrosomes and Flemming bodies, consistent with its effects on microtubules and abscission. These novel and unexpected roles were found in cells deleted for ELMOD2 using the CRISPR/Cas9 system in immortalized mouse embryonic fibroblasts (MEFs). These lines were generated in part due to our inability to document its knockdown by siRNA because of its low abundance in cultured cells (Turn, et al 2020). Interestingly, deletion of neither ELMOD1 nor ELMOD3 in MEFs resulted in any of the phenotypes described previously (or below) (manuscript in preparation), suggesting a high degree of specificity of ELMOD2 within this small family.

With the knowledge that (1) ELMOD2 localizes to centrosomes, (2) many regulators of cell cycle also have close links to cilia, (3) multiple ARF family members (including at least

ARL2/3/6/13B) are implicated in ciliary signaling (Fisher et al., 2020), and (4) ELMOD2 has in vitro GAP activity for at least two of these ciliary ARFs, we hypothesized that ELMOD2 may also play a role in ciliary function. Primary cilia serve as signaling hubs that mediate essential intracellular and intercellular functions, particularly during development (Gigante and Caspary, 2020; Higginbotham et al., 2012). Within the past few decades, there has been a steady increase in the study of primary cilia because of their link to a range of human pathologies. These diseases, collectively called ciliopathies, include polycystic kidney disorder, Bardet-Biedl Syndrome, situs inversus, primary cilia dyskinesia, and Joubert Syndrome, as well as others (Chen et al., 2020; Goetz and Anderson, 2010; Waters and Beales, 2011). Further studies have implicated primary cilia as signaling hubs, sequestering receptors needed for development, metabolism, recognition of sensory stimuli, cell cycle, and others.

Primary cilia are composed of (1) a basal body tethered to the plasma membrane by pinwheel-like structures called distal appendages (DA), (2) microtubules that project from the distal end of the basal body to create a single, intact axoneme, and (3) a ciliary membrane encasing the axoneme as it projects into the extracellular space. Cells grown in culture typically lack cilia until they approach confluence, or enter G_0, which is promoted by serum starvation. Ciliogenesis is tightly regulated to ensure that one and only one primary cilium is formed per cell. The process of ciliogenesis involves a series of incompletely understood steps that include movement of centrosomes toward the cell surface, where the mother centriole becomes established as the basal body. During this process, the centrosomal protein Cep164 is recruited to the distal appendages of the mother centriole, giving them license to subsequently recruit TTBK2, a kinase that phosphorylates Cep83, and MPP9. These players lead to the release of the capping protein complex CP110-Cep97. Afterward, ciliary vesicles dock at the basal body and proceeds with building the

transition zone and extending the axoneme to generate the elongating cilium. The commitment to initiate ciliogenesis, which we term licensing, is often monitored by the obligate recruitment of Cep164 and later release of CP110 as markers of this process.

Both during ciliogenesis and in existing cilia, protein traffic in and out of cilia is regulated by the transition zone acting as a presumptive physical barrier and by active transport involving at least three protein complexes: IFT-A, IFT-B, and the BBSome. Once inside cilia, proteins can be actively transported along the axoneme via kinesin or dynein driven motors. The selective traffic in and out of cilia is important not only to build a stable organelle but is also a critical aspect of signaling that is transduced from receptors in the ciliary membrane to the cell body. Perhaps the best known or studied of signaling pathways in primary cilia is that of Sonic Hedgehog (SHH). In this pathway, SHH acts as a ligand that binds to the receptor Patched (Ptch2) on the ciliary membrane. Ligand-binding leads to Ptch2 removal and the entry of another receptor, Smoothened (Smo). While some other ciliary membrane proteins also change in localization in response to ligand, the G-protein coupled receptor 161 (GPR161) is exported after SHH stimulation, while others (including the Somatostatin Receptor 3 (SSTR3) and adenylyl cyclase III (ACIII)) are unaltered in abundance in cilia. Even less well understood than traffic in and out of cilia is specific transport of newly synthesized proteins from the ER, through the Golgi, to cilia. Such ciliary traffic may be targeted directly to the basal body for regulated import, but a number of findings have also implicated a role for rootlets in traffic to cilia.

Rootlets are cytoskeleton-like structures that project from the proximal end of the basal body and are composed primarily of the ~225 kDa protein rootletin. The gene encoding rootletin in mice is termed Crocc (ciliary rootlet coiled-coil; Gene ID 230872) though because the protein is consistently termed rootletin in the literature we will conform to this usage throughout, except

when referring to specific alleles. Other proteins reported to localize to rootlets include kinesins, amyloid precursor protein (APP), and presenilins (Yang and Li, 2005). The rootlet's function is incompletely understood. To date, though, rootletin is predicted to help stabilize cilia against external flow and to regulate ciliary traffic (Yang et al., 2005; Yang and Li, 2005; Yang and Li, 2006; Yang et al., 2002). Rootletin and rootlets have also been shown to be important in centrosomal cohesion, along with centrosomal proteins C-NAP1, Cep68, and Cep44 (which is believed to help anchor the rootlet to the centrosome) (Hossain et al., 2020).

To test the model that ELMOD2 plays a role at cilia, we used our previously generated ELMOD2 KO mouse embryonic fibroblast (MEF) lines, looking for any changes in cilia compared to WT lines. Ten KO lines from two different guides were generated (Turn et al., 2020). We discovered novel roles for ELMOD2 at cilia and ciliary rootlets, and we were able to cleanly resolve these effects from its roles in microtubule and mitochondrial function as well as cytokinesis. Furthermore, we were surprised to find close functional links between ELMOD2 and rootletin in both centrosome cohesion and ciliogenesis. We then used well known markers of steps in ciliary licensing to identify the site or step(s) at which ELMOD2 and rootletin act in ciliogenesis, as well as the ARF family GTPase involved. Together, we believe that these data provide several new insights into fundamental aspects of ciliary biology, including ciliogenesis and rootlet function.

Materials and Methods

Reagents, antibodies, plasmids: The commercially obtained antibodies and dilutions used in imaging herein include those directed towards: γ-tubulin (1:5000) (Sigma; T6557), γ-tubulin (1:5000) (Abcam; ab11317), centrin (1:1000) (Sigma; 04-1624), myc (1:1000) (Invitrogen; R950-25), HA (1:1000) (Covance; MMS-101P), acetylated tubulin (1:2000) (Sigma; T6793-2ML),

ARL13B (1:500) (Proteintech; 10083-118), ARL13B (1:500) (Abcam; ab136648), Gli3 (1:1000) (R&D Systems; AF3690), Cep164 (1:100) (Santa Cruz; sc-515403), CP110 (1:100) (VWR; 76045-052), IFT88 (1:500) (VWR; 10088-640), NPHP4 (1:100) (VWR; 10091-250), Cep290 (1:100) (VWR; 10084-648), rootletin (1:500) (Millipore-Sigma; ABN1686), TTBK2 (1:100) (Sigma; HPA018113-100UL), Cep44 (1:100) (Proteintech; 10084-652). Rabbit polyclonal antibodies against the following human proteins were generated by our lab and have been previously characterized: ARL2 (Sharer and Kahn, 1999; Sharer et al., 2002), ARL3 (Cavenagh et al., 1994), and ELMOD2 (Newman et al., 2014). We are grateful for the generous gifts of other antibodies: ARF6 polyclonal antibody from Jim Casanova (Univ. of Virginia) (REF), Smoothened from Katherine Anderson (REF).

As described in our previous manuscripts (REFERENCE), the CRISPR-Cas9 system used to generate the null lines involved use of a plasmid obtained from Addgene (pSpCas9(BB)-2A-Puro (PX459) V2.0 (#62988)). Plasmids directing expression of human ARL2, ARL2[Q70L], ELMOD2-myc, or ELMOD2[R167K]-myc/his in pcDNA3.1 were described previously (Bowzard et al., 2007; East et al., 2012; Zhou et al., 2006). Jim Casanova provided us with plasmids used for transient expression of ARF6-HA, ARF6[Q71L]-HA, or ARF6[T157A]-HA (Altschuler et al., 1999; Santy, 2002). All fast cycling point mutants were generated in pcDNA3.1 vectors using site-directed mutagenesis and confirmed by DNA sequencing. The following drugs were purchased for this study: ciliobrevin D (Sigma; 250401-10MG). SHH-induction medium was kindly gifted to us by the Caspary lab. Human bronchial cells (NH BE009) were graciously gifted to us by Mike Koval.

Cell Culture: All CRISPR/Cas9 knockout lines were grown under the same conditions, maintaining cells at low passage (below passage 10). We avoid maintaining cells at higher passage to prevent potential selection against certain phenotypes. WT MEFs were purchased from ATCC (CRL-2991), and all knockout lines were generated from this original line. Cells were grown in DMEM (Fisher; 11965092) with 10% FBS (Atlanta Biologicals; S11150) and 2mM glutamine at 37°C, 5% CO_2 and were screened at least monthly for mycoplasma contamination. Serum starvation was used to induce ciliation and involved growth of cells in 0.5% FBS and 2mM glutamine supplemented DMEM for 24hrs. No antibiotics were used in the routine maintenance of cells. We treat replicates of individual lines on separate days as technical replicates, and we treat the average of these technical replicates for each line as biological replicates.

Generation of CRISPR null lines: : ELMOD2 and Rootletin KO lines were generated using CRISPR-Cas9, as described in our previous publications (Turn et al., 2020). In brief, low passage WT (ATCC CRL-2991) immortalized MEFs were used as the parental population for all lines generated. Four guides (20 nt long) were generated using Benchling software, for each gene. These guides were cloned into pSpCas9(BB)-2A-Puro (PX459) V2.0 using BbsI restriction sites and then transfected into WT MEFs (~90% dense per well of 6-well dish) at a 1:3 ratio of DNA (4 µg) to Lipofectamine 2000 (12 µg) for 4 hours in Opti-MEM medium (Fisher; 31985070). Transfected cells were then replated into 10 cm dishes and allowed to grow up overnight. The next day, puromycin selection (3 µg/ml, Sigma #P8833) was initiated and lasted for a total of 4 days to enrich for transfected cells. Cells were then grown to near confluence in our regular culture medium (DMEM + 10% FBS). Cloning was performed by plating into 2 96-well plates at ~3 cells/well. These clones were grown up and screened for frameshifting mutations in both strands

using DNA sequencing, with primers flanking the predicted cut site. At least two clones from each of two guides were generated to ensure that any phenotypes studied were not the result of off-target effects or clonal abnormalities.

Lentiviral Transduction: The mouse ELMOD2-myc open reading frame was cloned into the pFUGW vector using EcoRI and BamHI sites, used to generate lentivirus by Emory's Viral Vector Core, as previously described (REF). Cells were incubated with virus for 48 hrs and then fresh medium was exchanged, cells were grown up and frozen for storage. The transduction efficiency was determined to be ~70-90%, based upon myc staining. Because of this high transduction efficiency, use of these lines in "rescue" experiments involved counting all cells in the population, rather than only those expressing ELMOD2. Therefore, because 10-30% of the cells scored in such experiments are not expressing ELMOD2-myc, less than complete rescue is expected, as routinely observed.

Transfection of MEFs: As described in our previous manuscript (REF), Lipofectamine 2000 proved toxic to many null genotypes (particularly in the case of ELMOD2). Therefore, transfections after the original generation of CRISPR nulls used polyethyleneimine (PEI) due to its reduced cellular toxicity. The day before transfection, cells were plated at 70% density in 6-well dishes. These cells were transfected with a 1:3 ratio of DNA to PEI for 24 hours in medium containing 2% FBS in DMEM. Cells were replated onto Matrigel coated coverslips at the appropriate density, serum starved for 24hrs, and processed using standard IF protocols. Unless otherwise stated, 4 µg of DNA, 12 µg PEI, and 100 µL of serum-free medium per reaction were

combined in an Eppendorf tube, vortexed, and incubated for 20 minutes at room temperature before being added dropwise to the sample.

For GTPase cross-rescue experiments, jetOPTIMUS transfection reagent was used (VWR; 76299-634). Similar to transfection with PEI, cells were plated at 70% density in 6-well dishes before being transfected with a 1:1 ratio of DNA to JetOPTIMUS for 24 hours. The cells were incubated in 2% FBS in DMEM. For each reaction, 4µg of DNA was combined with 4µL JetOptimus transfection reagent in 400µL JetOptimus buffer according to the provided protocol, vortexed, incubated for 10 min at room temperature, and added dropwise onto cells. Cells grew up for 24 hours before being replated onto Matrigel coated coverslips at appropriate density, as described above for PEI transfection.

Western blot: Cells were plated at approximately 90% density and harvested the next day by incubating with 5mM EDTA for 10 minutes. Cells were collected and the supernatant was aspirated. The cell pellets were resuspended into 1x Laemmli sample buffer, heated at 95˚C for 5 minutes, and insolubles removed by centrifugation before being samples were loaded onto a 7.5% polyacrylamide gel. Proteins were later transferred on nitrocellulose overnight at 20V. Membranes were stained for Ponceau to check for equal loading, blocked with filtered 5% blotto in PBST (BioRad; 1706404) for 1hr at room temperature, and stained with primary antibody against rootletin at a 1:500 dilution overnight at 4˚C. Membranes were washed 3x for 10 min in 1xPBST, incubated with HRP-anti-chicken secondary antibody for 1hr at room temperature and developed using enhanced chemilluminescence, as previously described.

General phenotyping using immunofluorescence: After plating cells onto coverslips and performing other drug/serum starvation treatments as needed, we used a number of different fixation and permeabilization conditions, depending upon what was being imaged. The following conditions were used:

- *PFA fixation*: For ciliary markers (except for γ-tubulin) such as ARL13B, Gli3, or IFT88, cells were removed from the incubator and immediately fixed with pre-warmed (37˚C) 4% PFA for 15 minutes on the bench top. Cells were then rinsed 4x with PBS before being permeabilized with 0.1% TritonX-100 for 10 minutes and blocked with 1%BSA in PBS for 1 hr at room temperature. After diluting the antibody in blocking solution and spinning down to remove insoluble debris, staining with primary antibody was overnight at 4˚C. Cells were rinsed 4x with PBS, incubated in 2˚ antibody (1:500) for 1hr at room temperature in the dark, rinsed 4x with 1xPBS, stained with Hoechst (1:5000), and coverslips were mounted on slides using MOWIOL + PPD (9:1 ratio).
- *5 min methanol fixation:* For centrosomal markers (centrin, γ-tubulin, ARL2, ELMOD2, TTBK2) and rootletin, cells on coverslips were fixed for 5 min at -20˚C in ice-cold methanol. Coverslips were then rinsed 4x with PBS, blocked and incubated with antibodies as described above. TTBK2 was unique in that it worked better with 3% BSA or 10% FBS for blocking.
- *10 min methanol fixation:* Some centrosomal and ciliary markers (*e.g.* Cep164, CP110, Cep290, NPHP4, rootletin) require longer fixation; cells were fixed at -20˚C with ice-cold methanol for 10 minutes before being washed on a rocker with PBS for 3 washes, 5 minutes each at room temperature. Cells were blocked with 10% FBS for 30 minutes, primary antibodies added in 10% FBS and incubated overnight at 4˚C. Coverslips were rinsed 3x

on a shaker, 5 minutes each, with PBS and then incubated in secondary antibody for 1hr at RT in the dark. Coverslips were rinsed and mounted onto slides as described above.

Ciliobrevin treatment: To inhibit retrograde transport in cilia, cells were plated onto Matrigel-coated coverslips and serum-starved for 24 hours as described above. Ciliobrevin (0 µM or 30 µM) (Sigma-Aldrich; 250401-10MG) was added to the cultures for 1hr at 37˚C before fixing cells with 4% PFA for 15 minutes at 37˚C. Samples were processed as described above, except PBS containing 0.1% Tween detergent (PBST) was used for washes to remove autofluorescent residue left by the drug.

qPCR of SHH pathway targets: Cellular signaling in response to SHH involved measuring transcriptional changes in Gli1 and Ptch1 mRNAs, as previously described (REF). Cells were incubated with SHH conditioned medium or serum starvation medium (0.5% FBS) for 48hrs. The cells were then harvested, and the RNA was extracted using the Qiagen RNeasy Kit with QIAshredder homogenizer columns according to manufacturer's protocols. RNA (200 ng) was used to generate cDNAs using BioRad iScript Reverse Transcription supermix . The following primers were used during qPCR to detect transcript levels:

Pold3 (loading control) F:5'-ACGCTTGACAGGAGGGGGCT-R:5'-AGGAGAAAAGCAGGGGCAAGCG-3'

Ptchd1 F:5'-TGCTGTGCCTGTGGTCATCCTGATT-3';R:5'-CAGAGCGAGCATAGCCCTGTGGTTC-3'

Gli1 F: 5'-CTTCACCCTGCCATGAAACT-3'; R: 5'-TCCAGCTGAGTGTTGTCCAG–3'

qPCR was performed as previously described (REF). In brief, the cDNA was combined with primers and Bio-Rad SsoAdvanced Universal SYBR Supermix (1725270). The samples were run on a Bio-Rad CFX96 Touch Real-Time PCR Detection System, and the data were collected and analyzed using Bio-Rad CFX Manager 3.1. The following program conditions were used: 95°C for 5 min; 45 cycles of 95°C for 15 s; 57°C for 30 s. The samples were then read, and a melt curve was generated from 65°C to 95°C to ensure that the individual samples were pure and that no cross-contamination occurred. All samples were performed in both biological and technical triplicate, with normalization to the Pold3 loading control. Results were analyzed for statistical significance using One-Way ANOVA.

Microscopy: All fixed immunofluorescence experiments were performed using Matrigel (BD Bioscience) coated 18 mm glass coverslips (#1.5, Fisher Scientific; 12-545-81) prepared in the lab. Samples were visualized using confocal (Olympus FV1000 microscope and Olympus Fluoview v1.7 software; 100x magnification (1.45 NA, Oil); 405, 488, 543, and 635 laser lines) and widefield microscopes (Olympus IX81 microscope and Slidebook software; 100x magnification (UPIanFI, 1.30 NA Oil). For the majority of the images shown (as indicated in the figure legends), confocal microscopy was used to collect z-stacks (0.37µm steps) to later generate z-stacks using image processing to ensure that the full cilium/basal body/rootlet are visible. The same acquisition settings (gain, laser power, offset, etc) were used for every sample in each individual experiment. FIJI imaging software was used to process the z-projections, and the same brightness, contrast, cropping, and other processing settings were used across the experimental test group to ensure the accuracy of comparisons.

Super resolution microscopy: 3D-SIM images of cilia were collected using a Nikon superresolution microscope (N-SIM) at 100x magnification (1.49 NA, Oil) using a 488-laser line. An EMCCD - Andor iXon3 DU-897E-CS0-#BV camera was used. Data were acquired and processed using Nikon Elements v5.0.2 software. Widefield images along with raw SIM data were collected for every cilium studied. Nikon Elements was used to reconstruct images collected via SIM, and reconstruction parameters were adjusted as needed to prevent the introduction of artifacts that did not coincide with the original widefield image.

g-STED images were collected using a Leica gSTED 3× microscope at 100x magnification (NA 1.4, oil). Z-stack projections were collected for each cell with a 0.22 μm step-size, and images were collected using 488 and 561 laser lines for excitation and 592 and 660 laser lines for depletion. Images were acquired and processed using Leica X software. Confocal, gSTED, and deconvolved gSTED images were collected.

Live cell Imaging: Wild-type cells were transfected with plasmid directing expression of GFP-rootletin for 24 hours, using the jetOPTIMUS protocol described above, and cells were replated onto 35 mm MatTek dishes (#P35GC-1.5-14-C). The next day, cells were imaged using a BioTek Lionheart FX widefield microscope at 20x magnification (NA .45) using the 488 channel and phase-contrast. Images were collected every 5 minutes for 12 hours immediately after serum starvation (10% DMEM +0.5% FBS). Cells were maintained with constant CO_2 (5%) and temperature (37˚C) throughout the imaging window. Videos were processed via Lionheart imaging software.

Reproducibility/Statistics: Unless otherwise stated, 100 cells were scored per each replicate, and all experiments were performed in at least triplicate and scored in at least duplicate.

Data were processed using Excel and graphed using GraphPad Prism, and error bars shown indicate the standard error of the mean (SEM) for the data set. Individual data points signify the average of technical replicates for each individual cell line. For all quantified data, statistical significance of the difference between individual test groups was assessed using either One-Way or Two-Way ANOVA tests: * = $p < 0.05$; ** = $p < 0.01$; *** = $p < 0.0001$. Technical replicates are considered the replicates of individual lines performed on separate days, while biological replicates are considered the average of the technical replicates for individual lines.

Results

ELMOD2 deletion causes increased ciliation and multiciliation

We have shown previously (Turn et al., 2020) that deletion of ELMOD2 results in centrosome amplification as well as decreased microtubule stability and nucleation from centrosomes in immortalized mouse embryonic fibroblasts (MEFs). Given the roles of centrosomes/basal bodies and microtubules in ciliogenesis and ciliary functions, we explored effects of ELMOD2 deletion on ciliation in these cells, predicting there to be defects in ciliation. We used the same 10 KO clones described previously (Turn et al., 2020) in which frame shifting mutations in ELMOD2 were introduced by CRISPR/Cas9 and confirmed by DNA sequencing, as well as a parental and a "CRISPR WT" line that underwent transfection and cloning but had no mutations in the targeted region of the ELMOD2 gene. Four of the KO clones were transduced with a lentivirus directing expression of ELMOD2-myc to assess rescue of any observed phenotypes and to protect against off-target effects of CRISPR.

We stained cells for ciliary (ARL13B, acetylated tubulin) and centrosomal (γ-tubulin, centrin) markers with and without serum starvation (0.5% fetal bovine serum (FBS) for 24 hr) to

induce ciliation, as described under Materials and Methods. In contrast to our predictions, ELMOD2 KO lines displayed *increased* ciliation compared to WT controls (Figure 1A) in both normal medium (10% FBS) or after serum starvation. All 10 ELMOD2 KO lines displayed higher rates of ciliation compared to WT, without (*62.5% (n = 10, range = 43-78%) versus 16.0% (n = 3, range = 13-19%), respectively*) or with (*89.1% (n = 10, range = 61-97%) versus 42.7% (n = 3, range = 32-51%) respectively*) serum starvation to induce ciliation. This increase in the percentage of cells displaying cilia in ELMOD2 KO lines was reversed upon expression of ELMOD2-myc via lentivirus. These "rescued" KO lines had clearly reduced ciliation rates compared to their uninfected KO cells: 28.0% *((n = 4) range = 15-43%)* in normal medium and 42.8% *((n = 4) range = 30-55%)* after serum starvation, approaching numbers seen in WT lines (Fig. 1B-C). In contrast, there was no difference in the percentage of ciliated cells in WT compared to WT transduced with the lentivirus directing expression of ELMOD2-myc (Fig. 1B-C).

In addition to increased ciliation, we also observed clear increases in instances of multiciliation. This is unusual, as WT MEFs typically have a single, long primary cilium with fairly uniform staining of acetylated tubulin and ARL13B throughout its length; each cilium has a single basal body. The four ELMOD2 null lines tested revealed an increase in multiciliation, with an average of 24.4% *(n = 4, range = 20-32%)* of ciliated cells having at least two cilia (compared to 1.2% *(n = 2, range = 1-1.3%)* of WT cells) (Fig. 1D-E). Though it was far more common to see 2-3 cilia per cell, some cells had 9 or more cilia (Figure 1E). Our previous paper (Turn et al., 2020) reported that ELMOD2 KO cells have supernumerary centrosomes at an increased frequency, which would enable the increase in ciliation. Cilia in ELMOD2 KOs also varied in length and morphology, having stubby, short cilia in some cells and normal length cilia in others. Thus, it appears that ELMOD2 normally may act to suppress ciliation, as the loss of ELMOD2 in

MEFs results in both an increase in the number of cells that ciliate and also alterations in the processes that control ciliation numbers and morphologies.

ELMOD2 KO cells display abnormal ciliary morphology and protein content

We next asked if the cilia displayed normal morphology and function, as we predicted that spurious ciliation may be accompanied with failed regulation of ciliary structure, as previously described (REFs). We noted an increase in cilia with non-uniform ARL13B and/or acetylated tubulin staining. Using structured illumination microscopy (SIM), these abnormalities in staining could be resolved into what appear to be buds coming off the surface along the length of the cilium (Figure 1H). There are even instances in which these buds appear to form branches or result in ciliary splaying, as detected by widefield microscopy (Figure 1G). Individual buds and branches that stained positive for ARL13B often, but not always, co-stained with acetylated tubulin. This suggests that these aberrant morphologies may occur from the ciliary membrane alone but could also be in response to changes in the axonemal structure. While 22.8% of cilia in ELMOD2 KO cells have abnormal morphology *(n = 4, range = 14-30.3%)*, this is true in only 2.7% *(n = 2, range = 2-3.3%)* of cilia in WT MEFs, based on widefield immunofluorescence imaging (Figure 1F).

We typically use centrosomal markers, such as centrin, to mark and facilitate the identification of cilia, particularly when ciliary markers display background staining. A quite surprising but even more common change found in the ELMOD2 KO lines was the presence of centrin staining *inside* cilia (in an average of 86.2% of KO cells *(n = 4, range = 81.3-89.3%)* versus 12.8% *(n = 2, range = 12-13.7%)* of WT cells) (Figure 1I). Centrin is a canonical centriolar protein used to mark the basal bodies and has not previously been reported in primary cilia (except in the transition zone of retinal cells and olfactory epithelia (REF)), though there have been reports

of it being recruited to motile cilia (Huang et al., 1988; Piperno et al., 1992). Because of the striking increase in centrin staining inside cilia, we tested whether conditions might be found in which centrin may also be found in WT cilia. That is, perhaps centrin can always enter cilia but, under normal conditions, it is rapidly exported so it only rarely reaches levels detectible by antibody staining. To test this, we inhibited retrograde ciliary transport by treating cells with the dynein motor inhibitor ciliobrevin (30μM for 1 hour) before fixing cells and staining for centrin. As a positive control, we stained for Gli3 with and without ciliobrevin treatment. Without ciliobrevin, little to no Gli3 staining was present in cilia of WT or ELMOD2 null cells. However, ciliobrevin treatment led to increased Gli3 ciliary staining and, in many cases, Gli3 accumulation at the ciliary tip in both WT and ELMOD2 KOs. When we stained ciliobrevin-treated cells for centrin, we detected centrin in WT cilia at levels comparable to those seen in cilia of ELMOD2 KO lines without ciliobrevin treatment (Figure 1 I-K). Ciliobrevin-treatment of ELMOD2 KOs resulted in even higher levels of centrin staining, including a subpopulation of cells demonstrating accumulation of centrin at the ciliary tip. Thus, these data are consistent with the conclusion that centrin enters cilia in WT cells but is normally rapidly exported back out. In ELMOD2 KO lines, export of centrin appears to be compromised, resulting in its accumulation there, though we cannot exclude potential effects of ELMOD2 deletion on centrin protein half-life or rate of import. Interestingly, no differences were observed in Gli3 staining in WT vs ELMOD2 KO lines, suggesting that there is selectivity to the effects of ELMOD2 KO on the ciliary proteome.

Defects in ciliary morphology and/or protein traffic are often associated with defects in ciliary functions and signaling. Ciliary signaling, in turn, is linked to regulated import/export of membrane receptors, so we asked if loss of ELMOD2 disrupted canonical ciliary signaling pathways. The G protein coupled receptor (GPCR) somatostatin receptor 3 (SSTR3) was expressed

as a GFP-tagged protein in WT and ELMOD2 KO lines, which were then induced to ciliate by serum starvation to assess its localization to cilia. Every ciliated GFP-positive WT cell displayed SSTR3-GFP in cilia. In contrast, we observed few, if any, ELMOD2 KO cells with cilia positive for SSTR3-GFP (Figure 2A). While useful for tracking exogenous proteins, the presence of GFP in a fusion protein always risks altering functionality. Thus, we also examined import of the endogenous protein and its sensitivity to pathway activation. We found an antibody with sufficient sensitivity to label endogenous SSTR3, and the results were the same as those coming from the GFP tagged protein. However, this antibody has been discontinued by the commercial supplier (Santa Cruz), so any further studies of SSTR3 used the tagged protein.

Smoothened (Smo) is a G_i linked GPCR that is imported into cilia in response to activation of the Sonic Hedgehog (SHH) pathway. Cells were treated with conditioned medium containing SHH under serum starvation conditions and were stained 24 hours later with antibodies directed against acetylated tubulin and Smo. Controls included serum starved cells that were not exposed to SHH. WT cells displayed marked recruitment of Smo to cilia upon SHH treatment *(76.5% strong staining (range = 72.5%-81.0%), 15.3% weak staining (range = 10.0-25.0%), 8.0% no Smo staining (range = 7.0-9.0%); n = 2)*. In contrast, ELMOD2 nulls showed markedly reduced Smo staining in SHH-treated cells *(26.4% strong staining (range = 15.0-33.5%), 6.6% weak staining (range = 1.5-16.0%), 67.0% no Smo staining in cilium (range = 50.5-83.5%); n = 4)* (Figure 2C). Expression of ELMOD2-myc reversed the defect in Smo recruitment *(62.6% strong staining (range = 55.0-77.5%), 14.6% weak staining (range = 11.5 – 17.5%), 22.8% no Smo staining in cilium (range = 11.0-29.0%); n = 4)* (Figure 2C).

We also tested whether the reduction in Smo recruitment was accompanied by defects in downstream transcriptional regulation in the SHH pathway, using qPCR to monitor levels of *Gli1*

and *Ptch1* mRNAs (REFs). We observed that ELMOD2 KO caused decreases in the magnitude of responses to SHH in both mRNAs (Figure 2D), consistent with decreased SHH signaling. Because these cells are polyploid and multinucleated, due to cell cycle defects described previously (Turn et al., 2020), it is difficult to draw many conclusions regarding the defective SHH signaling and downstream transcriptional output in ELMOD2 KO cells. Together, though, both the immunofluorescence and qPCR data monitoring the SHH pathway reveal defects in ciliary signaling.

To assess the extent to which ELMOD2 deletion results in defects in import of ciliary signaling proteins, we also looked at two other ciliary membrane proteins. The GPCR GPR161 and adenylyl cyclase ACIII each displayed reduced ciliary localization in ELMOD2 KO compared to WT cells (Figure 2B), and these defects were reversed upon expression of ELMOD2-myc. Together, these results show that deletion of ELMOD2 leads to changes in the levels of ciliary proteins both under basal conditions and in response to SHH stimulation. These changes include both increases (*e.g.*, centrin) or decreases (*e.g.*, SSTR3, ACIII, CPR161) in protein abundance that might result from defects in import, export, half-life, or ciliary retention.

ELMOD2 localizes to the basal body in MEFs and can be found in cilia after treatment of cells with ciliobrevin

Based on the strong evidence pointing to effects of ELMOD2 deletion on ciliary function, we sought to explore the likelihood of it acting directly in cilia or at basal bodies, rather than through indirect effects e.g., on microtubule nucleation or stability. In previous studies, we and others have found that ELMOD2 localizes to the endoplasmic reticulum (ER), lipid droplets, mitochondria, Flemming bodies, and centrosomes Because of ELMOD2's presence at

centrosomes, we examined whether ELMOD2 may also localize to cilia or cilia-associated compartments. Using our rabbit polyclonal ELMOD2 antibody, we found no convincing evidence of ELMOD2 localization to cilia after 24-hour serum starvation and fixation with either methanol or PFA. We then asked if ELMOD2 may behave like centrin (*i.e.*, showing increased staining in cilia after inhibition of retrograde traffic via ciliobrevin treatment). We incubated serum-starved WT MEFs with or without 30 μM ciliobrevin for 1hr, fixed cells with 4% PFA and immunostained for ELMDO2 and ARL13B. No sign of ELMOD2 staining was seen in WT MEFs without drug treatment. However, ELMOD2 staining was evident, though weak, in cilia from cells treated with ciliobrevin (Figure S1). No such staining is evident in the ELMOD2 KO cells, indicating that the staining is specific. It is uncertain whether ELMOD2 functions inside cilia, but these results indicate that it can at least transiently localize there.

To see if ELMOD2 localizes to basal bodies, we serum starved WT MEFs, fixed with cold methanol for 5 minutes, and immunostained for acetylated tubulin and ELMOD2. We observed specific staining of ELMOD2 at both the basal bodies (at the base of cilia) (Figure 3A) as well as at non-ciliary centrosomes (as previously reported (Turn et al., 2020)). Our previous studies reported strong co-localization with both γ-tubulin and centrin, though appearing more similar in size/shape with γ-tubulin (Turn et al., 2020). We interpret this as evidence of specific localization of ELMOD2 in the PCM (pericentriolar material) rather than the centriole, as its staining co-localizes but extends beyond centrin (a classic centriolar marker). We cannot exclude its presence at specific sites along centrioles, though. ELMOD2 staining in the cilium itself was not observed under these conditions.

Interestingly, we noted that ELMOD2 staining at the basal body did not localize exclusively to a tight focus, but also showed staining of a “foot-like” structure emanating

apparently from the proximal end of the basal body, away from the cilium (Figure 3A). Though there are many instances in which ELMOD2 staining appeared as a single foot, extending from the basal body at a clearly distinct angle from the ciliary axoneme (acetylated tubulin staining), in other cases multiple smaller, fibrillar projections were apparent, and these varied in length. This staining was absent in ELMOD2 KO cells (Figure 3A). These projections did not co-localize with acetylated tubulin, suggesting that ELMOD2 was localizing to a distinct structure. Based on this staining, we predicted that perhaps ELMOD2 may also be localizing to ciliary rootlets, a cytoskeletal structure projecting from basal bodies of cilia and made up of polymers of the protein rootletin. To test this, serum-starved WT MEFs were co-stained with acetylated tubulin (to mark cilia), rootletin (to mark rootlets), and ELMOD2 to assess co-localization. Rootletin staining is apparent in all cells, with or without cilia, and strongly concentrated at centrosomes. In practically all cells studied, this staining appears as long tendrils/feet surrounding and extending from the centrosome, as described previously (REFs). There was heterogeneity in the morphology of these rootlets, as some have many feet, and their length and shape varied from cell to cell. When comparing rootlets in ciliated versus non-ciliated cells, we note that rootlets at the base of cilia typically appeared as one, thick rootlet rather than many thinner, more tendril-like rootlets more typical of non-ciliary rootlets, also as previously described (REFs). Interestingly, ELMOD2-positive “feet” clearly overlapped and partially co-localized with the rootletin fibers/feet (Figure 3A). Not only did their staining not completely overlap, but there were cases in which there were rootletin-positive tubules extending from the basal bodies that showed no sign of ELMOD2 staining. ELMOD2 staining appears to co-localize to rootlets only when the rootlets are associated with the centrosome, and co-localization is most extensive when the strands of rootletin are compact (Figure S5).

MEFs were originally chosen as our model system to study ELMOD2 as we were testing its role in mitochondrial fusion and later noted effects of deletion on abscission and microtubule stability (Turn, et al 2020). With these more recent, and unexpected, observations regarding its functions and localizations at cilia, we tested to see the likely generalities of its presence at cilia using a better model system of ciliary structure/function. Photoreceptor cells (rods and cones) in the retina are perhaps the most commonly used model for ciliary signaling due to their large cilia resulting from their specialized role in phototransduction. Such a model system allows for detailed structural analyses and protein localization under normal and pathological conditions (REFs). Mouse and human retinas were obtained and processed for immunofluorescence imaging, as described under Methods and previously (REFs). Staining of centrin, to mark the connecting cilium and inner segment of photoreceptor cells, and ELMOD2 are shown in Figure 4A-B. In both human and mouse tissue, we observe that ELMOD2 is localized adjacent to the ciliary rootlet at the base of the connecting cilium (a structure that connects the outer (including the ciliary rootlet) and inner segments of the retinal cell that is equivalent to the transition zone of other primary cilia). These data, coupled with the work done in ELMOD2 null cells, point to potential roles for ELMOD2 as acting from potentially multiple cellular locations to mediate essential ciliary functions including traffic of ciliary cargoes and ciliogenesis.

Loss of ELMOD2 leads to fragmentation and abnormal morphology of ciliary rootlets

Using the same conditions described above to look at ciliary rootlets in WT MEFs, we repeated the experiment in ELMOD2 KO lines and found striking differences. In general, ELMOD2 KO lines displayed more fragmented rootletin staining throughout the cell body, rather than bright fibrillar staining focused at centrosomes (Figure 3B). On average, 65.0% of KO cells

show rootlet fragmentation *i.e.*, the rootletin staining is dispersed throughout the cell as bright puncta) *(n = 4, range = 56.0-77.5%)*, while only 4.0% of WT cells had such fragmented rootlets *(n = 2, range = 1.5-6.5%)* (Figure 3E). Expression of ELMOD2-myc brought the extent of rootlet fragmentation back down to near WT levels *(12.5%, n = 4, range = 10.5-20.0%)* (Figure 3E). In ciliated ELMOD2 KO cells, rootletin stains the proximal end of basal bodies as bright puncta but no obvious rootlets, or what we define as a foot-like structure projecting from the base of the cilium (Figure 3C). While 100.0% of WT cilia have a rootlet *(n = 2)*, only 29.6% of ELMOD2 KO cilia have a rootlet *(n = 4, range = 21.5-38.5%)* (Figure 3F). Once again, this phenotype is rescued upon lentiviral transduction with ELMOD2-myc *(79.0%, n = 4, range = 75.5-83.5%)* (Figure 3F). Together, these data provide evidence that ELMOD2 is important in regulating rootlet recruitment to or organization at basal bodies.

Previous studies have revealed that rootletin is a critical component of centrosome linkage, along with C-Nap1, Cep44, and Cep68 (Bahe et al., 2005; Conroy et al., 2012; Flanagan et al., 2017; Graser et al., 2007b; Hossain et al., 2020; Vlijm et al., 2018; Yang et al., 2006). Disruption of centrosome linkage can lead to spurious centrosomal separation with potentially severe downstream consequences in the cell, such as aneuploidy and supernumerary centrosomes (REF). We tested whether loss of ELMOD2 leads to increased centrosome separation by scoring the number of cells with centrosomes >2µm apart, a common metric in the field (REF). An average of 14.0% of WT cells had separated centrosomes *(n = 2, range = 13.0-15.0%)*, while 59.3% of ELMOD2 null cells had separated centrosomes *(n = 4, range = 54.0-65.5%)* (Figure 3D, 3G). The centrosome cohesion defect was largely reversed upon expression of ELMOD2-myc *(23.6%, n = 4, range = 21.0-26.0%)* (Figure 3G). Thus, ELMOD2 is found to play a role in docking or retention

of rootletin to centrosomal proteins. Based on these data, we predict ELMOD2 is important to both centrosome cohesion and ciliary licensing.

ELMOD2 localization and rootlet morphology change dynamically during early ciliogenesis

Based on early impressions, we noted a trend in which ciliated cells tended to have tighter, more compact rootlets that extended from the basal body. On the other hand, non-ciliated cells tended to have larger, more spread out rootlets encasing their centrosomes, looking like thin tendrils. We asked if rootlets undergo changes in morphology to suit the ciliary needs of the cell. Previous literature has already suggested that rootlets are dynamic structures, particularly with regards to centrosome separation and the free diffusion of rootletin to form rootlets (Mahen, 2018). Yet, the relationship between rootlet dynamics and cilia-inducing conditions has not been closely studied. We performed live-cell imaging of rootlets using widefield microscopy of GFP-rootletin transfected cells at low magnification (20x) (Figure S11). Wild-type cells were imaged with and without serum starvation to observe if cilia-inducing conditions promote changes in rootlet morphology. As shown in Figure S11, rootlet fragmentation was observed upon induction of serum starvation, in which regions of strong rootletin staining began to separate from the centrosomes and PCM. These fragmentation events began within the first 5 minutes of imaging (not including the 10-15 minutes it took to swap out medium, find a field on the microscope, and set imaging parameters). These changes in rootletin dynamics were only observed after serum starvation. In serum-enriched medium, the rootlet morphology did not appear to change during the hour imaging window (Figure S11).

Based on the finding that rootlets dynamically change morphology in response to serum starvation, we next asked if ELMOD2 also changed in localization to rootlets at different time

points after serum starvation. We tracked the changes in rootlet morphology and ELMOD2 localization during ciliogenesis by monitoring the proteins at varying times after initiation of serum starvation. Under serum enriched conditions, rootlets typically appeared as large, dense networks of anemone-like structures encasing both centrosomes (Figure 3H), though in mitotic cells there is little or no rootletin staining at centrosomes. Cells were fixed at different time points after serum starvation and stained for rootletin, ELMOD2, and acetylated tubulin. When rootletin staining is present, it localizes to small puncta that align with centrosomes. Without serum starvation, ELMOD2 staining only partially co-localizes with that of rootletin, though staining of ELMOD2 is relatively weak in intensity and can be difficult to discern at basal bodies over background. As early as 10 minutes after serum starvation, ELMOD2 staining at rootlets surrounding centrosomes becomes very bright and co-localizes almost completely with rootletin (Figure 3H). By 30-60 min, ELMOD2 staining becomes more compacted around centrosomes, while rootlets remain large/branching. With increasing time, the rootlets followed the same trend as ELMOD2 and also became more compact around the basal body. Instead of appearing as thin tendrils, the rootlets became more bundled around the centrosome(s). By 6hr, ELMOD2 and rootletin co-localize tightly around the centrosome as thick roots (Figure 3H), and this staining pattern is maintained at the 24hr time point. Interestingly, the vast majority of cells with compacted rootlets were ciliated while cells that still had less-compact, tendril-like rootlet staining lacked a cilium.

Rootletin KO MEFs phenocopy ELMOD2 KO phenotypes

As a result of the (partial) co-localization of ELMOD2 and rootletin and effects of ELMOD2 loss on rootlets, we hypothesized that ELMOD2 and rootletin act in the same pathway to affect ciliogenesis. To test this model, we knocked out rootletin in MEFs, using the same

approaches as described for ELMOD2 null cells (Turn et al., 2020) (Figure S2A-B). Mouse rootletin is a ~225kDa protein composed of 2009 amino acids encoded in 37 exons on chromosome IV. NCBI predicts (gene ID: 230872) two transcripts that differ at the 5' end, impacting N-terminal sequences. For this reason, we targeted exons downstream of these differences so that each transcript would be frame shifted in the same way. We generated guide RNAs targeting exons 6, 7, 8, or 9 to induce frame shifting mutations with the goal of making non-functional protein products. Screening was performed by immunofluorescence of MEF lines cloned by limiting dilution, followed by DNA sequencing surrounding the targeted exon to identify frame shifting mutations in both alleles. We generated 5 predicted KO lines from three different guide RNAs (see Fig. S2A-B). Western blotting of total cell lysates and probing with an antibody to rootletin confirmed the loss of the major band at ~240 kDa (seen in all WT lines, based on protein standards) in all KO lines (Figure 5A). This rootletin antibody was raised against a C-terminal fragment of the holoprotein and failed to reveal any shorter bands, consistent with the loss of rootletin protein products.

These rootletin KO lines were then used to test the hypothesis that ELMOD2 and rootletin work in the same pathway to negatively regulate ciliogenesis. As seen in our ELMOD2 KO lines, loss of rootletin leads to increased centrosome separation *(68.2% in rootletin KO (n = 5, range = 53-81%) versus 19.5% in WT (n = 3, range = 17-23%),* which is consistent with previous reports of rootletin regulating centrosome cohesion (Bahe et al., 2005; Yang et al., 2006) (Figure 5D). Rootletin KO cells also have increased ciliation *(94.7%, n = 5, range = 93.5-97%)* and multiciliation *(23.3%, n = 5, range = 17.0-30.0%)* compared to WT cells *(38.7%, n = 3, range = 35.0-43.0% for ciliation, 0.0% for multiciliation, n = 3)* (Figure 5B-C). Yet, rootletin nulls are distinct from ELMOD2 nulls in that they do not have cold sensitive microtubules, multinucleation,

or evidence of cytokinesis defects (Turn et al., 2020). Furthermore, while ELMOD2 nulls tend to have a wide range of number of cilia per cell (typically 2-3, but can be 9 or more), multiciliated rootletin KO cells almost never have more than two cilia. Thus, ELMOD2 and rootletin KO cells share commonalities in defects in centrosome cohesion, increased ciliation, and multiciliation, yet there are also somewhat subtle differences in aspects of these phenotypes.

During the immunofluorescence screening for rootletin null cells, we noticed in a few instances evidence of much stronger staining of rootletin rather than loss of rootletin (Figure 5B). One of these lines (called G1, #21) was preserved and analyzed by DNA sequencing. This clone was found to have frameshifting mutations on both alleles. One allele is a 1bp insertion, differing from the 1bp insertion found in G1,#31 only in the base inserted. Clone G1,#31 produced no rootletin staining. The other allele, though, was a 2bp insertion that was unique to that clone (Figure S2). Based on previous results from CRISPR/Cas9 KO in cultured cells, we predict that one or both alleles in this clone allow the use of a downstream methionine to generate an N-terminal truncated protein, rather than no protein. The predicted use of what is normally Met240 as the initiating methionine would result in a protein that is 239 residues shorter than the long transcript of mouse rootletin, or a total of 1770 residues (~195 kDa). An immunoblot of total cell lysate from these cells, probed with the rootletin antibody, shows the loss of the band at ~240 kDa and replacement by one slightly smaller, at ~215 kDa, consistent with our prediction of an N-terminal truncation mutant being generated (Figure 5A, see Figure S3 for original blot). The level of this truncated protein (which we term *Crocc*$^{\Delta 239}$) is clearly higher than that of the WT by both immunofluorescence and immunoblotting (Figs. 5A-B). We speculate that the N-terminus of rootletin may contain one or more sites of post-translational modification (*e. g.*, ubiquitination) that normally shortens the protein half-life. When the *Crocc*$^{\Delta 239}$ cells were stained for rootletin, we

observed that there are indeed still rootlets, though they are abnormally large, bright, and fibrous compared to WT rootlets (Fig. 5B). *Crocc*$^{\Delta 239}$ expressing cells showed no increase in centrosome separation (Figure 5D). Instead, they appear to have severely reduced ciliation compared to WT cells, with on average of only 6.5% of cells being ciliated (compared to 38.7% in WT cells) even after serum starvation. These cells also show no sign of multiciliation (Figure 5C). Thus, the N-terminal truncation mutant *Crocc*$^{\Delta 239}$ is expressed under its own promoter and results in higher levels of protein and reduced ciliation under standard or serum-starvation conditions. This observation is consistent with previous data indicating that, like ELMOD2, rootletin expression is associated with suppression of ciliation while its absence results in increased ciliation and multiciliation.

ELMOD2 localization is disrupted in rootletin KO cells

Because ELMOD2 and rootletin KO lines share similarities in phenotypes and the proteins extensively co-localize at rootlets and centrosomes, we predict that they act in a shared biochemical pathway. Both proteins are reorganized/recruited to basal bodies early in ciliogenesis, and ELMOD2 KO disrupted rootlet organization. We speculated that perhaps the converse is also true: *i.e.*, that rootletin deletion would alter the localization/organization of ELMOD2 at the basal body, though not elsewhere in cells. Rootletin null cells were serum starved for 24hr, fixed, and stained for ELMOD2, acetylated tubulin, and γ-tubulin. As described above, ELMOD2 typically localizes to basal bodies and rootlets in WT cells. As expected, rootletin KO results in loss of ELMOD2 localization at rootlets (as they are absent). They still appear to have at least some basal body localization. Interestingly, though, there is an acquisition of strong ciliary localization of ELMOD2 (Figure 5E). This staining is punctate and distributes preferentially to the distal tip of a

subpopulation of cilia. In *Crocc*$^{\Delta 239}$ cells, in which rootlets are retained and even magnified, ELMOD2 staining is strongly rootlet-associated, even more so than in WT rootlets (Figure 5E). We examined ELMOD2 localization at other sites (*e.g.* midbodies and mitochondria) and found no changes in ELMOD2 at those sites in rootletin KO cells (Figure S4). This suggests that rootletin specifically plays a role in ELMOD2 localization to cilia/rootlets but not other cellular compartments. Together, these data reveal that rootletin and ELMOD2 localization at basal bodies and rootlets are co-dependent and that loss of either results in very similar phenotypic consequences at that site.

Rootletin over-expression rescues ELMOD2 null phenotypes

Given the close physical and functional properties of ELMOD2 and rootletin, null cells of each were each transfected with a plasmid that directs the expression of myc-rootletin to determine if over-expression could reverse the phenotypes resulting from the loss of either rootletin or ELMOD2. Transfected cells were fixed and stained for myc, acetylated tubulin, γ-tubulin, and rootletin to assess ciliary, centrosomal, and rootlet phenotypes. Transfected cells were scored for ciliation (Figure 6A) and centrosome separation (Figure 6B). An empty vector transfection control (pcDNA3.1) was also performed to ensure that the act of transfection itself did not lead to changes in centrosome separation or ciliation. Transfected cells were scored for number of ciliated cells and for number of cells with centrosomes >2μm apart. In summary, expression of empty vector had no effect on % ciliation *(WT: 33.3%, n = 2, range 30.0-36.5%; ELMOD2 KO: 92.8%, n = 4, range 87.5-97.0%; rootletin KO: 89.0%, n = 4, range 87.0-90.5%;* Crocc$^{\Delta 239}$*: 0.5, n = 1)* or centrosome separation *(WT: 17.3%, n = 2, range 17.0-17.5%; ELMOD2 KO: 75.0%, n = 4, range 71.5-81.0%; rootletin KO: 74.9%, n = 4, range 65.5-84.5%;* Crocc$^{\Delta 239}$*: 14.0, n = 1)* in transfected

cells. On the other hand, myc-rootletin reversed both increased ciliation *(WT: 27.3%, n = 2, range 23.5-31.0%; ELMOD2 KO: 36.9%, n = 4, range 30.0-42.5%; rootletin KO: 37.8%, n = 4, range 32.5-40.0%;* Crocc$^{\Delta 239}$*: 1.5%, n = 1)* and increased centrosome separation defects *(WT: 14.8%, n = 2, range 14.0-15.5%; ELMOD2 KO: 21.4%, n = 4, range 17.0-30.0%; rootletin KO: 17.1%, n = 4, range 14.0-22.0%;* Crocc$^{\Delta 239}$*: 12.5%, n = 1)* in both ELMOD2 KO and rootletin KO cells (Figure 6A-B). This result further supports a close functional link between ELMOD2 and rootletin and even suggests that ELMOD2 may play a regulatory role in recruiting rootletin to basal bodies that can be overcome in its absence by excess rootletin. Expression of myc-rootletin fails to reverse the phenotypes in *Crocc$^{\Delta 239}$* expressing cells, consistent with these phenotypes resulting from an already increased level of rootletin activity.

ELMOD2 functions in cilia are at least in part independent of its GAP activity

With the strong evidence for a role of ELMOD2 in aspects of ciliary and rootlet biology (above) and the history of ARF family GAPs acting as both GAPs and effectors (REFs), we asked whether GAP activity is required for its actions at cilia or rootlets. To test this, we used the point mutation that has previously been shown to result in loss of GAP activity as a result of the mutation of the "arginine finger" in the GAP domain (REFs). We transfected WT and ELMOD2 KO cells with either empty vector control, ELMOD2-myc, or ELMOD2[R167K]-myc. The next day, cells were serum starved for 24 hours. Percentage of ciliated cells was scored using myc staining to identify transfected cells along with acetylated tubulin to mark cilia. Transient transfection of ELMOD2-myc reversed increased ciliation in ELMOD2 null cells (similar to what we observed previously using lentiviral transduction) but failed to reverse ciliation defects in rootletin KO or *Crocc$^{\Delta 239}$ (WT: 28.5%, n = 2, range 27.0-30.0%; ELMOD2 KO: 26.1%, n = 4, range 21.5-34.0%;*

Rootletin KO: 89.6%, n = 4, range 88.0-91.0%; Crocc$^{\Delta 239}$*: 1.0%, n = 1)* (Figure 6A). ELMOD2-myc expression also failed reversed centrosome separation in rootletin KO and *Crocc$^{\Delta 239}$* cells, though it did reverse the increased centrosome defects in ELMOD2 KO cells *(WT: 22.5%, n = 2, range 21.0-24.0%; ELMOD2 KO: 25.4%, n = 4, range 14.0-33.0%; Rootletin KO: 74.5%, n = 4, range 67.5-80.0%;* Crocc$^{\Delta 239}$*: 13.0%, n = 1)* (Figure 6B). These data suggest that ELMOD2 alone is not sufficient to regulate ciliation or centrosome cohesion. Surprisingly, the expression of GAP-dead ELMOD2-myc mirrored the phenotypes of ELMOD2-myc expression in both ciliation and centrosome cohesion, in that both GAP-dead ELMOD2 and WT ELMOD2 reverse increased ciliation defects and increased centrosome separation defects in ELMOD2 KO cells (Figure 6A-B). ELMOD2[R167K]-myc expression had little to no effect on ciliary *(WT: 28.5%, n = 2, range 25.5-31.5%; ELMOD2 KO: 26.6%, n = 4, range 19.0-33.0%; rootletin KO: 90.1%, n = 4, range 81.0-94.0%; Crocc$^{\Delta 239}$: 0.0, n = 1)* and centrosome separation defects *(WT: 19.8%, n = 2, range 19.5-20%; ELMOD2 KO: 20.9%, n = 4, range 16.0-26.5%; rootletin KO: 61.6%, n = 4, range 59.5-64.5%;* Crocc$^{\Delta 239}$*: 14.0%, n = 1)* in rootletin KO and *Crocc$^{\Delta 239}$* cell lines (Figure 6A-B).

We also asked if ELMOD2 functions at rootlets might also be independent of GAP activity. We transfected empty vector, ELMOD2-myc plasmid, and ELMOD2[R167K]-myc plasmid in WT controls and ELMOD2 KO lines and scored for rootlet fragmentation (Figure 6C). We discovered that ELMOD2 function at rootlets also appears to be independent of GAP activity as the ELMOD2[R167K]-myc mutant showed similar levels of rescue to ELMOD2-myc. In the case of rootlet fragmentation, neither ELMOD2-myc nor ELMOD2[R167K]-myc expression had any effect on rootlet morphology in WT cells *(empty vector: 9.8%, n = 2, range 7.0-12.5%; ELMOD2-myc: 13.8%, n = 2, range 12.0-15.5%; ELMOD2[R167K]-myc: 13.0%, n = 2, range 12.5-13.5%)* (Figure 6C). On the other hand, expression of ELMOD2-myc or ELMOD2[R167K]-myc reversed

rootlet fragmentation in ELMOD2 KO cells to levels quite similar to those seen in WT cells *(empty vector: 78.0%, n = 4, range 68.0-84.5%; ELMOD2-myc: 18.8%, n = 4, range 13.0-23.5%; ELMOD2[R167K]-myc: 23.9%, n = 4, range 18.5-30.0%)* (Figure 6C). Together, these data suggest that ELMOD2 does not rely on GAP activity to mediate ciliary or rootlet functions. Note that the GAP-dead [R167K] mutant retains binding affinity to activated ARF family GTPases. Therefore, we predict that ELMOD2 is acting as a downstream effector rather than as a terminator of GTPase signaling.

ARL2 can rescue ciliary and centrosomal defects in Rootletin and ELMOD2 KO cells and specifically localizes to rootlets

Because ELMODs are single domain proteins that bind the activated conformation of a number of ARF family GTPases, though likely not acting primarily as a GAP at basal bodies or rootlets, we predict that an ARF family GTPase is also involved in the basal body/rootlet actions of ELMOD2. A number of ARF family GTPases have been linked to ciliary functions including ARL2, ARL3, ARL6, and ARL13B (REFs). In our previous work, we showed that ELMOD2 acts with ARL2 in mitochondria and tubulin assembly, and with ARF6 at recycling endosomes and Flemming bodies (Turn et al., 2020). To determine whether any of these GTPases can rescue the loss of ELMOD2, we expressed WT or activated mutants of each of these GTPases and scored effects on ciliation, rootlet fragmentation, and centrosome separation. Although by far the most commonly exploited activating mutation in regulatory GTPases is that of changing the glutamine in the G-3 motif to leucine (Q to L), we have found that expression of such mutants are often quite toxic to cells, making analyses of their cellular actions difficult (Turn et al., 2020; Zhou et al., 2006). As a result, we have increasingly relied upon “fast cycling” point mutants, in which a

conserved residue in the G-5 motif is mutated resulting in decreased affinity for GDP with retention of GTP binding (Aspenstrom, 2018; Santy, 2002). This allows for ready binding and inactivation by GAPs and prevents toxicity that may result from excess activity. We used vectors that direct expression of the following proteins: empty vector, ARL2, and (fast-cycling mutants of) ARL2[V160A], ARL3[L131A]-myc, ARF6[T157A]-HA, and ARL6[I165A]-myc. Of the numerous constructs expressed, only ARL2 and ARL2[V160A] demonstrated the ability to reverse rootlet fragmentation, elevated ciliation, and defective centrosome cohesion. ARL2 WT led to reversal of increased ciliation defects *(WT: 28.8%, n = 2, range 25.0-32.5%; ELMOD2 KO: 36.8%, n = 4, range 26.5-49.0%; rootletin KO: 41.4%, n = 4, range 26.5-49.0%;* Crocc$^{\Delta 239}$*: 1.0%, n = 1)* as well as centrosome separation defects *(WT: 17.8%, n = 2, range 17.5-18.5%; ELMOD2 KO: 28.9%, n = 4, range 23.5-36.5%; rootletin KO: 35.3%, n = 4, range 29-39.5%;* Crocc$^{\Delta 239}$*: 23.5, n = 1)* in both ELMOD2 KO and rootletin KO. Surprisingly, ARL2[V160A] reversed increased ciliation defects *(WT: 28.3%, n = 2, range 26.5-30.0%; ELMOD2 KO: 30.0%, n = 4, range 23.5-33.5%; rootletin KO: 30.1%, n = 4, range 26.0-32.5%;* Crocc$^{\Delta 239}$*: 1.0%, n =1)* and centrosome separation defects *(WT: 18.0%, n = 2, range 17.5-18.5%; ELMOD2 KO: 30.9%, n = 4, range 29-32%; rootletin KO: 41.1%, n = 4, range 35-45%;* Crocc$^{\Delta 239}$*: 13.0%, n = 1)* to similar levels as ARL2 WT. Furthermore, ELMOD2 KO cells transfected with either ARL2 or ARL2[V160A] showed reversal of their rootlet fragmentation defects *(ARL2: 24.8%, n = 4, range 21.5-28.5%; ARL2[V160A]: 24.6%, n = 4 range 17.0-32.0%)*. None of the constructs expressed could reverse the *Crocc$^{\Delta 239}$* ciliation defects, suggesting that loss of rootletin's N-terminus alters the ability of ELMOD2 and ARL2 to regulate its dynamics. None of the other GTPases tested in this experiment rescued the above-described defects to the same extent as ARL2, suggesting specificity of function for ARL2 in this pathway. Even ARL3, ARL2's closest paralog, did not

show evidence of rescuing ELMOD2 KO or rootletin KO defects. Fast-cycling ARL13B was also tested in this study; it also showed no signs of rescuing ciliary, rootlet, or centrosome defects in either ELMOD2 KO or rootletin KO but was not quantified. It is interesting to note that overexpression of ARL2, but not ELMOD2, reverses rootletin KO defects and that ARL2 rescued rootlet fragmentation in ELMOD2 KO cells. We take this to mean that ARL2 negatively regulates spurious ciliogenesis and centrosome separation in the same pathway as ELMOD2 and rootletin, though through different mechanisms than those of ELMOD2.

Previous work in our lab and others uncovered specific localization and roles for ARL2 at centrosomes, mediating microtubule nucleation as well as tubulin folding (REF). Other studies have also implicated ARL2 in stabilizing photoreceptor cilia (Wright et al., 2018) and in regulating ciliary length (Davidson et al., 2013). We immunostained for ARL2 under multiple different fixation and permeabilization conditions (methanol versus PFA for different time points, permeabilization with Triton X-100, etc), but did not detect clear evidence of ciliary staining. Instead, and in addition to centrosomal or basal body staining, we observed that ARL2 also co-localizes with rootletin staining at rootlets and that this staining competes (Figure 8A-B). This staining was detected after 5 minutes ice-cold methanol fixation, the same fixation conditions previously shown in our lab to detect ARL2 and ELMOD2 centrosomal staining (Turn et al., 2020; Zhou et al., 2006). Like ELMOD2, ARL2 stains the PCM strongly, but also can be detected along rootlets. Thus, we found a high degree of specificity among ARF family members in the ability of ARL2 to restore basal body and rootletin functionalities in the absence of ELMOD2. In ELMOD2 KO cells, ARL2 still localizes to rootlets, suggesting that ELMOD2 is not required for ARL2's recruitment to rootlets (Figure 8C). We found specific localization of ARL2 to the same two

structures, consistent with ARL2 acting in concert with ELMOD2 and rootletin in the regulation of ciliogenesis and centrosome separation.

Because ARL2 has not previously been found at rootlets, and rootlets have not typically been studied in MEFs, we again turned to the far better characterized retinal cells to assess if ARL2 shares the same staining pattern as ELMOD2 in mouse and human retinal cells (Figure 8D-F). Other studies have explored ARL2 staining in photoreceptor cells, but they did not tease apart ARL2's site of action (Wright et al., 2018). Unlike ELMOD2, ARL2 localizes to the rootlet itself in photoreceptor cells in both mice and humans (Figure 8D-F). These data would suggest that while ARL2 and ELMOD2 are both working at rootlets to regulate ciliary function, it is likely that the two players have discrete functions in these pathways.

ELMOD2 and rootletin regulate the ciliogenesis pathway by preventing spurious licensing through CP110 release

Many of the phenotypes described above might be explained by defects in intraflagellar transport (IFT) or transition zone (TZ) functionalities. Therefore, we screened a number of markers of these processes as a quick way to assess their integrity (Figure S9). IFT88 is a common marker for IFT and is a component of the IBT-B complex, active in anterograde ciliary traffic. It displays bright punctate staining (often with preferential staining at the base and tip) throughout the length of the cilium (Figure S9C). No differences were evident in the staining of IFT88 in WT vs ELMOD2 KO lines. Two TZ markers, NPHP4 and Cep290, each localize strongly to the TZ at the proximal end of the cilium, and again no differences were evident for these proteins in WT vs ELMOD2 KOs (Figure S9A-B). Thus, despite the evidence described above that loss of ELMOD2

results in apparent defects in ciliary protein import, export, and/or retention, we found no gross changes in the transition zone or localization of IFT based on use of a few markers of each.

Previous studies have revealed a role for Cep44 as a critical player in anchoring rootletin to centrosomes to generate rootlets (Hossain et al., 2020). They discovered it was the last known player to recruit that was essential for rootletin to bind. Therefore, we asked if loss of ELMOD2 or rootletin disrupted Cep44 localization (Figure S6). Neither rootletin nor ELMOD2 KO showed defective Cep44 localization to centrosomes, suggesting that ELMOD2 and rootletin are acting downstream of Cep44 in their actions at basal bodies. Interestingly, though, we noticed that a subpopulation of cilia showed faint Cep44 recruitment to cilia in both rootletin and ELMOD2 nulls. No such ciliary staining is apparent in WT cells. This trend of abnormal localization of centrosomal proteins to cilia is reminiscent of the spurious localization of centrin to cilia in ELMOD2 nulls and the spurious ELMOD2 enrichment in cilia of rootletin nulls (as described above). Altogether, though, these data suggest that ELMOD2 is acting downstream of Cep44 to regulate rootletin anchoring to centrosomes.

In marked contrast to the unaltered appearance of markers of the TZ and IFT, we observed spurious localization of proteins involved in ciliary activation (sometimes referred to as “licensing”). Early in ciliary assembly, the basal body is primed to dock to the plasma membrane and to project a cilium by sequentially recruiting/releasing a number of proteins. Key regulators of this process include Cep164 (a distal appendage protein that facilitates basal body docking to the membrane) (Schmidt et al., 2012), TTBK2 (a kinase that binds to Cep164 at distal appendages and phosphorylates key players that facilitate CP110 release) (Goetz et al., 2012; Lo et al., 2019), and CP110 (a centriolar capping protein that must be removed to allow docking of the ciliary vesicle which will eventually fuse with the plasma membrane to initiate growth of the cilium at

the cell surface (Spektor et al., 2007). In a WT cell, a centriole that is ready to assemble a cilium will stain positive for Cep164 and TTBK2 but negative for CP110. To ensure that only one cilium is generated per cell, any other centrosome(s) in a cell should show the opposite staining pattern so that they cannot recruit ciliary vesicles or dock at the plasma membrane. This predicted outcome was confirmed in our WT MEFs, which display at most one centrosome per cell that stains positive for Cep164 and TTBK2 but negative for CP110.

ELMOD2 KO cells displayed multiple centrosomes that fit these conditions ($Cep164^{+}$, $TTBK2^{+}$ and $CP110^{-}$) (Figure 9). Only 2.0% of WT cells *(n = 2, range 1.0–3.0%)* versus 33.8% of ELMOD2 KO cells *(n = 4, range 32.0-35.5%)* had >1 centrosome positive for Cep164 (Figure 9A-B). TTBK2 followed a similar trend as Cep164, as 37.4% of ELMOD2 KO cells had >1 centrosome positive for TTBK2 *(n = 4, range 32.5-45.0%)* compared to WT with only 1.3% of cells having >1 centrosome positive for TTBK2 (*n = 2, range 1.0-1.5%)* (Figure 9C-D). On the other hand, 8.5% of WT *(n = 2, range = 8-9%)* versus 42.3% of ELMOD2 KO *(n = 4, range 35.0-52.0%)* cells have >1 centrosome negative for CP110 (Figure 9E-F). This spurious activation of centrioles into basal bodies is reversed in ELMOD2 MEFs transduced with ELMOD2-myc (8.4% of cells have >1 centrosome positive for Cep164 *(n = 4, range 7-10.5%)*; 15.8% of cells have >1 centrosome without CP110) (Figure 9). We interpret these data as evidence that ELMOD2 normally plays a role in preventing spurious ciliary activation and that its loss leads to misregulation of the licensing events that ensure that only one centriole becomes a basal body per cell, resulting in multiciliation.

Because rootletin KO lines phenocopied ELMOD2 KO in several respects related to cilia, we stained rootletin KO and *Crocc*$^{\Delta 239}$ cells for Cep164, TTBK2, and CP110 as described above. Like in ELMOD2 KOs, loss of rootletin led to an increased percentage of cells with >1 centrosome

being positive for Cep164 *(42.7% (n = 5, range 37.0-48.5%)* compared to WT cells *(3.5% (n = 3, range 3.0-4.0%)* (Figure 9G). The same was true with TTBK2, with rootletin KO cells having 35.6% cells with >1 centrosome being positive for TTBK2 *(n = 4, range 33.5-38.5%)* (Figure 9H). Furthermore, an increased percentage of rootletin KOs had 2 or more centrosomes with no CP110 staining *(44.5% of rootletin KO (n = 5, range 40.5-50.0%) versus 7.3% of WT (n = 3, range 4-9%))* (Figure 9). Both phenotypes are consistent with spurious licensing of ciliogenesis and resemble results obtained in ELMOD2 KO lines in both phenotype and magnitude.

Interestingly, the *Crocc$^{\Delta 239}$* line had only slightly decreased levels of Cep164 localization at centrosomes, compared to WT *(46.3% of cells with ≥1 centrosome positive for Cep164 in WT vs 26.5% in* Crocc$^{\Delta 239}$*)* (Figure 9G). The same was true for TTBK2 *(29.0% in WT (n = 2, range 27.5-30.5%) vs 29.0% in* Crocc$^{\Delta 239}$*)* (Figure 9H). Instead, it appears that the site at which ciliogenesis is blocked in *Crocc$^{\Delta 239}$* cells is CP110 removal as 96.5% of *Crocc$^{\Delta 239}$* cells, versus 58.7% of WT cells, have all their centrosomes positive for CP110 (Figure 9I). This mutant line also has much lower percentages (6.5%) of ciliated cells after serum starvation. We interpret these data as evidence that both ELMOD2 and rootletin can act in cells to decrease or block ciliogenesis, specifically blocking spurious CP110 release.

Taken together, we propose that ELMOD2 is acting in close cooperation with rootletin and ARL2e to limit the timing and extent of ciliogenesis. We further argue that their site of action is downstream of the recruitment of Cep164 and TTBK2 and upstream of the release of CP110 (see Discussion).

Discussion

This study has provided new insight into the cellular functions of ELMOD2, close functional links to rootlets at basal bodies, and roles of both in ciliogenesis. Though previous studies have established roles for ELMOD2 in mitochondrial fusion (Newman et al., 2017a; Newman et al., 2017b; Newman et al., 2014; Schiavon et al., 2019), microtubule nucleation from centrosomes (Turn et al., 2020), cytokinesis (Echard et al., 2004; Turn et al., 2020), oogenesis (Zhou et al., 2017), and lipase recruitment to lipid droplets (Suzuki et al., 2015), this is the first evidence of ELMOD2 playing regulatory role(s) at cilia. We found that loss of ELMOD2 leads to increased ciliation, multiciliation, abnormal ciliary morphology, increased ciliary centrin, decreased recruitment of a subset of ciliary membrane receptors, loss of rootlet attachment to centrosomes/basal bodies, and loss of centrosome cohesion. These phenotypes were reversed upon expression of WT or activated ARL2, linking this GTPase and GAP as active in the same pathway(s). These results prompted us to (re-)examine the localization of ELMOD2 and ARL2 in MEF cells and retina where we found them at basal bodies and rootlets. The connection between ELMOD2 and rootlets was greatly strengthened by the observations that deletion of rootletin resulted in many of the same phenotypes seen in cells lacking ELMOD2 and that increased expression of rootletin reversed the phenotypes found in ELMOD2 KO lines. We propose that ELMOD2 (with ARL2) and rootletin inhibit spurious ciliogenesis by regulating rootlet morphology, thereby affecting the ability of mother centrioles to develop into basal bodies and to carry out the regulated recruitment and release of key factors that drive ciliogenesis. This work also provides some unexpected insights into the functional domains that control rootletin function, as loss of the first 239 amino acids of rootletin leads to increased levels of rootletin, loss of ciliation, increased CP110 retention, and decreased Cep164 and TTBK2 recruitment. We

summarize these observations with our proposed model for the actions of ELMOD2, ARL2, and rootletin in ciliary licensing in Figure 10.

ELMOD2$^{-/-}$ MEFs exhibit multiple ciliary defects, including multiciliation, increased ciliation, abnormal ciliary morphology including splaying, and changes in ciliary protein content. Given our previous data showing roles for ELMOD2 at centrosomes and in microtubule nucleation and stability we were initially concerned that these changes in ciliary integrity may be indirect, resulting from alterations in microtubules or axonemes. Or that the centrosome amplification described previously in ELMOD2 null MEFs (Turn et al., 2020) may explain the increased ciliation. This concern was perhaps increased by the finding that increasing ARL2 activity is sufficient to rescue each. While we do not believe that we can completely separate these actions of ELMOD2 in cells we currently believe they are distinct actions resulting from distinct protein-protein interactions. For example, there are numerous examples in the literature in which centrosome amplification is not accompanied by increased ciliation. In addition, we showed that expression of activated ARF6 reversed the centrosome amplification phenotype in ELMOD2$^{-/-}$ MEFs, consistent with it being a consequence of failed abscission events (Turn et al., 2020), but expression of the same ARF6 construct had no effect on ciliary phenotypes (Fig. 7). Also, while loss of microtubule nucleation or stability might be expected to compromise ciliation we found *increased* ciliation in ELMOD2 null lines. Perhaps the strongest single piece of evidence arguing for distinct actions of ELMOD2 in microtubule and ciliary functions is the finding that expression of the GAP dead mutant (ELMOD2[R167K]) was equally active as WT to restore ciliary integrity (Fig. 6) but failed to reverse the defects at microtubules/centrosomes (Turn et al., 2020). Thus, the GAP activity of ELMOD2 is required at centrosomes/microtubules but not at cilia. In addition, the multiple commonalities found between deletion of ELMOD2 and rootletin strongly support the

conclusion that they act together, yet previous studies of rootlets consistently find no clear links to microtubules. We also found no signs of differences in microtubule density or sensitivity to nocodazole in *Crocc*$^{-/-}$ MEFs, compared to WT, further suggesting clear distinctions between ELMOD2 acting on microtubules and with rootletin at basal bodies and rootlets. Perhaps its unique position as regulator of ciliogenesis, microtubule anchoring, and cytokinesis positions it to mediate between all three pathways, allowing communication that ensures proper regulation of cell cycling and signaling (East and Kahn, 2011; Francis et al., 2016).

The molecular details of neither the early steps in ciliogenesis (licensing) nor the later steps that are critical to the formation of a complete and functional cilia are well understood, despite significant advances in recent years (Chen et al., 2020; Gigante and Caspary, 2020; Nachury, 2018; Nachury and Mick, 2019; Satir, 2017). We used the previous identification of specific steps or components in licensing as markers in the pathway to pinpoint likely sites of action for ELMOD2 and rootletin. An incomplete model of this pathway is shown in Fig. 10. Cep44 is consistently found at the proximal ends of centrioles, where it plays a role in attachment of rootletin and centrosome biogenesis and cohesion (Atorino et al., 2020; Hossain et al., 2020). Cep164 recruits to distal appendages early in this process (Graser et al., 2007a; Schmidt et al., 2012), to allow for the docking of the serine-threonine kinase, TTBK2. TTBK2 is required for the removal of the CP110-Cep97 protein complex from the basal body, allowing ciliary vesicle docking (Goetz et al., 2012). Just how CP110-Cep97 removal occurs is uncertain. Recent work has revealed that TTBK2 phosphorylates M-phase phosphoprotein 9 (MPP9) (Huang et al., 2018), a factor that recruits to the distal appendages to mediate CP110-Cep97 docking. MPP9 phosphorylation by TTBK2 promotes its degradation, leading to the release of CP110-Cep97 complex. Cep83 has also been identified as a substrate for TTBK2, as its phosphorylation by TTBK2 is critical for Cep83 to drive

pre-ciliary vesicle docking to distal appendages, CP110 release, and the formation of the ciliary vesicle (Lo et al., 2019).

Because the deletion of either ELMOD2 or rootletin results in increased ciliation, we conclude that each protein normally acts to prevent (spurious or excessive) ciliation. Staining of Cep44 is not altered in response to deletion of either ELMOD2 or rootletin, thus we argue their sites of action lie downstream of Cep44. The first step in the pathway shown in our model that displayed differences in the KO lines is increased staining of Cep164 and TTBK2 in both ELMOD2 and rootletin nulls. Because Cep44 is unaltered in either ELMOD2 or Rootletin KO, while Cep164 and TTBK2 are increased at centrioles, we propose that ELMOD2 acts in the regulated recruitment of rootlets/rootletin to centrioles, perhaps in concert with Cep44. Consistent with this conclusion is the observation that rootlet attachment at basal bodies (and centrosomes) is lost in cells that lack ELMOD2. The normal, physical linkages between centrioles and rootlets may present a physical barrier to proteins being recruited or removed. Thus, the loss of rootlet attachment to the basal body also may explain the increased recruitment of Cep164 and TTBK2 (Fig. 10). Alternatively, the rootlets linked to centrioles may serve a scaffolding function for recruitment of regulators of ciliogenesis. In ELMOD2 KO cells, the increases in both Cep164 and TTBK2 are predicted to cause the spurious release of the CP110 complex that caps and prevents ciliation. Taken together, we also predict that rootletin inhibits spurious ciliogenesis in a very similar way to ELMOD2 by preventing recruitment of Cep164 and TTBK2 and the release of the CP110 cap.

How are these steps and processes regulated? In short, we don't know. We believe the evidence strongly supports a role for the regulatory GTPase ARL2 acting with ELMOD2 in these processes. This could provide a link between the cell cycle and ciliary licensing, as ciliation only

occurs when cells are in the G_0 or G_1 phases of the cell cycle. We also speculate that TTBK2 may phosphorylate rootletin and, in so doing, regulate its actions or half-life. TTBK2 is a relatively understudied kinase but is predicted to have a highly unusual preference for a phosphotyrosine at the +2 position relative to its site of serine/threonine phosphorylation (Bouskila et al., 2011). ELMOD2 contains no (S/T)XY sequence, but rootletin does: serine 155 is followed by tyrosine at residue 157, making it a potential substrate for TTBK2. Interestingly, the *Crocc*$^{\Delta 239}$ mutant is missing these residues, and the truncated protein is expressed to much higher levels than the wild type protein. Thus, the N-terminus of rootletin may include sites of regulated protein-protein interaction and protein half-life. Results from our studies of cells expressing rootletin[Δ239] are also consistent with those from the Li lab and others that have used the pre-designed N-terminal truncation protein, termed R234, that lacks 500 residues from the N-terminus (Akiyama et al., 2017; Yang et al., 2006; Yang et al., 2002). Both truncation mutants retain the ability to form rootlets. Recent structural studies confirm the importance of more C-terminal portions of rootletin, specifically coiled-coil domain 3 to oligomerization and centrosome binding (Ko et al., 2020) though these previous studies have not investigated protein half-lives or roles in ciliation.

We propose that, like ELMOD2, rootletin plays a role in inhibiting spurious ciliation by preventing the release of CP110 and inhibiting the recruitment of Cep164 and TTBK2. Consistent with this, rootletin KO cells display increased staining of Cep164 and TTBK2 at centrosomes and decreased CP110, each of which should lead to increased ciliogenesis. Indeed, we found increased percentages of ciliated cells in the nulls as well as an increase in biciliated cells. Previous work demonstrated roles for rootlets (including the ~225 kDa homopolymer rootletin) to form fibrous structures that surround centrosomes and maintain their cohesion throughout the cell cycle, with loss during cell division. C-Nap1 is structurally and evolutionarily linked to rootletin while Nek2

and Cep68 are also implicated in these actions. Knockdown of rootletin leads to spurious centrosome separation (Bahe et al., 2005; Graser et al., 2007b; Hossain et al., 2020; Meraldi and Nigg, 2001; Vlijm et al., 2018; Yang et al., 2006). Failure to regulate centrosome cohesion can lead to cell cycle defects, such centrosome amplification or aneuploidy. In addition to centrosome cohesion, rootlets have also been implicated in ciliary stabilization. Deleting the *Crocc* gene in mice caused increased degeneration of photoreceptor cells in adult animals and decreased mucosal clearance in lung epithelia (Yang et al., 2005). Evidence for direct binding between kinesin light chains and rootletin was interpreted as potential functions in vesicular cargo docking or transport to cilia (Yang and Li, 2005). Work in flies suggests that the rootlet is required for attachment of centrioles to cilia in chordotonal neurons (Styczynska-Soczka and Jarman, 2015), but rootlets are not required for ciliogenesis. Loss of rootletin leads to severe mechanosensory defects in flies. There is some debate in the field over the role that rootlets play in ciliogenesis, as Nigg's group (Graser et al., 2007a) reported no change in ciliogenesis upon knockdown of rootletin, though the Morrison group reported a *reduction* in ciliogenesis in RPE cells upon knockdown of rootletin (Conroy et al., 2012). Our data add to this debate, as we propose that rootletin normally *inhibits* (spurious) ciliogenesis in MEFs, and thus its loss causes increased ciliation. Differences in findings between labs could result from cell type differences (MEFs vs RPE cells), as much of the other work was either performed in multiciliated cells (in which it may be difficult to see *increased* ciliation) or in the highly specialized retinal cells in which additional control mechanisms may be in place. Alternatively, differences in conclusions may be the result of the approaches used,;*i.e.*, knockout vs knockdown, as the latter is known to result in only incomplete loss of protein. The rootletin antibodies employed in our studies target the C-terminus of the protein and thus is

expected to identify any N-terminal truncated mutants (*e.g.*, Crocc$^{\Delta 293}$) or protein fragments that might remain after genome editing, but we see none.

In contrast to the deletion of rootletin, with consequent increases in ciliation, we found what we believe to be a cell line that expresses an N-terminal truncation mutant of rootletin (Crocc$^{\Delta 239}$) to higher levels and displays a profound loss of ciliation. It is not clear at this time whether the phenotypes observed in this line result from the increased expression, the loss of key N-terminal residues, or both. These cells display increased CP110 retention at both centrosomes, despite the presence of Cep164 and its near normal increase in response to serum starvation. The discovery of the Crocc$^{\Delta 239}$ allele highlights once again both advantages and cautions in the use of CRISPR/Cas9 genome editing. It was discovered as a result of increased staining of rootlets when screening potential rootletin KO clones by immunofluorescence. DNA sequencing around the targeted exon revealed frameshifting mutations in both alleles; one is a 2 bp insertion and the other is a 1 bp insertion (see Fig. S2). In fact, the single bp insertion is at the same site as that found in clone #31, though has an A inserted instead of the C in both alleles in the other clone. Because clone #31 displays no evidence of rootletin protein, we suspect that it is the 2 bp insertion allele that is responsible for the large amount of rootletin-positive signal in both immunoblots and immunostained cells. We believe the resulting frame shift results in the use of a downstream methionine (Met240) to initiate translation, resulting in the N-terminal truncation mutant that lacks the first 239 amino acids. The faster migrating band in the immunoblot (Fig. 5A) is consistent with this interpretation. Why a 2bp insertion results in use of a downstream methionine when the 1bp insertion or deletion does not is unclear. This result, though, is consistent with and adds to the conclusions reached by Smits, et al (Smits et al., 2019) and their well-documented examples of unexpected outcomes from genome editing, that include use of downstream start codons.

Rescue experiments resulted in evidence linking ARL2 to ELMOD2 and rootletin in ciliogenesis as well as the conclusion that ELMOD2 is acting as an effector in this pathway, and not solely a GAP (Fig. 6, 7). ARL2, ARL2[V160A], and myc-rootletin each rescue ciliary and centrosome cohesion defects (and rootletin defects in the case of ELMOD2 KOs) in both rootletin and ELMOD2 KO cells (Fig. 6, 7). This effect is quite specific to ARL2 as its closest structural paralog, ARL3, or functionally linked paralogs ARL6 or ARF6 fail to rescue these defects. Further, expression of ELMOD2-myc or the GAP dead point mutant, ELMOD2[R167K]-myc, each reverse ciliary, rootlet, and centrosome cohesion defects seen in ELMOD2 KO, showing quite clearly that GAP activity is not required and instead indicating a role for ELMOD2 here as an effector (East and Kahn, 2011; Zhang et al., 2003; Zhang et al., 1998). While ELMOD2 expression does not rescue ciliary phenotypes in rootletin KO cells, the converse is true; *i.e.*, increased expression of rootletin does reverse defects seen in ELMOD2 KO lines. the former is perhaps not surprising as deletion of rootletin results in the loss of an important cytoskeletal polymer with clear roles in centrosome cohesion. Still, we believe this finding also suggests that rootletin acts very close to ELMOD2 and likely immediately downstream of it in this pathway, playing a non-essential but critical role in regulating rootletin morphology to direct ciliogenesis. Perhaps ELMOD2 facilitates the proper tethering and bundling of rootlets to accommodate cellular needs (*e.g.*, ciliation, mitosis).

Surprisingly, in contrast to ELMOD2, activated ARL2 (ARL2[V160A]) and ARL2 reverse ciliary defects in both ELMOD2 and rootletin KO lines. We might have predicted that ARL2 would rescue ELMOD2 KO phenotypes but not rootletin KO phenotypes, especially given the previously pointed out importance of rootletin as a cytoskeletal polymer. There are several possibilities for why or how ARL2 may rescue the loss of rootletin. One possibility is that ARL2

may have an action downstream of rootletin in its inhibitory functions. Perhaps in WT cells rootlets allow for anchorage and recruitment of ARL2 so that it may regulate ciliogenesis, and therefore loss of the rootlet leads to the dilution of ARL2's signal and prevents it from inhibiting ciliation. Overexpression of ARL2 or the fast-cycling ARL2[V160A] would override the system, allowing for diffusion of ARL2 to the site, and therefore restore inhibition of ciliogenesis. This would be consistent with GTPase biology, as the tight regulation of an ARF's localization in time and space is pivotal for the proper coordination of cell functions (D'Souza-Schorey and Chavrier, 2006; Fisher et al., 2020; Jackson and Casanova, 2000; Kahn, 2009; Kahn et al., 2005; Mizuno-Yamasaki et al., 2012; Nie et al., 2003; Sztul et al., 2019). Another possibility is that ARL2 is acting through another component of the rootlet rather than rootletin directly. One predicted structural component of the ciliary rootlet/ centrosome linker is Cep68, a protein which also forms a dense network that binds to C-Nap1 (Vlijm et al., 2018). Perhaps ARL2 works through Cep68 or another structural component of the rootlet, and therefore increasing ARL2 activity may be sufficient to compensate for the loss of rootletin, resulting in improved rootlet function, reversal of ciliary, centrosome separation, and rootlet defects despite the absence of rootletin. Additional experiments along any of these lines may well further extend our understanding of this pathway and how it is regulated.

Our studies also increase both the number of sites and pathways at which ARL2 and ELMOD2 have been shown to act. These add to the growing list of family members and pathways affected by them, with functional links to cilia. The ARF family includes at least four members with known roles in ciliary biology, including ARL2, ARL3, ARL6, and ARL13B. Previous studies revealed that ELMOD2 has *in vitro* GAP activity toward ARL2, ARL3, ARF1, ARF3, and ARF6, but not ARL13B (Ivanova et al., 2014), thus despite the specificity observed in our rescue experiments (Figs. 6, 7) we cannot exclude ELMOD2 acting with one or more of these other

GTPases to regulate aspects of ciliary biology. ARL2, ARL3 and RP2, that can act as a GAP for them, are implicated in protein traffic to cilia, particularly that of prenylated (acting with PDE6δ) or N-myristoylated protein cargos (acting with UNC119) (Evans et al., 2010; Hanke-Gogokhia et al., 2016; Jaiswal et al., 2016; Veltel et al., 2008; Wright et al., 2011; Wright et al., 2016). Clean dissection of the actions of each of these ARF family GTPases, and their GAPs clearly requires additional studies that are predicted to further our currently incomplete understanding of the pathways as well as links to other aspects of cell biology, including cell division and cancer.

In MEFs, we observe that ELMOD2 and ARL2 each localize to rootlets and basal bodies. Specificity is evident from antigen competition (ARL2; see Fig. 8B) and loss of signaling in ELMOD2 KO cells. Our findings are also consistent with previous proteomic studies in which ELMOD2 is one of the hits in photoreceptor sensory cilia that is disrupted in rootletin KO mice (Liu et al., 2007). It is interesting to note that ELMOD2 and ARL2 do not completely co-localize with rootlets. There are some rootlet branches that do not stain for ELMOD2 or ARL2, and there are some cases in which it looks like ARL2 or ELMOD2 create their own rootlet-like projections that are negative for rootletin. This suggests that these factors work together, though they may also interact with other components of rootlets, *e.g.*, Cep68, as suggested above.

In ELMOD2 KO, much of the rootletin structure at centrosomes is disrupted, and ARL2 still co-localizes to centrosome-associated rootletin though not to rootletin positive structures at other sites in the cell. ARL2 and ELMOD2 still localize to basal bodies without rootletin, though they no longer appear to form rootlet-like projections. Together, these data would suggest that rootletin is needed for ARL2 and ELMOD2 to recruit to the rootlet and that ELMOD2 helps with rootletin anchoring, but ELMOD2 is not required for ARL2 to recruit to rootletin. Complicating these interpretations is the fact that we previously described ARL2 as present in the pericentriolar

material, where along with its binding partner cofactor D (aka tubulin specific co-chaperone D or TBCD), and able to influence recruitment there of gamma-tubulin ring complex. This current study lacks the resolution to discriminate between protein localization/binding at centrioles, presence in the PCM, and localization to rootlets that surround each. It is likely that a detailed, high resolution study of these proteins at these sites will further increase our understanding of how each is acting, likely in more than one process each.

Further adding to the complexity in defining roles, there appears to be some level of tissue or cell type specificity to the localizations observed. ARL2 localizes to the rootlet of primary mouse retinal cells, while ELMOD2 localizes to the connecting cilium, potentially serving a role in anchoring the rootlet to the centrioles. In contrast, ARL2 localizes almost exclusively to the length of the cilium in bronchial cells, while ELMOD2 shows strong staining at the ciliary tip as well as faint co-localization with ciliary rootlets (Figure S8). The proximity of these locations is expected to allow them to interact directly, and in addition ARF family GTPases are known to bind some structures, e.g., membranes, only transiently and in a highly regulated fashion. This is the first evidence of ELMOD2 having ciliary/cilia-associated localizations and of both ARL2/ELMOD2 working with rootlets. Perhaps, the steady state distribution of ELMOD2 and ARL2 localization to rootlets, cilia, and other compartments varies, depending upon the ciliary requirements of a given tissue. Because ELMOD2 is an ancient and highly conserved protein, it will be interesting in the future to examine its role in multiciliated organisms/cells to perhaps test for a role in the licensing of multiciliation. These findings suggest the possibility, if not likelihood, of tissue specificity to ELMOD2 and ARL2 localization and action, perhaps changing in response to different cellular requirements. Although there has been no published follow up to the earlier signs of linkage between the ELMOD2 gene and idiopathic pulmonary fibrosis (Hodgson et al.,

2006; Pulkkinen et al., 2010), we note the importance of multiciliated cells in this condition and perhaps an argument to look deeper into these questions.

In addition to large changes in ciliation in the KO lines described, and for which we are proposing a specific model and pathway (Fig. 10), we also found a number of changes in ciliary content for which we lack sufficient prior understanding of detailed pathways to formulate a working model. With respect to the abnormal localization of proteins to cilia seen in ELMOD2 KO and rootletin KO MEFs, these defects may simply be secondary to ciliogenesis structural defects, *e.g.*, resulting from dissociation or loss of rootlets/rootletin. Mahjoub and Stearns reported (Mahjoub, 2013; Mahjoub and Stearns, 2012) that PLK4 induces centrosome amplification that leads to the production of multiple primary cilia. They suggested that multiciliation may lead to diluted ciliary signaling, which is consistent with what we observed in ELMOD2 KO cells. ELMOD2 KO caused decreased recruitment of multiple signaling proteins, including SSTR3, Smo, GPR161, and ACIII (Figure 2) and decreased SHH pathway output (Fig. 2). Therefore, receptor traffic and signaling defects could be secondary to a fundamental defect in multiciliation leading to a dilution of cell signal.

We do, however, see monociliated cells that also display reduced recruitment of ciliary receptors so simply dilution of components into multiple cilia cannot fully explain these differences between cell lines. We also see a number of other proteins that spuriously localize to cilia upon loss of ELMOD2 or rootletin, including centrin, Cep44, ELMOD2, and ARL2. One possibility to explain the spurious localization of these proteins is that IFT or transition zone are defective in ELMO2 or rootletin KO cells. We did not observe defects in transition zone or IFT based upon gross immunofluorescence analysis (Figure S1), but future studies should be directed

to examination of IFT traffic and TZ integrity, perhaps using super resolution or electron microscopy.

Ciliobrevin is a retrograde inhibitor of dynein motors whose presence led to increased staining of centrin, ELMOD2, and ARL2 in cilia of WT cells, similar to what we observed in ELMOD2 nulls. Thus, we speculate that each of these proteins (and no doubt others) can enter cilia in perhaps all cells but under normal conditions are rapidly exported, preventing accumulation to a level detectible by immunofluorescence. The increase presence of centrin inside cilia might be particularly interesting as centrin2 has been shown to interact directly with CP110 (Tsang et al., 2006) and other studies suggest that centrin2 is required for the removal of CP110 to induce ciliogenesis (Prosser and Morrison, 2015). Previous labs have indicated that centrin localizes to motile cilia and to the transition zone of retinal cilia and olfactory cilia (REF), but no studies to our knowledge have identified centrin in primary cilia. Other studies have noted that centrin can localize to rootlets, particularly in the case of multiciliate protists, bovine photoreceptors, and insect sensilla (Lemullois et al., 2004; Levy et al., 1996; Wolfrum, 1992). Perhaps rootletin, ELMOD2, and ARL2 regulate CP110's access to centrin, and during ciliogenesis, rootletin morphology is adapted to allow centrin association with CP110 and CP110 release. These speculations may be worth further exploration to probe for ELMOD2, ARL2, and rootletin ciliary function(s).

Also unexplained are the abnormalities in ciliary morphology found in our KO lines. We observed both defects in the axoneme (acetylated tubulin) and ciliary membrane (ARL13B), noting branching and splaying of cilia that is virtually nonexistent in WT primary cilia. Though we do not have clear answers as to the source of these abnormal morphologies, there are a number of possibilities. One, the increase in spurious ciliogenesis may lead to the skipping of checkpoints

that are critical for ensuring proper ciliary morphology. Other reports of cells with increased ciliation have also noted abnormal ciliary morphologies, so are unlikely specific to the proteins or cells used in our study (Yasar et al., 2017).

Together, this study has uncovered critical new functions for the ARF GAP ELMOD2 in ciliary and rootlet function. This sheds much needed insight into teasing apart how GTPases and their regulators facilitate interpathway communication. There are still many more questions than answers concerning how ELMOD2 directs so many different essential cellular functions and how precisely ELMOD2 works with rootletin to direct ciliogenesis (Figure 10). With this additional information, we hope to incentivize future work into understanding the signaling events that mediate the communication between cilia, cell cycle, microtubule dynamics, and other essential cellular functions.

Acknowledgements This work was supported by NIH Grants R35GM122568 (R.A.K.) and 1F31CA236493-02 to (R.E.T). We thank colleagues for their generous sharing of key reagents. We give special thanks to Monica Bettencourt-Diaz, Max Nachury, Win Sale, Dorothy Lerit, Maureen Barr, Rytis Prekeris, Tim Stearns, and Peter Jackson for providing input to help us better test and explore models. Emory University Integrated Cellular Imaging (ICI) Microscopy Core and Emory Viral Vector Core of the Emory Neuroscience NINDS Core Facilities Grant 5P30NS055077 provided access to key reagents and instrumentation.

Author Contributions RET designed and performed all experiments shown in this paper, except for the qPCR performed by EDG and retinal immunohistochemistry by JL. RET and RAK wrote the manuscript, analyzed data, and generated all figures/tables, except for the qPCR data generated

by EDG and retinal immunohistochemistry data generated by JL. RET, TC, and RAK worked together to develop the story and make interpretation of findings. RET, JL, TC, EDG, UW, and RAK reviewed the results, provided feedback on the manuscript, and approved the submitted final product.

References

Adari, H., D.R. Lowy, B.M. Willumsen, C.J. Der, and F. McCormick. 1988. Guanosine triphosphatase activating protein (GAP) interacts with the p21 ras effector binding domain. *Science*. 240:518-521.

Agromayor, M., and J. Martin-Serrano. 2013. Knowing when to cut and run: mechanisms that control cytokinetic abscission. *Trends Cell Biol*. 23:433-441.

Ahmadian, M.R., P. Stege, K. Scheffzek, and A. Wittinghofer. 1997. Confirmation of the arginine-finger hypothesis for the GAP-stimulated GTP-hydrolysis reaction of Ras. *Nat Struct Biol*. 4:686-689.

Akiyama, T., A. Inoko, Y. Kaji, S. Yonemura, K. Kakiguchi, H. Segawa, K. Ishitsuka, M. Yoshida, O. Numata, P. Leproux, V. Couderc, T. Oshika, and H. Kano. 2017. SHG-specificity of cellular Rootletin filaments enables naive imaging with universal conservation. *Sci Rep*. 7:39967.

Altschuler, Y., S. Liu, L. Katz, K. Tang, S. Hardy, F. Brodsky, G. Apodaca, and K. Mostov. 1999. ADP-ribosylation factor 6 and endocytosis at the apical surface of Madin-Darby canine kidney cells. *J Cell Biol*. 147:7-12.

Antoshechkin, I., and M. Han. 2002. The C. elegans evl-20 gene is a homolog of the small GTPase ARL2 and regulates cytoskeleton dynamics during cytokinesis and morphogenesis. *Dev Cell*. 2:579-591.

Aspenstrom, P. 2018. Fast-cycling Rho GTPases. *Small GTPases*:1-8.

Atorino, E.S., S. Hata, C. Funaya, A. Neuner, and E. Schiebel. 2020. CEP44 ensures the formation of bona fide centriole wall, a requirement for the centriole-to-centrosome conversion. *Nature communications*. 11:903.

Bahe, S., Y.D. Stierhof, C.J. Wilkinson, F. Leiss, and E.A. Nigg. 2005. Rootletin forms centriole-associated filaments and functions in centrosome cohesion. *J Cell Biol*. 171:27-33.

Beghin, A., S. Honore, C. Messana, E.L. Matera, J. Aim, S. Burlinchon, D. Braguer, and C. Dumontet. 2007. ADP ribosylation factor like 2 (Arl2) protein influences microtubule dynamics in breast cancer cells. *Exp Cell Res*. 313:473-485.

Bhamidipati, A., S.A. Lewis, and N.J. Cowan. 2000. ADP ribosylation factor-like protein 2 (Arl2) regulates the interaction of tubulin-folding cofactor D with native tubulin. *J Cell Biol*. 149:1087-1096.

Boman, A.L., J. Kuai, X. Zhu, J. Chen, R. Kuriyama, and R.A. Kahn. 1999. Arf proteins bind to mitotic kinesin-like protein 1 (MKLP1) in a GTP-dependent fashion. *Cell Motil Cytoskel*. 44:119-132.

Borowicz, S., M. Van Scoyk, S. Avasarala, M.K. Karuppusamy Rathinam, J. Tauler, R.K. Bikkavilli, and R.A. Winn. 2014. The soft agar colony formation assay. *J Vis Exp*:e51998.

Bouchoux, J., F. Beilstein, T. Pauquai, I.C. Guerrera, D. Chateau, N. Ly, M. Alqub, C. Klein, J. Chambaz, M. Rousset, J.M. Lacorte, E. Morel, and S. Demignot. 2011. The proteome of cytosolic lipid droplets isolated from differentiated Caco-2/TC7 enterocytes reveals cell-specific characteristics. *Biol Cell*. 103:499-517.

Bouskila, M., N. Esoof, L. Gay, E.H. Fang, M. Deak, M.J. Begley, L.C. Cantley, A. Prescott, K.G. Storey, and D.R. Alessi. 2011. TTBK2 kinase substrate specificity and the impact of spinocerebellar-ataxia-causing mutations on expression, activity, localization and development. *Biochem J*. 437:157-167.

Bowzard, J.B., D. Cheng, J. Peng, and R.A. Kahn. 2007. ELMOD2 is an Arl2 GTPase-activating protein that also acts on Arfs. *J Biol Chem*. 282:17568-17580.

Brugnera, E., L. Haney, C. Grimsley, M. Lu, S.F. Walk, A.C. Tosello-Trampont, I.G. Macara, H. Madhani, G.R. Fink, and K.S. Ravichandran. 2002. Unconventional Rac-GEF activity is mediated through the Dock180-ELMO complex. *Nat Cell Biol*. 4:574-582.

Bugnard, E., K.J. Zaal, and E. Ralston. 2005. Reorganization of microtubule nucleation during muscle differentiation. *Cell Motil Cytoskeleton*. 60:1-13.

Burd, C.G., T.I. Strochlic, and S.R. Gangi Setty. 2004. Arf-like GTPases: not so Arf-like after all. *Trends Cell Biol*. 14:687-694.

Casalou, C., A. Ferreira, and D.C. Barral. 2020. The Role of ARF Family Proteins and Their Regulators and Effectors in Cancer Progression: A Therapeutic Perspective. *Frontiers in Cell and Developmental Biology*. 8.

Cavenagh, M.M., M. Breiner, A. Schurmann, A.G. Rosenwald, T. Terui, C. Zhang, P.A. Randazzo, M. Adams, H.G. Joost, and R.A. Kahn. 1994. ADP-ribosylation factor (ARF)-like 3, a new member of the ARF family of GTP-binding proteins cloned from human and rat tissues. *J Biol Chem*. 269:18937-18942.

Cavenagh, M.M., J.A. Whitney, K. Carroll, C. Zhang, A.L. Boman, A.G. Rosenwald, I. Mellman, and R.A. Kahn. 1996. Intracellular distribution of Arf proteins in mammalian cells. Arf6 is uniquely localized to the plasma membrane. *J Biol Chem*. 271:21767-21774.

Chabin-Brion, K., J. Marceiller, F. Perez, C. Settegrana, A. Drechou, G. Durand, and C. Pous. 2001. The Golgi complex is a microtubule-organizing organelle. *Mol Biol Cell*. 12:2047-2060.

Chen, H.Y., R.A. Kelley, T. Li, and A. Swaroop. 2020. Primary cilia biogenesis and associated retinal ciliopathies. *Semin Cell Dev Biol*.

Chipperfield, R.G., S.S. Jones, K.M. Lo, and R.A. Weinberg. 1985. Activation of Ha-ras p21 by substitution, deletion, and insertion mutations. *Mol Cell Biol*. 5:1809-1813.

Conroy, P.C., C. Saladino, T.J. Dantas, P. Lalor, P. Dockery, and C.G. Morrison. 2012. C-NAP1 and rootletin restrain DNA damage-induced centriole splitting and facilitate ciliogenesis. *Cell Cycle*. 11:3769-3778.

Cunningham, L.A., and R.A. Kahn. 2008. Cofactor D functions as a centrosomal protein and is required for the recruitment of the gamma-tubulin ring complex at centrosomes and organization of the mitotic spindle. *J Biol Chem*. 283:7155-7165.

Cuthbert, E.J., K.K. Davis, and J.E. Casanova. 2008. Substrate specificities and activities of AZAP family Arf GAPs in vivo. *American journal of physiology. Cell physiology*. 294:C263-270.

D'Souza-Schorey, C., and P. Chavrier. 2006. ARF proteins: roles in membrane traffic and beyond. *Nat Rev Mol Cell Biol*. 7:347-358.

D'Souza-Schorey, C., G. Li, M.I. Colombo, and P.D. Stahl. 1995. A regulatory role for ARF6 in receptor-mediated endocytosis. *Science*. 267:1175-1178.

D'Souza-Schorey, C., E. van Donselaar, V.W. Hsu, C. Yang, P.D. Stahl, and P.J. Peters. 1998. ARF6 targets recycling vesicles to the plasma membrane: insights from an ultrastructural investigation. *J Cell Biol*. 140:603-616.

D'Souza, R.S., J.Y. Lim, A. Turgut, K. Servage, J. Zhang, K. Orth, N. Sosale, M. Lazzara, J. Allegood, and J.E. Casanova. 2020. Calcium-stimulated disassembly of focal adhesions mediated by an ORP3/IQSec1 complex. *Elife*. 9.

Davidson, A.E., N. Schwarz, L. Zelinger, G. Stern-Schneider, A. Shoemark, B. Spitzbarth, M. Gross, U. Laxer, J. Sosna, P.I. Sergouniotis, N.H. Waseem, R. Wilson, R.A. Kahn, V. Plagnol, U. Wolfrum, E. Banin, A.J. Hardcastle, M.E. Cheetham, D. Sharon, and A.R. Webster. 2013. Mutations in ARL2BP, encoding ADP-ribosylation-factor-like 2 binding protein, cause autosomal-recessive retinitis pigmentosa. *Am J Hum Genet*. 93:321-329.

Donaldson, J.G., and C.L. Jackson. 2011. ARF family G proteins and their regulators: roles in membrane transport, development and disease. *Nat Rev Mol Cell Biol*. 12:362-375.

Donaldson, J.G., and H. Radhakrishna. 2001. Expression and properties of ADP-ribosylation factor (ARF6) in endocytic pathways. *Methods Enzymol*. 329:247-256.

East, M.P., J.B. Bowzard, J.B. Dacks, and R.A. Kahn. 2012. ELMO Domains, Evolutionary and Functional Characterization of a Novel GTPase-activating Protein (GAP) Domain for Arf Protein Family GTPases. *J Biol Chem*. 287:39538-39553.

East, M.P., and R.A. Kahn. 2011. Models for the functions of Arf GAPs. *Semin Cell Dev Biol*. 22:3-9.

Echard, A., G.R. Hickson, E. Foley, and P.H. O'Farrell. 2004. Terminal cytokinesis events uncovered after an RNAi screen. *Curr Biol*. 14:1685-1693.

Efimov, A., A. Kharitonov, N. Efimova, J. Loncarek, P.M. Miller, N. Andreyeva, P. Gleeson, N. Galjart, A.R. Maia, I.X. McLeod, J.R. Yates, 3rd, H. Maiato, A. Khodjakov, A. Akhmanova, and I. Kaverina. 2007. Asymmetric CLASP-dependent nucleation of noncentrosomal microtubules at the trans-Golgi network. *Dev Cell*. 12:917-930.

Evans, R.J., N. Schwarz, K. Nagel-Wolfrum, U. Wolfrum, A.J. Hardcastle, and M.E. Cheetham. 2010. The retinitis pigmentosa protein RP2 links pericentriolar vesicle transport between the Golgi and the primary cilium. *Hum Mol Genet*. 19:1358-1367.

Fidyk, N., J.B. Wang, and R.A. Cerione. 2006. Influencing cellular transformation by modulating the rates of GTP hydrolysis by Cdc42. *Biochemistry*. 45:7750-7762.

Fielding, A.B., E. Schonteich, J. Matheson, G. Wilson, X. Yu, G.R. Hickson, S. Srivastava, S.A. Baldwin, R. Prekeris, and G.W. Gould. 2005. Rab11-FIP3 and FIP4 interact with Arf6 and the Exocyst to control membrane traffic in cytokinesis. *EMBO J*. 24:3389-3399.

Fisher, S., D. Kuna, T. Caspary, R.A. Kahn, and E. Sztul. 2020. ARF family GTPases with links to cilia. *Am J Physiol Cell Physiol*. 319:C404-C418.

Flanagan, A.M., E. Stavenschi, S. Basavaraju, D. Gaboriau, D.A. Hoey, and C.G. Morrison. 2017. Centriole splitting caused by loss of the centrosomal linker protein C-NAP1

reduces centriolar satellite density and impedes centrosome amplification. *Mol Biol Cell*. 28:736-745.

Francis, J.W., D. Goswami, S.J. Novick, B.D. Pascal, E.R. Weikum, E.A. Ortlund, P.R. Griffin, and R.A. Kahn. 2017a. Nucleotide Binding to ARL2 in the TBCDARL2beta-Tubulin Complex Drives Conformational Changes in beta-Tubulin. *J Mol Biol*. 429:3696-3716.

Francis, J.W., L.E. Newman, L.A. Cunningham, and R.A. Kahn. 2017b. A Trimer Consisting of the Tubulin-specific Chaperone D (TBCD), Regulatory GTPase ARL2, and beta-Tubulin Is Required for Maintaining the Microtubule Network. *J Biol Chem*. 292:4336-4349.

Francis, J.W., R.E. Turn, L.E. Newman, C. Schiavon, and R.A. Kahn. 2016. Higher order signaling: ARL2 as regulator of both mitochondrial fusion and microtubule dynamics allows integration of 2 essential cell functions. *Small GTPases*. 7:188-196.

Frank, S.R., J.C. Hatfield, and J.E. Casanova. 1998. Remodeling of the actin cytoskeleton is coordinately regulated by protein kinase C and the ADP-ribosylation factor nucleotide exchange factor ARNO. *Mol Biol Cell*. 9:3133-3146.

Gigante, E.D., and T. Caspary. 2020. Signaling in the primary cilium through the lens of the Hedgehog pathway. *Wiley Interdiscip Rev Dev Biol*:e377.

Gillingham, A.K., and S. Munro. 2007. The small G proteins of the Arf family and their regulators. *Annu Rev Cell Dev Biol*. 23:579-611.

Goetz, S.C., and K.V. Anderson. 2010. The primary cilium: a signalling centre during vertebrate development. *Nat Rev Genet*. 11:331-344.

Goetz, S.C., K.F. Liem, Jr., and K.V. Anderson. 2012. The spinocerebellar ataxia-associated gene Tau tubulin kinase 2 controls the initiation of ciliogenesis. *Cell*. 151:847-858.

Graser, S., Y.D. Stierhof, S.B. Lavoie, O.S. Gassner, S. Lamla, M. Le Clech, and E.A. Nigg. 2007a. Cep164, a novel centriole appendage protein required for primary cilium formation. *J Cell Biol*. 179:321-330.

Graser, S., Y.D. Stierhof, and E.A. Nigg. 2007b. Cep68 and Cep215 (Cdk5rap2) are required for centrosome cohesion. *J Cell Sci*. 120:4321-4331.

Gumienny, T.L., E. Brugnera, A.C. Tosello-Trampont, J.M. Kinchen, L.B. Haney, K. Nishiwaki, S.F. Walk, M.E. Nemergut, I.G. Macara, R. Francis, T. Schedl, Y. Qin, L. Van Aelst, M.O. Hengartner, and K.S. Ravichandran. 2001. CED-12/ELMO, a novel member of the CrkII/Dock180/Rac pathway, is required for phagocytosis and cell migration. *Cell*. 107:27-41.

Hanai, A., M. Ohgi, C. Yagi, T. Ueda, H.W. Shin, and K. Nakayama. 2016. Class I Arfs (Arf1 and Arf3) and Arf6 are localized to the Flemming body and play important roles in cytokinesis. *Journal of biochemistry*. 159:201-208.

Hanke-Gogokhia, C., H. Zhang, J.M. Frederick, and W. Baehr. 2016. The Function of Arf-like Proteins ARL2 and ARL3 in Photoreceptors. *Advances in experimental medicine and biology*. 854:655-661.

Hickson, G.R.X., J. Matheson, B. Riggs, V.H. Maier, A.B. Fielding, R. Prekeris, W. Sullivan, F.A. Barr, and G.W. Gould. 2003. Arfophilins Are Dual Arf/Rab 11 Binding Proteins That Regulate Recycling Endosome Distribution and Are Related to Drosophila Nuclear Fallout. *Mol. Biol. Cell*. 14:2908-2920.

Higginbotham, H., T.Y. Eom, L.E. Mariani, A. Bachleda, J. Hirt, V. Gukassyan, C.L. Cusack, C. Lai, T. Caspary, and E.S. Anton. 2012. Arl13b in primary cilia regulates the migration and placement of interneurons in the developing cerebral cortex. *Dev Cell*. 23:925-938.

Hodgson, U., V. Pulkkinen, M. Dixon, M. Peyrard-Janvid, M. Rehn, P. Lahermo, V. Ollikainen, K. Salmenkivi, V. Kinnula, J. Kere, P. Tukiainen, and T. Laitinen. 2006. ELMOD2 is a candidate gene for familial idiopathic pulmonary fibrosis. *Am J Hum Genet*. 79:149-154.

Horgan, C.P., and M.W. McCaffrey. 2009. The dynamic Rab11-FIPs. *Biochem Soc Trans*. 37:1032-1036.

Hosaka, M., K. Toda, H. Takatsu, S. Torii, K. Murakami, and K. Nakayama. 1996. Structure and intracellular localization of mouse ADP-ribosylation factors type 1 to type 6 (ARF1-ARF6). *J Biochem (Tokyo)*. 120:813-819.

Hossain, D., S.Y. Shih, X. Xiao, J. White, and W.Y. Tsang. 2020. Cep44 functions in centrosome cohesion by stabilizing rootletin. *J Cell Sci*. 133.

Hoyt, M.A., T. Stearns, and D. Botstein. 1990. Chromosome instability mutants of Saccharomyces cerevisiae that are defective in microtubule-mediated processes. *Mol Cell Biol*. 10:223-234.

Huang, B., D.M. Watterson, V.D. Lee, and M.J. Schibler. 1988. Purification and characterization of a basal body-associated Ca2+-binding protein. *J Cell Biol*. 107:121-131.

Huang, N., D. Zhang, F. Li, P. Chai, S. Wang, J. Teng, and J. Chen. 2018. M-Phase Phosphoprotein 9 regulates ciliogenesis by modulating CP110-CEP97 complex localization at the mother centriole. *Nat Commun*. 9:4511.

Inoue, H., and P.A. Randazzo. 2007. Arf GAPs and their interacting proteins. *Traffic*. 8:1465-1475.

Ismail, S.A., Y.X. Chen, A. Rusinova, A. Chandra, M. Bierbaum, L. Gremer, G. Triola, H. Waldmann, P.I. Bastiaens, and A. Wittinghofer. 2011. Arl2-GTP and Arl3-GTP regulate a GDI-like transport system for farnesylated cargo. *Nature chemical biology*. 7:942-949.

Ivanova, A.A., M.P. East, S.L. Yi, and R.A. Kahn. 2014. Characterization of recombinant ELMOD (cell engulfment and motility domain) proteins as GTPase-activating proteins (GAPs) for ARF family GTPases. *J Biol Chem*. 289:11111-11121.

Jackson, C.L., and S. Bouvet. 2014. Arfs at a glance. *J Cell Sci*. 127:4103-4109.

Jackson, C.L., and J.E. Casanova. 2000. Turning on ARF: the Sec7 family of guanine-nucleotide-exchange factors. *Trends Cell Biol*. 10:60-67.

Jaiswal, M., E.K. Fansa, S.K. Kösling, T. Mejuch, H. Waldmann, and A. Wittinghofer. 2016. Novel biochemical and structural insights into the interaction of myristoylated cargo with Unc119 and their release by Arl2/3. *J Biol Chem*.

Jaworek, T.J., E.M. Richard, A.A. Ivanova, A.P. Giese, D.I. Choo, S.N. Khan, S. Riazuddin, R.A. Kahn, and S. Riazuddin. 2013. An alteration in ELMOD3, an Arl2 GTPase-activating protein, is associated with hearing impairment in humans. *PLoS genetics*. 9:e1003774.

Johnson, K.R., C.M. Longo-Guess, and L.H. Gagnon. 2012. Mutations of the mouse ELMO domain containing 1 gene (Elmod1) link small GTPase signaling to actin cytoskeleton dynamics in hair cell stereocilia. *PloS one*. 7:e36074.

Kahn, R.A. 2009. Toward a model for Arf GTPases as regulators of traffic at the Golgi. *FEBS Lett*. 583:3872-3879.

Kahn, R.A., L. Volpicelli-Daley, B. Bowzard, P. Shrivastava-Ranjan, Y. Li, C. Zhou, and L. Cunningham. 2005. Arf family GTPases: roles in membrane traffic and microtubule dynamics. *Biochem Soc Trans*. 33:1269-1272.

Klinger, C.M., A. Spang, J.B. Dacks, and T.J. Ettema. 2016. Tracing the Archaeal Origins of Eukaryotic Membrane-Trafficking System Building Blocks. *Molecular biology and evolution*. 33:1528-1541.

Ko, D., J. Kim, K. Rhee, and H.J. Choi. 2020. Identification of a Structurally Dynamic Domain for Oligomer Formation in Rootletin. *J Mol Biol*. 432:3915-3932.

Kuriyama, R., S. Dragas-Granoic, T. Maekawa, A. Vassilev, A. Khodjakov, and H. Kobayashi. 1994. Heterogeneity and microtubule interaction of the CHO1 antigen, a mitosis-specific kinesin-like protein. Analysis of subdomains expressed in insect sf9 cells. *J Cell Sci*. 107 (Pt 12):3485-3499.

Lahbib, S., C.S. Leblond, M. Hamza, B. Regnault, L. Lemée, A. Mathieu, H. Jaouadi, R. Mkaouar, I.B. Youssef-Turki, A. Belhadj, I. Kraoua, T. Bourgeron, and S. Abdelhak. 2018. Homozygous 2p11.2 deletion supports the implication of ELMOD3 in hearing loss

and reveals the potential association of CAPG with ASD/ID etiology. *Journal of Applied Genetics*.

Lemullois, M., G. Fryd-Versavel, and A. Fleury-Aubusson. 2004. Localization of centrins in the hypotrich ciliate Paraurostyla weissei. *Protist*. 155:331-346.

Levy, Y.Y., E.Y. Lai, S.P. Remillard, M.B. Heintzelman, and C. Fulton. 1996. Centrin is a conserved protein that forms diverse associations with centrioles and MTOCs in Naegleria and other organisms. *Cell Motil Cytoskeleton*. 33:298-323.

Li, W., Y. Feng, A. Chen, T. Li, S. Huang, J. Liu, X. Liu, Y. Liu, J. Gao, D. Yan, J. Sun, L. Mei, X. Liu, and J. Ling. 2019. Elmod3 knockout leads to progressive hearing loss and abnormalities in cochlear hair cell stereocilia. *Hum Mol Genet*. 28:4103-4112.

Li, W., J. Sun, J. Ling, J. Li, C. He, Y. Liu, H. Chen, M. Men, Z. Niu, Y. Deng, M. Li, T. Li, J. Wen, S. Sang, H. Li, Z. Wan, E.M. Richard, P. Chapagain, D. Yan, X.Z. Liu, L. Mei, and Y. Feng. 2018. ELMOD3, a novel causative gene, associated with human autosomal dominant nonsyndromic and progressive hearing loss. *Human genetics*. 137:329-342.

Li, Y., W.G. Kelly, J.M. Logsdon, Jr., A.M. Schurko, B.D. Harfe, K.L. Hill-Harfe, and R.A. Kahn. 2004. Functional genomic analysis of the ADP-ribosylation factor family of GTPases: phylogeny among diverse eukaryotes and function in C. elegans. *FASEB J*. 18:1834-1850.

Lin, R., S. Bagrodia, R. Cerione, and D. Manor. 1997. A novel Cdc42Hs mutant induces cellular transformation. *Curr Biol*. 7:794-797.

Lin, R., R.A. Cerione, and D. Manor. 1999. Specific contributions of the small GTPases Rho, Rac, and Cdc42 to Dbl transformation. *J Biol Chem*. 274:23633-23641.

Liu, Q., G. Tan, N. Levenkova, T. Li, E.N. Pugh, Jr., J.J. Rux, D.W. Speicher, and E.A. Pierce. 2007. The proteome of the mouse photoreceptor sensory cilium complex. *Mol Cell Proteomics*. 6:1299-1317.

Lo, C.H., I.H. Lin, T.T. Yang, Y.C. Huang, B.E. Tanos, P.C. Chou, C.W. Chang, Y.G. Tsay, J.C. Liao, and W.J. Wang. 2019. Phosphorylation of CEP83 by TTBK2 is necessary for cilia initiation. *J Cell Biol*. 218:3489-3505.

Loi, E., L. Moi, S. Blois, E. Bacchelli, A.F. Vega Benedetti, C. Cameli, R. Fadda, E. Maestrini, M. Carta, G. Doneddu, and P. Zavattari. 2019. ELMOD3-SH2D6 gene fusion as a possible co-star actor in autism spectrum disorder scenario. *Journal of cellular and molecular medicine*.

Lu, M., J.M. Kinchen, K.L. Rossman, C. Grimsley, C. deBakker, E. Brugnera, A.C. Tosello-Trampont, L.B. Haney, D. Klingele, J. Sondek, M.O. Hengartner, and K.S. Ravichandran. 2004. PH domain of ELMO functions in trans to regulate Rac activation via Dock180. *Nat Struct Mol Biol*. 11:756-762.

Mahen, R. 2018. Stable centrosomal roots disentangle to allow interphase centriole independence. *PLoS Biol*. 16:e2003998.

Mahjoub, M.R. 2013. The importance of a single primary cilium. *Organogenesis*. 9:61-69.

Mahjoub, M.R., and T. Stearns. 2012. Supernumerary centrosomes nucleate extra cilia and compromise primary cilium signaling. *Curr Biol*. 22:1628-1634.

Makyio, H., M. Ohgi, T. Takei, S. Takahashi, H. Takatsu, Y. Katoh, A. Hanai, T. Ueda, Y. Kanaho, Y. Xie, H.W. Shin, H. Kamikubo, M. Kataoka, M. Kawasaki, R. Kato, S. Wakatsuki, and K. Nakayama. 2012. Structural basis for Arf6-MKLP1 complex formation on the Flemming body responsible for cytokinesis. *EMBO J*. 31:2590-2603.

McElver, J., D. Patton, M. Rumbaugh, C. Liu, L.J. Yang, and D. Meinke. 2000. The TITAN5 gene of Arabidopsis encodes a protein related to the ADP ribosylation factor family of GTP binding proteins. *The Plant cell*. 12:1379-1392.

Meraldi, P., and E.A. Nigg. 2001. Centrosome cohesion is regulated by a balance of kinase and phosphatase activities. *J Cell Sci*. 114:3749-3757.

Miryounesi, M., S. Bahari, S. Salehpour, N. Alipour, and S. Ghafouri-Fard. 2019. ELMO Domain Containing 1 (ELMOD1) Gene Mutation Is Associated with Mental Retardation and Autism Spectrum Disorder. *Journal of molecular neuroscience : MN*. 69:312-315.

Mizuno-Yamasaki, E., F. Rivera-Molina, and P. Novick. 2012. GTPase networks in membrane traffic. *Annu Rev Biochem*. 81:637-659.

Moravec, R., K.K. Conger, R. D'Souza, A.B. Allison, and J.E. Casanova. 2012. BRAG2/GEP100/IQSec1 interacts with clathrin and regulates alpha5beta1 integrin endocytosis through activation of ADP ribosylation factor 5 (Arf5). *J Biol Chem*. 287:31138-31147.

Muromoto, R., Y. Sekine, S. Imoto, O. Ikeda, T. Okayama, N. Sato, and T. Matsuda. 2008. BART is essential for nuclear retention of STAT3. *International immunology*. 20:395-403.

Nachury, M.V. 2018. The molecular machines that traffic signaling receptors into and out of cilia. *Curr Opin Cell Biol*. 51:124-131.

Nachury, M.V., and D.U. Mick. 2019. Establishing and regulating the composition of cilia for signal transduction. *Nat Rev Mol Cell Biol*. 20:389-405.

Nahse, V., L. Christ, H. Stenmark, and C. Campsteijn. 2017. The Abscission Checkpoint: Making It to the Final Cut. *Trends Cell Biol*. 27:1-11.

Nakayama, K. 2016. Regulation of cytokinesis by membrane trafficking involving small GTPases and the ESCRT machinery. *Critical reviews in biochemistry and molecular biology*. 51:1-6.

Newman, L.E., C.R. Schiavon, R.E. Turn, and R.A. Kahn. 2017a. The ARL2 GTPase regulates mitochondrial fusion from the intermembrane space. *Cellular logistics*. 7:e1340104.

Newman, L.E., C.R. Schiavon, C. Zhou, and R.A. Kahn. 2017b. The abundance of the ARL2 GTPase and its GAP, ELMOD2, at mitochondria are modulated by the fusogenic activity of mitofusins and stressors. *PloS one*. 12:e0175164.

Newman, L.E., C.J. Zhou, S. Mudigonda, A.L. Mattheyses, E. Paradies, C.M. Marobbio, and R.A. Kahn. 2014. The ARL2 GTPase is required for mitochondrial morphology, motility, and maintenance of ATP levels. *PloS one*. 9:e99270.

Nie, Z., D.S. Hirsch, and P.A. Randazzo. 2003. Arf and its many interactors. *Curr Opin Cell Biol*. 15:396-404.

Nithianantham, S., S. Le, E. Seto, W. Jia, J. Leary, K.D. Corbett, J.K. Moore, and J. Al-Bassam. 2015. Tubulin cofactors and Arl2 are cage-like chaperones that regulate the soluble alphabeta-tubulin pool for microtubule dynamics. *eLife*. 4.

Peterman, E., and R. Prekeris. 2019. The postmitotic midbody: Regulating polarity, stemness, and proliferation. *J Cell Biol*. 218:3903-3911.

Petry, S., and R.D. Vale. 2015. Microtubule nucleation at the centrosome and beyond. *Nat Cell Biol*. 17:1089-1093.

Piperno, G., K. Mead, and W. Shestak. 1992. The inner dynein arms I2 interact with a "dynein regulatory complex" in Chlamydomonas flagella. *J Cell Biol*. 118:1455-1463.

Price, H.P., A. Peltan, M. Stark, and D.F. Smith. 2010. The small GTPase ARL2 is required for cytokinesis in Trypanosoma brucei. *Mol Biochem Parasitol*. 173:123-131.

Prigent, M., T. Dubois, G. Raposo, V. Derrien, D. Tenza, C. Rosse, J. Camonis, and P. Chavrier. 2003. ARF6 controls post-endocytic recycling through its downstream exocyst complex effector. *J Cell Biol*. 163:1111-1121.

Prosser, S.L., and C.G. Morrison. 2015. Centrin2 regulates CP110 removal in primary cilium formation. *J Cell Biol*. 208:693-701.

Pulkkinen, V., S. Bruce, J. Rintahaka, U. Hodgson, T. Laitinen, H. Alenius, V.L. Kinnula, M. Myllarniemi, S. Matikainen, and J. Kere. 2010. ELMOD2, a candidate gene for idiopathic pulmonary fibrosis, regulates antiviral responses. *FASEB J*. 24:1167-1177.

Radcliffe, P.A., L. Vardy, and T. Toda. 2000. A conserved small GTP-binding protein Alp41 is essential for the cofactor-dependent biogenesis of microtubules in fission yeast. *FEBS Lett*. 468:84-88.

Radhakrishna, H., and J.G. Donaldson. 1997. ADP-ribosylation factor 6 regulates a novel plasma membrane recycling pathway. *J Cell Biol*. 139:49-61.

Randazzo, P.A., H. Inoue, and S. Bharti. 2007. Arf GAPs as regulators of the actin cytoskeleton. *Biol Cell*. 99:583-600.

Reinstein, J., I. Schlichting, M. Frech, R.S. Goody, and A. Wittinghofer. 1991. p21 with a phenylalanine 28----leucine mutation reacts normally with the GTPase activating protein GAP but nevertheless has transforming properties. *J Biol Chem*. 266:17700-17706.

Rios, R.M. 2014. The centrosome-Golgi apparatus nexus. *Philos Trans R Soc Lond B Biol Sci*. 369.

Sankaran, S., L.M. Starita, A.C. Groen, M.J. Ko, and J.D. Parvin. 2005. Centrosomal microtubule nucleation activity is inhibited by BRCA1-dependent ubiquitination. *Mol Cell Biol*. 25:8656-8668.

Santy, L.C. 2002. Characterization of a Fast Cycling ADP-ribosylation Factor 6 Mutant. *J Biol Chem*. 277:40185-40188.

Santy, L.C., K.S. Ravichandran, and J.E. Casanova. 2005. The DOCK180/Elmo complex couples ARNO-mediated Arf6 activation to the downstream activation of Rac1. *Curr Biol*. 15:1749-1754.

Satir, P. 2017. CILIA: before and after. *Cilia*. 6:1.

Schiavon, C.R., M.E. Griffin, M. Pirozzi, R. Parashuraman, W. Zhou, H.A. Jinnah, D. Reines, and R.A. Kahn. 2018. Compositional complexity of rods and rings. *Mol Biol Cell*. 29:2303-2316.

Schiavon, C.R., R.E. Turn, L.E. Newman, and R.A. Kahn. 2019. ELMOD2 regulates mitochondrial fusion in a mitofusin-dependent manner, downstream of ARL2. *Mol Biol Cell*. 30:1198-1213.

Schiel, J.A., G.C. Simon, C. Zaharris, J. Weisz, D. Castle, C.C. Wu, and R. Prekeris. 2012. FIP3-endosome-dependent formation of the secondary ingression mediates ESCRT-III recruitment during cytokinesis. *Nat Cell Biol*. 14:1068-1078.

Schlacht, A., K. Mowbrey, M. Elias, R.A. Kahn, and J.B. Dacks. 2013. Ancient Complexity, Opisthokont Plasticity, and Discovery of the 11th Subfamily of Arf GAP Proteins. *Traffic*. 14:636-649.

Schmidt, K.N., S. Kuhns, A. Neuner, B. Hub, H. Zentgraf, and G. Pereira. 2012. Cep164 mediates vesicular docking to the mother centriole during early steps of ciliogenesis. *J Cell Biol*. 199:1083-1101.

Schonteich, E., M. Pilli, G.C. Simon, H.T. Matern, J.R. Junutula, D. Sentz, R.K. Holmes, and R. Prekeris. 2007. Molecular characterization of Rab11-FIP3 binding to ARF GTPases. *Eur J Cell Biol*. 86:417-431.

Schweitzer, J.K., and C. D'Souza-Schorey. 2002. Localization and Activation of the ARF6 GTPase during Cleavage Furrow Ingression and Cytokinesis. *J Biol Chem*. 277:27210-27216.

Schweitzer, J.K., and C. D'Souza-Schorey. 2005. A requirement for ARF6 during the completion of cytokinesis. *Exp Cell Res*. 311:74-83.

Schweitzer, J.K., A.E. Sedgwick, and C. D'Souza-Schorey. 2011. ARF6-mediated endocytic recycling impacts cell movement, cell division and lipid homeostasis. *Semin Cell Dev Biol*. 22:39-47.

Seixas, E., M. Barros, M.C. Seabra, and D.C. Barral. 2013. Rab and Arf proteins in genetic diseases. *Traffic*. 14:871-885.

Sharer, J.D., and R.A. Kahn. 1999. The ARF-like 2 (ARL2)-binding protein, BART. Purification, cloning, and initial characterization. *J Biol Chem*. 274:27553-27561.

Sharer, J.D., J.F. Shern, H. Van Valkenburgh, D.C. Wallace, and R.A. Kahn. 2002. ARL2 and BART enter mitochondria and bind the adenine nucleotide transporter. *Mol Biol Cell*. 13:71-83.

Shiba, T., H. Koga, H.W. Shin, M. Kawasaki, R. Kato, K. Nakayama, and S. Wakatsuki. 2006. Structural basis for Rab11-dependent membrane recruitment of a family of Rab11-interacting protein 3 (FIP3)/Arfophilin-1. *Proc Natl Acad Sci U S A*. 103:15416-15421.

Shultz, T., M. Shmuel, T. Hyman, and Y. Altschuler. 2008. Beta-tubulin cofactor D and ARL2 take part in apical junctional complex disassembly and abrogate epithelial structure. *FASEB J*. 22:168-182.

Smits, A.H., F. Ziebell, G. Joberty, N. Zinn, W.F. Mueller, S. Clauder-Munster, D. Eberhard, M. Falth Savitski, P. Grandi, P. Jakob, A.M. Michon, H. Sun, K. Tessmer, T. Burckstummer, M. Bantscheff, L.M. Steinmetz, G. Drewes, and W. Huber. 2019. Biological plasticity rescues target activity in CRISPR knock outs. *Nat Methods*. 16:1087-1093.

Song, J., Z. Khachikian, H. Radhakrishna, and J.G. Donaldson. 1998. Localization of endogenous ARF6 to sites of cortical actin rearrangement and involvement of ARF6 in cell spreading. *J Cell Sci*. 111 (Pt 15):2257-2267.

Spang, A., Y. Shiba, and P.A. Randazzo. 2010. Arf GAPs: gatekeepers of vesicle generation. *FEBS Lett*. 584:2646-2651.

Spektor, A., W.Y. Tsang, D. Khoo, and B.D. Dynlacht. 2007. Cep97 and CP110 suppress a cilia assembly program. *Cell*. 130:678-690.

Stearns, T., M.A. Hoyt, and D. Botstein. 1990. Yeast mutants sensitive to antimicrotubule drugs define three genes that affect microtubule function. *Genetics*. 124:251-262.

Steinborn, K., C. Maulbetsch, B. Priester, S. Trautmann, T. Pacher, B. Geiges, F. Kuttner, L. Lepiniec, Y.D. Stierhof, H. Schwarz, G. Jurgens, and U. Mayer. 2002. The Arabidopsis

PILZ group genes encode tubulin-folding cofactor orthologs required for cell division but not cell growth. *Genes Dev*. 16:959-971.

Styczynska-Soczka, K., and A.P. Jarman. 2015. The Drosophila homologue of Rootletin is required for mechanosensory function and ciliary rootlet formation in chordotonal sensory neurons. *Cilia*. 4:9.

Suzuki, M., T. Murakami, J. Cheng, H. Kano, M. Fukata, and T. Fujimoto. 2015. ELMOD2 is anchored to lipid droplets by palmitoylation and regulates adipocyte triglyceride lipase recruitment. *Mol Biol Cell*. 26:2333-2342.

Sztul, E., P.W. Chen, J.E. Casanova, J. Cherfils, J.B. Dacks, D.G. Lambright, F.S. Lee, P.A. Randazzo, L.C. Santy, A. Schurmann, I. Wilhelmi, M.E. Yohe, and R.A. Kahn. 2019. ARF GTPases and their GEFs and GAPs: concepts and challenges. *Mol Biol Cell*. 30:1249-1271.

Takahashi, S., T. Takei, H. Koga, H. Takatsu, H.W. Shin, and K. Nakayama. 2011. Distinct roles of Rab11 and Arf6 in the regulation of Rab11-FIP3/arfophilin-1 localization in mitotic cells. *Genes to cells : devoted to molecular & cellular mechanisms*. 16:938-950.

Tassin, A.M., B. Maro, and M. Bornens. 1985a. Fate of microtubule-organizing centers during myogenesis in vitro. *J Cell Biol*. 100:35-46.

Tassin, A.M., M. Paintrand, E.G. Berger, and M. Bornens. 1985b. The Golgi apparatus remains associated with microtubule organizing centers during myogenesis. *J Cell Biol*. 101:630-638.

Tian, G., Y. Huang, H. Rommelaere, J. Vandekerckhove, C. Ampe, and N.J. Cowan. 1996. Pathway leading to correctly folded beta-tubulin. *Cell*. 86:287-296.

Tian, G., S. Thomas, and N.J. Cowan. 2010. Effect of TBCD and its regulatory interactor Arl2 on tubulin and microtubule integrity. *Cytoskeleton (Hoboken)*. 67:706-714.

Tsang, W.Y., A. Spektor, D.J. Luciano, V.B. Indjeian, Z. Chen, J.L. Salisbury, I. Sanchez, and B.D. Dynlacht. 2006. CP110 cooperates with two calcium-binding proteins to regulate cytokinesis and genome stability. *Mol Biol Cell*. 17:3423-3434.

Tulu, U.S., C. Fagerstrom, N.P. Ferenz, and P. Wadsworth. 2006. Molecular requirements for kinetochore-associated microtubule formation in mammalian cells. *Curr Biol*. 16:536-541.

Turn, R.E., M.P. East, R. Prekeris, and R.A. Kahn. 2020. The ARF GAP ELMOD2 acts with different GTPases to regulate centrosomal microtubule nucleation and cytokinesis. *Mol Biol Cell*. 31:2070-2091.

Ueda, T., A. Hanai, T. Takei, K. Kubo, M. Ohgi, H. Sakagami, S. Takahashi, H.W. Shin, and K. Nakayama. 2013. EFA6 activates Arf6 and participates in its targeting to the Flemming body during cytokinesis. *FEBS Lett*. 587:1617-1623.

Van Valkenburgh, H., J.F. Shern, J.D. Sharer, X. Zhu, and R.A. Kahn. 2001. ADP-ribosylation factors (ARFs) and ARF-like 1 (ARL1) have both specific and shared effectors: characterizing ARL1-binding proteins. *J Biol Chem*. 276:22826-22837.

Veltel, S., R. Gasper, E. Eisenacher, and A. Wittinghofer. 2008. The retinitis pigmentosa 2 gene product is a GTPase-activating protein for Arf-like 3. *Nat Struct Mol Biol*. 15:373-380.

Vitali, T., S. Girald-Berlingeri, P.A. Randazzo, and P.W. Chen. 2017. Arf GAPs: A family of proteins with disparate functions that converge on a common structure, the integrin adhesion complex. *Small GTPases*:1-9.

Vitali, T., S. Girald-Berlingeri, P.A. Randazzo, and P.W. Chen. 2019. Arf GAPs: A family of proteins with disparate functions that converge on a common structure, the integrin adhesion complex. *Small GTPases*. 10:280-288.

Vlijm, R., X. Li, M. Panic, D. Ruthnick, S. Hata, F. Herrmannsdorfer, T. Kuner, M. Heilemann, J. Engelhardt, S.W. Hell, and E. Schiebel. 2018. STED nanoscopy of the centrosome linker

reveals a CEP68-organized, periodic rootletin network anchored to a C-Nap1 ring at centrioles. *Proc Natl Acad Sci U S A*. 115:E2246-E2253.

Waters, A.M., and P.L. Beales. 2011. Ciliopathies: an expanding disease spectrum. *Pediatr Nephrol*. 26:1039-1056.

Watzlich, D., I. Vetter, K. Gotthardt, M. Miertzschke, Y.X. Chen, A. Wittinghofer, and S. Ismail. 2013. The interplay between RPGR, PDEdelta and Arl2/3 regulate the ciliary targeting of farnesylated cargo. *EMBO Rep*. 14:465-472.

Wilson, G.M., A.B. Fielding, G.C. Simon, X. Yu, P.D. Andrews, R.S. Hames, A.M. Frey, A.A. Peden, G.W. Gould, and R. Prekeris. 2005. The FIP3-Rab11 protein complex regulates recycling endosome targeting to the cleavage furrow during late cytokinesis. *Mol Biol Cell*. 16:849-860.

Wolfrum, U. 1992. Cytoskeletal elements in arthropod sensilla and mammalian photoreceptors. *Biol Cell*. 76:373-381.

Wright, K.J., L.M. Baye, A. Olivier-Mason, S. Mukhopadhyay, L. Sang, M. Kwong, W. Wang, P.R. Pretorius, V.C. Sheffield, P. Sengupta, D.C. Slusarski, and P.K. Jackson. 2011. An ARL3-UNC119-RP2 GTPase cycle targets myristoylated NPHP3 to the primary cilium. *Genes Dev*. 25:2347-2360.

Wright, Z.C., Y. Loskutov, D. Murphy, P. Stoilov, E. Pugacheva, A.F.X. Goldberg, and V. Ramamurthy. 2018. ADP-Ribosylation Factor-Like 2 (ARL2) regulates cilia stability and development of outer segments in rod photoreceptor neurons. *Sci Rep*. 8:16967.

Wright, Z.C., R.K. Singh, R. Alpino, A.F. Goldberg, M. Sokolov, and V. Ramamurthy. 2016. ARL3 regulates trafficking of prenylated phototransduction proteins to the rod outer segment. *Hum Mol Genet*. 25:2031-2044.

Wu, J., and A. Akhmanova. 2017. Microtubule-Organizing Centers. *Annu Rev Cell Dev Biol*. 33:51-75.

Yang, J., M. Adamian, and T. Li. 2006. Rootletin interacts with C-Nap1 and may function as a physical linker between the pair of centrioles/basal bodies in cells. *Mol Biol Cell*. 17:1033-1040.

Yang, J., J. Gao, M. Adamian, X.H. Wen, B. Pawlyk, L. Zhang, M.J. Sanderson, J. Zuo, C.L. Makino, and T. Li. 2005. The ciliary rootlet maintains long-term stability of sensory cilia. *Mol Cell Biol*. 25:4129-4137.

Yang, J., and T. Li. 2005. The ciliary rootlet interacts with kinesin light chains and may provide a scaffold for kinesin-1 vesicular cargos. *Exp Cell Res*. 309:379-389.

Yang, J., and T. Li. 2006. Focus on molecules: rootletin. *Exp Eye Res*. 83:1-2.

Yang, J., X. Liu, G. Yue, M. Adamian, O. Bulgakov, and T. Li. 2002. Rootletin, a novel coiled-coil protein, is a structural component of the ciliary rootlet. *J Cell Biol*. 159:431-440.

Yasar, B., K. Linton, C. Slater, and R. Byers. 2017. Primary cilia are increased in number and demonstrate structural abnormalities in human cancer. *J Clin Pathol*. 70:571-574.

Zhang, C.J., J.B. Bowzard, A. Anido, and R.A. Kahn. 2003. Four ARF GAPs in Saccharomyces cerevisiae have both overlapping and distinct functions. *Yeast*. 20:315-330.

Zhang, C.J., M.M. Cavenagh, and R.A. Kahn. 1998. A family of Arf effectors defined as suppressors of the loss of Arf function in the yeast Saccharomyces cerevisiae. *J Biol Chem*. 273:19792-19796.

Zhang, C.J., A.G. Rosenwald, M.C. Willingham, S. Skuntz, J. Clark, and R.A. Kahn. 1994. Expression of a dominant allele of human ARF1 inhibits membrane traffic in vivo. *J Cell Biol*. 124:289-300.

Zhou, C., L. Cunningham, A.I. Marcus, Y. Li, and R.A. Kahn. 2006. Arl2 and Arl3 regulate different microtubule-dependent processes. *Mol Biol Cell*. 17:2476-2487.

Zhou, C.X., L.Y. Shi, R.C. Li, Y.H. Liu, B.Q. Xu, J.W. Liu, B. Yuan, Z.X. Yang, X.Y. Ying, and D. Zhang. 2017. GTPase-activating protein Elmod2 is essential for meiotic progression in mouse oocytes. *Cell Cycle*. 16:852-860.

Zhu, X., and I. Kaverina. 2013. Golgi as an MTOC: making microtubules for its own good. *Histochem Cell Biol*. 140:361-367.

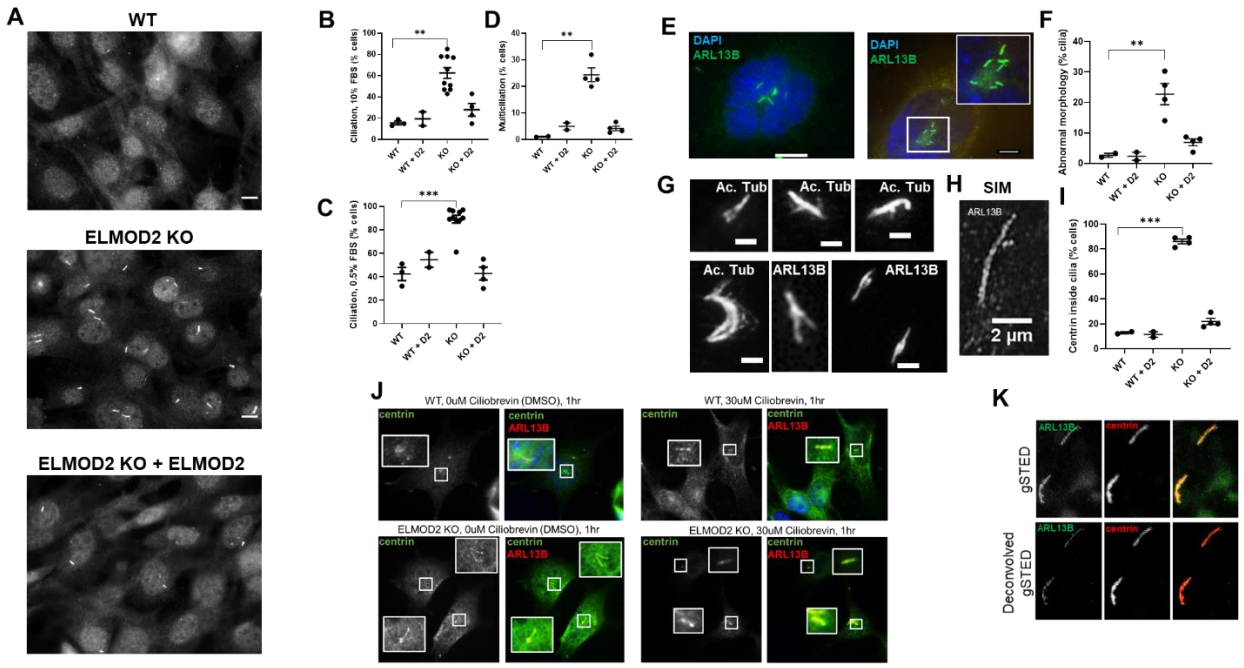

Figure 1: *Deletion of ELMOD2 causes ciliary defects.* **(A)** ELMOD2 KO cells display increased ciliation as well as multiciliation compared to WT MEFs in normal (10% FBS) medium. Cells were grown to ~80% confluence, fixed with 4% PFA, permeabilized with 0.1% Triton X-100, and stained for ARL13B as a marker of ciliation. Representative images were collected at 60x magnification using widefield microscopy. Scale bar = 10 µm. **(B)** Using the same conditions described in (A), ciliation was scored in 2 WT, 10 ELMOD2 KO, and 4 ELMOD2-rescued lines. One hundred cells per cell line were scored for the presence of one or more cilia. ARL13B and acetylated tubulin were used as markers to detect cilia. (**C)** The same experiment was performed as described for (B), except cells were serum starved and plated at 90-100% confluence. **(D)** The same experiment was performed as described for (C), except multiciliation (>1 cilia) was scored. **(E)** Loss of ELMOD2 leads to increased multiciliation. Cells were fixed with 4% PFA, permeabilized with 0.1% Triton X-100, and stained for ARL13B to detect cilia and with Hoechst to identify individual cells. Images were collected using widefield microscopy at 100x magnification. The two panels each show single cells with 4 and 10 cilia (2 of the cilia did not fit

inside the inset) from left to right. The cell on the left is also multinucleated, which is typical of ELMOD2 KO cells. Scale bar = 10 µm. (**F)** Serum-starved cells stained for ARL13B and acetylated tubulin were scored for abnormal morphology (*i.e.*, branching or splaying rather than having a single, relatively straight cilium). Only ciliated cells (2 WT, 10 ELMOD2 KO, and 4 ELMOD2 KO + ELMOD2-myc) were scored. (**G)** Examples of cilia with abnormal morphology are shown. Images were collected using widefield microscopy at 100x magnification, zoomed in to highlight the branching/splaying. Panels are labeled to indicate if the image shows ARL13B or acetylated tubulin staining, though no differences were noted. Scale bar = 2 µm. **(H)** An image of a branching cilium stained with ARL13B is shown using structured illumination microscopy at 100x magnification. Scale bar = 2 µm **(I)** ELMOD2 KO cells show increased centrin localization inside cilia compared to WT cells. Cells were stained for ARL13B and centrin and scored for number of cells with cilia positive for centrin. **(J)** Centrin staining in cilia is increased in both WT and ELMOD2 KO cells after treatment with ciliobrevin. Representative images collected via widefield microscopy (100x magnification) are shown. WT and KO cells were serum starved for 24 hours before being treated with either DMSO or 30µM ciliobrevin for 1hr at 37˚C. Cells were fixed, stained, and permeabilized as described in (I). Insets highlight individual cilia and whether centrin localizes to them. **(K)** g-STED microscopy (100x magnification) confirms the localization of centrin to cilia in non-treated ELMOD2 KO cells. Cilia shown in this image come from a single cell. These cilia have centrin localization along the length of the cilium as well as at buds coming off the surface. In each case of scoring, experiments were performed in triplicate, and the average of the triplicate for each line was plotted. Results were tabulated in an interleaved scatterplot via GraphPad Prism. Statistical significance was assessed using One-Way ANOVA; *=$p<0.05$; **=$p<0.01$; ***=$p<0.0001$.

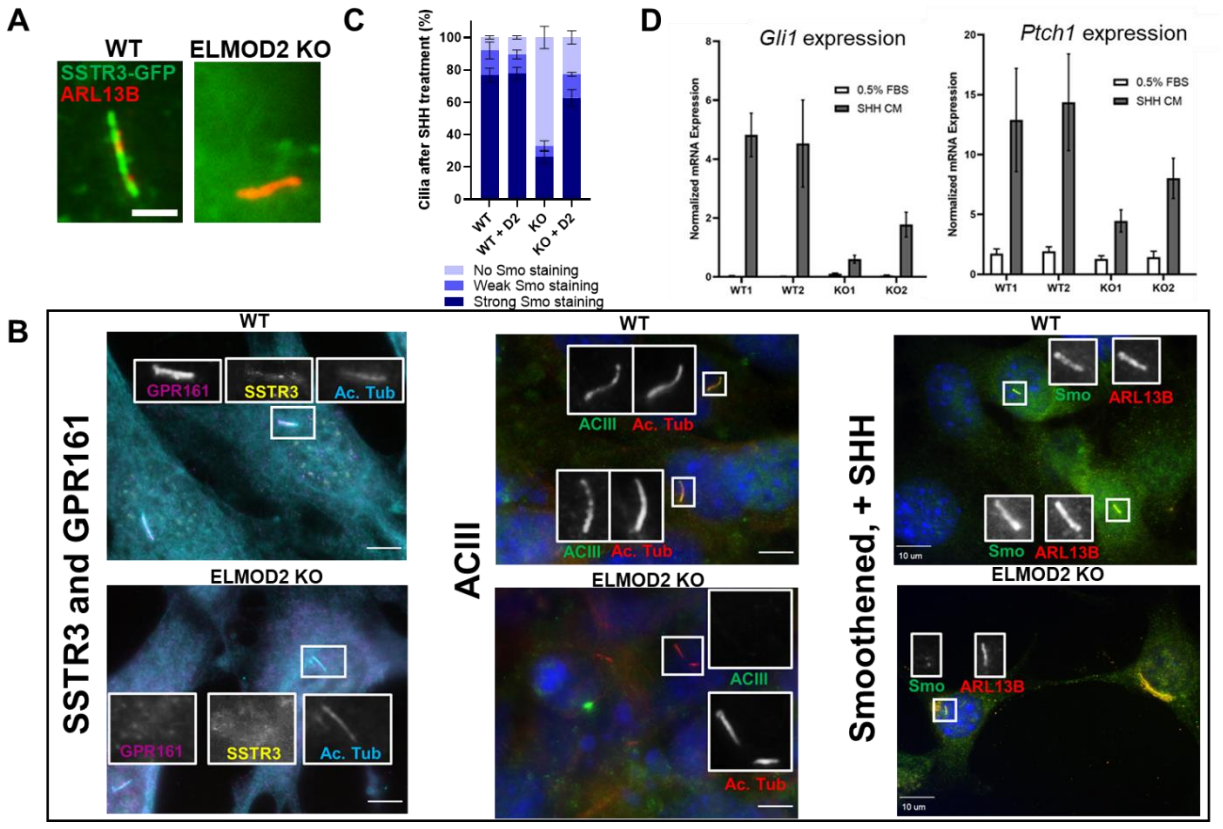

Figure 2: *Ciliary signaling is disrupted in ELMOD2 KO lines.* **(A)** WT or ELMOD2 KO cells were transfected with plasmid directing expression of SSTR3-GFP and serum starved. KO cells displayed strongly reduced presence of SSTR3 in cilia. Cells were fixed with 4% PFA, permeabilized with 0.1% Triton X-100, and co-stained with ARL13B. Representative images were collected using widefield microscopy (100x magnification). Scale bar = 2 µm. **(B)** ELMOD2 KO cells show decreased recruitment of (endogenous) SSTR3, GPR161, Smo, and ACIII. Serum-starved cells were fixed and stained using protocols required for detecting the appropriate antigen. Representative images were collected via widefield microscopy at 100x magnification. Samples were co-stained with either acetylated tubulin or ARL13B to mark cilia. Scale bar = 10 µm. **(C)** ELMOD2 KO cells show decreased Smo recruitment after SHH treatment, compared to WT cells. Cells (2 WT, 4 ELMOD2 KO, and 4 ELMOD2 KO + ELMOD2-myc) were serum starved, treated with SHH-enriched medium for 24 hours to induce, fixed with 4% PFA, and permeabilized with

0.1% Triton X-100. Cells were co-stained for Smo and ARL13B, and 100 cells were scored per line in triplicate. Ciliated cells were binned into either having strong, weak, or no Smo staining. The average of the triplicates for each line was determined, and the data were plotted as a stacked bar graph. Error bars indicate SEM. **(D)** ELMOD2 KO MEFs show reduced Shh-stimulated transcriptional responses compared to WT cells. Cells were collected 48 hours after SHH treatment and levels of *Gli1* and *Ptch1* mRNAs were determined using qPCR. Error bars indicate SD, and bar graphs indicate normalized mRNA expression.

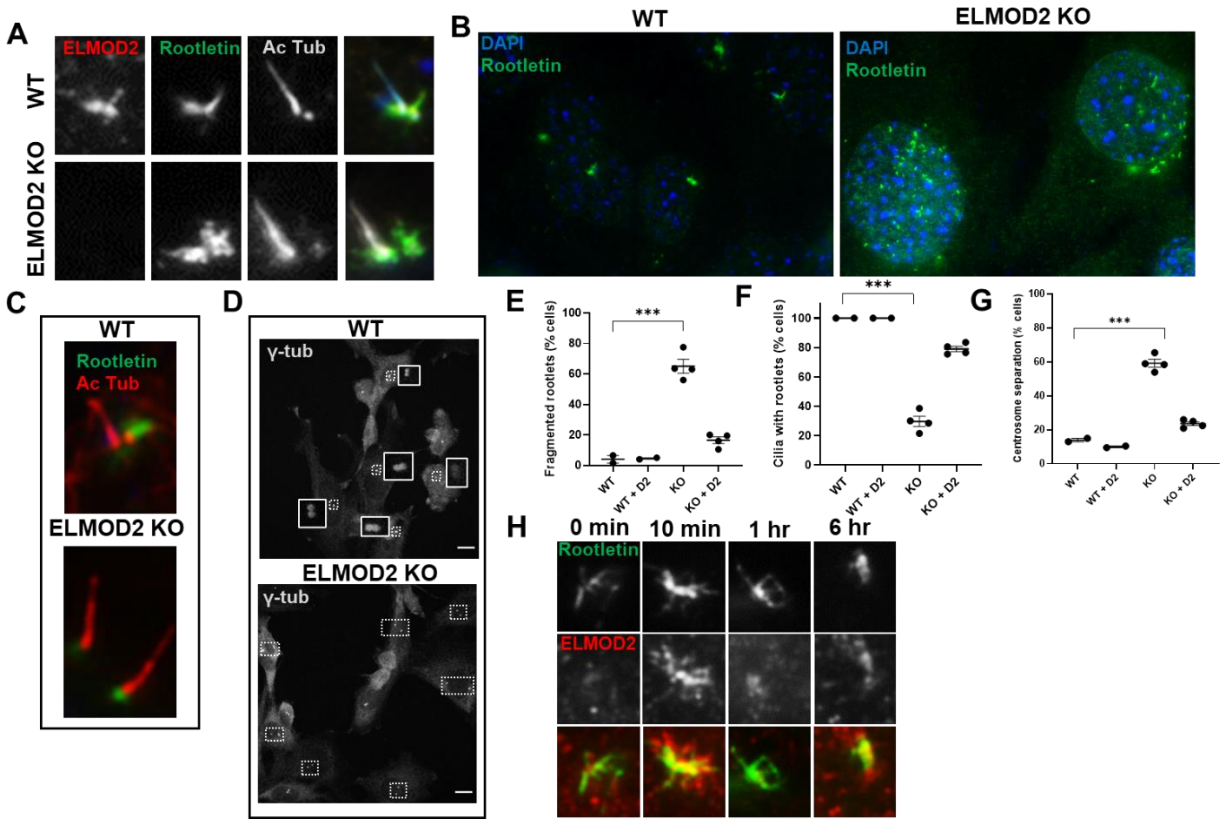

Figure 3: *ELMOD2 localizes to rootlets and its deletion causes rootlet defects.* **(A)** ELMOD2 localizes to rootlets in WT MEFs. WT or KO cells were fixed for 5 min in ice-cold methanol and stained for ELMOD2, acetylated tubulin, and rootletin, as described under Methods. Images were collected via widefield microscopy at 100x magnification. Scale = 10 µm. **(B)** ELMOD2 KO cells have increased rootlet fragmentation. Serum-starved, methanol fixed cells were stained for rootletin and Hoechst. Images were collected using widefield microscopy at 100x magnification. **(C)** When focusing specifically on cilia-associated rootletin, rootletin staining in ELMOD2 KO cells is limited to the base of cilia and has lost the bulk of the filamentous rootlet staining. Cilia in ELMOD2 KO cells have smaller, less root-like rootlets than WT cilia. Growth and fixation conditions were the same as described in (B). Cells were stained with rootletin and acetylated tubulin (to mark cilia). Images were collected via widefield microscopy at 100x magnification. **(D)** ELMOD2 KO cells show increased centrosome separation. Serum-starved cells were fixed with

ice-cold methanol, stained for γ-tubulin, and imaged via confocal microscopy at 100x magnification, with z-projections. Scale bar = 10 μm. **(E)** Serum starved cells were fixed with ice cold methanol, stained for rootletin, and scored in duplicate for fragmented rootlets. **(F)** The same conditions as described for (E) were used to score cell lines for cilia with rootlets, except only ciliated cells were scored. **(G)** Using the same conditions described in (B), cells were scored for centrosome separation using FIJI image processing software with the provided measuring tool. Cells were counted as "separated" if they were more than 2μm apart. **(H)** ELMOD2 and rootletin staining each change after serum starvation. WT MEFs were fixed at different times after initiation of serum starvation using ice-cold methanol and stained for ELMOD2 and rootletin. Representative widefield images were collected at 100x magnification. Staining of each at basal bodies is strongly increased within 10 min, showing extensive overlap. At later times each, becomes more concentrated into a smaller area, but filamentous staining of ELMOD2 is lost before that of rootletin. When scoring was performed, the average of duplicates of individual lines were plotted using an interleaved scatterplot. Error bars indicate SEM. Statistical significance was assessed using One-Way ANOVA; *=$p<0.05$; **=$p<0.01$; ***=$p<0.0001$.

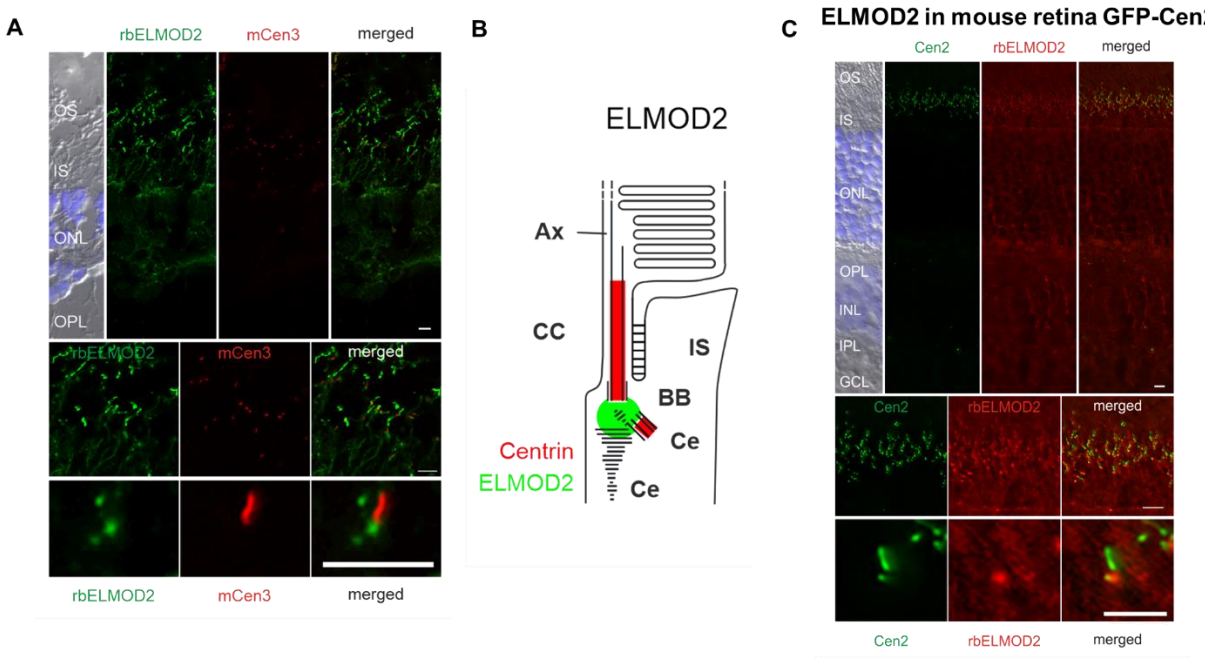

Figure 4: *ELMOD2 localizes to the base of the connecting cilium of both human and mouse retinal epithelium.* Human **(A)** and mouse **(B)** photoreceptor cells were harvested from WT mice and sectioned. Cells were stained for ELMOD2 and centrin (a marker of the connecting cilium). Representative images shown here indicate that ELMOD2 localizes specifically to the base of the connecting cilium.

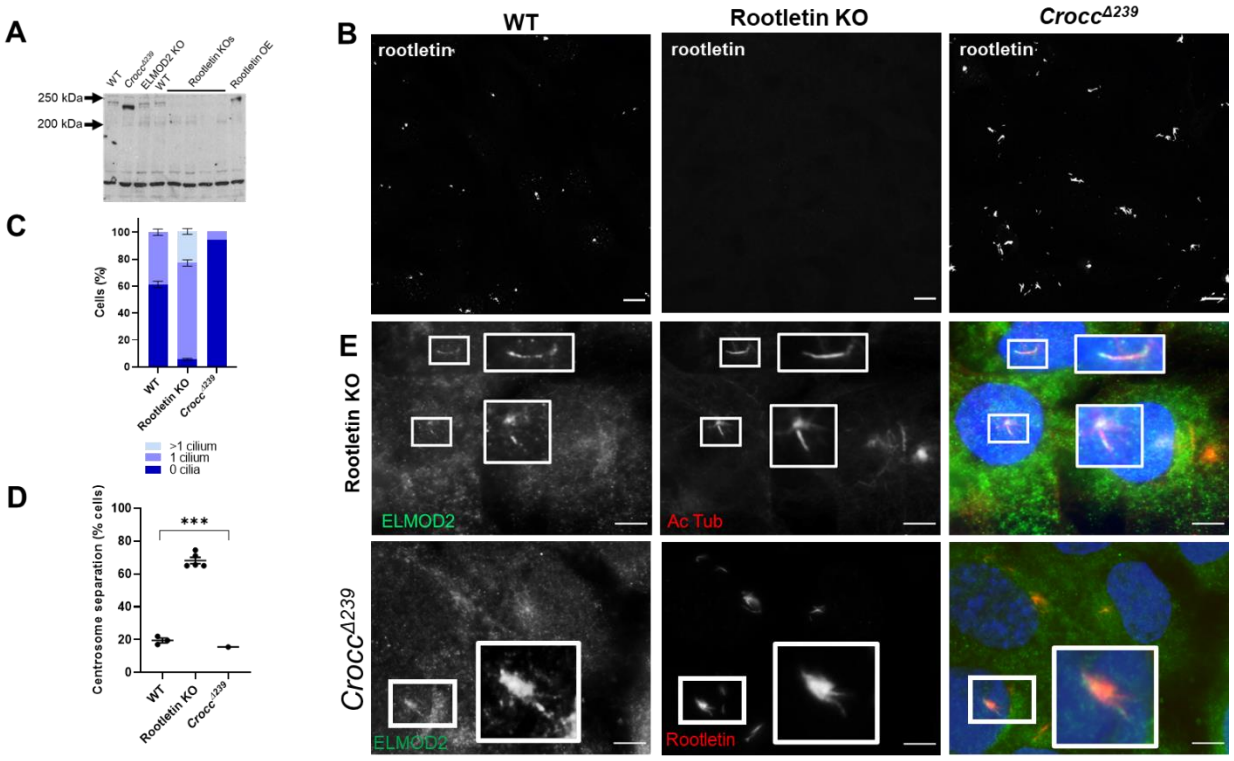

Figure 5: *Rootletin KO lines phenocopy ELMOD2 null ciliary and centrosomal cohesion defects.* **(A)** Immunoblotting shows the absence of rootletin in CROCC KO, no changes from WT in ELMOD2 KO cells, and strongly increased expression in *Crocc*$^{\Delta 239}$ cells. Equal protein was loaded into a 7.5% polyacrylamide gel before being transferred onto nitrocellulose membrane and stained for rootletin, as described under Methods. The band migrating at ~240 kDa, based on comparison to protein standards, in WT and ELMOD2 KO MEFs is absent in rootletin KO lines. This band is increased in intensity upon expression of myc-rootletin (far right lane). The *Crocc*$^{\Delta 239}$ cell lysate, instead, has a stronger staining band that migrates ~20 kDa faster compared to WT. A representative image of this after 1-minute exposure to film is shown. See Fig. S3 for other images. **(B)** Representative confocal images (100x magnification, z-stacks) of WT, rootletin KO, and *Crocc*$^{\Delta 239}$ cells are shown. Cells were fixed with ice cold methanol and stained for rootletin. Scale = 10µm. **(C)** Scoring of cilia in serum starved WT, rootletin KO, and *Crocc*$^{\Delta 239}$ cells reveal that loss of rootletin leads to increased ciliation while expression of rootletin [Δ239] prevents ciliation.

Cells were stained for acetylated tubulin or ARL13B and scored for having either 0, 1, or >1 cilia. Scoring of 3 WT, 5 rootletin KO, and the *Crocc*$^{\Delta 239}$ lines was performed in duplicate. Data were graphed in GraphPad Prism using a stacked bar graph. Error bars indicate SEM. **(D)** Rootletin KO cells have increased centrosome separation compared to WT. 3 WT, 5 rootletin KO, and 1 *Crocc*$^{\Delta 239}$ cell lines were fixed with ice cold methanol and stained for γ-tubulin to mark centrosomes. Fields of cells at 100x magnification were taken and processed using the measuring tool in FIJI imaging software to measure the distance between centrosomes. Centrosomes that were more than 2μm apart were considered separated. This experiment was performed in duplicate, and the average of the duplicates of each line was plotted in an interleaved scatterplot. Error bars indicate SEM. Statistical significance was assessed using One-Way ANOVA; *=$p<0.05$; **=$p<0.01$; ***=$p<0.0001$. **(E)** Representative images of rootletin KO and *Crocc*$^{\Delta 239}$ cells show different localization of ELMOD2 at the centrosomal/ciliary compartment compared to WT. ELMOD2 localizes to cilia in rootletin KO and strongly to rootlets in the *Crocc*$^{\Delta 239}$ mutant. Serum starved cells were fixed with ice cold methanol and stained for ELMOD2 and either rootletin or acetylated tubulin. Images were collected via widefield microscopy at 100x magnification. Scale = 10μm.

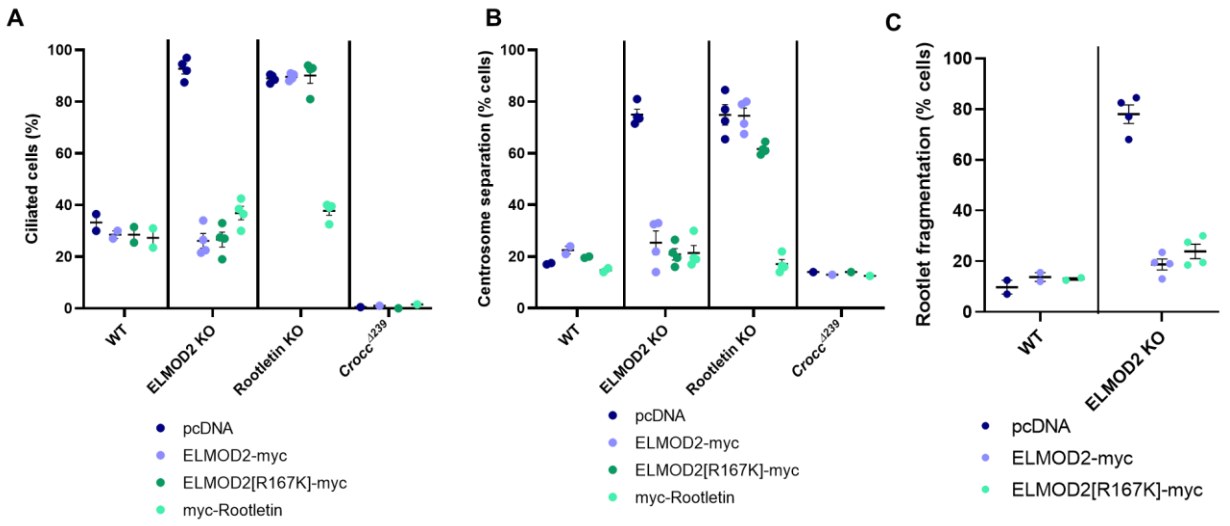

Figure 6: *ELMOD2-myc and ELMOD2[R167K]-myc rescue ciliation and centrosomal cohesion defects in ELMOD2 KO but not rootletin KO cells.* Cells (2 WT, 4 ELMOD2 KO, 4 rootletin KO, and *Crocc*$^{\Delta 239}$ mutant) were transfected with either empty vector, or plasmids directing expression of ELMOD2-myc or ELMOD2[R167K]-myc before being re-plated onto coverslips, serum starved, fixed with ice cold methanol, and stained for rootletin (to mark rootlets), acetylated tubulin (to mark cilia), and γ-tubulin (to mark centrosomes). Cells were scored in duplicate for either **(A)** % ciliation, **(B)** centrosome separation (centrosomes >2µm apart), or **(C)** rootlet fragmentation. 100 cells were scored per replicate. The averages of individual lines were plotted as individual points in leafed scatterplots. Error bars indicate SEM. Statistical significance was assessed using One-Way ANOVA; *=p<0.05; **=p<0.01; ***=p<0.0001.

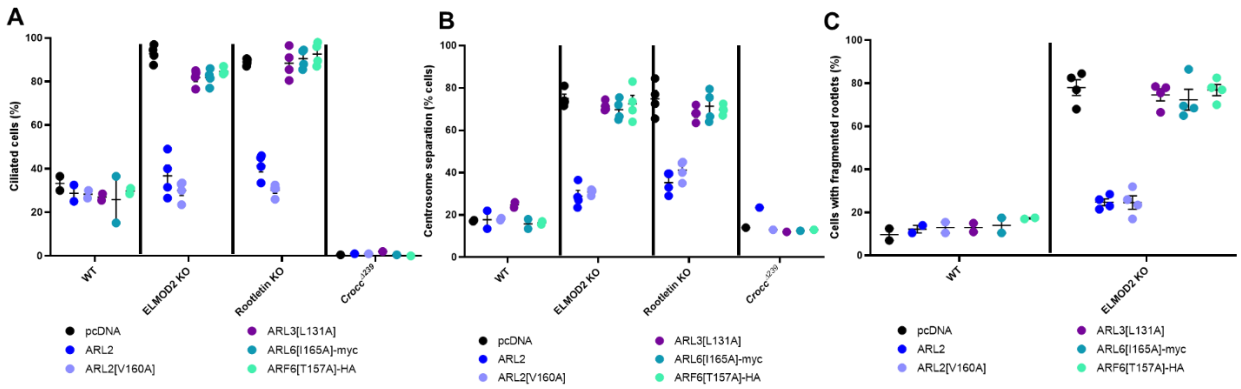

Figure 7: *ARL2 and ARL2[V160A] reverse increased ciliation, rootlet fragmentation, and increased centrosome separation defects in ELMOD2 and rootletin KO cells.* Cells (2 WT, 4 ELMOD2 KO, 4 rootletin KO, and *Crocc*$^{\Delta 239}$ mutant) were transfected with one of the following constructs: pcDNA (empty vector control), ARL2, ARL2[V160A], ARL3[L131A], ARL6[I165A]-myc, or ARF6[T157A]-HA and were plated onto glass coverslips before being serum starved for 24 hours. Samples were fixed with ice cold methanol before being immunostained for rootletin (to mark rootlets), acetylated tubulin (to mark cilia), and γ-tubulin (to mark centrosomes). Cells were scored in duplicate for either **(A)** % of cells with at least one cilium, **(B)** centrosome separation (centrosomes >2µm apart), or **(C)** rootlet fragmentation. 100 cells were scored per replicate. The averages of individual lines were plotted as individual points in leafed scatterplots. Error bars indicate SEM. Statistical significance was assessed using One-Way ANOVA; *=p<0.05; **=p<0.01; ***=p<0.0001.

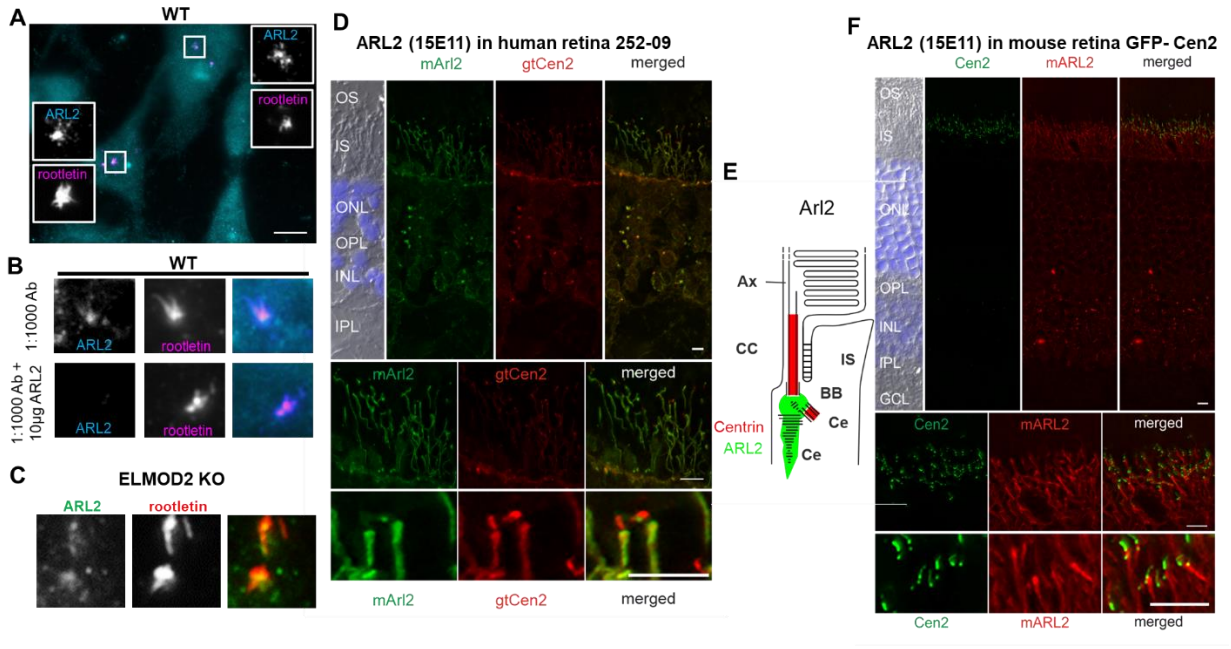

Figure 8: *ARL2 localizes to ciliary rootlets in WT MEFs and human/mouse photoreceptor cells.* **(A)** Ice-cold methanol fixed WT cells show ARL2 co-localization with rootletin. A representative image is shown here which was collected via widefield microscopy at 100x magnification. Scale = 10µm. **(B)** ARL2 staining at rootlets is lost with antigen competition. Images were collected using the same conditions described in (A), except that in the lower panel the primary antibody was incubated with 10 µg purified recombinant human ARL2 prior to use in cell staining. **(C)** ARL2 localization to rootlets in maintained in ELMOD2 KO cells. Images were collected using the same conditions as described in (A), except that ELMOD2 KO cells rather than WT MEFs were used. **(D-F)** ARL2 localizes strongly to the ciliary rootlet in human and mouse retinal epithelial cells. As described in Figure 4, photoreceptors were fixed and stained for ARL2 and centrin (as marker of basal bodies/connecting cilium).

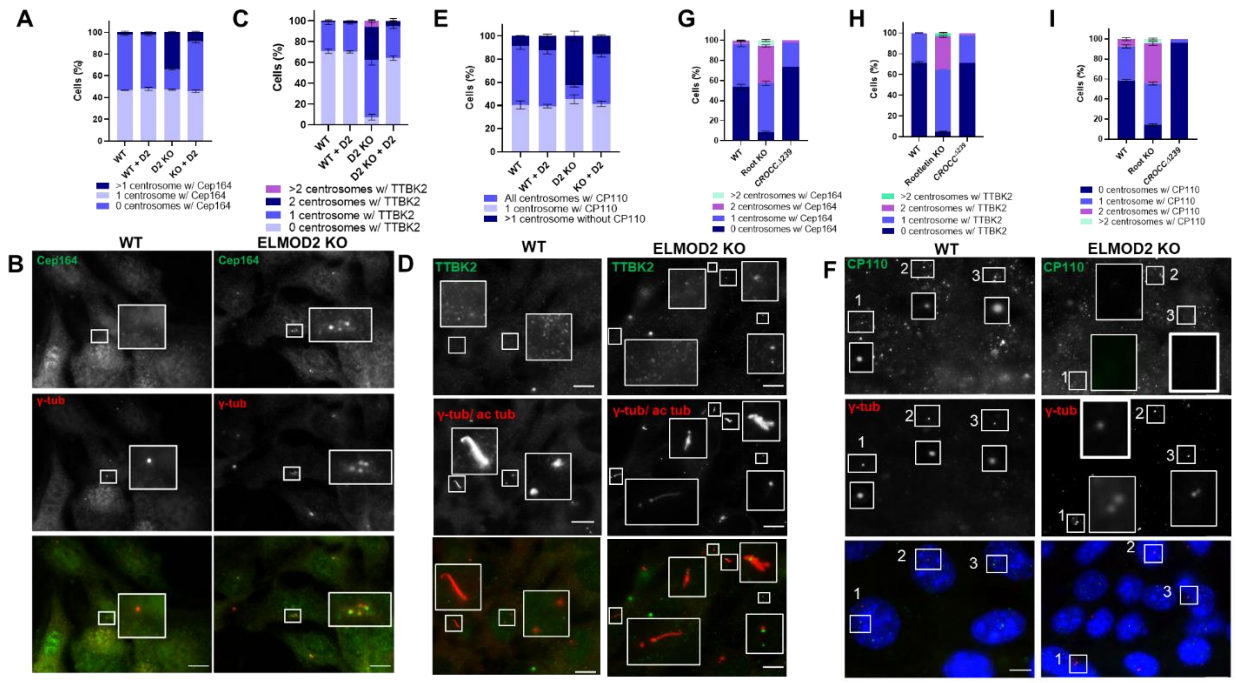

Figure 9: *ELMOD2 KO causes misregulation of markers of different steps in the ciliogenesis process.* **(A-B)** Loss of ELMOD2 leads to increased Cep164 recruitment. Cells (2 WT, 4 ELMOD2 KO, and 4 ELMOD2 KO + ELMOD2-myc) were serum starved and scored for changes in Cep164 localization, using γ-tubulin to mark cilia, as described under Methods. Representative images are shown in (**B**); scale bar = 10µm. Cells were scored in duplicate and binned as either having 0, 1, or >1 centrosome positive for Cep164. Data were plotted in a stacked bar graph, and error bars indicate SEM. **(C-D)** TTBK2 is increased at centrosomes in ELMOD2 KO cells. The same conditions as shown for (A-B) were used to monitor changes in TTBK2 recruitment, except cells were co-stained with both γ-tubulin and acetylated tubulin to track both centrosomes and cilia, and cells were fixed for only 5 minutes. **(E-F)** Loss of ELMOD2 leads to increased CP110-negative centrosomes, even cells with >1 centrosome being negative for CP110. The same conditions as shown for (A-B) were used to determine if CP110 localization to centrosomes changes in ELMOD2 KO cells. The same experiments were also performed in rootletin KO and *Crocc*$^{\Delta 239}$ mutant cells to look at Cep164 **(G)**, TTBK2 **(H)**, and CP110 **(I),** respectively. Together, these data

all point to loss of ELMOD2 and rootletin leading to increased Cep164 and TTBK2 recruitment to centrosomes and increased CP110 release from centrosomes. In contrast, in the *Crocc*$^{\Delta 239}$ mutant, there is a decrease in Cep164 and TTBK2 recruitment and a particularly strong retention of CP110 at centrosomes.

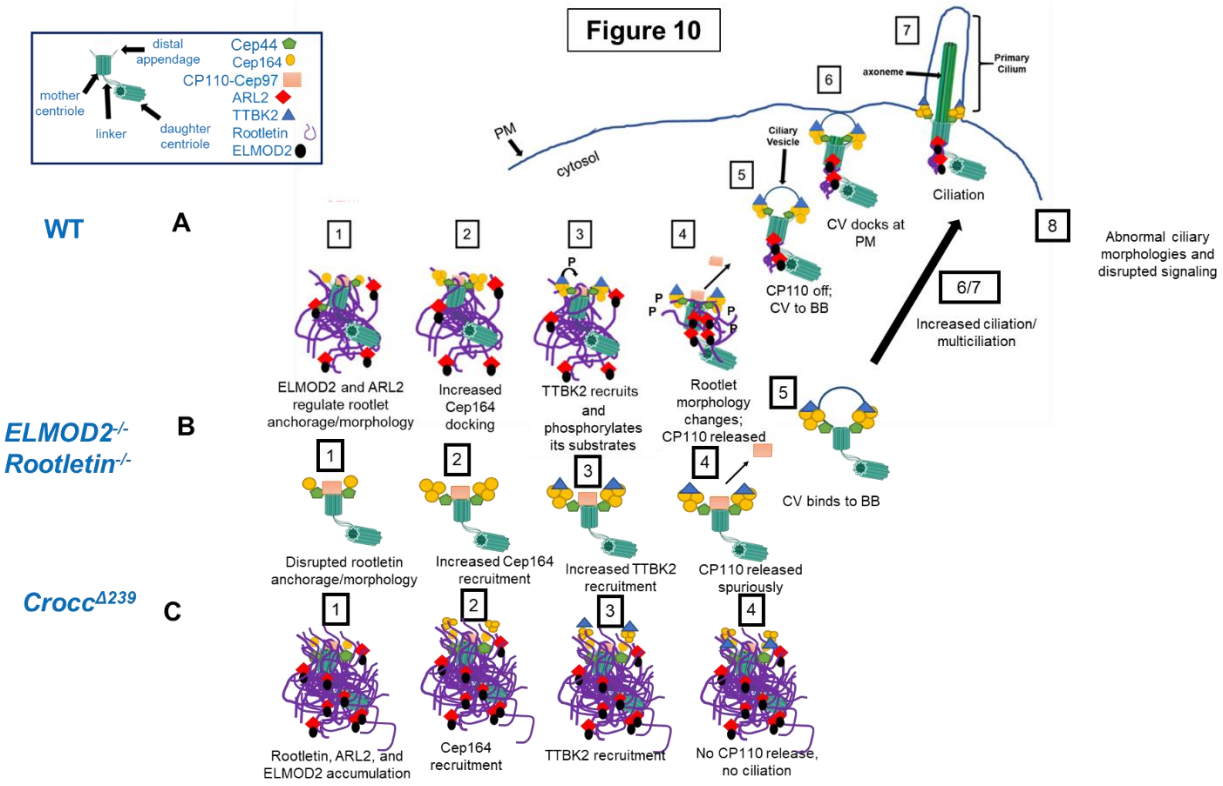

Figure 10: *ELMOD2, ARL2, and rootletin work together to prevent spurious ciliogenesis*. **(A)** We propose that ELMOD2, ARL2, and rootletin work in concert to inhibit spurious ciliogenesis. we argue that rootletin/rootlet acts to block CP110 release, and that ELMOD2 and ARL2 regulate rootletin anchoring and possibly activity at basal bodies. Previous studies have revealed early steps in ciliogenesis that include (1) Cep164 recruitment to centrosomes, (2) TTBK2 recruitment to basal bodies by Cep164, (3)TTBK2 phosphorylation of substrates, (4) CP110-Cep97 capping complex release, (5) docking of the ciliary vesicle at the distal end of the basal body, (6) docking of the basal body at the plasma membrane, and (7) projection of the axoneme and elaboration of the cilium. We believe that ELMOD2 and rootletin act early in ciliogenesis to regulate licensing, by preventing spurious CP110-Cep97 complex release. **(B)** Consistent with this model in the absence of ELMOD2 or rootletin (KO lines), we see increased Cep164 and TTBK2 recruitment resulting in increased CP110 release, with consequent increased ciliation and even multiciliation.

(C) The *CROCC*$^{\Delta 239}$ line shows increased localization of rootletin, ARL2, and ELMOD2 at centrosomes and strongly reduced ciliation compared to WT. These cells have slightly reduced Cep164 and TTBK2 recruitment and a severe loss of CP110 release. Together, these data point to a specific role for rootletin in inhibiting the spurious release of CP110, and that over-activation of rootletin at centrosomes leads to inhibition of ciliation.

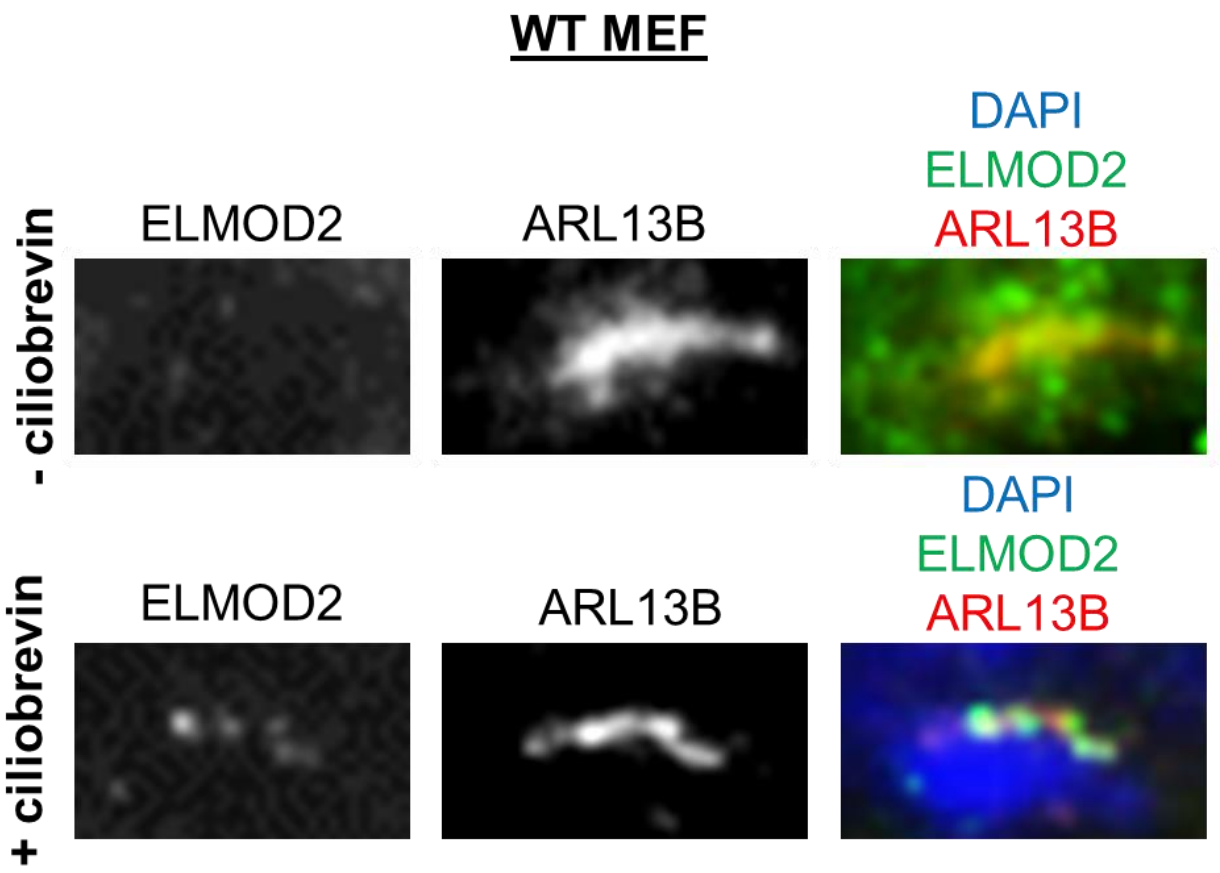

Figure S1: *ELMOD2 localizes to cilia in WT MEFs upon ciliobrevin treatment.* WT MEFs treated either with 0.6% DMSO (top) or 30µM ciliobrevin (bottom) for 1hr were fixed with 4% PFA, permeabilized with 0.1% Triton X-100, and stained for ELMOD2 and ARL13B. Only upon blocking of ciliary retrograde transport via ciliobrevin do we observe ELMOD2 localization to cilia. Representative images are shown. Images were collected via widefield imaging at 100x magnification.

A

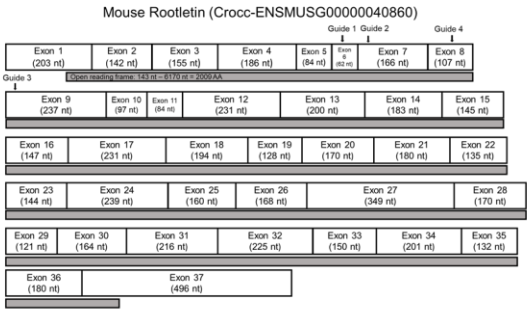

B

Clone ID	Guide	Alleles
G1, #12	1	Both alleles: 1 bp deletion (C); **AA sequence:** …TEHSQDLDSALLR*
G1, #31	1	Both alleles: 1 bp insertion (C); **AA sequence:** …TEHSQDLDSALLRPRGGTAEVRGWDSPWAPSG*
G2, #17	2	Both alleles: 1 bp insertion (C); **AA sequence:** …VSKCPLNTPTPPRSASLAQVNAMLREQLDQANLANQALSEDIPQGD Q*
G2, #20	2	Both alleles: 4bp deletion (TACG); **AA sequence:** …VSKCPLNTPTPPRSASLAQVNAMLREQLDQANLANQALSEDTR*
G4, #2	4	Both alleles: 1 bp insertion (A) ; **AA sequence:** …SFNAYFSSEHSRLLRLWRQVMGLRQAGQRGEDGHGEVRLLGAQG ASCPG*
Rootletin Δ239	1	1: 1 bp insertion (A); **AA sequence: …**TEHSQDLDSALLRHRGGTAEVRGWDSPWAPSG* 2: 2 bp insertion (CT); **AA sequence: …** TEHSQDLDSALLRP*

Figure S2: *Summary of Crocc frame shifting alleles in KO and* Crocc$^{\Delta 239}$ *MEFs.* **(A)** We designed 4 guides to use in CRISPR/Cas9 genome editing and the sites they target are shown above the targeted exons. The mouse *Crocc* gene encodes 37 exons shown, with the open reading frame shown below the spliced exons. **(B)** A total of 5 *Crocc* KO lines were generated, along with one *Crocc*$^{\Delta 239}$ line (G1, #21). Two clones were generated using guide 1, two clones were generated using guide 2, and 1 clone was generated using guide 4. The *Crocc*$^{\Delta 239}$ mutant was generated from guide 1. Genomic DNA sequencing was performed on clones that had lost staining of rootletin by immunofluorescence of fixed cells, to identify frame-shifting mutations in potential null lines. The black font indicates WT protein sequence while the red font indicates nonsense protein sequence resulting from a frame shift and an asterisk indicates a stop codon. Each of the knockout clones led to frameshifting mutations which were predicted to generate non-functional protein products, as later confirmed by Western blot. In contrast, the line termed *Crocc*$^{\Delta 239}$ displays very strong staining of rootletin, despite having both alleles frameshifted at the targeted site. The use of a

downstream methionine to initiate protein translation is proposed as an explanation of the shorter protein product seen in immunoblots.

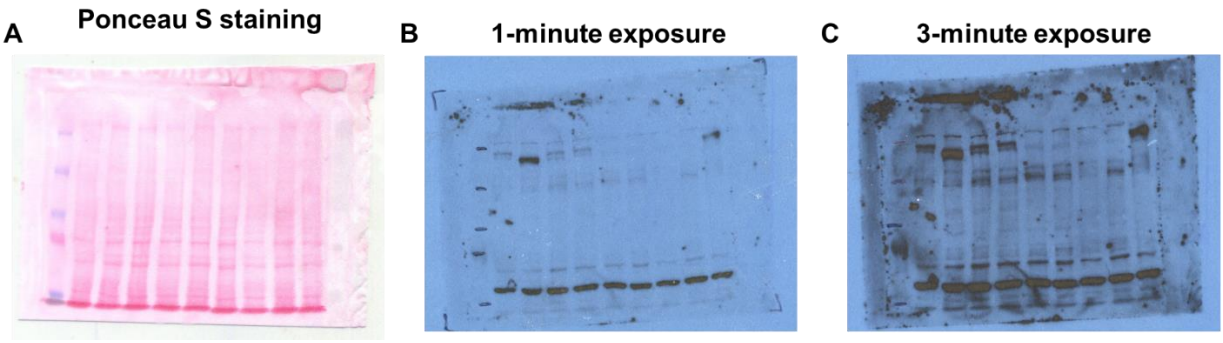

Figure S3: *Western blot for rootletin in WT, Rootletin KO, ELMOD2 KO, and* Crocc$^{\Delta 239}$ *MEFs.* Raw data of the Western shown in Figure 5A are shown, including **(A)** Ponceau S staining of the nitrocellulose membrane to confirm equal protein loading, and **(B-C)** uncropped images of the films collected at 1 min and 3 min exposures respectively. Membranes were stained with chicken-anti-rootletin at 1:1000 dilution in 5% Blotto.

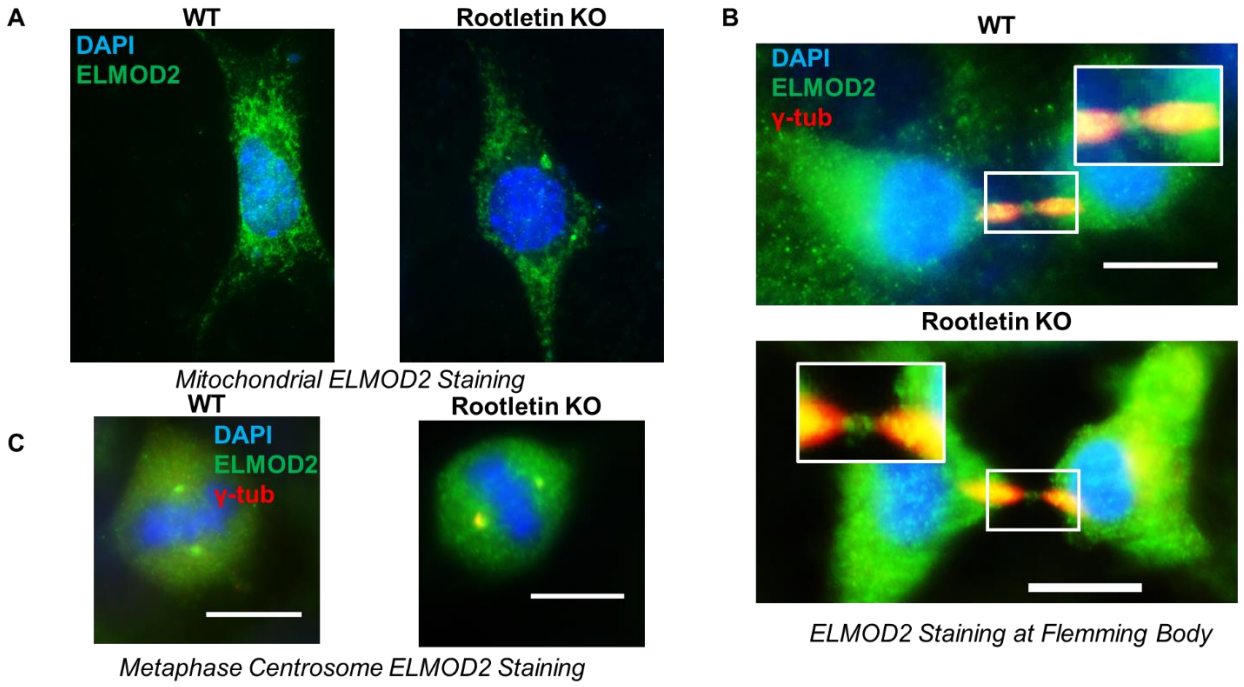

Figure S4: *ELMOD2 still localizes to mitochondria, Flemming bodies, and centrosomes in rootletin KO cells.* To test whether the deletion of rootletin alters ELMOD2 staining at sites other than rootlets, we used a number of fixation conditions to stain rootletin KO cells for ELMOD2. (**A**) Loss of rootletin does not alter ELMOD2 staining of mitochondria. ELMOD2 localization at Flemming bodies **(B)** and metaphase centrosomes **(C)** also remained unchanged in rootletin KO cells. Cells were fixed with ice cold methanol for 5 minutes and stained for ELMOD2 and γ-tubulin (to mark both midbodies and centrosomes). Together, these data point to ELMOD2 specifically working with rootletin at cilia but not other cellular compartment at which ELMOD2 localizes. Widefield images at 100x magnification are shown. Scale = 10μm.

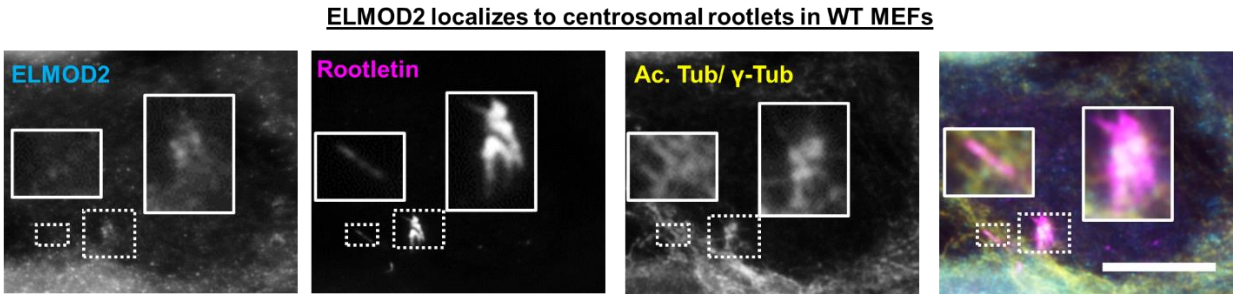

Figure S5: *ELMOD2 does not localize to non-centrosomal rootlets.* Representative images show that ELMOD2 specifically localizes to centrosome-associated rootlets rather than all rootletin staining. Serum-starved, WT MEFs were fixed with ice-cold methanol and stained for ELMOD2, acetylated tubulin, and rootletin. Widefield images were collected at 100x magnification. Scale = 10µm.

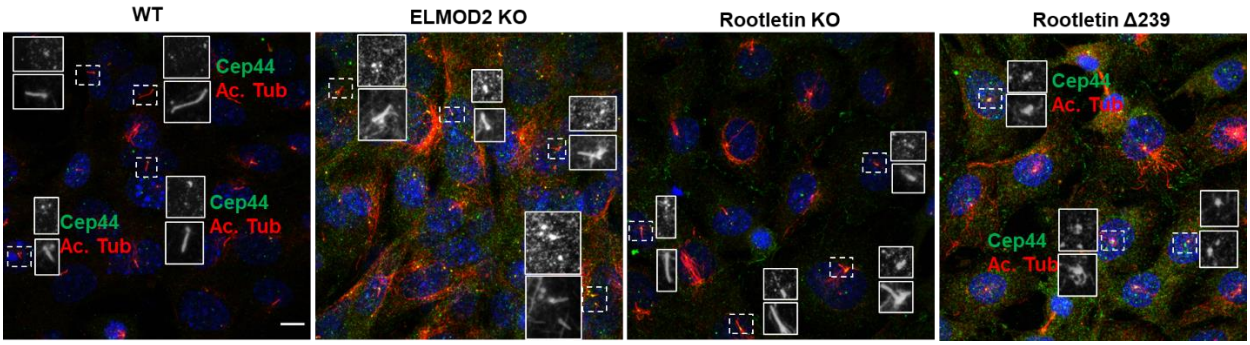

Figure S6: *Cep44 localization to centrosomes is unaltered in ELMOD2 KO or rootletin KO cells*. Serum-starved WT, ELMOD2 KO, rootletin KO, and *Crocc*$^{\Delta 239}$ cells were fixed with ice cold methanol for 10 minutes and stained for Cep44 and acetylated. Cep44 localization remains unchanged at centrosomes, though there is some staining of cilia in both ELMOD2 KO and rootletin KO. Z-stack projects were collected via confocal microscopy at 100x magnification. Scale = 10 µm.

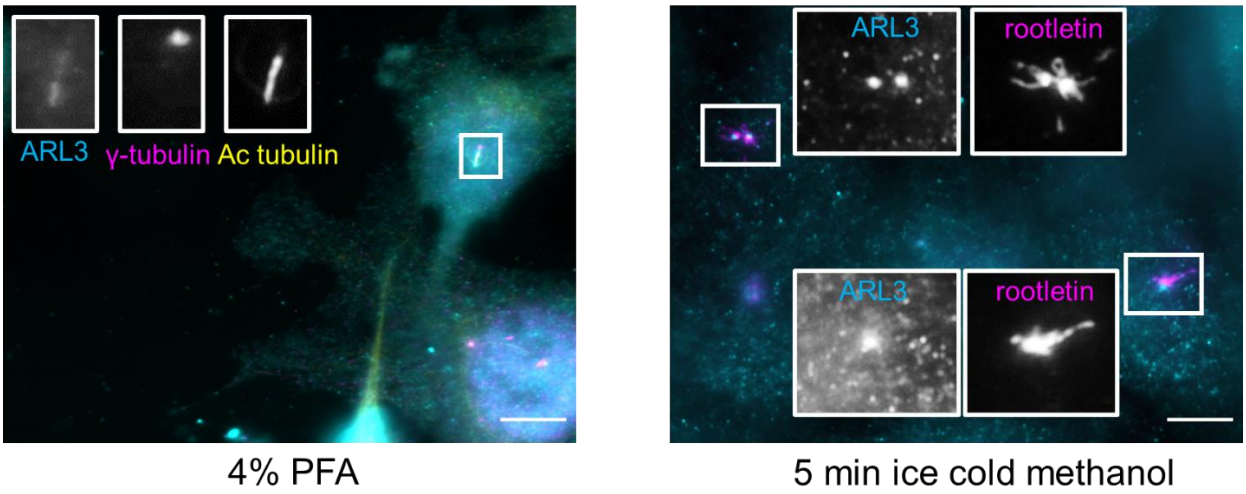

Figure S7: *ARL3 localizes to cilia and centrosomes but not rootlets in WT MEFs.* Representative widefield images (100x magnification) of ARL3 localization in WT MEFs are shown. With 4% PFA fixation, ARL3 staining at cilia is observed, as seen by co-staining with γ-tubulin and acetylated tubulin. With ice-cold methanol fixation, centrosomal staining of ARL3 is evident, but it does not extend to rootlets (using conditions in which one can readily detect ELMOD2 and ARL2 at rootlets). Scale = 10μm.

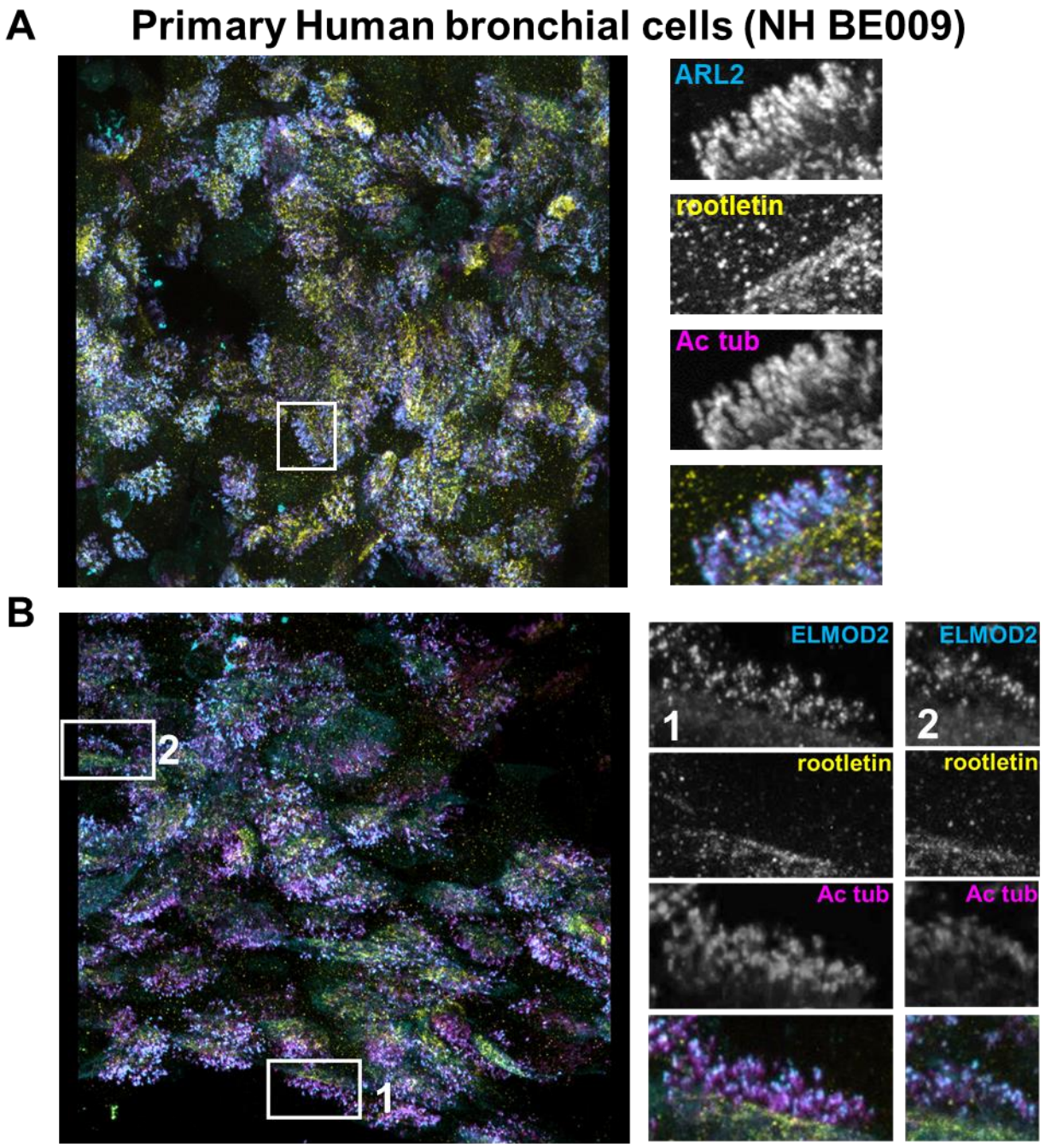

Figure S8: *ARL2 localizes along the length of cilia in human (multiciliated) bronchial epithelial cells, while ELMOD2 localizes to the tips of cilia and rootlets in human bronchial cells.* Wild-type primary cultures of human bronchial cells were grown on transwell plates over a few weeks before being fixed with ice-cold methanol and stained for rootletin (to mark rootlets), acetylated tubulin

(to mark cilia) and either **(A)** ARL2 or **(B)** ELMOD2. Confocal images were collected at 100x magnification, and z-projections were generated. Representative images of fields of bronchial cells are shown on the left. On the right, insets that highlight cells in which one can readily distinguish cilia from plasma membrane from rootlets. ARL2 is found almost exclusively at cilia in these cells, while ELMOD2 stains both the tip of cilia as well as (more faintly) the rootlets.

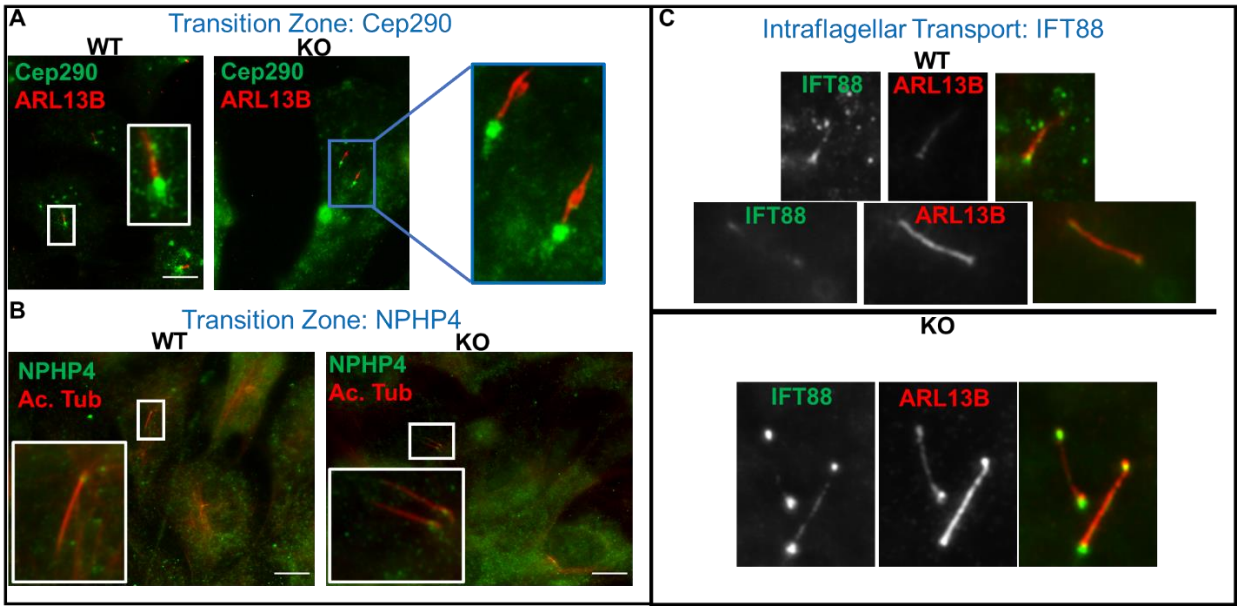

Figure S9: *ELMOD2 KO does not alter the localization of IFT or transition zone (TZ) markers.* Cells were fixed and stained for either markers of transition zone **(A-B)** or intraflagellar transport **(B)** to determine if there are overt defects in these compartments in ELMOD2 KO cells. For transition zone, cells were fixed for 10 min with ice-cold methanol, blocked with 10% FBS, and stained for either NPHP4 or Cep290, along with a ciliary marker (ARL13B or acetylated tubulin). To look at IFT, cells were fixed with 4% PFA, permeabilized with 0.1% Triton X-100, and stained for IFT88 (a marker of intraflagellar transport). Representative images were collected via widefield microscopy at 100x magnification. Scale = 10µm. Together, these data indicate no obvious changes in IFT or transition zone.

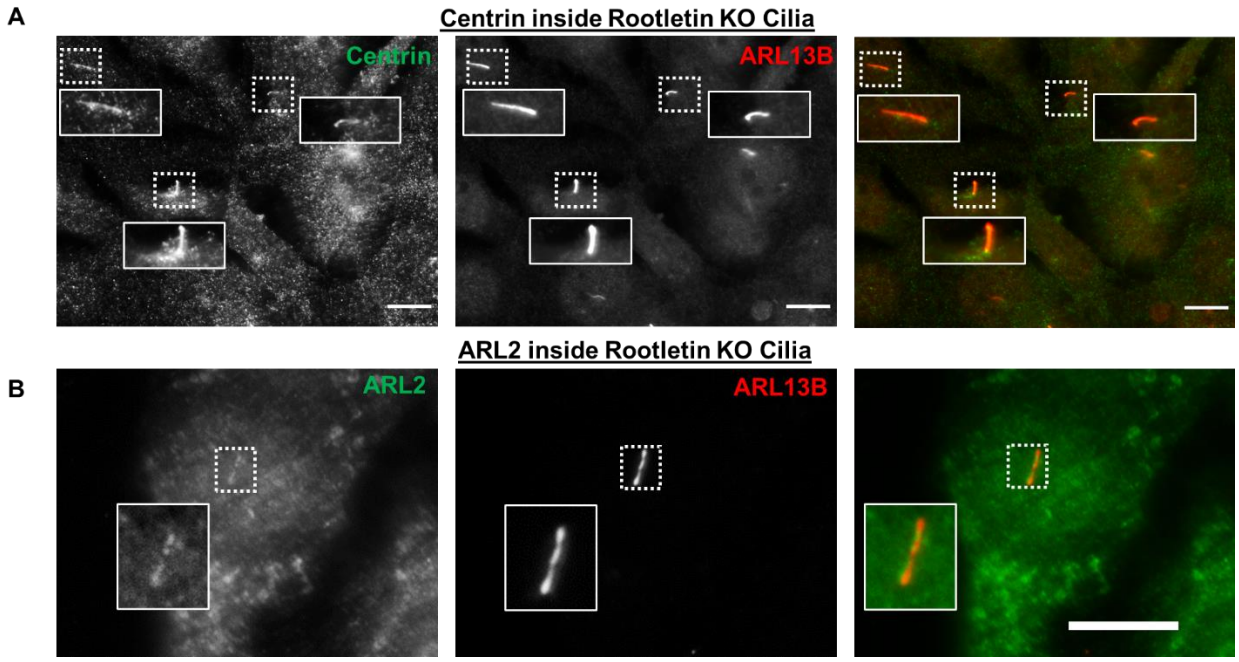

Figure S10: *Centrin and ARL2 localize to rootletin KO cilia.* Representative images collected via widefield microscopy show that serum-starved rootletin KO cells have increased recruitment of both ARL2 and centrin. Cells were fixed with 4% PFA, permeabilized with 0.1% Triton X-100, and stained for ARL13B as a marker of cilia and either centrin or ARL2. Images were collected at 100x magnification. Scale = 10µm.

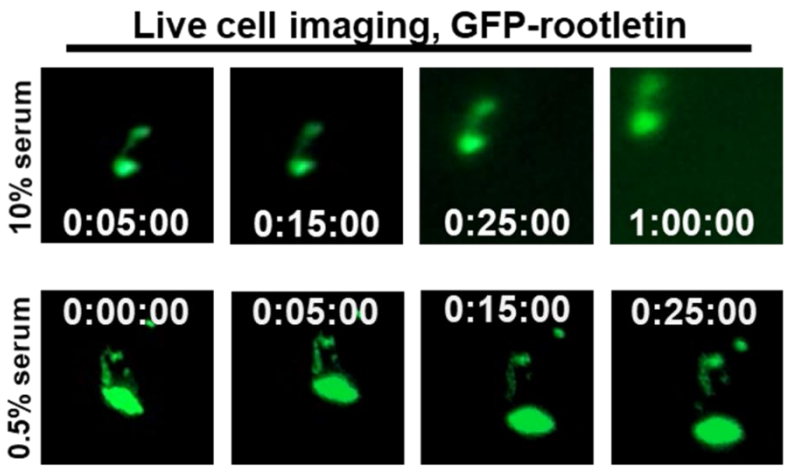

Figure S11: *Live cell imaging of GFP-rootletin transfected WT MEFs reveal that serum starvation induces rootlet tendrils to fall off*. Cells were imaged every 5 minutes over a 1-hour imaging window using widefield microscopy, 20x magnification. Temperature was maintained at 37˚C, and CO_2 was maintained at 5%. Cells were either images for 1 hour without serum starvation or imaged for ~1 hour after serum starvation. While no rootlet fragmentation was obvious without serum starvation, after serum starvation rootlets begin to fragment within minutes. Representative images are shown.

Chapter 4: Discussion

Summary

Increasing study of ARF GTPases and their regulators has revealed critical roles for these proteins in multiple different cellular compartments and signaling pathways. ARFs and their respective GEFs/GAPs serve as drivers of cellular functions, ensuring that downstream signals are propagated at the right time and place. Because of their position at the crossroads of diverse signaling pathways (ranging from cell cycle, cytoskeletal organization, mitochondrial dynamics, cell attachment, cell motility, ciliary function, and more), our lab has proposed a model in which ARFs are pivotal regulators of inter-pathway communication (Francis et al., 2016). To date, much of our approach to studying signaling has been restricted to linear, confined signaling pathways where a single protein will only communicate with a single downstream player. As our knowledge concerning signaling in distinct pathways has advanced, it has become increasingly clear that there needs to be various degrees of communication between individual organelles/compartments to drive essential cellular processes as well as coordinate those acting at different sites. For example, cell division alone requires dramatic changes in microtubules, nuclei, cilia, actin, endosomes, plasma membrane, centrosomes, mitochondria, and other cellular compartments to communicate with one another to ensure that two healthy cells are generated after each division. It is when communication is disrupted between these compartments that pathologies often arise. We predict that ARF GTPases and their regulators play a key role in making these connections in the signaling network. Thus, a fundamental goal for our lab has been to one day understand the mechanisms by which ARFs, ARF GEFs, and ARF GAPs selectively drive one function versus another in a temporally and spatially specific manner.

I have contributed to our lab's fundamental goal through my dissertation research exploring the diverse and overlapping functions of the ELMOD family of ARF GAPs. As the first family to

exhibit GAP activity for both ARFs and ARLs in vitro (East et al., 2012; Ivanova et al., 2014), these players served as strong candidates for regulators of inter-pathway communication. Yet, since discovery of their GAP activity for ARL2 in 2007 (Bowzard et al., 2007), very little has been published concerning their cellular functions. Previous work implicated these players in a number of pathologies (Hodgson et al., 2006; Pulkkinen et al., 2010; Lawson et al., 2011; Johnson et al., 2012; Jaworek et al., 2013; Li et al., 2018; Lahbib et al., 2019; Li et al., 2019; Miryounesi et al., 2019), yet the cellular functions of these proteins remained largely uncharacterized. Our lab took the first step towards exploring ELMOD1, ELMOD2, and ELMOD3 activities in cells with the discovery that ELMOD1 localizes to Golgi (East et al., 2012) and that ELMOD2 directs mitochondrial fusion downstream of ARL2 and upstream of the mitofusins (Newman et al., 2014; Schiavon et al., 2019). I carried this work forward by investigating novel functions for all the family members and using these data to tease apart the degree of functional redundancy versus specificity among ELMOD1, ELMOD2, and ELMOD3. To do so, I generated knockout lines of each of the family members in MEFs using CRISPR-Cas9. The use of cells devoid of each ELMOD proved to be a powerful tool for identifying novel phenotypes in each cell line that points to a far great number of cellular functions for ELMODs than any of us had imagined before I began my research. By gaining a basic understanding of how the ELMODs function in cells, I have laid the groundwork for exploring the regulatory events that drive ARF GTPase function. Together, I have also contributed to the lab's overall goal of probing for the mechanisms that drive ARFs and their regulators in inter-pathway communication. It is quite common in dissertations to describe the field before and after the research presented to highlight the impact on the field. This seems unnecessary as so little was known about the cellular roles of the ELMODs. So instead, I have

summarized the novel functionalities I discovered for ELMOD2 during my research in the model below (see Figure 1).

The majority of my dissertation research was focused on teasing apart novel functions for ELMOD2 in cells. In Chapter 2 ("The ARF GAP ELMOD2 acts with different GTPases to regulate centrosomal microtubule nucleation and cytokinesis" (Turn et al., 2020)), I document for the first time a role for ELMOD2 in microtubule anchoring and cytokinesis. In initial characterization of ELMOD2 KO MEFs, I observed that loss of ELMOD2 led to cold sensitive microtubules, nocodazole super-sensitive microtubules, multinucleation, polyploidy, supernumerary centrosomes, loss of contact inhibition, and increased mitotic indices. I investigated to see where ELMOD2 may be acting that would lead to these downstream defects, and I discovered two new localizations: in what appears to be the pericentriolar material (PCM) of centrosomes and the Flemming body (the dense, proteinaceous section of the midbody that recruits factors pivotal for abscission). I probed for ELMOD2's cellular functions that would propagate these microtubule and cell cycle defects and soon discovered that ELMOD2 is working in concert with ARL2 and TBCD to regulate γ-tubulin recruitment to centrosomes. Previous data from our lab reported that ARL2 and TBCD regulate the recruitment of the γTuRC (γ-tubulin ring complex) to centrosomes and organizes the mitotic spindle (Cunningham and Kahn, 2008). Loss of ELMOD2 leads to delayed recruitment of all these players to centrosomes after removing microtubules with either cold or nocodazole treatment. A delay in recruitment in γ-tubulin to centrosomes would explain the disordered microtubule network and the slowed recovery from microtubule depolymerizing conditions. Because expression of ARL2 activating mutants reversed cold sensitivity defects in ELMOD2 KO lines, I interpret these data as evidence that ELMOD2 is acting with ARL2 in a pathway to regulate microtubule stability. On the other hand, ARL2 activating mutants failed to

reverse supernumerary centrosome and multinucleation defects, suggesting that ELMOD2 has yet another cellular function beyond regulating microtubule anchoring. I discovered that ELMOD2 is acting in the FIP3-Rab11-ARF6 pathway to direct cytokinesis, leading to the disrupted localization of these proteins at recycling endosome clusters and failure of ARF6 to recruit to Flemming bodies. Together, these findings contribute both to our fundamental understanding of ELMOD actions in cells and paves the way for functional insight into the mechanisms that drive cytokinesis and microtubule biology. Note that this clear distinction between phenotypic reversal by different GTPases acting with one GAP is, I believe, the first instance in which such cross specificity has been demonstrated in cells for one GAP.

In Chapter 3 ("Roles for ELMOD2 and Rootletin in Ciliogenesis"), I explored yet another novel cellular function for ELMOD2. To our surprise, loss of ELMOD2 led to *increased* ciliation, multiciliation, abnormal ciliary morphology, disrupted signaling, and mis-localization of "non-ciliary" proteins into cilia. Though I failed to identify the source of all the lesions in ciliary function, my findings do point to at least one central defect in ciliogenesis. I noted that ELMOD2 not only localizes to basal bodies, but also to ciliary rootlets- a poorly studied structure that both regulates centrosome cohesion and projects from the proximal end of basal bodies. In non-ciliated cells, rootlets look like a dense network of fibers surrounding both centrosomes. On the other hand, ciliated cells often have only a single or a few condensed rootlets that project from the distal end of the basal body. The precise function of rootlets with respect to cilia remains poorly defined, though the general consensus is that they regulate ciliary stability in retinal cells (Yang et al., 2002; Yang et al., 2005; Yang and Li, 2005; Yang and Li, 2006; Liu et al., 2007). Loss of ELMOD2 leads to rootlet fragmentation and stubby/punctate rootlets at the base of cilia. Expression of ELMOD2-myc and myc-rootletin each rescue ELMOD2 KO ciliary defects. I proceeded to test

the hypothesis that ELMOD2, in concert with the ciliary rootlet, are acting as negative regulators of ciliogenesis. I generated rootletin KO cells and observed that they presented with increased ciliation, multiciliation, mis-localization of centrin to cilia, and abnormal ciliary morphology, similar to ELMOD2 KO. Yet, rootletin KO cells do not have multinucleation, supernumerary centrosomes, or cold sensitive microtubules. These data would suggest that rootletin, while having overlapping functions with ELMOD2, is not working with ELMOD2 in all its cellular functions. Furthermore, rootletin KO cells still had normal localization of ELMOD2 in all other locations examined (including mitochondria, metaphase centrosomes, and Flemming bodies). Surprisingly, both ARL2 and fast-cycling ARL2 reverse ciliary defects in both ELMOD2 KO and rootletin KO cells. However, ELMOD2-myc alone is insufficient to reverse ciliary defects in rootletin KO cells. One potential explanation for this unusual finding is that the rootlet is acting as a scaffold for such components as ARL2 so that it can inhibit ciliogenesis. Therefore, overexpressing the ARL2 or fast-cycling ARL2 can flood the system and allow for the free diffusion of ARL2 to block spurious ciliogenesis in rootletin and ELMOD2 KO cells. Perhaps ARL2 is acting in a different pathway than ELMOD2 and rootletin to block spurious ciliogenesis. Further study will be critical to tease apart the relationship of ELMOD2, rootletin, and ARL2 in ciliogenesis. We tested further to narrow down the source of the lesion in ciliogenesis in both ELMOD2 and rootletin KO cells, and we believe that the fundamental defect lies early in ciliogenesis, specifically in the release of CP110. Further study is necessary to understand the precise mechanisms by which ELMOD2, rootletin, and ARL2 inhibit spurious ciliogenesis and how the other ciliary phenotypes I observed along the way emerged (*e.g.* defective signaling, abnormal ciliary morphology, spurious localization of proteins like centrin to cilia), but these findings lay the groundwork for much-

needed study into the mechanisms that drive ciliogenesis and the regulators of ARF GTPases at cilia.

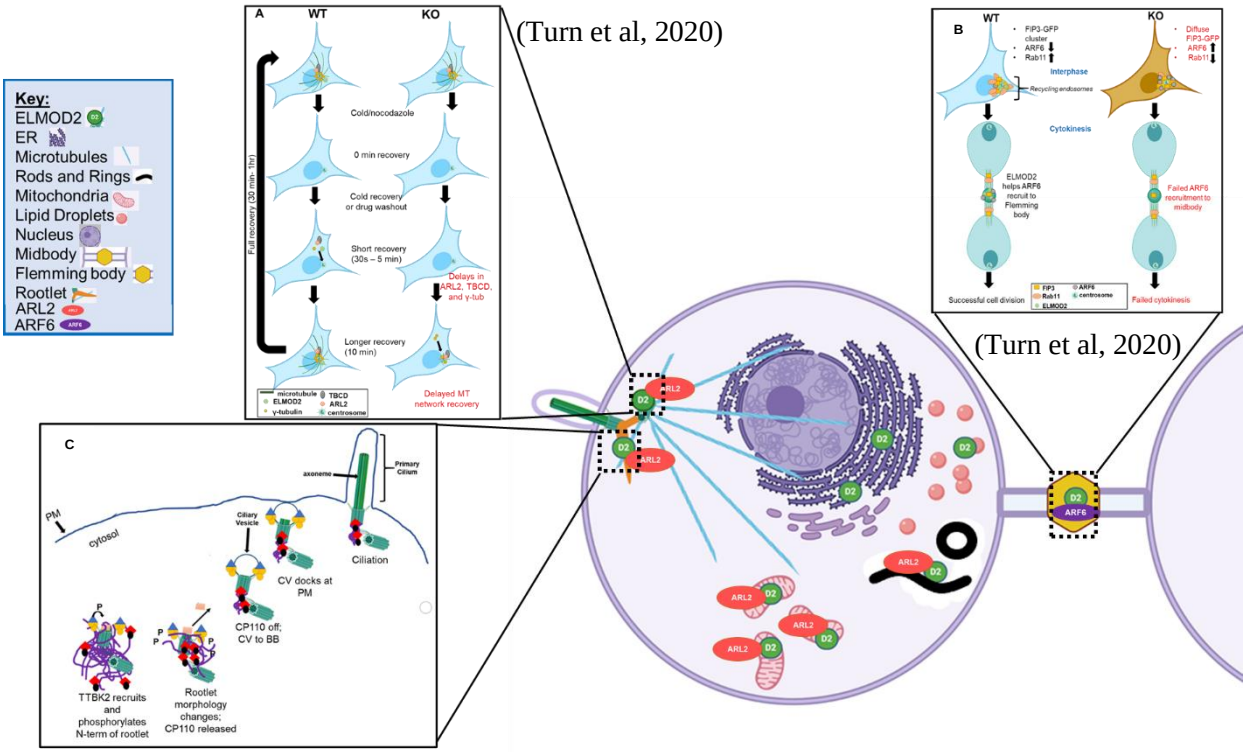

Figure 1: Summary of contributions to the field. *As part of my dissertation research, I have moved the field of ARF GAP biology forward by identifying three novel functions for ELMOD2 in mammalian cells:* ***(A)*** *microtubule anchoring at centrosomes,* ***(B)*** *cytokinesis, and* ***(C)*** *ciliogenesis. My work shed light on the mechanisms that drive each of these functions and opens up exciting new questions concerning inter-pathway communication. The key in the upper left highlights different compartments/proteins shown in the model cell. This figure was generated using BioRender.*

Future Directions

In many ways, the summation of this work brings forth more questions than answers concerning ARF GTPase signaling and fundamental aspects of cellular biology. Here, I will pose logical future directions for this work that the next generation of researchers may pursue.

1. ELMOD Family

As the previous chapters of this work demonstrate, the vast majority of my research was focused on exploring novel cellular functions for ELMOD2 in cells. I identified ELMOD2 as a novel regulator of ciliogenesis, cytokinesis, and microtubule anchoring. One direction that I did not have the opportunity to pursue in my dissertation research, though, was exploring the functions of ELMOD1 and ELMOD3. I generated knockout lines for all three family members, and I collaborated with future generations of lab members to begin pursuing their cellular functions. Early studies suggest that ELMOD2 is quite different from ELMOD1 and ELMOD3 in cell activities. Neither ELMOD1 nor ELMOD3 display evidence of defects in microtubule anchoring or cytokinesis. Although they have ciliary defects, these phenotypes are the *opposite* of ELMOD2's: loss of ciliation and reduced recruitment of ARL13B and ARL3 to cilia. Furthermore, ELMOD1 and ELMOD3 have novel phenotypes: they have severe attachment defects that are exacerbated in ELMOD1/ELMOD3 DKO cells. Attachment defects are reversed upon pre-coating of cell culture plates with fibronectin. Previous data generated by former lab member Kate Hardin, our collaborator Jim Casanova, and myself suggest that focal adhesions are altered in ELMOD1 and ELMOD3 nulls. The lab is currently collaborating with members of Jim Casanova's lab

(University of Virginia), an expert in integrins and actions of ARF6 and actin at the cell surface, to identify lesions resulting from the deletion of ELMOD1, ELMOD3, or both.

After determining if these phenotypes can be rescued, one logical future direction for this project would be to determine the source of the lesion for cell attachment. Likely candidates would include vesicular traffic of key attachment particles to the plasma membrane or defects in actin cytoskeleton. Previous data from our lab demonstrated that ELMOD1 localizes to Golgi and may function at this site (East et al., 2012). Furthermore, ARF GTPases and ARF GAPs have a long history of working in vesicular traffic to regulate transport of cellular cargoes, especially in the case of cell attachment (Serafini et al., 1991; Boman et al., 2000; Derby et al., 2004; Godi et al., 2004; Volpicelli-Daley et al., 2005; Zhou et al., 2006; Donaldson and Jackson, 2011; Yu and Lee, 2017). Together, these data make a strong argument for a disruption in vesicular traffic being the source of the lesion. However, previous lab member Dr. Michael East generated unpublished data showing ELMOD3 localization to actin stress fibers and has preliminary data suggesting that ELMOD3 may be acting in a RHO/ROCK-dependent pathway. Together, these findings point to logical new directions to pursue for this project. We have not ruled out the possibility that ELMOD1 and ELMOD3 may be acting in different pathways that impose downstream consequences on cell attachment and therefore will need to perform cross-rescues to see if ELMOD1 and/or ELMOD3 can rescue the other's phenotypes. Future tests that should be performed to probe for function include cell spreading, cell motility, fibronectin secretion, integrin recruitment, actin morphology assessment, among others.

Further study should also be dedicated to understanding how loss of ELMOD1 and ELMOD3 compromises ARL3 and ARL13B localization to cilia. So far, markers of ciliogenesis, transition zone, and IFT appear unchanged in KO cells at least by widefield microscopy.

Surprisingly, these phenotypes are reminiscent of Skylar Fisher's data looking at ARL16 KO lines. Perhaps we have identified more than one regulator of ARL13B and ARL3 import into cilia, something which to date has been a mystery in the field of ciliary biology. Future directions would be to look at other regulators of ciliary import and transition zone (*e.g.* IFT20, TULP3) and to work towards building the signaling pathway.

Finally, I would be interested in further investigating what features of the ELMODs allows them to regulate such a variety of signaling pathways. What about each ELMOD drives it to distinct locations to perform one function versus another? Is it possible to identify targeting motifs that selectively drive their localization, such as import into mitochondria versus centrosomal localization in the case of ELMOD2? Study of potential post-translational modifications and deeper investigation into specific binding partners for each of these players will prove pivotal for building individual signaling pathways and eventually networks. Though previous attempts have been made to identify novel binding partners for these proteins, these efforts have been unsuccessful to date, probably because of the transient nature of ARF GAP interactions and the low levels of expression in cells and tissues. Perhaps more sensitive yeast two-hybrid approaches (*e.g.*, DEEPN; (Pashkova et al., 2016; Peterson et al., 2018)) or further optimization of APEX-2 (Lam et al., 2015; Hung et al., 2017; Bersuker et al., 2018) may help us find these answers. Altogether, there are many exciting directions to pursue with respect to the ELMOD family and how they mediate such essential cellular functions.

2. *Rootlets*

As described in Chapter 3, I have uncovered novel functions for the ciliary rootlet, a relatively poorly understood cellular structure. By identifying it as an inhibitor of ciliogenesis, I have placed this cell compartment on the map as not simply a passive, stabilizing component.

Rather, it is a dynamic structure that plays an active role in ensuring that ciliogenesis occurs at the right time and place. These findings suggest that we have merely brushed the surface of rootletin's cellular functions and that we still have much to learn about rootlet biology. First and foremost, how precisely does the rootlet inhibit ciliogenesis? Is it solely one component of the rootlet (rootletin) that inhibits ciliogenesis, or are other players, like Cep68, involved in this process (Graser et al., 2007; Vlijm et al., 2018)? Is the rootlet acting as a scaffold for key players to recruit, or is it behaving more as a physical barrier inhibiting the release/recruitment of ciliogenesis-related factors? How are ELMOD2 and ARL2 regulating the ciliary rootlet- are they acting upon it directly, or are there other intervening factors? One logical first step is to identify the rootlet's direct binding partners, as this may shed light on cellular mechanism. Also performing more detailed live cell imaging to capture both ciliogenesis and rootlet dynamics would prove useful for pinpointing the relationship of cilia and rootlet during ciliogenesis. My discovery of the Δ239 mutant also poses exciting new directions, as we believe that the N-terminus may contain critical information that regulates rootletin's dynamics. Perhaps performing systematic mutagenesis or creating smaller and smaller truncations may help us identify how rootletin is being regulated. One interesting possibility is that it is the target of TTBK2, a kinase that plays a critical role in promoting ciliogenesis (see Chapter 3). Basic sequence analysis revealed that the N-terminus of rootletin contains a putative phosphorylation motif that is recognized by TTBK2 (Bouskila et al., 2011). Therefore, it would be interesting to mutate these residues to see if this induces loss of ciliogenesis.

Beyond probing for the mechanism of rootlet function in ciliogenesis, I am fascinated by the question of tissue specificity. Like the cilium, the ciliary rootlet varies in morphology between tissue/cell types. I noted that while the monociliated retinal cell has a very long rootlet that appears

homogeneous across the cell population, multiciliated cells had very small rootlets (see Chapter 3). Could the size and morphology of the rootlet vary from cell to cell based on the ciliary requirements? Does the composition of the rootlet also vary? Further research into tissue specificity of rootlets may uncover critical information regarding how these rootlets work and how diseases may arise when they are disrupted.

3. Ciliogenesis

Beyond further investigation into ciliogenesis from a rootlet perspective, another direction that requires additional research is probing the mechanisms that drive ciliogenesis upstream of Cep164 recruitment to distal appendages. Very little is known concerning the signaling events that give the cell license to project a cilium and the precise mechanisms that ensure one and only one cilium is generated. For example, why does deletion of ELMOD2 cause increased ciliation and massive multinucleation while deletion of rootletin only promotes the former? What provides these layers of control? This is perhaps a very difficult and open-ended question that may serve as the foundation for future study. I predict that the use of genome-wide screens to identify novel ciliogenesis-regulating genes to start adding more pieces to the puzzle will be required. Defining all the stages that drive ciliogenesis is instrumental for our fundamental understanding of cell biology and for getting at the root of how ciliopathies arise.

4. Cytokinesis

Like ciliogenesis, the signaling events that drive cytokinesis also remain unclear. Though I have added another piece to the puzzle with the addition of ELMOD2 as a novel regulator of cytokinesis in the same pathway as ARF6, I have not teased apart the mechanism by which ELMOD2 regulates this pathway. Is ELMOD2 helping to dock endosomes from the PCM? Does

it dock onto endosome clusters that later traffic to midbody, and would that explain how it ends up in the Flemming body? There are still many open-ended questions concerning what upstream signaling events drive Rab11-FIP3-ARF6 clustering to centrosomes and how these players traffic to the midbody to promote cytokinesis. Furthermore, there is debate in the field about the relationship between these players and whether they truly act as a trimer complex, or if Rab11 and ARF6 compete for FIP3 binding (which is what my data suggest). Use of live cell imaging approaches and super-resolution microscopy to track the relationship of these players throughout cytokinesis may help us get at the root of these questions.

5. Higher order signaling

As we continue developing our fundamental understanding of ARF GTPase-mediated signaling networks, the next big question that remains is how ARFs and their regulators selectively turn on and off specific signaling pathways as well as mediate inter-pathway regulation. To understand how such cell processes as cell motility, cell division, apoptosis, and so many more occur, we need to start tying together the individual signals that make up these large signaling networks. The next step is to start probing for binding partners and post-translational modifications for proteins at the crossroads of the signaling cascades. These findings may help us tease apart how cell signaling is regulated and how disruption of a single protein can propagate such a wide range of cellular defects. It would be amazing to figure out how the cell precisely titers how much of a specific protein is at a given site at a given time. Such research will pave the way for a better understanding of diseases and how a complex range of phenotypes/symptoms can result from a single defect.

Concluding Remarks

Taken together, my findings add several more pieces to the model that ARF GTPases and their regulators facilitate higher order signaling. My findings have uncovered novel roles for ELMOD2 in three distinct cellular pathways: cytokinesis, ciliogenesis, and microtubule anchoring at centrosomes. Before this work, the only known functions for ELMOD2 were in mitochondrial fusion and predicted functions in lipid droplets. Before my dissertation research, the only known GTPase ELMOD2 was known to act upon was with ARL2. My studies have expanded ELMOD2's functions and highlight the fact that ARF GTPases as well as their regulators are capable of mediating diverse cellular pathways.

Beyond expanding our fundamental understanding of ARF GAP biology, my findings have shed light on poorly understood signaling pathways. With respect to the ARF6 pathway of cytokinesis, I believe that I have discovered a novel upstream player that promotes the recruitment of FIP3-positive endosomes to centrosomes. The mechanisms that drive the movement of endosomes from centrosomes to midbodies and Flemming bodies remain poorly understood, and the discovery of ELMOD2 in this pathway may help shed light on these upstream mechanisms. My work has uncovered the first ARF GAP to regulate microtubule anchoring at centrosomes, as well as revealed pivotal new insight into the upstream mechanisms driving ciliogenesis. Together, I hope that my work may provide tools for future generations to continue teasing apart the pathways that make cells function.

Together, my research has moved forward both the field of ARF GTPase and cellular biology. These findings will lay the foundation for future researchers both in my lab and outside the lab to get at the heart of the signaling mechanisms that drive essential cellular functions. Perhaps with our continued efforts we will gather enough pieces to our puzzle to begin assembling

signaling networks and will begin to define the approaches that the cell employs to promote inter-pathway communication between disparate signaling compartments. Together, these contributions to basic research will lay the groundwork for identifying the source of pathologies and will aid in the development of therapeutics that target the precise lesion.

References

Bersuker, K., C.W.H. Peterson, M. To, S.J. Sahl, V. Savikhin, E.A. Grossman, D.K. Nomura, and J.A. Olzmann. 2018. A Proximity Labeling Strategy Provides Insights into the Composition and Dynamics of Lipid Droplet Proteomes. *Dev Cell*. 44:97-112 e117.

Boman, A.L., C. Zhang, X. Zhu, and R.A. Kahn. 2000. A family of ADP-ribosylation factor effectors that can alter membrane transport through the trans-Golgi. *Mol Biol Cell*. 11:1241-1255.

Bouskila, M., N. Esoof, L. Gay, E.H. Fang, M. Deak, M.J. Begley, L.C. Cantley, A. Prescott, K.G. Storey, and D.R. Alessi. 2011. TTBK2 kinase substrate specificity and the impact of spinocerebellar-ataxia-causing mutations on expression, activity, localization and development. *Biochem J*. 437:157-167.

Bowzard, J.B., D. Cheng, J. Peng, and R.A. Kahn. 2007. ELMOD2 is an Arl2 GTPase-activating protein that also acts on Arfs. *J Biol Chem*. 282:17568-17580.

Cunningham, L.A., and R.A. Kahn. 2008. Cofactor D functions as a centrosomal protein and is required for the recruitment of the gamma-tubulin ring complex at centrosomes and organization of the mitotic spindle. *J Biol Chem*. 283:7155-7165.

Derby, M.C., C. van Vliet, D. Brown, M.R. Luke, L. Lu, W. Hong, J.L. Stow, and P.A. Gleeson. 2004. Mammalian GRIP domain proteins differ in their membrane binding properties and are recruited to distinct domains of the TGN. *J Cell Sci*. 117:5865-5874.

Donaldson, J.G., and C.L. Jackson. 2011. ARF family G proteins and their regulators: roles in membrane transport, development and disease. *Nat Rev Mol Cell Biol*. 12:362-375.

East, M.P., J.B. Bowzard, J.B. Dacks, and R.A. Kahn. 2012. ELMO Domains, Evolutionary and Functional Characterization of a Novel GTPase-activating Protein (GAP) Domain for Arf Protein Family GTPases. *J Biol Chem*. 287:39538-39553.

Francis, J.W., R.E. Turn, L.E. Newman, C. Schiavon, and R.A. Kahn. 2016. Higher order signaling: ARL2 as regulator of both mitochondrial fusion and microtubule dynamics allows integration of 2 essential cell functions. *Small GTPases*. 7:188-196.

Godi, A., A. Di Campli, A. Konstantakopoulos, G. Di Tullio, D.R. Alessi, G.S. Kular, T. Daniele, P. Marra, J.M. Lucocq, and M.A. De Matteis. 2004. FAPPs control Golgi-to-cell-surface membrane traffic by binding to ARF and PtdIns(4)P. *Nat Cell Biol*. 6:393-404.

Graser, S., Y.D. Stierhof, and E.A. Nigg. 2007. Cep68 and Cep215 (Cdk5rap2) are required for centrosome cohesion. *J Cell Sci*. 120:4321-4331.

Hodgson, U., V. Pulkkinen, M. Dixon, M. Peyrard-Janvid, M. Rehn, P. Lahermo, V. Ollikainen, K. Salmenkivi, V. Kinnula, J. Kere, P. Tukiainen, and T. Laitinen. 2006. ELMOD2 is a candidate gene for familial idiopathic pulmonary fibrosis. *Am J Hum Genet*. 79:149-154.

Hung, V., S.S. Lam, N.D. Udeshi, T. Svinkina, G. Guzman, V.K. Mootha, S.A. Carr, and A.Y. Ting. 2017. Proteomic mapping of cytosol-facing outer mitochondrial and ER membranes in living human cells by proximity biotinylation. *eLife*. 6.

Ivanova, A.A., M.P. East, S.L. Yi, and R.A. Kahn. 2014. Characterization of recombinant ELMOD (cell engulfment and motility domain) proteins as GTPase-activating proteins (GAPs) for ARF family GTPases. *J Biol Chem*. 289:11111-11121.

Jaworek, T.J., E.M. Richard, A.A. Ivanova, A.P. Giese, D.I. Choo, S.N. Khan, S. Riazuddin, R.A. Kahn, and S. Riazuddin. 2013. An alteration in ELMOD3, an Arl2 GTPase-activating protein, is associated with hearing impairment in humans. *PLoS genetics*. 9:e1003774.

Johnson, K.R., C.M. Longo-Guess, and L.H. Gagnon. 2012. Mutations of the mouse ELMO domain containing 1 gene (Elmod1) link small GTPase signaling to actin cytoskeleton dynamics in hair cell stereocilia. *PloS one*. 7:e36074.

Lahbib, S., C.S. Leblond, M. Hamza, B. Regnault, L. Lemee, A. Mathieu, H. Jaouadi, R. Mkaouar, I.B. Youssef-Turki, A. Belhadj, I. Kraoua, T. Bourgeron, and S. Abdelhak. 2019. Homozygous 2p11.2 deletion supports the implication of ELMOD3 in hearing loss and reveals the potential association of CAPG with ASD/ID etiology. *J Appl Genet*. 60:49-56.

Lam, S.S., J.D. Martell, K.J. Kamer, T.J. Deerinck, M.H. Ellisman, V.K. Mootha, and A.Y. Ting. 2015. Directed evolution of APEX2 for electron microscopy and proximity labeling. *Nat Methods*. 12:51-54.

Lawson, W.E., J.E. Loyd, and A.L. Degryse. 2011. Genetics in pulmonary fibrosis--familial cases provide clues to the pathogenesis of idiopathic pulmonary fibrosis. *Am J Med Sci*. 341:439-443.

Li, W., Y. Feng, A. Chen, T. Li, S. Huang, J. Liu, X. Liu, Y. Liu, J. Gao, D. Yan, J. Sun, L. Mei, X. Liu, and J. Ling. 2019. Elmod3 knockout leads to progressive hearing loss and abnormalities in cochlear hair cell stereocilia. *Hum Mol Genet*. 28:4103-4112.

Li, W., J. Sun, J. Ling, J. Li, C. He, Y. Liu, H. Chen, M. Men, Z. Niu, Y. Deng, M. Li, T. Li, J. Wen, S. Sang, H. Li, Z. Wan, E.M. Richard, P. Chapagain, D. Yan, X.Z. Liu, L. Mei, and Y. Feng. 2018. ELMOD3, a novel causative gene, associated with human autosomal dominant nonsyndromic and progressive hearing loss. *Human genetics*. 137:329-342.

Liu, Q., G. Tan, N. Levenkova, T. Li, E.N. Pugh, Jr., J.J. Rux, D.W. Speicher, and E.A. Pierce. 2007. The proteome of the mouse photoreceptor sensory cilium complex. *Mol Cell Proteomics*. 6:1299-1317.

Miryounesi, M., S. Bahari, S. Salehpour, N. Alipour, and S. Ghafouri-Fard. 2019. ELMO Domain Containing 1 (ELMOD1) Gene Mutation Is Associated with Mental Retardation and Autism Spectrum Disorder. *Journal of molecular neuroscience : MN*. 69:312-315.

Newman, L.E., C.J. Zhou, S. Mudigonda, A.L. Mattheyses, E. Paradies, C.M. Marobbio, and R.A. Kahn. 2014. The ARL2 GTPase is required for mitochondrial morphology, motility, and maintenance of ATP levels. *PloS one*. 9:e99270.

Pashkova, N., T.A. Peterson, V. Krishnamani, P. Breheny, M. Stamnes, and R.C. Piper. 2016. DEEPN as an Approach for Batch Processing of Yeast 2-Hybrid Interactions. *Cell reports*. 17:303-315.

Peterson, T.A., M.A. Stamnes, and R.C. Piper. 2018. A Yeast 2-Hybrid Screen in Batch to Compare Protein Interactions. *Journal of visualized experiments : JoVE*.

Pulkkinen, V., S. Bruce, J. Rintahaka, U. Hodgson, T. Laitinen, H. Alenius, V.L. Kinnula, M. Myllarniemi, S. Matikainen, and J. Kere. 2010. ELMOD2, a candidate gene for idiopathic pulmonary fibrosis, regulates antiviral responses. *Faseb J*. 24:1167-1177.

Schiavon, C.R., R.E. Turn, L.E. Newman, and R.A. Kahn. 2019. ELMOD2 regulates mitochondrial fusion in a mitofusin-dependent manner, downstream of ARL2. *Mol Biol Cell*. 30:1198-1213.

Serafini, T., G. Stenbeck, A. Brecht, F. Lottspeich, L. Orci, J.E. Rothman, and F.T. Wieland. 1991. A coat subunit of Golgi-derived non-clathrin-coated vesicles with homology to the clathrin-coated vesicle coat protein beta-adaptin. *Nature*. 349:215-220.

Turn, R.E., M.P. East, R. Prekeris, and R.A. Kahn. 2020. The ARF GAP ELMOD2 acts with different GTPases to regulate centrosomal microtubule nucleation and cytokinesis. *Mol Biol Cell*. 31:2070-2091.

Vlijm, R., X. Li, M. Panic, D. Ruthnick, S. Hata, F. Herrmannsdorfer, T. Kuner, M. Heilemann, J. Engelhardt, S.W. Hell, and E. Schiebel. 2018. STED nanoscopy of the centrosome linker reveals a CEP68-organized, periodic rootletin network anchored to a C-Nap1 ring at centrioles. *Proc Natl Acad Sci U S A*. 115:E2246-E2253.

Volpicelli-Daley, L.A., Y. Li, C.J. Zhang, and R.A. Kahn. 2005. Isoform-selective effects of the depletion of ADP-ribosylation factors 1-5 on membrane traffic. *Mol Biol Cell*. 16:4495-4508.

Yang, J., J. Gao, M. Adamian, X.H. Wen, B. Pawlyk, L. Zhang, M.J. Sanderson, J. Zuo, C.L. Makino, and T. Li. 2005. The ciliary rootlet maintains long-term stability of sensory cilia. *Mol Cell Biol*. 25:4129-4137.

Yang, J., and T. Li. 2005. The ciliary rootlet interacts with kinesin light chains and may provide a scaffold for kinesin-1 vesicular cargos. *Exp Cell Res*. 309:379-389.

Yang, J., and T. Li. 2006. Focus on molecules: rootletin. *Experimental eye research*. 83:1-2.

Yang, J., X. Liu, G. Yue, M. Adamian, O. Bulgakov, and T. Li. 2002. Rootletin, a novel coiled-coil protein, is a structural component of the ciliary rootlet. *J Cell Biol*. 159:431-440.

Yu, C.J., and F.J. Lee. 2017. Multiple activities of Arl1 GTPase in the trans-Golgi network. *J Cell Sci*. 130:1691-1699.

Zhou, C., L. Cunningham, A.I. Marcus, Y. Li, and R.A. Kahn. 2006. Arl2 and Arl3 regulate different microtubule-dependent processes. *Mol Biol Cell*. 17:2476-2487.